Durham E-Theses

CP-violation in cascade decays at the LHC

TATTERSALL, JAMIE

How to cite:

TATTERSALL, JAMIE (2010) *CP-violation in cascade decays at the LHC*, Durham theses, Durham University. Available at Durham E-Theses Online: http://etheses.dur.ac.uk/523/

CP-violation in cascade decays at the LHC

Jamie Tattersall

A Thesis presented for the degree of

Doctor of Philosophy

Institute for Particle Physics Phenomenology

Department of Physics

University of Durham

U.K.

September 2010

CP-violation in cascade decays at the LHC

Jamie Tattersall

Abstract

We study the potential to observe CP-violating effects in various supersymmetric cascade decay chains at the LHC. Asymmetries composed by triple products of momenta of the final state particles are sensitive to CP-violating effects. We analytically calculate the cascade decays including the relevant spin correlations to compute the parton level asymmetry. In addition, we use Monte Carlo simulations to estimate the sensitivity of the LHC to the CP-violating observables.

Due to large boosts that dilute the asymmetries, these can be difficult to observe at the LHC. However, if all particle masses in a cascade decay are known, it may be possible to reconstruct all momenta in the decay chains. We can then recover the full asymmetry on an event-by-event basis even when we have missing momentum due to a stable lightest supersymmetric particle. After the reconstruction, the non-diluted CP-violating signal gets significantly enhanced so that an observation may become feasible.

A fully hadronic study has also been completed to produce the best estimate of the viability of these obseravbles at the LHC. We include both standard model and SUSY backgrounds in the study. Our conclusions state that given a favourable scenario, CP-violation may be observed in SUSY at the 3σ-level over a wide range of CP-phases with 500 fb^{-1} of data.

Declaration

The work in this thesis is based on research carried out at the Institute for Particle Physics Phenomenology, Department of Physics, University of Durham, United Kingdom. No part of this thesis has been submitted elsewhere for any other degree or qualification and it is based on the work in the following publications and articles:

- J. Tattersall, G. Moortgat-Pick, and K. Rolbiecki,
  CP-violation in SUSY cascades at the LHC,
  arXiv:1009.0294 [hep-ph].

- G. Moortgat-Pick, K. Rolbiecki, J. Tattersall,
  Momentum reconstruction at the LHC for probing CP-violation in the stop sector,
  arXiv:1008.2206 [hep-ph].

- K. Rolbiecki, G. Moortgat-Pick, J. Tattersall, and P. Wienemann,
  Probing CP Violation with Kinematic Reconstruction at the LHC,
  Fortsch. Phys. 58 (2010) 699-702, arXiv:1003.0087 [hep-ph].

- G. Moortgat-Pick, K. Rolbiecki, J. Tattersall, and P. Wienemann,
  CP Violation in SUSY Cascade Decay Chains at the LHC,
  AIP Conf. Proc. 1200 (2010) 337-340, arXiv:0910.1371 [hep-ph].

- A. De Roeck and others,
  From the LHC to Future Colliders,
  Eur. Phys. J. C66 (2010) 525-583, arXiv:0909.3240 [hep-ph].

- K. Rolbiecki, J. Tattersall, and G. Moortgat-Pick,
  Measuring the Stop Mixing Angle at the LHC,
  arXiv:0909.3196 [hep-ph].

- G. Moortgat-Pick, K. Rolbiecki, J. Tattersall, and P. Wienemann,
  Probing CP Violation with and without Momentum Reconstruction at the LHC,
  JHEP 01 (2010) 004, arXiv:0908.2631 [hep-ph].

- J. Ellis, F. Moortgat, G. Moortgat-Pick, J. M. Smillie, and J. Tattersall,
  Measurement of CP Violation in Stop Cascade Decays at the LHC,
  Eur. Phys. J. C60 (2009) 633651, arXiv:0809.1607 [hep-ph].

Acknowledgements

First and foremost I would really like to thank my supervisor, Gudi. I don't think that she could have done a better job in providing a PhD that was both stimulating but also so much fun. Yes, we have our regular arguments but the smiles always return just as quickly. Importantly, I think we complement each other well in the studies. One thing I won't miss is continuously being out-drunk when we head down to the pub (but with Georg as a training partner, maybe that's not so surprising).

Special thanks must also go to Krzysztof Rolbiecki who I've now collaborated with over three papers. We've got at least another 3 to come and I definitely hope to carry on working together for the foreseeable future. I must also mention my other collaborators, Jenni Smillie, Filip Moortgat, John Ellis and Peter Wienemann (especially the Germans who put up with my awful English, despite being a native speaker).

Continuing with the physics theme I would especially like to thank the Herwig++ help-desk at Durham. Peter Richardson (I'm not sure the rules allow me to thank an examiner), David Grellschied and Martyn Gigg all gave up valuable hours to help get our simulations working. Likewise Frank Siegert and Hendrik Hoeth provided invaluable Rivet help.

The final physics thanks go to Frank Krauss, whose abuse in a seminar turned a very quick small paper into something that took a whole lot longer (but which is hopefully a lot more useful).

Moving on to the personal, I would like to say a big thank you to Charlotte. I probably would have finished quite a bit earlier and with a good deal less stress if you hadn't been around. Then again, life would certainly have been a lot less enjoyable! I can't wait for our new life to start in Germany and I do appreciate you

following me to the land of Bratwurst and sauerkraut!

I would also like to mention everyone at the IPPP for making the place such a great one to do a PhD. In particular (but in no special order) Aoife Bharucha, James Currie, Alison Fowler, Tracey Li, Katharine Morgan, Eimear O'Callaghan, Sophy Palmer, Andrew Papanastasiou, Joao Pires, Karina Williams, David Wilson. I've also got to say thanks to Ciaran, who wasted many of my valuable hours with TuxKart. How many extra papers would have been finished without that distraction?

Finally, I've got to say thanks to my family. Firstly my mum who at least is now getting rid of me to Germany (if I pass). Also my brother, who shouldn't get any thanks at all. He sabotaged this thesis by dragging me off to Alaska for a month to get cold and climb a hill when I should have been working.

Contents

Contents ix

Chapter 1

Introduction

1.1 The Standard Model

The Standard Model of particle physics is an extremely successful theory that describes all of the fundamental constituents of matter and their interactions (apart from gravity). The model describes to very high accuracy, a wealth of experimental data that has been collected over the past 40 years. Despite the fact that the precision and energy of the experiments has rapidly advanced, there are still no unambiguous hints of new structure (if we add neutrino masses to the model).

The model is built from three generations of quarks, q, and leptons, ℓ, that form the fermionic matter fields. These matter fields interact via three fundamental forces, the electromagnetic force, the weak force and the strong force which are carried by various bosonic exchange particles.

Electromagnetism and the weak force are combined in the model to produce the Glashow-Weinberg-Salam electroweak interaction [1–3]. This theory describes the massless photon, γ, and the massive $W^{\pm}$ and Z^0 bosons which interact with both the quarks and leptons. The strong force is described by Quantum Chromodynamics (QCD) [4–6] which explains the interaction between the massless gluon, g, and the quarks.

All of the above particles and forces have now been thoroughly investigated in experiments all over the world. However, one ingredient of the Standard Model still remains to be discovered and this is the Higgs boson [7–11]. The Higgs boson

is required to spontaneously break the electroweak symmetry so that we can give masses to the weak gauge bosons. In addition, the mechanism allows us to give masses to all the fermions in the model. Despite the success of the rest of the theory we are still yet to find any direct evidence for a Higgs boson at a collider. So far, we have only been able to place a bound on the mass of the particle from the Large Electron Positron Collider (LEP) of, $m_H > 114.4$ GeV (at the 95% confidence level) [12]. Recently, the Tevatron has also started excluding certain masses for the Higgs and the most recent exclusion is between 158 and 175 GeV (at the 95% confidence level) [13]. Over the next few years, the discovery or exclusion of the Higgs boson is one of the principle tasks of both the Tevatron and the newly operational Large Hadron Collider [14, 15].

1.2 Standard Model problems

Whilst the Standard Model has been incredibly successful, we know that the model cannot be the final theory of physics, since it does not include gravity. In addition, the model faces other theoretical challenges and there are experimental hints (particularly from cosmology) that we require new physics to explain the universe satisfactorily.

Probably the most discussed issue concerning the Standard Model is the so called 'hierarchy problem' [16, 17]. Phenomenologically, the mass of the Higgs boson must be around the electroweak scale, $\mathcal{O}(100 \text{ GeV})$, to preserve the unitarity of WW scattering amplitudes [18, 19]. Indeed, indirect fits from electroweak observables constrain the mass to be, $m_H = 87^{+35}_{-26}$ GeV, or $m_H < 157$ GeV at 95% confidence level [20, 21]. However, if we calculate the quantum corrections to the Higgs mass we find that the result contains a quadratic divergence. Fig. 1.1 shows the correction to the Higgs mass, m_H from a fermion, f, with mass, m_f. If we evaluate this contribution we find,

$$\Delta m_H^2 = -2 \frac{N|\lambda_f|^2}{16\pi^2} (\Lambda_{UV}^2 - 2m_f^2 \ln(\Lambda_{UV}/m_f) + ...) , \qquad (1.1)$$

where λ_f is the coupling constant, N is a multiplicative factor (for example $N(t) = 3$ for top quarks due to summation over colour) and Λ_{UV} is an ultraviolet momentum
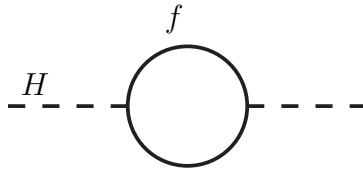
Figure 1.1: Loop corrections to m_H^2 from a fermion, f, with mass, m_f.

cut-off. We see that the correction to the Higgs mass is proportional to the square of this ultraviolet momentum cut-off. Now, if we believe that the Standard Model is correct apart from the inclusion of gravity, we have no new physics in the model until quantum gravitation effects become important. Hence, we have to set the ultraviolet cut-off at the scale when we expect these effects to become important and this scale can be assumed to be close to the Planck mass, $M_P \sim 10^{19}$ GeV. Calculating with this scale, we find that the correction to the Higgs mass is $\sim 10^{30}$ larger than the mass of the Higgs itself. In principle we can renormalise the quadratic divergences away but this requires an incredible fine-tuning between an extremely large bare mass and the loop correction to result in a physical Higgs mass of $\mathcal{O}(100$ GeV$)$. The precise cancellation over so many orders of magnitude is therefore thought to be highly unnatural.

Another problem with the Standard Model is the lack of a suitable candidate for cold dark matter. Dark matter was first presented as an idea to explain the shape of galaxy rotation curves [22], which required the presence of additional matter that was not luminous. New data from the gravitational lensing [23] and fits to the currently favoured cosmological model [24] also support the idea that most of the universe is composed of a non-relativistic, weakly interacting, stable particle. However, the Standard Model does not contain a particle that matches this criteria. For a recent review on the evidence and candidates for dark matter see [25].

Finally, we would also like to mention that the Standard Model is unable to satisfactorily explain the baryon asymmetry of the universe. To produce an excess of matter over anti-matter in the universe any theory must contain CP-violation [26]. Whilst the Standard Model contains a CP-violating phase in the CKM matrix [27], the model produces an asymmetry many orders of magnitude smaller than that
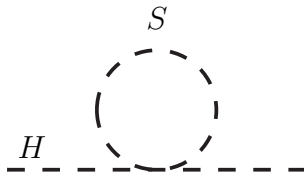
Figure 1.2: Loop corrections to m_H^2 from a scalar, S, with mass, m_S.

observed in the universe [28–31].

1.3 Supersymmetry

A potential solution to all the problems discussed above is provided by Supersymmetry (SUSY) [32,33]. SUSY is postulated as a new symmetry that exists between fermions and bosons. It is theoretically interesting as it is the only non-trivial extension of the Poincaré group [34]. Excellent introductions to SUSY are given in [35,36].

Phenomenologically, SUSY predicts that all bosons in the theory have a fermionic partner and vice versa for the fermions. However all of the properties (i.e. charges and masses) of the partners should be same. Instantly, we see that if SUSY is to exist in nature, it must be a broken symmetry as we have not seen any partners to the Standard Model particles yet. Thus, the mass of all of the partners that have electric or colour charge must be higher than thus far probed in experiments.

In Sec. 1.2 we discussed the hierarchy problem that is often considered the most pressing issue within the Standard Model. SUSY provides a solution to this problem with the new partners of the Standard Model particles [37–39]. For example, Fig. 1.2 shows the correction to the Higgs mass, m_H from a scalar, S, with mass, m_S. If we evaluate this contribution we find,

$$\Delta m_H^2 = -\frac{N\tilde{\lambda}_S}{16\pi^2}(\Lambda_{UV}^2 - 2m_S^2\ln(\Lambda_{UV}/m_S) + ...)\,,\tag{1.2}$$

where λ_S is the coupling constant. We must also remember that for each on-shell fermionic degree of freedom we require a scalar partner and consequently we have two scalar partners for each Standard Model particle. Therefore, comparing Eq. (1.1) to

Eq. (1.2), if we set,

$$\tilde{\lambda}_S = -\lambda_f^2 \qquad (1.3)$$

we are able to cancel the UV divergence to the Higgs mass for each individual Standard Model fermion.

However, we must note that we still have the logarithmic terms in both Eq. (1.1) and Eq. (1.2). These will only cancel completely if we set,

$$m_S = m_f \,. \qquad (1.4)$$

but we know that for the SUSY partners this relation cannot be true, as they have not been discovered yet. However, since this is just a logarithmic dependence, the correction will stay small as long as the mass difference between the Standard Model and SUSY states is small. Consequently, we come to the conclusion that the mass splitting between the states should be around the weak scale $\mathcal{O}(1\text{ TeV})$. In addition, electroweak data points to a SUSY spectrum below 1 TeV [40–42]. Therefore, we come to the conclusion that if SUSY exists in nature, there is a good chance of it being seen at the LHC.

As well as solving the hierarchy problem, models of SUSY can also contain a suitable candidate for dark matter [43, 44]. If we impose R-parity on our models (see Sec. 2.3 for more details) the lightest SUSY partner (LSP) has to be stable. If in addition, the particle only interacts weakly, then it can reproduce the required abundance from cosmological considerations very accurately [45].

Finally, new SUSY models also offer the possibility of providing many new CP-violating phases to the theory. These phases may be large and in particular scenarios they have the potential to allow SUSY to generate the required baryon asymmetry that we see in the universe [28, 46–48]. In this thesis we concentrate on the discovery potential of the LHC to be able to observe any new CP-violation that may be present if SUSY is seen.

1.4   Thesis outline

We start the thesis in Chapter 2 by briefly describing the complex Minimal Supersymmetric Standard Model (MSSM) and its interactions. This is the simplest SUSY

extension of the Standard Model and is the theory that has been most studied phenomenologically. In particular we fix the notation that will be used in the rest of the thesis and also point out the specific CP-violating phases that we will concentrate on.

In Chapter 3 we summarise some of the various studies that have looked at CP-violation in the MSSM at the LHC. We start with a general introduction to the transformation properties of the C, P and T symmetries before explaining their use at colliders. The T-odd triple product correlations are discussed in detail as these are the observables that are suitable to find hints for CP-violation at colliders. In addition we also discuss constraints on CP-violating phases in SUSY from the low energy electric dipole moment (EDM) experiments.

Our first study is presented in Chapter 4, where we investigated the pair production of SUSY top quarks (stops, $\tilde{t}_i$) at the LHC,

$$pp \rightarrow \tilde{t}_i \tilde{t}_i^* \,. \tag{1.5}$$

These are then followed by the decay,

$$\tilde{t}_i \rightarrow \tilde{\chi}_j^0 + t \rightarrow \tilde{\chi}_1^0 \ell^+ \ell^- + Wb. \tag{1.6}$$

where $\tilde{\chi}^0$'s are called neutralinos and are mixed states comprising the SUSY partners of the photon, Z and neutral Higgs bosons. We find that the three-body decay of neutralinos are sensitive to CP-violating triple product asymmetries due to spin correlations between the production and decay of the relevant $\tilde{\chi}_j^0$. We also explain in detail how to calculate the asymmetries at the parton level and derive the origin of the CP-violating terms.

In Chapter 5 we discuss 1st and 2nd generation SUSY quark (squark) production but investigate the corresponding decay chain to Eq. (1.6). We chose to investigate this decay, as firstly, the production cross section is substantially higher than for stops which results in better a statistical significance for our asymmetry. Secondly, when we investigate squark production in association with a SUSY gluon (gluino), we find that we are able to kinematically reconstruct the event. With the reconstruction, we find that the CP-asymmetry will be significantly larger.

Our final study is presented in Chapter 6 where we return to discuss the pair production of stops but we now consider the following two-body decay chain,

$$\tilde{t}_i \to \tilde{\chi}_j^0 + t \to \tilde{\ell}^\pm + \ell^\mp + Wb \to \tilde{\chi}_1^0 \ell^\pm \ell^\mp + Wb. \tag{1.7}$$

where $\tilde{\ell}^\pm$ is a SUSY lepton (slepton). The advantage of studying the two-body decay chain is that the single cascade in Eq. (6) is fully reconstructible. In addition, we complete a fully hadronic study to try to accurately estimate the luminosity that will be required to observe CP-violation in SUSY at the LHC.

Finally, we conclude the thesis in Chapter 7. In addition, we present the Lagrangian and couplings for all interactions used in the thesis in Appendix A. In Appendix B we give the amplitudes for all of the processes calculated and in Appendix C we present details of the phase-space calculation.

Chapter 2

The complex MSSM

The simplest supersymmetric extension of the Standard Model is known as the Minimal Supersymmetric Standard Model (MSSM) [49–52]. The model introduces the minimal number of new particles and couplings that are necessary for a consistent supersymmetric (SUSY) model. This results in each Standard Model particle (left and right states) receiving a new 'superpartner' and in addition we require an extended Higgs sector of two doublets, see Sec. 2.1.

If SUSY is realised in nature the symmetry must be broken since we have not seen any of the additional particles yet and in unbroken SUSY, these would have the same mass as the Standard Model fields. In the MSSM we choose to break SUSY 'softly', which means allowing any terms into the Lagrangian that break the symmetry but do not induce any new quadratic divergences, see Sec. 2.2. These terms are introduced in the most general way and with no assumption as to how the SUSY breaking mechanism occurs in nature.

2.1 Introduction

The MSSM extends the particle content of the Standard Model by introducing the superpartners. The gauge group is the same as the Standard Model so the superpartners have the same quantum numbers as the Standard Model fields but differ by spin-$\frac{1}{2}$. Firstly, all the quarks and leptons get new spin-0 partners called squarks and sleptons as shown in Tab. 2.1. It must be noted that a superpartner is

Name	Particle (Spin-$\frac{1}{2}$)	Superpartner (Spin-0)	$SU(3)_C, SU(2)_L, U(1)_Y$
Quarks, Squarks (x3 families)	(u_L, d_L)	$(\tilde{u}_L, \tilde{d}_L)$	$(3, 2, \frac{1}{3})$
	$u_R^\dagger$	$\tilde{u}_R^*$	$(\overline{3}, 1, -\frac{4}{3})$
	$d_R^\dagger$	$\tilde{d}_R^*$	$(\overline{3}, 1, \frac{2}{3})$
Leptons, Sleptons (x3 families)	(ν, e_L)	$(\tilde{\nu}, \tilde{e}_L)$	$(1, 2, -1)$
	$e_R^\dagger$	$\tilde{e}_R^*$	$(1, 1, 2)$

Table 2.1: The quarks, squarks, leptons and sleptons of the MSSM. The spin-0 fields are complex scalars, whilst the spin-$\frac{1}{2}$ fields are two component Weyl fermions. $SU(3)_C$ is the gauge group of colour charge, $SU(2)_L$ is the gauge group of weak isospin and $U(1)_Y$ is the gauge group of Weak hypercharge.

Name	Particle (Spin-1) (Spin-1)	Superpartner (Spin-$\frac{1}{2}$)	$SU(3)_C, SU(2)_L, U(1)_Y$
Gluon, Gluino	g	$\tilde{g}$	$(8, 1, 0)$
W bosons, Winos	W_μ^i	$\tilde{W}^i$	$(1, 3, 0)$
B boson, Binos	B_μ	$\tilde{B}^0$	$(1, 1, 0)$

Table 2.2: The gauge and gaugino fields of the MSSM. $SU(3)_C$ is the gauge group of colour charge, $SU(2)_L$ is the gauge group of weak isospin and $U(1)_Y$ is the gauge group of Weak hypercharge.

required for each on-shell Standard Model degree of freedom, therefore two scalar states are required per Standard Model fermion. These are called the 'left' and 'right' states $(\tilde{f}_L, \tilde{f}_R)$ as the partners of the corresponding Standard Model fermions but actually have no helicity themselves since they are spin-0.

The gauge bosons of the Standard Model also receive superpartners that are called gauginos with spin-$\frac{1}{2}$, see Tab. 2.2. In analogy to the Standard Model photon, Z, and the $W^\pm$ bosons, one can form a photino, $\tilde{\gamma}$, a Zino, $\tilde{Z}$, and $\tilde{W}^\pm$ from the $\tilde{B}$ and $\tilde{W}^i$ fields. The superpartners of the gluons are the gluinos $\tilde{g}$.

In the MSSM we not only require superpartners to the Standard Model Higgs bosons but we also need to enlarge the Standard Model Higgs Boson sector, see Tab. 2.3. We now require two complex Higgs doublets with hypercharges $U(1)_Y =$

Name	Particle (Spin-0)	Superpartner (Spin-$\frac{1}{2}$)	$SU(3)_C,\ SU(2)_L,\ U(1)_Y$
Higgs, Higgsinos	$(H_{11},\ H_{12})$	$(\tilde{H}_{11},\ \tilde{H}_{12})$	$(1,\ 2,\ -1)$
	$(H_{21},\ H_{22})$	$(\tilde{H}_{21},\ \tilde{H}_{22})$	$(1,\ 2,\ 1)$

Table 2.3: The Higgs and higgsino fields of the MSSM. $SU(3)_C$ is the gauge group of colour charge, $SU(2)_L$ is the gauge group of weak isospin and $U(1)_Y$ is the gauge group of Weak hypercharge.

± 1 to give masses to both the up and down type quarks and leptons and also to cancel the new anomalies caused by adding extra fermions to the model. The superpartners of the new Higgs fields are called higgsinos. For a detailed account of the Higgs sector in the MSSM, see for example [53–55].

In analogy with the Standard Model, the gauge eigenstates of the MSSM do not in general correspond directly to the mass eigenstates but instead mix. This is due to the electroweak symmetry, $SU(2)_L \times U(1)_Y$, being broken, allowing fields with the same $SU(3)_C \times U(1)_{em}$, spin and R-parity (Sec. 2.3) to mix. In the Standard Model we have already seen that the B_μ and W_μ^i mix to form the physical states: γ, Z^0 and $W^\pm$. The same is also true for the quarks and leptons of the Standard Model.

For the MSSM this also occurs; the individual squarks, sleptons, gauginos and higgsinos can all mix with particles of the same quantum number. The only exception are the gluinos which are the only colour octet fermions that exist in the model. The gauge eigenstates along with the physical mass eigenstates that are formed are shown in Tab. 2.4. A particular point to note is that the gauginos and higgsinos are able to mix together. These form new mass eigenstates called neutralinos, $\tilde{\chi}_i^0$, for the neutral particles ($U(1)_{em} = 0$) and charginos, $\tilde{\chi}_i$, for those that have charge ($U(1)_{em} = \pm 1$).

Name	Spin	Gauge Eigenstate	Mass Eigenstate
Higgs Bosons	0	$H_1^0,\ H_2^0,\ H_1^-,\ H_2^+$	$h^0,\ H^0,\ A^0,\ H^\pm$
Squarks	0	$\tilde{u}_L,\ \tilde{u}_R,\ \tilde{d}_L,\ \tilde{d}_R$ $\tilde{c}_L,\ \tilde{c}_R,\ \tilde{s}_L,\ \tilde{s}_R$ $\tilde{t}_L,\ \tilde{t}_R,\ \tilde{b}_L,\ \tilde{b}_R$	$\tilde{u}_1,\ \tilde{u}_2,\ \tilde{d}_1,\ \tilde{d}_2$ $\tilde{c}_1,\ \tilde{c}_2,\ \tilde{s}_1,\ \tilde{s}_2$ $\tilde{t}_1,\ \tilde{t}_2,\ \tilde{b}_1,\ \tilde{b}_2$
Sleptons	0	$\tilde{e}_L,\ \tilde{e}_R,\ \tilde{\nu}_e$ $\tilde{\mu}_L,\ \tilde{\mu}_R,\ \tilde{\nu}_\mu$ $\tilde{\tau}_L,\ \tilde{\tau}_R,\ \tilde{\nu}_\tau$	$\tilde{e}_1,\ \tilde{e}_2,\ \tilde{\nu}_e$ $\tilde{\mu}_1,\ \tilde{\mu}_2,\ \tilde{\nu}_\mu$ $\tilde{\tau}_1,\ \tilde{\tau}_2,\ \tilde{\nu}_\tau$
Neutralinos	$\frac{1}{2}$	$\tilde{B}^0,\ \tilde{W}^3,\ \tilde{H}_1^0,\ \tilde{H}_2^0$	$\tilde{\chi}_1^0,\ \tilde{\chi}_2^0,\ \tilde{\chi}_3^0,\ \tilde{\chi}_4^0$
Charginos	$\frac{1}{2}$	$\tilde{W}^-,\ \tilde{W}^+,\ \tilde{H}_1^-,\ \tilde{H}_2^+$	$\tilde{\chi}_1^\pm,\ \tilde{\chi}_2^\pm$
Gluino	$\frac{1}{2}$	$\tilde{g}$	$\tilde{g}$

Table 2.4: Gauge and mass eigenstates of the additional particles in the MSSM.

2.2 Soft SUSY breaking

Since no superpartners have (as yet) been discovered, we know that if SUSY exists, it must be broken to allow the masses of the particles to be large enough to have escaped detection. SUSY breaking is not currently fully understood and we therefore formulate the MSSM in a model independent way. This is accomplished by introducing any terms that break SUSY without inducing new quadratic divergences into the theory. The different terms that we can add are as follows [56]:

- Gaugino mass terms, $-\frac{1}{2}M_a\bar{\lambda}_a\lambda_a$;

- Scalar mass terms, $-M_{\phi_i}^2|\phi_i|^2$;

- Trilinear scalar interactions, $-A_{ijk}\phi_i\phi_j\phi_k$;

- Bilinear terms, $-B_{ij}\phi_i\phi_j$.

These breaking terms lead to the explicit form of the 'soft' SUSY breaking Lagrangian,

$$-\mathcal{L}_{soft} = \frac{1}{2}M_1\tilde{B}\tilde{B} + \frac{1}{2}M_2\tilde{W}\tilde{W} + \frac{1}{2}M_3\tilde{g}\tilde{g} + m_{H_1}^2|H_1|^2 + m_{H_2}^2|H_2|^2$$
$$+M_{\tilde{Q}}^2|\tilde{q}_L|^2 + M_{\tilde{U}}^2|\tilde{u}_R^*| + M_{\tilde{D}}^2|\tilde{d}_R^*|^2 + M_{\tilde{L}}^2|\tilde{\ell}_L|^2 + M_{\tilde{E}}^2|\tilde{e}_R^*|^2 \qquad (2.1)$$
$$+(h_E A_E H_1\tilde{\ell}_L\tilde{e}_R^* + h_D A_D H_1\tilde{q}_L\tilde{d}_R^* + h_U A_U H_2\tilde{q}_L\tilde{u}_R^* + B\mu H_1 H_2 + h.c.).$$

M_1, M_2 and M_3 are the $U(1)$, $SU(2)$ and $SU(3)$ gaugino mass terms respectively whilst $m_{H_1}^2$, $m_{H_2}^2$ and $B\mu$ are the Higgs mass terms. The scalar mass terms are 3×3 Hermitian matrices in generation space which are represented by $M_{\tilde{Q}}^2$, $M_{\tilde{U}}^2$, $M_{\tilde{D}}^2$, $M_{\tilde{L}}^2$ and $M_{\tilde{E}}^2$ while the terms $h_E A_E$, $h_D A_D$ and $h_U A_U$ are general 3×3 matrices. If we allow the parameters in Eq. (2.1) to be complex we have over 100 new free parameters compared with the Standard Model.

If SUSY is discovered at the LHC the task will immediately turn to attempting to measure these parameters in the hope of shedding light on the precise mechanism of SUSY breaking. This may seem like a daunting task but luckily, for individual processes, only a small subset should be important (at least at tree level).

The above implementation of the MSSM assumes no particular model for the SUSY breaking mechanism. However, many ideas have now been presented as to how SUSY may be broken in realistic models. In addition, these models try to significantly reduce the number of free parameters so that the theory becomes far more predictive and testable. A detailed discussion of different SUSY breaking models is beyond the scope of this thesis but we will briefly introduce the model that most of our scenarios are based around.

The model that we use is known as minimal supergravity (mSUGRA)[1] [57, 58]. In this model, we specify a common gaugino mass, $M_{1/2}$, a common scalar mass, M_0 and a universal trilinear coupling, A_0, at the GUT scale. In addition we need to specify $\tan\beta = \nu_2/\nu_1$ which is the ratio of the vacuum expectation values of the

---

[1]It must be noted that although the models are commonly known as mSUGRA, those presented here do not contain any gravitation interactions. Therefore, the presence in the model of a gravitino is ignored. Another name used in the literature for models with this parameter set but without gravitation is the constrained minimal supersymmetric Standard Model (CMSSM).

two Higgs fields and the sign of μ_0. All of these parameters are defined at the GUT scale however. We therefore need to evolve the various parameters down to the electroweak scale using the renormalisation group equations (RGEs) calculated to a particular loop order. This calculation will produce the various soft breaking terms given in Eq. 2.1.

In chapter 4, we also examine a particular scenario within a non-universal Higgs mass (NUHM) model [59–61]. These models allow the soft breaking Higgs masses, m_{H_1} and m_{H_2} to be different to M_0 at the GUT scale and consequently offer more freedom in the phenomenology. In addition, we occasionally introduce 'phenomenological' models where we vary the soft breaking parameters individually. We do this to examine the dependence of individual parameters and alternative coupling schemes. For example in chapter 4 we investigate a scenario (scenario C) where the second lightest neutralino is higgsino-like whilst keeping the kinematics similar.

Finally, we add CP-violation into the model by adding arbitrary CP-phases to particular soft breaking terms in Eq. (2.1) for simplicity.

2.3 R-parity

One important point to mention is the lack of R-parity, P_R, violating terms in Eq. (2.1) and more generally, in the whole of the MSSM. For example, we could have the following terms in the Lagrangian,

$$\mathcal{L}_{\Delta L} = \lambda \tilde{u}_L^* \bar{d}_R e_L, \tag{2.2}$$

$$\mathcal{L}_{\Delta B} = \lambda' \tilde{d}_R \bar{d}_R \bar{u}_R. \tag{2.3}$$

These terms break lepton (ΔL) and baryon (ΔB) number though. Therefore, if both kinds of terms are allowed, rapid proton decay would occur and this places strong constraints on the couplings (in the example of Eq. (2.2-2.3), λ and λ') [62, 63]. Throughout this thesis we use the definition of the MSSM where all R-parity violating couplings are set to zero for both theoretical minimality and phenomenological reasons.

It must be stated however, that R-parity is applied by hand assuming the strict minimality of the MSSM and it gives a new quantum number to all the particles in

the MSSM. R-parity is defined as,

$$P_R = (-1)^{3(B-L)+2s},\qquad(2.4)$$

where B is baryon number, L is lepton number and s is the spin of the particle. All the ordinary Standard Model particles and the Higgs bosons have even R-parity ($P_R = 1$) whereas all the superpartners have odd R-parity ($P_R = -1$). If R-parity is exactly conserved, then none of the Standard Model particles can mix with the superpartners. Furthermore, the symmetry imposes that each vertex in the theory must contain an even number of superpartners and this condition has extremely important phenomenological implications.

Due to R-parity, a single superpartner can only decay into an odd number of lighter superpartners. Consequently, the lightest supersymmetric particle (LSP) must be stable as it cannot decay to a purely Standard Model final state and it cannot kinematically decay into any other superpartner. This property gives the MSSM the possibility of explaining the dark matter that is currently favoured for many cosmological models of the universe. As the LSP is stable, any LSPs produced in the big bang will have survived to the current day (neglecting annihilation), enabling the abundance to be calculated and compared to cosmological measurements. Searches for 'exotic isotopes' have put stringent bounds on stable particles that have either electric or colour charge and therefore the LSP must only interact weakly [64].

R-parity also leads to distinctive phenomenology at collider experiments. Firstly, since R-parity conservation leads to all interactions containing an even number of superpartners, we can always expect to see the pair production of superpartners at a collider. This also means, once a superpartner is produced, any possible decay must leave another superpartner in the final state. This leads to a characteristic prediction for many SUSY models. Cascade decays produce many final-state particles that may be detected at the LHC. As one example, squark production $pp \rightarrow \tilde{q}\tilde{q}^*$ in particular may be followed by the decay,

$$\tilde{q} \quad \rightarrow \quad \tilde{\chi}_2^0 q,\qquad(2.5)$$

$$\tilde{\chi}_2^0 \quad \rightarrow \quad \tilde{\ell}^+\ell^-,\qquad(2.6)$$

$$\tilde{\ell}^+ \quad \rightarrow \quad \tilde{\chi}_1^0 \ell^+.\qquad(2.7)$$

where the $\tilde{\chi}_1^0$ is the LSP in this example and the $\tilde{q}^*$ can follow the same decay chain.

We notice that there will be two LSPs in the final state and from cosmological considerations these must only interact weakly. Therefore, we will have the distinctive signature that the two LSPs will leave the detector without being seen. Consequently a large momentum imbalance should be observed in many MSSM events at colliders. In the MSSM, the two most popular choices for the LSP is a sneutrino $\tilde{\nu}$ or the lightest neutralino $\tilde{\chi}_1^0$ as shown in the example decay chain, see Eq. (2.7).

2.4 Mass matrices

Due to electroweak and SUSY symmetry breaking, many of the superpartners have the same quantum numbers. Therefore the gauge eigenstates can mix to create mass eigenstates that are not flavour diagonal. The corresponding gauge and mass eigenstates are shown in Tab. 2.4. Hence we have to deal with the mixing of fields and diagonalise the mass matrices in order to determine the mass eigenstates.

Whilst the mass eigenstates are the particles that will be physically produced at the LHC, the mixing matrices define the couplings of a particular particle and are therefore of crucial importance. As the inputs of the mixing matrices are the SUSY breaking parameters, measuring these matrices will also give important information on the pattern of SUSY breaking. Finally, since the mixing matrices are in general complex, any CP-violating phases that are present in the model manifest themselves via the mixing (i.e. in mass eigenvalues and couplings).

2.4.1 Squarks

In the most general case, it is possible that all the squarks with the same charge, R-parity ($P_R = -1$) and colour can mix together. We would therefore have to diagonalise two 6×6 squark mass matrices to find the mass eigenstates. However, mixing between generations of squarks can cause severe problems due to large loop corrections to flavour changing neutral current (FCNC) reactions [65,66]. Therefore, we ignore intergenerational mixing and instead decompose the two 6×6 matrices into

six 2×2 matrices which describe each flavour separately. The matrix in the basis of the gauge eigenstates, $(\tilde{q}_L, \tilde{q}_R)$ is,

$$\mathcal{M}_{\tilde{q}}^2 = \begin{pmatrix} m_{\tilde{q}_L}^2 + m_q^2 & m_{\tilde{q}_{LR}}^* \, m_q \\ m_{\tilde{q}_{LR}} \, m_q & m_{\tilde{q}_R}^2 + m_q^2 \end{pmatrix}, \tag{2.8}$$

where

$$m_{\tilde{q}_L}^2 = M_{\tilde{Q}}^2 + m_Z^2 \cos 2\beta \left(I_{3L}^q - e_q \sin^2 \theta_W \right), \tag{2.9}$$

$$m_{\tilde{q}_R}^2 = M_{\{\tilde{U},\tilde{D}\}}^2 + e_q m_Z^2 \cos 2\beta \, \sin^2 \theta_W, \tag{2.10}$$

$$m_{\tilde{q}_{LR}} = A_q - \mu^* \{\cot \beta, \tan \beta\}. \tag{2.11}$$

for {up, down} quarks respectively. e_q, I_{3L}^q and m_q are the charge, the third component of the weak isospin and the mass of the partner quark respectively. θ_W is the weak mixing angle and m_Z is the mass of the Z-boson. The soft scalar masses are $M_{\tilde{Q}}$, $M_{\tilde{U}}$ and $M_{\tilde{D}}$ which are soft breaking terms in the Lagrangian, Eq. (2.1). μ and A_q are the higgsino mass parameter and soft SUSY-breaking trilinear coupling respectively. Finally, $\tan \beta = \nu_2/\nu_1$ and is the ratio of the vacuum expectation value of the two Higgs fields.

From the above parameters, μ and A_q can take complex values,

$$A_q = |A_q| \, e^{i\phi_q}, \qquad \mu = |\mu| \, e^{i\phi_\mu}, \qquad (0 \le \phi_q, \phi_\mu < 2\pi), \tag{2.12}$$

thus yielding CP-violation in the squark sector.

The off-diagonal terms of the mass matrix $\mathcal{M}_{\tilde{q}}^2$, Eq. (2.8), are proportional to the mass of the Standard Model partner. Therefore, for the first two generations of quarks, a very good approximation is to assume that the mass eigenstates are equal to the interaction eigenstates. For the third generation however, this is no longer true. The large mass of the top quark produces large mixing effects in the stop sector and if $\tan \beta$, μ or A_q is large enough, sizable mixing effects can also be seen in the sbottom sector.

In general, the mass matrix $\mathcal{M}_{\tilde{q}}^2$ are hermitian and can be diagonalised by a unitary matrix $\mathcal{R}_{\tilde{q}}$. This unitary matrix rotates the gauge eigenstates, $\tilde{q}_L$ and $\tilde{q}_R$, into the mass eigenstates $\tilde{q}_1$ and $\tilde{q}_2$,

$$\mathcal{R}_{\tilde{q}} \, \mathcal{M}_{\tilde{q}}^2 \, \mathcal{R}_{\tilde{q}}^\dagger = \begin{pmatrix} m_{\tilde{q}_1}^2 & 0 \\ 0 & m_{\tilde{q}_2}^2 \end{pmatrix}. \tag{2.13}$$

We choose the convention $m_{\tilde{q}_1}^2 < m_{\tilde{q}_2}^2$ for the masses of $\tilde{q}_1$ and $\tilde{q}_2$. The matrix $\mathcal{R}_{\tilde{q}}$ rotates the gauge eigenstates, $\tilde{q}_L$ and $\tilde{q}_R$, into the mass eigenstates $\tilde{q}_1$ and $\tilde{q}_2$ as follows,

$$
\begin{pmatrix} \tilde{q}_1 \\ \tilde{q}_2 \end{pmatrix} = \mathcal{R}_{\tilde{q}} \begin{pmatrix} \tilde{q}_L \\ \tilde{q}_R \end{pmatrix} = \begin{pmatrix} \cos\theta_{\tilde{q}} & \sin\theta_{\tilde{q}}\, e^{-i\phi_{\tilde{q}}} \\ -\sin\theta_{\tilde{q}}\, e^{i\phi_{\tilde{q}}} & \cos\theta_{\tilde{q}} \end{pmatrix} \begin{pmatrix} \tilde{q}_L \\ \tilde{q}_R \end{pmatrix}, \qquad (2.14)
$$

where $\theta_{\tilde{q}}$ and $\phi_{\tilde{q}}$ are the mixing angle and the CP-violating phase of the squark sector, respectively. The masses are given by,

$$
m_{\tilde{q}_{1,2}} = \frac{1}{2}\left(2m_q^2 + m_{LL}^2 + m_{RR}^2 \mp \sqrt{(m_{LL}^2 - m_{RR}^2)^2 + 4|m_{LR}|^2 m_q^2} \right), \qquad (2.15)
$$

whereas for the mixing angle and the CP phase we have,

$$
\cos\theta_{\tilde{q}} = \frac{-m_q|m_{LR}|}{\sqrt{m_q^2|m_{LR}|^2 + (m_{\tilde{q}_1}^2 - m_{LL}^2)^2}}, \qquad (2.16)
$$

$$
\sin\theta_{\tilde{q}} = \frac{m_{LL}^2 - m_{\tilde{q}_1}^2}{\sqrt{m_q^2|m_{LR}|^2 + (m_{\tilde{q}_1}^2 - m_{LL}^2)^2}}, \qquad (2.17)
$$

$$
\phi_{\tilde{q}} = \arg(A_q - \mu^*\{\cot\beta,\, \tan\beta\}). \qquad (2.18)
$$

for {up, down} type quarks respectively.

By convention we take $0 \le \theta_{\tilde{q}} < \pi$ and $0 \le \phi_{\tilde{q}} < 2\pi$. It must be noted that $\phi_{\tilde{q}}$ is an 'effective' phase and does not directly correspond to the phase of any MSSM parameter. Instead, the phase will have contributions from both ϕ_{A_q} and ϕ_μ.

If $m_{\tilde{q}_L} < m_{\tilde{q}_R}$ then $\cos^2\theta_{\tilde{q}} > \frac{1}{2}$ and $\tilde{q}_1$ has a predominantly left gauge character. On the other hand, if $m_{\tilde{q}_L} > m_{\tilde{q}_R}$ then $\cos^2\theta_{\tilde{q}} < \frac{1}{2}$ and $\tilde{q}_1$ has a predominantly right character.

2.4.2 Sleptons

The mass matrix for the sleptons is arranged in the same way as for the squarks,

$$
\mathcal{M}_{\tilde{\ell}}^2 = \begin{pmatrix} m_{\tilde{\ell}_L}^2 + m_\ell^2 & m_{\tilde{\ell}_{LR}}^* m_\ell \\ m_{\tilde{\ell}_{LR}} m_\ell & m_{\tilde{\ell}_R}^2 + m_\ell^2 \end{pmatrix}, \qquad (2.19)
$$

where

$$
m_{\tilde{\ell}_L}^2 = M_{\tilde{L}}^2 - m_Z^2 \cos 2\beta \left(\frac{1}{2} - \sin^2\theta_W \right), \qquad (2.20)
$$

$$
m_{\tilde{\ell}_R}^2 = M_{\tilde{E}}^2 - m_Z^2 \cos 2\beta \sin^2\theta_W, \qquad (2.21)
$$

$$
m_{\tilde{\ell}_{LR}} = A_\ell - \mu^* \tan\beta. \qquad (2.22)
$$

For the selectrons and smuons the left and right eigenstates can be considered to be equal to the mass eigenstates due to the small mass of the Standard Model particles. However, for the staus, mixing can occur in a similar way to the sbottoms if $\tan \beta$ is large enough. In this case, all the formulae for squark mixing are applicable and we can parametrise the stau sector with a mixing angle $\theta_{\tilde{\tau}}$ and phase $\phi_{\tilde{\tau}}$,

$$
\begin{pmatrix} \tilde{\tau}_1 \\ \tilde{\tau}_2 \end{pmatrix} = \begin{pmatrix} \cos \theta_{\tilde{\tau}} & \sin \theta_{\tilde{\tau}} \, \mathrm{e}^{-\mathrm{i}\phi_{\tilde{\tau}}} \\ -\sin \theta_{\tilde{\tau}} \, \mathrm{e}^{\mathrm{i}\phi_{\tilde{\tau}}} & \cos \theta_{\tilde{\tau}} \end{pmatrix} \begin{pmatrix} \tilde{\tau}_L \\ \tilde{\tau}_R \end{pmatrix} . \tag{2.23}
$$

For the sneutrinos, $\tilde{\nu}$, we only consider superpartners to the left handed Standard Model states. As the masses of the Standard Model particles are so low, a good approximation is to assume that the mass for each generation is,

$$
m_{\tilde{\nu}_L}^2 = M_{\tilde{L}}^2 + \frac{1}{2}m_Z^2 \cos 2\beta . \tag{2.24}
$$

2.4.3 Neutralinos

In the MSSM, the four neutralinos $\tilde{\chi}_i^0$ ($i = 1, 2, 3, 4$) are mixtures of the neutral $U(1)$ and $SU(2)$ gauginos, $\tilde{B}$ and $\tilde{W}^3$, and the higgsinos, $\tilde{H}_1^0$ and $\tilde{H}_2^0$. In general, both the gauge and mass eigenstates are Majorana fermions where the sparticle and anti-sparticle are identical. The mass term of the Lagrangian in the basis $\psi^0 = (\tilde{B}, \tilde{W}^3, \tilde{H}_1^0, \tilde{H}_2^0)$ is given by,

$$
\mathcal{L}_{\tilde{\chi}^0} = -\frac{1}{2}(\psi^0)^T \mathcal{M}_N \psi^0 + h.c. \tag{2.25}
$$

Where the mass matrix,

$$
\mathcal{M}_N = \begin{pmatrix} M_1 & 0 & -m_Z c_\beta s_W & m_Z s_\beta s_W \\ 0 & M_2 & m_Z c_\beta c_W & -m_Z s_\beta c_W \\ -m_Z c_\beta s_W & m_Z c_\beta c_W & 0 & -\mu \\ m_Z s_\beta s_W & -m_Z s_\beta c_W & -\mu & 0 \end{pmatrix} \tag{2.26}
$$

is built up by the fundamental SUSY parameters: the $U(1)$ and $SU(2)$ gaugino masses M_1 and M_2, the higgsino mass parameter μ, and $\tan \beta = v_2/v_1$ ($c_\beta = \cos \beta$, $s_W = \sin \theta_W$ etc.). In addition to the μ parameter, a non-trivial CP phase can also

be attributed to the M_1 parameter (the phase of M_2 can be rotated away with a redefinition of the fields [67–70]),

$$M_1 = |M_1| \, e^{i\phi_1}, \qquad (0 \le \phi_1 < 2\pi) \,. \tag{2.27}$$

Since the complex matrix $\mathcal{M}_N$ is symmetric, one unitary matrix N is sufficient to rotate the gauge eigenstate basis $(\tilde{B}, \tilde{W}^3, \tilde{H}_1^0, \tilde{H}_2^0)$ to the mass eigenstate basis of the Majorana fields $\tilde{\chi}_i^0$,

$$\mathrm{diag}(m_{\tilde{\chi}_1^0}, m_{\tilde{\chi}_2^0}, m_{\tilde{\chi}_3^0}, m_{\tilde{\chi}_4^0}) = N^* \mathcal{M}_N N^\dagger, \qquad (m_{\tilde{\chi}_1^0} < m_{\tilde{\chi}_2^0} < m_{\tilde{\chi}_3^0} < m_{\tilde{\chi}_4^0}) \,. \tag{2.28}$$

The masses $m_{\tilde{\chi}_i^0}$ ($i = 1, 2, 3, 4$) can be chosen to be real and positive by a suitable definition of the unitary matrix N [71].

The character of the mass eigenstates can be examined by looking at the relative strength of the input, M_1, M_2 and μ. If, for example $|M_{\{1,2\}}| < |\mu|$, the two lightest neutralinos will be dominated by the gaugino components and the two heavier states will be mainly higgsino-like. In addition, a unification of the gaugino masses is often assumed at some GUT scale. When the unified masses are run down to the electroweak scale using the renormalisation group equations (RGE) the following relation is found,

$$M_1(M_Z) = \frac{5}{3} \tan^2 \theta_W M_2(M_Z) \simeq \frac{1}{2} M_2(M_Z). \tag{2.29}$$

Consequently, we find that in the scenario presented above, the lightest neutralino, $\tilde{\chi}_1^0$, is mainly bino, $\tilde{B}$, in character while the 2nd lightest neutralino, $\tilde{\chi}_2^0$, is mainly wino, $\tilde{W}^0$, in character. In addition, Eq. (2.29) implies that the masses will closely follow the relation, $m_{\tilde{\chi}_1^0} \simeq \frac{1}{2} m_{\tilde{\chi}_2^0}$.

If we now inspect scenarios where the higgsino mass parameter is less than the gaugino mass parameters, $|\mu| < |M_{\{1,2\}}|$, the phenomenology of the neutralinos has the opposite characteristics. The two lightest neutralinos will now mostly be higgsino-like with masses close to that of $|\mu|$ whilst the heavier neutralinos will be gauginos. Finally, if the higgsino and gaugino parameters are similar, $|\mu| \simeq |M_{\{1,2\}}|$ then some of the mass states will have mixed higgsino, gaugino characteristics.

2.4.4 Charginos

Analogously to the neutralinos, the charged partners of the $W^\pm$ and $H^\pm$ also mix. The mass eigenstates of these particles are called charginos $\tilde{\chi}^\pm$ but are normal Dirac fermions as the sparticle and anti-particle are different. The mass term of the Lagrangian in the basis $\psi^+ = (-i\tilde{W}^+, \tilde{H}_2^+)$, $\psi^- = (-i\tilde{W}^-, \tilde{H}_1^-)$ is given by,

$$
\mathcal{L}_{\tilde{\chi}^\pm} = -\frac{1}{2}(\psi^+, \psi^-) \begin{pmatrix} 0 & \mathcal{M}_C^T \\ \mathcal{M}_C & 0 \end{pmatrix} \begin{pmatrix} \psi^+ \\ \psi^- \end{pmatrix} + h.c. \tag{2.30}
$$

where the mass matrix is,

$$
\mathcal{M}_C = \begin{pmatrix} M_2 & \sqrt{2}m_W \sin\beta \\ \sqrt{2}m_W \cos\beta & \mu \end{pmatrix}. \tag{2.31}
$$

Since the mass matrix is not hermitian we need two different unitary matrices to diagonalise it,

$$
U^* \mathcal{M}_C V^\dagger = \begin{pmatrix} m_{\tilde{\chi}_1^\pm} & 0 \\ 0 & m_{\tilde{\chi}_2^\pm} \end{pmatrix} \quad \text{with} \quad m_{\tilde{\chi}_1^\pm} < m_{\tilde{\chi}_2^\pm}. \tag{2.32}
$$

Applying the U and V matrices on the gauge eigenstates $\psi_j^\pm$ gives the physical mass eigenstates, $\tilde{\chi}_1^\pm$ and $\tilde{\chi}_2^\pm$ as follows,

$$
\tilde{\chi}_i^+ = V_{jk}\psi_j^+, \qquad \tilde{\chi}_i^- = U_{ij}\psi_j^-, \qquad i,j = 1,2, \tag{2.33}
$$

The relative strength of M_1 and μ define the couplings of the charginos in a similar way to that of the neutralinos. If $M_2 < \mu$ the lightest chargino, $\tilde{\chi}_1^\pm$, is mainly wino, $\tilde{W}$, in character whilst the heavier chargino, $\tilde{\chi}_2^\pm$, will be a higgsino, $\tilde{H}^\pm$. If the parameter hierarchy is opposite, $\mu < M_2$, the mass eigenstates will also have the opposite characteristics. In contrast, if the parameters are of similar size, $M_2 \simeq \mu$, the mass states will be mixed. Additionally, if we have a non-mixed scenario where M_2 and μ are separated, the wino-like chargino will have a similar mass to the wino-like neutralino and the higgsino-like chargino will have similar mass to the higgsino-like neutralinos.

2.5 Electric dipole moment results

Some of the additional CP-violating phases of the MSSM are already constrained by the low energy measurement of Electric Dipole Moments (EDMs). The most demanding constraints come from the EDM of the Neutron [72], Thallium [73] and Mercury [74] with the following values,

$$|d_{\text{n}}| < 2.9 \times 10^{-26} e \text{ cm } (90\%\text{C.L.}), \tag{2.34}$$

$$|d_{\text{Tl}}| < 9.0 \times 10^{-25} e \text{ cm } (90\%\text{C.L.}), \tag{2.35}$$

$$|d_{\text{Hg}}| < 3.1 \times 10^{-29} e \text{ cm } (90\%\text{C.L.}). \tag{2.36}$$

If we ignore any CP-violation induced by a QCD θ-term, then the only CP-violating term in the Standard Model is the electroweak phase within the CKM matrix. The phase only contributes at the 2-loop level to the above observables and thus is expected to be small, for example $|d_{\text{n}}| \sim 10^{-32} e$ cm [75–77].

In the MSSM however, more sizable contributions can be expected, especially from the phases of the Higgs mass parameter, the gaugino mass parameter and the trilinear couplings of the first generation squarks (ϕ_μ, ϕ_{M_1}, ϕ_{M_3}, ϕ_{A_u}, ϕ_{A_d}) as they can produce effects at 1-loop. Out of these, the experimental measurements most severely constrain the phase of the Higgs mass parameter, $\phi_\mu \lesssim 0.01\pi$ [78, 79]. The constraint on the phase of the other parameters mentioned is less severe due to the coupling structure of the corrections [80]. The constraints on the phases of the other CP-violating MSSM parameters that have been investigated with respect to triple product correlations (ϕ_{A_t}, ϕ_{A_b}, ϕ_{A_τ}) at the LHC are weaker. The reason is that they only contribute at the 2-loop level and can essentially be thought of as being unconstrained at the current time [80].

A possible solution to allow for larger phases in the gaugino sector is to increase the mass of the first and second generation squarks [81–83]. The larger mass suppresses the loop contribution to the EDM. However, this possibility allows the third generation of squarks to remain light so that electroweak symmetry breaking still take place and the MSSM continues to provide an explanation for the hierarchy problem. Another way to alleviate the constraints on the phases of the gaugino

sector is to allow cancellations between different phases of the model [84–87]. While the phase of the Higgs mass parameter, ϕ_μ, is still very constrained, this approach can help other parameters in the theory. For example, the phase of the $U(1)$ gaugino mass term, ϕ_{M_1} can now become essentially unconstrained in many models [88].

A recent comprehensive review of the CP-violating constraints within the MSSM is given in [80] whilst a review of some of the issues regarding the different EDM measurements and the reliability of the theoretical predictions is given in [89]. For our studies, we set $\phi_\mu = 0$ due to the severity of the constraints on this particular phase. However, we leave all other CP-violating phases free to vary from $0 < \phi < 2\pi$ to see the full range of their dependencies at the LHC.

Chapter 3

CP-violation studies at the LHC

If the MSSM is discovered at the LHC and if the model contains sizable CP-violating phases, there are many potential observables that could be used to detect the CP-violation. For example, masses [90–94], total cross sections [95, 96] and branching ratios [97, 98] can all change when CP-phases are present in the model and could in principle be used. However, these observables are all CP-even quantities and consequently display the same behaviour for both the particle and the anti-particle. In a model like the MSSM with so many free parameters this can cause a problem as the CP effect can potentially be 'faked' by changing some of the soft breaking parameters. In addition, loop corrections can be sizable to all of the observables mentioned and can produce additional uncertainty when trying to determine the CP-phase.

Therefore, in order to make the unambiguous observation of a complex parameter, we should use CP-odd observables where the CP conjugate process has an opposite sign and cannot be faked by other model parameters. Examples of CP-odd observables include rate asymmetries of branching ratios [99–103], rate asymmetries in cross sections [104] and angular distributions [105]. However, all of these observables only exhibit CP-violating properties when we go to the loop level and consequently we expect the effects to be relatively small. Another possibility to consider, are observables that are T_N-odd, Sec. 3.1, and can be defined using the triple product correlations of momenta and/or spins of particles [106–116]. For the case of SUSY at the LHC, we can do this using triple products of the final-state

particles of cascade decays.

Two recent reviews of CP violation in the MSSM are given in [117, 118].

3.1 C, P and T transformations

We begin by briefly reviewing the transformation properties of C, P and T on a single particle before explaining their use in reactions at colliders [119–121].

A single incoming particle, X, with momentum, P, and spin state, S, can be written as,

$$|X; \vec{P}, \vec{S}\rangle_{in}. \tag{3.1}$$

If we apply a parity transformation, P, to the state, the momentum is reversed while the spin remains fixed,

$$\mathrm{P}|X; \vec{P}, \vec{S}\rangle_{in} = |X; -\vec{P}, \vec{S}\rangle_{in}. \tag{3.2}$$

The anti-unitarity time reversal operator, T, reverses the momentum and spin of a particle and also exchanges the initial and final states,

$$\mathrm{T}|X; \vec{P}, \vec{S}\rangle_{in} = |X; -\vec{P}, -\vec{S}\rangle_{out}. \tag{3.3}$$

Finally, the charge conjugation operation, C, replaces the particle by its antiparticle,

$$\mathrm{C}|X; \vec{P}, \vec{S}\rangle_{in} = |\bar{X}; \vec{P}, \vec{S}\rangle_{in}. \tag{3.4}$$

It it also possible to have the combined action of all three transformations,

$$\mathrm{CPT}|X; \vec{P}, \vec{S}\rangle_{in} = |\bar{X}; \vec{P}, -\vec{S}\rangle_{out}. \tag{3.5}$$

Using the CPT-theorem [122, 123], it is possible to show that relativistic quantum field theories with usual spin-statistics relations have to be invariant under a CPT-transformation. This invariance guarantees that the masses and also the total widths of particles and antiparticles are the same.

Thus, due to CPT-invariance, any theory can only violate T if it also violates CP, where,

$$\mathrm{CP}|X; \vec{P}, \vec{S}\rangle_{in} = |\bar{X}; -\vec{P}, \vec{S}\rangle_{in}. \tag{3.6}$$

and therefore CP and T violation can be considered as equivalent.

In this thesis we concentrate on the violation of CP (or T) in cascade decays and we therefore need to consider how the transformations work with the S-matrix. We define an initial (final) state of n_i (n_f) particles as,

$$|i\rangle \;=\; |\vec{P}_a, \vec{P}_b, ..., \vec{S}_a, \vec{S}_b, ...\rangle_{in}\,, \tag{3.7}$$

$$|f\rangle \;=\; |\vec{P}_1, \vec{P}_2, ..., \vec{S}_1, \vec{S}_2, ...\rangle_{out}\,. \tag{3.8}$$

The transformation properties under C, P and CP follow from those of the single particle,

$$|f_{\mathrm{P}}\rangle \;=\; |-\vec{P}_1, -\vec{P}_2, ..., \vec{S}_1, \vec{S}_2, ...\rangle_{out}\,, \tag{3.9}$$

$$|f_{\mathrm{C}}\rangle \;=\; |\vec{P}_{\bar{1}}, \vec{P}_{\bar{2}}, ..., \vec{S}_{\bar{1}}, \vec{S}_{\bar{2}}, ...\rangle_{out}\,, \tag{3.10}$$

$$|f_{\mathrm{CP}}\rangle \;=\; |-\vec{P}_{\bar{1}}, -\vec{P}_{\bar{2}}, ..., \vec{S}_{\bar{1}}, \vec{S}_{\bar{2}}, ...\rangle_{out}\,, \tag{3.11}$$

and likewise for $|i_{\mathrm{P}}\rangle$, $|i_{\mathrm{C}}\rangle$ and $|i_{\mathrm{CP}}\rangle$.

For the T transformation, we also have to exchange the initial and final states,

$$|f_{\mathrm{T}}\rangle \;=\; |-\vec{P}_1, -\vec{P}_2, ..., -\vec{S}_1, -\vec{S}_2, ...\rangle_{in}\,, \tag{3.12}$$

$$|i_{\mathrm{T}}\rangle \;=\; |-\vec{P}_a, -\vec{P}_b, ..., -\vec{S}_a, -\vec{S}_b, ...\rangle_{out}\,. \tag{3.13}$$

We define the S-matrix as the usual,

$$\langle f|S|i\rangle = S_{fi}\,, \tag{3.14}$$

The transformation properties can then be written as,

$$S_{fi} \;\xrightarrow{\mathrm{P}}\; S_{f_P i_P}\,, \tag{3.15}$$

$$S_{fi} \;\xrightarrow{\mathrm{C}}\; S_{f_C i_C}\,, \tag{3.16}$$

$$S_{fi} \;\xrightarrow{\mathrm{CP}}\; S_{f_{CP} i_{CP}}\,, \tag{3.17}$$

with the T transformation also exchanging the initial and final states,

$$S_{fi} \;\xrightarrow{\mathrm{T}}\; S_{i_T f_T}\,. \tag{3.18}$$

In a collider experiment however, it is extremely hard to test T due to the requirement of exchanging the initial and final states. Therefore, it is often more practical to experimentally probe what is known as a naïve time reversal operation , T$_N$. This operation is the same as a T transformation but we do not exchange the initial and final states,

$$S_{fi} \xrightarrow{\text{T}_N} S_{f_T i_T} \,. \tag{3.19}$$

3.2   T$_N$ transformation

To clarify the properties of the T$_N$ operator, we will consider the unitarity of the S-matrix as explained in [121]. Using the optical theorem (e.g [120]) we can write the S-matrix in terms of the scattering amplitude, $\hat{T}$,

$$S = 1 + i\hat{T} \,. \tag{3.20}$$

For the reaction, $i \to f$, we can write $\hat{T}$ in terms of the reduced scattering amplitude, $\hat{\tau}$,

$$\hat{T}_{fi} \quad = \quad \langle f|\hat{T}|i \rangle \,, \tag{3.21}$$

$$= \quad (2\pi)^4 \delta^4(p_f - p_i)\langle f|\hat{\tau}|i \rangle \,, \tag{3.22}$$

where p_f (p_i) is the momentum of the final (initial) states.

We use the unitarity relation, $S^\dagger S = 1$ to obtain,

$$\hat{T}_{fi} - \hat{T}_{if}^* = i \sum_x \hat{T}_{xf}^* \hat{T}_{xi} \,, \tag{3.23}$$

where x denotes all possible intermediate states between i and f.

In terms of the reduced scattering amplitude, $\hat{\tau}$, this becomes,

$$\hat{\tau}_{fi} - \hat{\tau}_{if}^* = i(2\pi)^4 \sum_x \delta^4(p_x - p_i)\hat{\tau}_{xf}^* \hat{\tau}_{xi} \,. \tag{3.24}$$

If we now assume that there are no re-scattering effects ($\hat{\tau}_{ii} = \hat{\tau}_{ff} = 0$), and that the initial and final states are stable, for each possible intermediate state, x, the rhs of Eq. (3.24) vanishes. Therefore, in the absence of re-scattering, the reduced scattering amplitude, $\hat{\tau}$, is hermitian,

$$\hat{\tau}_{if} = \tau_{fi}^* \,. \tag{3.25}$$

Hence, if $\hat{\tau}$ is CP invariant, then it must also be T invariant due to the CPT theorem. Consequently,

$$\langle f|\hat{\tau}|i\rangle \;=\; \langle i_T|\hat{\tau}|f_T\rangle\,, \tag{3.26}$$

$$=\; \langle f_T|\hat{\tau}|i_T\rangle^*\,. \tag{3.27}$$

which leads to,

$$|\langle f|\hat{\tau}|i\rangle|^2 = |\langle f_T|\hat{\tau}|i_T\rangle|^2\,, \tag{3.28}$$

which means that the modulus of $\langle f|\hat{\tau}|i\rangle$ is invariant under a T_N transformation.

As the expectation value of any operator depends only on $|\langle f|\hat{\tau}|i\rangle|$, Eq. (3.28) implies that in the absence of any re-scattering, only T_N-even operators can have a non-zero expectation value if CP is conserved. Hence, a T_N-odd observable can only be seen if CP-violation is present or re-scattering effects occur. Another way to make this statement is that in the absence of re-scattering (i.e. $\mathrm{Im}(\hat{\tau})=0$),

$$\mathrm{CPT} \to \mathrm{CPT}_N. \tag{3.29}$$

Therefore, if the expectation value of a T_N-odd observable is non-zero, CP-violation or re-scattering effects must be present.

To make a definite observation of CP-violation, we must rule out the possibility that a T_N-odd observation is due to re-scattering effects. We can do this by looking at the charge conjugated process $\left(\bar{i} \to \bar{f}\right.$ compared with $i \to f)$ to see if the transformation is CP-even or CP-odd. Hence we can unambiguously determine if the process is CP-violating.

Another implication of Eq. (3.25) and Eq. (3.28) is that a CP-odd, but T_N-even observable can only be seen if re-scattering effects are present. Hence, CP-odd, T_N-even observables cannot be present at the tree level.

3.3 Triple product correlations

The main observables we use to look for CP-violation in the MSSM at the LHC are triple product correlations. These are produced from three independent momentum or spin vectors combined as,

$$\mathcal{T} = \vec{p}_1 \cdot (\vec{p}_2 \times \vec{p}_3)\,, \tag{3.30}$$

where p is the momentum of the individual particle, but could also be a spin vector.

If we apply a T_N operation to the triple product we reverse the sign of all the momentum vectors and therefore the sign of the triple product. Hence, the observable is T_N-odd. Under the assumption of no re-scattering effects as explained in Sec. 3.2 and CPT_N invariance, this translates into a CP-odd observable.

The advantage of using triple product correlations to observe CP-violation in the MSSM is that these effects can occur at the tree level and we can expect the observables to be larger. We now explain the origin of the triple products and how they can be used to observe CP-violation in the MSSM.

As an example, we consider the following decay chain,

$$\tilde{t} \;\to\; \tilde{\chi}_2^0 \, t, \tag{3.31}$$

$$\tilde{\chi}_2^0 \to \ell^+ \, \ell^- \, \tilde{\chi}_1^0 . \tag{3.32}$$

where the $\tilde{t}$ undergoes a two body decay and the $\tilde{\chi}_2^0$ undergoes a three body decay. This decay channel will be considered in more detail in Chapter 4 and the explicit amplitudes will be shown.

We evaluate the above cascade decay chain by calculating the total amplitude for both processes including the spin correlation between the production and decay of the $\tilde{\chi}_2^0$. We find that the following trace appears in the amplitude, which results in an explicit covariant product of momentum,

$$A \cdot \mathrm{Tr}[\gamma^5 \gamma^\mu \gamma^\nu \gamma^\rho \gamma^\sigma] \to i A \cdot \epsilon_{\mu\nu\rho\sigma} p_{\tilde{\chi}_2^0}^\mu p_t^\nu p_{\ell^+}^\rho p_{\ell^-}^\sigma , \tag{3.33}$$

where A is the relevant coupling constant. We notice that the covariant product is multiplied by a factor of i and consequently Eq. (3.33) only contributes to the amplitude if A contains imaginary (CP-violating) terms. In the case of the above example, these terms can come from complex phases within the neutralino mixing matrix, Eq. (2.26). We also note that the covariant product appears in the amplitude at the tree level and hence any potential observables are not loop suppressed.

If we expand the covariant product in terms of the explicit 4-momentum,

$$\begin{aligned}
\epsilon_{\mu\nu\rho\sigma} p_{\tilde{\chi}_2^0}^\mu p_t^\nu p_{\ell^+}^\rho p_{\ell^-}^\sigma = \quad & E_{\tilde{\chi}_2^0} \; \vec{p_t} \cdot (\vec{p_{\ell^+}} \times \vec{p_{\ell^-}}) + E_{\ell^+} \; \vec{p_{\ell^-}} \cdot (\vec{p_{\tilde{\chi}_2^0}} \times \vec{p_t}) \\
& - E_t \; \vec{p_{\ell^+}} \cdot (\vec{p_{\ell^-}} \times \vec{p_{\tilde{\chi}_2^0}}) - E_{\ell^-} \; \vec{p_{\tilde{\chi}_2^0}} \cdot (\vec{p_t} \times \vec{p_{\ell^+}}).
\end{aligned} \tag{3.34}$$

we find the energy multiplied by the triple products of momenta $(\vec{p_1} \cdot (\vec{p_2} \times \vec{p_3}))$. In the rest frame of the $\tilde{\chi}_2^0$, $(p_{\tilde{\chi}_2^0} = (m_{\tilde{\chi}_2^0}, 0, 0, 0))$, the expression simplifies and produces a single triple product,

$$\mathcal{T} = m_{\tilde{\chi}_2^0} \; \vec{p_t} \cdot (\vec{p_{\ell^+}} \times \vec{p_{\ell^-}}) \tag{3.35}$$

since all terms containing $p_{\tilde{\chi}_2^0} \to 0$. We can therefore measure the final-state momenta and if we observe an overall triple product we can infer the presence of CP-violation.

Again we draw attention to the fact that we cannot perform a true time reversal, T, operation at a collider as it requires interchanging the initial and final states, Sec. 3.2, [121] . Instead we apply a naïve time reversal, T$_N$, operation that only reverses the momentum and spin of the final-state particles but does not exchange the initial and final states. In principle, absorptive phases that originate from final state interactions (FSI) or the finite width of unstable particles could enter and provide a T$_N$-odd contribution. If these effects are sizable then the triple product could be sensitive to CP-even, T$_N$-odd effects. These contributions can be removed however by looking at the charge conjugate process. If the sign of the observable is opposite for the charge conjugate process, we know that the observable must be CP-odd and not due to absorptive phases.

3.4 T$_N$-odd asymmetry

In order to measure any CP-violation at a collider it is useful to define a dimensionless parameter that can be used to easily understand the statistical significance of any result. We therefore define the T$_N$-odd asymmetry parameter,

$$\mathcal{A}_T = \frac{N_{\mathcal{T}_+} - N_{\mathcal{T}_-}}{N_{\mathcal{T}_+} + N_{\mathcal{T}_-}} \;\; = \;\; \frac{\int \mathrm{sign}\{\mathcal{T}\}|T|^2 d\,\mathrm{lips}}{\int |T|^2 d\,\mathrm{lips}}, \tag{3.36}$$

where $N_{\mathcal{T}_+}$ ($N_{\mathcal{T}_-}$) are the numbers of events for which $\mathcal{T}$ is positive (negative), T is the amplitude and d lips denotes Lorentz invariant phase space. The denominator in Eq. (3.36), $\int |T|^2 d\,\mathrm{lips}$, is equal to the total cross section which in the example
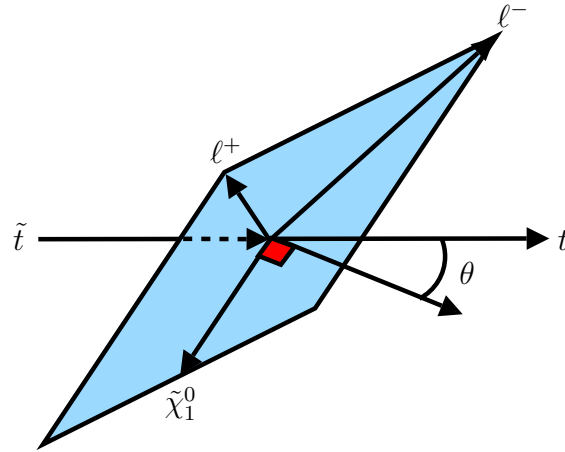
Figure 3.1: The reaction geometry in the $\tilde{\chi}_2^0$ rest frame. The triple product, $\mathcal{T}$, is given by the angle between the t and the plane formed between the ℓ^+ and the ℓ^- (in the $\tilde{\chi}_2^0$ rest frame, the $\tilde{\chi}_1^0$ also lies on this plane).

would be,

$$\int |T|^2 d\,\text{lips} = \sigma_{Tot},$$
$$= \sigma(pp \to \tilde{t}\tilde{t}^*) \cdot \text{BR}(\tilde{t} \to \tilde{\chi}_2^0 t) \cdot \text{BR}(\tilde{\chi}_2^0 \to \tilde{\chi}_1^0 \ell^+ \ell^-). \quad (3.37)$$

Fig. 3.1 shows that in the rest frame of the $\tilde{\chi}_2^0$, the $\tilde{\chi}_1^0$, ℓ^+ and ℓ^- define a plane. The triple product is given by the angle, θ, between the normal of this plane and the t that was produced in the $\tilde{t}$ decay alongside the $\tilde{\chi}_2^0$. In terms of the asymmetry parameter, events are regarded as $N_{\mathcal{T}_+}$ ($N_{\mathcal{T}_-}$) if the t was produced above (below) the plane. An alternative definition can also be given for the asymmetry in terms of the angular distribution,

$$\mathcal{A}_T = \frac{N_{\mathcal{T}_+} - N_{\mathcal{T}_-}}{N_{\mathcal{T}_+} + N_{\mathcal{T}_-}} = \frac{\int_1^0 \frac{d\sigma}{d\cos\theta} d\cos\theta - \int_0^{-1} \frac{d\sigma}{d\cos\theta} d\cos\theta}{\int_1^0 \frac{d\sigma}{d\cos\theta} d\cos\theta + \int_0^{-1} \frac{d\sigma}{d\cos\theta} d\cos\theta}, \quad (3.38)$$

where,

$$\cos\theta = \frac{\vec{p_t} \cdot (\vec{p_{\ell^+}} \times \vec{p_{\ell^-}})}{|\vec{p_t}| \cdot |(\vec{p_{\ell^+}} \times \vec{p_{\ell^-}})|}. \quad (3.39)$$

If CP-violation is present we expect a non-zero expectation value for $\mathcal{T}$ and therefore a non zero average angle between the plane and the produced t.

As stated above, a T_N-odd asymmetry can in principle be formed if absorptive phases are present from finite width effects or loop induced final state interactions.

Although these effects are expected to be small for electroweak processes as they are formally a higher order contribution we can remove them by defining a CP-odd asymmetry,

$$\mathcal{A}_{CP} = \frac{1}{2}(\mathcal{A}_T - \bar{\mathcal{A}}_T),\qquad(3.40)$$

where $\mathcal{A}_{CP}$ corresponds to the asymmetry for the CP-conjugated process.

3.5   Boosted frame asymmetry

Whilst the covariant product in the amplitude, Eq. (3.33), is inherently Lorentz invariant, the triple product, $\mathcal{T}$, Eq. (3.35) is not. At the LHC we can expect the particles produced to have substantial boosts in the laboratory frame that vary on an event-by-event basis. We therefore need to analyse the effect of such boosts on the triple product observable.

Ideally, we would like to reconstruct the rest frame of the $\tilde{\chi}_2^0$. We would then be able to boost the momentum of the triple product particles into this frame and access the value of the covariant product. However, the $\tilde{\chi}_1^0$ only interacts weakly and therefore will escape the detector without being seen, so the rest frame cannot of the $\tilde{\chi}_2^0$ cannot be trivially reconstructed.

If we analyse the covariant product in the laboratory frame,

$$\epsilon_{\mu\nu\rho\sigma}p_{\tilde{\chi}_2^0}^\mu p_t^\nu p_{\ell+}^\rho p_{\ell-}^\sigma \stackrel{lab}{=}\quad E_{\tilde{\chi}_2^0}\ \overrightarrow{p_t}\cdot(\overrightarrow{p_{\ell+}}\times\overrightarrow{p_{\ell-}}) + E_{\ell+}\ \overrightarrow{p_{\ell-}}\cdot(\overrightarrow{p_{\tilde{\chi}_2^0}}\times\overrightarrow{p_t})$$
$$-E_t\ \overrightarrow{p_{\ell+}}\cdot(\overrightarrow{p_{\ell-}}\times\overrightarrow{p_{\tilde{\chi}_2^0}}) - E_{\ell-}\ \overrightarrow{p_{\tilde{\chi}_2^0}}\cdot(\overrightarrow{p_t}\times\overrightarrow{p_{\ell+}}).\qquad(3.41)$$

we see that our triple product observable is only sensitive to the first term (we only exploit the sign). The other terms all require a measurement of the $\tilde{\chi}_1^0$ momentum to find the $\tilde{\chi}_2^0$ momentum. We therefore do not measure the sign of the true covariant product in the amplitude but instead only one component. As we have lost information on the true sign of the covariant product, the asymmetry can be significantly diluted for events at the LHC, Sec. 4.3.5.

Another way to understand the dilution of the asymmetry in the laboratory frame is to think about the relative orientation of the t and the plane defined by the ℓ^+ and ℓ^-, Fig. 3.1. These particles correspond to the triple product, $\mathcal{T} = \overrightarrow{p_t}\cdot(\overrightarrow{p_{\ell+}}\times\overrightarrow{p_{\ell-}})$

that is the first term in Eq. (3.41). In the rest frame of the $\tilde{\chi}_2^0$ the orientation is 'correct' and thus we measure the maximum asymmetry. However, in the laboratory frame, the orientation of the t and the ℓ^+, ℓ^- plane will in general be different. For some events, the difference in orientation can mean that the t 'flips' from one side of the plane to the other and consequently we record an opposite sign for the triple product.

3.6 Statistical error and significance

In order to determine whether a particular CP-asymmetry may be measured at a collider we have to understand the statistical significance of any result. The relative statistical error of the asymmetry Eq. (3.36) is given by,

$$\delta\mathcal{A}_T = \frac{\Delta(\mathcal{A}_T)^{\text{stat}}}{|\mathcal{A}_T|}. \tag{3.42}$$

We assume that $N_{\mathcal{T}_+}$ ($N_{\mathcal{T}_-}$) are the numbers of events where $\mathcal{T}$ is positive (negative), as in Eq. (3.36), and are binomially distributed, giving the following statistical error [124],

$$\Delta(\mathcal{A}_T)^{\text{stat}} = 2\sqrt{\epsilon(1-\epsilon)/N}, \tag{3.43}$$

where,

$$\epsilon = N_{\mathcal{T}_+}/(N_{\mathcal{T}_+} + N_{\mathcal{T}_-}) = \frac{1}{2}(1 + \mathcal{A}_T), \tag{3.44}$$

and $N = N_{\mathcal{T}_+} + N_{\mathcal{T}_-}$ is the total number of events. We can also write the total number of events in terms of the total cross section, σ_{Tot} (Eq. (3.37) in example) and luminosity, $\mathcal{L}$, with the relation, $N = \mathcal{L}\sigma_{Tot}$.

Combining Eq. (3.42) and Eq. (3.43), we can then write down the statistical significance of any asymmetry,

$$S = |A_T|\sqrt{\frac{\mathcal{L}\sigma_{Tot}}{1 - A_T^2}}. \tag{3.45}$$

For $S = 1$, the asymmetry can be measured at the 68% confidence level (CL), for S = 1.96 at the 95% CL, etc.

3.7 Triple product studies

There have now been many studies that have examined the possibility of searching for CP-violation in SUSY using triple products. The majority of these studies have been explored at a future linear collider and have mostly concentrated on CP-violation from the direct production and decay of sleptons (e.g. [125]), neutralinos (e.g. [106, 112]) and charginos (e.g [126]). The reason that the studies have been based on the linear collider is mainly because of the much cleaner experimental conditions when compared with the LHC. In addition, polarised beams and the known centre-of-mass system (cms) energy allows the initial state, e^+e^-, to become part of the T-odd observable (e.g [116, 127, 128]).

At the LHC, the situation is more challenging due to the composite QCD initial state. We no longer know the identity of the colliding particles, the collision centre-of-mass energy is undetermined and a large QCD background will be present. In addition, as the strong coupling constant is the largest, the cross section to coloured particles is dominant. Consequently, the electroweak initial states considered in the studies above are no longer competitive and the studies need to be based around the production of QCD charged particles. The main studies using triple product correlations in SUSY at the LHC are presented in Tab. 3.1.

The studies presented in this thesis, Chapters 4-6, are summarised briefly in this section for completeness and comparison.

3.7.1 Initial two-body decay studies

The initial study to consider the possibility of using triple product correlations in SUSY cascade decays at the LHC was [129]. This was a completely analytical, parton-level study and looked at the following two-body cascade decay of a stop,

$$\tilde{t} \to \tilde{\chi}_2^0 \, t \,, \tag{3.46}$$

$$\tilde{\chi}_2^0 \to \ell_N^\pm \, \tilde{\ell}^\mp \to \ell_N^\pm \, \ell_F^\mp \, \tilde{\chi}_1^0 \,, \tag{3.47}$$

$$t \to bW \to b \, \ell_t \, \nu_\ell \,, \tag{3.48}$$

Process	Sub Decay 1	Sub Decay 2	CP Phases	Max $\mathcal{A}_{\mathrm{CP}}$	Ref.
$\tilde{t} \to t\tilde{\chi}_i^0$	$t \to bW$ $\tilde{\chi}_i^0 \to \tilde{\ell}\ell$	$W \to \bar{\ell}\nu$ $\tilde{\ell} \to \ell\tilde{\chi}_1^0$	$\phi_{A_t}, \phi_\mu, \phi_{M_1}$	15(40)%	[129]
$\tilde{t} \to t\tilde{\chi}_i^0$	$\tilde{\chi}_i^0 \to \ell\bar{\ell}\tilde{\chi}_1^0$		ϕ_μ, ϕ_{M_1}	10[3]%	[130]
$\boldsymbol{\tilde{t} \to t\tilde{\chi}_i^0}$	$\boldsymbol{t \to bW}$ $\boldsymbol{\tilde{\chi}_i^0 \to \ell\bar{\ell}\tilde{\chi}_1^0}$		$\boldsymbol{\phi_{A_t}, \phi_\mu, \phi_{M_1}}$	$\boldsymbol{15[4]\%}$	**Ch. 4** **[131]**
$\tilde{t} \to t\tilde{\chi}_i^0$	$t \to bW$ $\tilde{\chi}_i^0 \to \tilde{\ell}\ell$	$W \to \bar{\ell}\nu$ $\tilde{\ell} \to \ell\tilde{\chi}_1^0$	$\phi_{A_t}, \phi_\mu, \phi_{M_1}$	18(40)[6]%	[132]
$\boldsymbol{\tilde{t} \to t\tilde{\chi}_i^0}$	$\boldsymbol{t \to bW}$ $\boldsymbol{\tilde{\chi}_i^0 \to \tilde{\ell}\ell}$	$\boldsymbol{W \to jj}$ $\boldsymbol{\tilde{\ell} \to \ell\tilde{\chi}_1^0}$	$\boldsymbol{\phi_{A_t}, \phi_\mu, \phi_{M_1}}$	$\boldsymbol{15[4]\%}$	**Ch. 6** **[133]**
$\tilde{b} \to t\tilde{\chi}_j^\pm$	$t \to bW$ $\tilde{\chi}_j^\pm \to \ell\tilde{\nu}$ $\tilde{\chi}_j^\pm \to \tilde{\ell}\nu$	$W \to \bar{\ell}\nu$ $\tilde{\ell} \to \ell\tilde{\chi}_1^0$	ϕ_{A_b}, ϕ_μ	10(40)% 15%	[134]
$\tilde{b} \to t\tilde{\chi}_j^\pm$	$t \to bW$ $\tilde{\chi}_j^\pm \to \ell\tilde{\nu}$	$W \to \bar{\ell}\nu$	ϕ_{A_b}, ϕ_μ	15(40)[7]%	[135]
$\boldsymbol{\tilde{q} \to q\tilde{\chi}_i^0}$ $\boldsymbol{\tilde{\chi}_i^0 \to \ell\bar{\ell}\tilde{\chi}_1^0}$			$\boldsymbol{\phi_\mu, \phi_{M_1}}$	$\boldsymbol{15[2]\%}$	**Ch. 5** **[136]**
$\tilde{t}_2 \to \tilde{t}_1\tau^-\tau^+$			ϕ_{A_t}	90%	[137]

Table 3.1: Overview of the SUSY cascade decays now studied to analyze CP phases at the LHC. Two-body decays are denoted by $a \to bc$ and three-body decays by $a \to bcd$. The column 'CP Phases' lists the phases the process is sensitive to. 'Max $\mathcal{A}_{\mathrm{CP}}$' gives the maximal asymmetries which have been found in the rest frame of the sfermion, the round brackets refer to the maximum asymmetry from non-observable final states and the square brackets to the laboratory frame asymmetry. The rows in bold correspond to the studies presented in this thesis along with the relevant chapter number. This list is not exhaustive but presents the most promising channels studied at the LHC. Some of the asymmetry numbers are not explicitly stated but have been extrapolated from plots presented.

where $\ell_N^\pm(\ell_F^\mp)$ is the lepton produced in the $\chi_2^0(\tilde{\ell}^\mp)$ decay and $N(F)$ denotes 'near' ('far'). ℓ_t is the lepton produced in the t decay.

The study was the first to consider using $\tilde{t}$ decays and therefore did not attempt to include the production process explicitly or try to estimate the dilution due to the boosted decay. Instead the study focused exclusively on the cascade decay and the triple products that could be formed

In the scenarios considered, the study found that the decay chain was most sensitive to the phase of the top trilinear coupling, ϕ_{A_t}, and T-odd asymmetries of up to 40% were found. Unfortunately however, the maximum asymmetry was found to occur with the triple product,

$$\mathcal{T} = \overrightarrow{p_{\ell_t}} \cdot (\overrightarrow{p_t} \times \overrightarrow{p_{\ell_N^\pm}}). \tag{3.49}$$

The triple product requires simultaneous knowledge of the top, t, and the lepton coming from the top, ℓ_t. The reason this triple product produces the largest asymmetry is that the lepton produced by the top, ℓ_t is sensitive to the polarisation of the W which in turn is sensitive to the polarisation of the top. This gives more information on the top production amplitude than the direction of the W alone (for example in the triple product, $\overrightarrow{p_W} \cdot (\overrightarrow{p_t} \times \overrightarrow{p_{\ell_N^\pm}})$) and therefore a larger asymmetry. However, the triple product requires simultaneous knowledge of the top, t, and the lepton coming from the top, ℓ_t. This neglects the fact that the missing neutrino, ν_ℓ, would seem to make this impossible at a collider.

The largest reconstructible T-odd asymmetries were found to be $\mathcal{A}_T \sim 15\%$ with the following triple products (labeling from [129]),

$$\mathcal{T}_1 = \overrightarrow{p_b} \cdot (\overrightarrow{p_t} \times \overrightarrow{p_{\ell_N^\pm}}), \tag{3.50}$$

$$\mathcal{T}_3 = \overrightarrow{p_{\ell_t}} \cdot (\overrightarrow{p_b} \times \overrightarrow{p_{\ell_N^\pm}}), \tag{3.51}$$

$$\mathcal{T}_5 = \overrightarrow{p_{\ell_t}} \cdot (\overrightarrow{p_{\ell_N^\pm}} \times \overrightarrow{p_{\ell_F^\mp}}). \tag{3.52}$$

The triple product from Eq. (3.50) is valid if we allow the top to decay hadronically while Eqs. (3.51,3.52) are possible if the leptonic decay of the top is preferred.

One outstanding issue with the triple products shown in Eqs. (3.50,3.51), is that they require that we can correctly distinguish the near and far lepton. This distinction may be possible with energy distributions but if we are not able to distinguish

the leptons, the asymmetry is diluted (to $\mathcal{A}_T \sim 10\%$) as the far lepton has a weaker spin correlation.

The same group also produced a study on the possibility of using cascade decays of sbottoms, $\tilde{b}$, as an alternative [134] with the following decay,

$$\tilde{b} \quad \rightarrow \quad t\tilde{\chi}^-, \tag{3.53}$$

$$\tilde{\chi}^- \quad \rightarrow \quad \ell^- + ME, \tag{3.54}$$

$$t \quad \rightarrow \quad b\ell_t\nu_\ell \,(bcs)\,[bjj], \tag{3.55}$$

where ME is the general missing energy that contains a single ν and $\tilde{\chi}_1^0$ in the final state.

The triple products of most interest are,

$$\mathcal{T}_A \quad = \quad \overrightarrow{p_\ell} \cdot (\overrightarrow{p_{(\ell_t,c)}} \times \overrightarrow{p_t}), \tag{3.56}$$

$$\mathcal{T}_B \quad = \quad \overrightarrow{p_\ell} \cdot (\overrightarrow{p_{\ell_t}} \times \overrightarrow{p_b}), \tag{3.57}$$

where ℓ is the lepton produced by the $\tilde{\chi}^-$ and ℓ_t is the lepton produced by the top.

Again, CP-violating asymmetries of up to, $\mathcal{A}_T \sim 40\%$ were found. However, this asymmetry was with the triple product $\mathcal{T}_A$, Eq. (3.56), which exploits the polarisation of the W. This would either require a leptonic top to be reconstructed or the other possibility explored in this paper was to use a c-quark final state that needs to be tagged. This will be extremely difficult at the LHC (or indeed a Linear Collider) and without this final state, the asymmetry drops to around, $\mathcal{A}_T \sim 10\%$, for the triple product $\mathcal{T}_B$, Eq. (3.57).

The study was also performed analytically at the parton level and the cascade decay was focused on without the production process being included.

3.7.2 Stop studies with 3-body $\tilde{\chi}_2^0$ decay

Stop cascade decay chains were again studied in [130] but focused on the three body decay of the $\tilde{\chi}_2^0$,

$$\tilde{t} \rightarrow \tilde{\chi}_2^0 t, \tag{3.58}$$

$$\tilde{\chi}_2^0 \rightarrow \ell^+\ell^-\tilde{\chi}_1^0. \tag{3.59}$$

The three body of the $\tilde{\chi}_2^0$ has the advantage that the amplitude of this process alone is sensitive to CP-phases in the neutralino sector and this study concentrated on these phases. Also, from an experimental point of view, the three body decay has the advantage that we do not need to distinguish the near and far leptons as we do for many triple products in the two body case.

The difference occurs due to the fact that in the case of two, two-body decays of the $\tilde{\chi}_2^0$,

$$\tilde{\chi}_2^0 \to \ell_N^{\pm} \, \tilde{\ell}^{\mp} \, , \tag{3.60}$$

$$\tilde{\ell}^{\mp} \to \ell_F^{\mp} \, \tilde{\chi}_1^0 \, , \tag{3.61}$$

we can factorise the two decays using the narrow width formalism, see Sec. 4.2.2. The narrow width formalism is applicable since both the $\tilde{\chi}_2^0$ and $\tilde{\ell}^{\mp}$ can be approximated as being on-shell. Consequently, the two decays are calculated separately and we have no interference effects between final-state particles produced in different decays.

However, for the three body decay shown in Eq. (3.59), the decay is mediated by various off-shell propagators (Z^0, $\tilde{\ell}_L^{\pm}$, $\tilde{\ell}_R^{\pm}$), see Fig. 4.2, that each contribute. Interference terms between these contributions give rise to the CP-violating triple products. For the explicit expressions that contribute see Appendix B.3.

The study found parton-level asymmetries in the rest frame of the $\tilde{\chi}_2^0$ of up to about, $\mathcal{A}_T \sim 10\%$, for CP-phases in the neutralino sector, Sec. 2.4.3, depending on the particular MSSM scenario. In addition, an estimate was made for the dilution of the asymmetry by the boosted initial state at the LHC. This was done by calculating the average boost of a $\tilde{t}$ produced at the LHC and applying this boost to the decay chain. The estimated dilution of the asymmetry was an order of magnitude.

We extended the above study by explicitly calculating the dominant production channel for $\tilde{t}\tilde{t}^*$ production at the LHC including the relevant parton distribution functions (PDFs) [131]. This study is explained in detail in Chapter 4.

We also added the top decay into the calculations,

$$t \to Wb, \tag{3.62}$$

and by including the top spin correlation, three independent triple products were sensitive to phases in the stop mixing matrix, Sec. 2.4.1.

We found that the rest frame parton-level asymmetry reached a maximum of $\mathcal{A}_T \sim 15\%$ for a particular scenario and this was most sensitive to the phase of the $U(1)$ gaugino mass term, ϕ_{M_1}, in the neutralino sector. However, phases in the stop sector could also be important and maximum asymmetry of $\mathcal{A}_T \sim 8\%$ could be seen as we vary ϕ_{A_t}.

When we introduce the production process and PDFs however, a large dilution in the asymmetry is seen due to the boosted stops. We find that the maximum asymmetry as we vary ϕ_{M_1} is reduced from $\mathcal{A}_T \sim 15\%$ to $\mathcal{A}_T \sim 4\%$ whilst the maximum asymmetry as we vary ϕ_{A_t} is reduced from $\mathcal{A}_T \sim 8\%$ to $\mathcal{A}_T \sim 3\%$. Predictably, the reduction in the observable asymmetry significantly increases the luminosity we would require to see CP-violating effects at the LHC. In this study we presented the first estimates of the luminosity needed to see statistically significant results and found that this would be particularly challenging. For example, we found that for the above decay chain and in the scenarios studied we would require at least $100\,\mathrm{fb}^{-1}$ to observe a 1σ-deviation from zero asymmetry for the CP-phase ϕ_{M_1}, Sec. 4.3.5. To observe a phase for the top trilinear coupling, ϕ_{A_t}, the situation is even more difficult and we require $500\,\mathrm{fb}^{-1}$ to observe a 1σ-deviation from zero asymmetry. For this early study experimental efficiencies or backgrounds were left for later consideration.

3.7.3 Extension of two-body studies

In [132] the same two body stop cascade decay chain as in [129], Sec. 3.7.1, was considered but the effect of the production process and PDFs were estimated. In addition, the relevant branching ratios were included to give an estimate of the required luminosity to see a statistically significant effect at the LHC.

The study found the same maximum asymmetry in the rest frame at parton level, $\sim 40\%$, for the unobservable triple product $\overrightarrow{p_{\ell_t}} \cdot (\overrightarrow{p_t} \times \overrightarrow{p_{\ell_N^\pm}})$, Eq. (3.50), as the phase, ϕ_{A_t} is varied. When the production process and PDFs are included a dilution factor that reduced the asymmetry, $\mathcal{A}_T$, by a factor of ~ 3 was noticed. For the

observable triple product, $\vec{p_{\ell_t}} \cdot (\vec{p_t} \times \vec{p_{\ell_N^\pm}})$, Eq. (3.51), the maximum asymmetry was again found to be significantly less, $\mathcal{A}_T \sim 18\%$ and this was also diluted by another factor of ~ 3 when we introduce the production process and PDFs. However, this triple product also has experimental difficulties as we need to be able to distinguish the near and far lepton in the $\tilde{\chi}_2^0$ decay which will be very challenging. The triple product, $\vec{p_{\ell_t}} \cdot (\vec{p_{\ell_N^\pm}} \times \vec{p_{\ell_F^\mp}})$, Eq. (3.52) avoids these problems but also has the smallest maximum asymmetry at $\mathcal{A}_T \sim 14\%$ in the rest frame and $\mathcal{A}_T \sim 4\%$ in the lab frame.

When estimating the statistical significance at the LHC the study unfortunately bases all of the results around the unobservable triple product that requires both the top momentum and the momentum of the lepton produced by the top. Using this triple product, a 1σ-deviation from zero asymmetry may be seen with as little as 5 fb^{-1}. However, if realistic triple products are used, substantially more luminosity can be expected to be required. Also, no experimental efficiencies or backgrounds were considered and these can be expected to make the situation significantly more challenging.

A similar update for two body sbottom cascade decay chains was presented in [135], c.f. [134] Sec. 3.7.1. The idea was again to include the production process including PDFs at the LHC to try and understand if CP-violating observables may be seen in these decay chains at the LHC.

The results of the study were similar to those presented in the stop study. A rest frame, parton-level asymmetry of up to $\sim 40\%$ could be seen for the unobservable asymmetry that simultaneously requires the momentum of the top and the momentum of the lepton produced by the top, $\mathcal{T}_A$, Eq. (3.56). For an observable, rest frame, parton-level asymmetry $\mathcal{T}_B$, Eq. (3.57), the maximum was up to $\sim 18\%$ and in the lab frame this would be reduced to $\sim 8\%$.

Unfortunately this study also decided to make luminosity estimates for the unobservable asymmetry and found that a minimum of $10\,\text{fb}^{-1}$ would be required to see 1σ-fluctuations at the LHC. Once again substantially more luminosity can be expected to be needed for the realistic triple products. In addition no experimental efficiencies or backgrounds were included.

3.7.4 Momentum reconstruction studies

The studies in Secs. 3.7.1-3.7.3 all suffer from a common problem. Although large rest frame parton-level asymmetries may be seen, these are severely diluted by the boosted production process in the lab frame. To overcome this issue, we examined how to use kinematical invariants in the decay chain to reconstruct the LSP, $\tilde{\chi}_1^0$, momentum. Once the $\tilde{\chi}_1^0$ momentum is known, the momentum of any other particle further up the decay chain can be trivially reconstructed. We first presented the idea in [136], Chapter 5, when it was applied to 1st and 2nd generation squark production. We also used the idea in [133], Chapter 6 when it was applied to $\tilde{t}\tilde{t}^*$ production. In addition, none of the studies presented so far had included any of the many experimental difficulties expected at the LHC. Our study in [136], Chapter 5, was the first to include the kinematical cuts required for the LHC and smearing on the final-state momentum. Also, the combinatorial issues of selecting the correct final-state particles were included. The $\tilde{t}\tilde{t}^*$ study went further by investigating fully hadronic events and their reconstruction. Both Standard Model and SUSY backgrounds were also included to try and gain a realistic idea of whether these measurements would be possible at the LHC.

Our squark study, Chapter 5 [136], investigated the same decay as presented in Sec. 3.7.2 but with a 1st or 2nd generation squark replacing the stop,

$$\tilde{q} \to \tilde{\chi}_2^0 q, \tag{3.63}$$

$$\tilde{\chi}_2^0 \to \ell^+ \ell^- \tilde{\chi}_1^0. \tag{3.64}$$

1st and 2nd generation squarks were chosen for the study as their production cross section at the LHC is significantly higher than stops for the scenarios we considered. Consequently, we hoped that statistically significant observations could occur for lower luminosities. In addition, $\tilde{q}\tilde{g}$ production via,

$$qg \to \tilde{q}\tilde{g}, \tag{3.65}$$

offers the possibility of reconstructing the $\tilde{\chi}_1^0$ momentum and thus, the decaying squark rest frame. This is not possible for $\tilde{t}\tilde{t}^*$ production in the scenarios studied with 3-body $\tilde{\chi}_2^0$ decay since we do not have enough kinematic constraints to solve

the system. A drawback to studying the squark decay however, is that we are only sensitive to CP-violating phases in the neutralino mass matrix. Since the quark will not transfer any spin correlations we are not sensitive to any imaginary couplings at the squark decay vertex.

Our study found that the rest frame parton-level asymmetry was similar to that of the stop study with $\mathcal{A}_T \sim 15\%$. However, after the PDFs and the production process is included, the asymmetry drops to $\mathcal{A}_T \sim 2\%$ (this also includes a dilution due to anti-squarks being present in the sample). When momentum reconstruction is performed though, the observable asymmetry rises to $\mathcal{A}_T \sim 15\%$ and shows the power of this technique.

When estimating the expected luminosity required to see CP-violating effects at the LHC, the study presented the first attempt at including some of the experimental factors that are expected to be important. Selection cuts were performed on the process and experimental smearing of the final-state particles was added. The minimum luminosity at which CP-phases may be seen at the statistically significant 3σ-level was estimated to be $100\,\text{fb}^{-1}$.

We then applied the same idea of momentum reconstruction to $\tilde{t}\tilde{t}^*$ production, Chapter 6 [133], with the decay chains discussed in Sec. 3.7.1 and Sec. 3.7.3 but with a fully hadronic top decay,

$$\tilde{t} \rightarrow \tilde{\chi}_2^0 t, \tag{3.66}$$

$$\tilde{\chi}_2^0 \rightarrow \ell_N^\pm \tilde{\ell}^\mp \rightarrow \ell_N^\pm \ell_F^\mp \tilde{\chi}_1^0, \tag{3.67}$$

$$t \rightarrow bW \rightarrow bjj. \tag{3.68}$$

We now have a two body decay of the $\tilde{\chi}_2^0$ and thus enough kinematic conditions to solve the system and find the $\tilde{\chi}_1^0$ momentum, Sec. 6.3. In addition, only a single $\tilde{t}$ decay chain is required for the momentum reconstruction, whereas for the $\tilde{q}\tilde{g}$ production discussed above, the decay chain of the both the $\tilde{q}$ and the $\tilde{g}$ needs to be included, Sec. 5.3.

We found the same maximum rest frame parton-level asymmetry as discussed before at $\mathcal{A}_T \sim 15\%$. When the production process and PDFs were included this

maximum asymmetry is reduced to $\mathcal{A}_T \sim 4\%$. The study then attempted to perform reconstruction at the hadronic level for complete events and found that this was a realistic proposal with the asymmetry returning to the rest frame level. None of the Standard Model backgrounds were found to be an issue within the limitations of the study as the reconstruction procedure severely reduces the background. The expected minimum luminosity required if we only consider $\tilde{t}\tilde{t}^*$ production is $300\,\mathrm{fb}^{-1}$ to see a 3σ-statistical deviation. The general SUSY background was found to be much more of an issue and extra cuts on top of the reconstruction procedure were required to improve the signal to background ratio. With the SUSY background included we would require a minimum of $500\,\mathrm{fb}^{-1}$ to see a 3σ-deviation.

For more information on both the studies presented in this section see Chapter 5 and Chapter 6.

3.7.5 Stop to taus

An additional study that considered using triple product correlations to search for CP-violation in SUSY cascade decays was [137]. The study considered the following two body decay chain,

$$\tilde{t}_2 \rightarrow H_i \tilde{t}_1, \tag{3.69}$$

$$H_i \rightarrow \tau^+ \tau^- \tag{3.70}$$

where the covariant product is built from the taus,

$$\epsilon^{\mu\nu\rho\sigma}(p_{\tau^+}^\mu, s_{\tau^+}^\nu, p_{\tau^-}^\rho, s_{\tau^-}^\sigma), \tag{3.71}$$

and $s_{\tau^\pm}^\mu$ are the spin vectors of the individual taus.

To generate large asymmetries, the study requires the interference between closely degenerate Higgs states, H_i. If this requirement is satisfied though, the asymmetries can reach the very large maximum of $\mathcal{A} \sim 90\%$.

However, the study does face formidable experimental challenges. Firstly, at least one of the tau spins in Eq. (3.71) must be measured on an event-by-event basis and this is expected to be very difficult at the LHC. Secondly, the backgrounds to hadronic taus will be substantial and it is not clear if the final-state of Eq. (3.69,3.70) will be reconstructible with a high enough signal to background ratio.

3.8   Decay rate asymmetries

Another potential way to observe CP-violation in SUSY at colliders is via decay rate asymmetries. As an example we choose the possible asymmetry for the decay of $\tilde{\chi}_1^{\pm} \to \tilde{\chi}_1^0 W^{\pm}$ [99],

$$\mathcal{A}_{\Gamma} = \frac{\Gamma_{(+)}(\tilde{\chi}_1^+ \to \tilde{\chi}_1^0 W^+) - \Gamma_{(-)}(\tilde{\chi}_1^- \to \tilde{\chi}_1^0 W^-)}{\Gamma_{(+)}(\tilde{\chi}_1^+ \to \tilde{\chi}_1^0 W^+) + \Gamma_{(-)}(\tilde{\chi}_1^- \to \tilde{\chi}_1^0 W^-)}, \tag{3.72}$$

where $\Gamma_{+(-)}$ is the decay rate for the positively (negatively) charged $\tilde{\chi}^{+(-)}$ respectively. The observable is therefore just a simple counting experiment between the different final states and the statistical significance will be the same as detailed in Sec. 3.6.

For most decays these asymmetries can be expected to be small as they can only contribute at the loop level. However, for certain decays, the loop corrections can become large ($\mathcal{A}_{\Gamma} \sim 15\%$) with the right couplings and kinematics [100].

Many different decay processes have now been investigated in the context of the MSSM at the LHC. For example in Higgs decays [100, 102], stop decays [138, 139] and charginos [99].

Chapter 4

Stop production and three body neutralino decay

4.1 Introduction

In this chapter we study the production of stops at the LHC and the subsequent cascade decay chain [131],

$$\tilde{t}_i \to \tilde{\chi}_j^0 + t \to \tilde{\chi}_1^0 \ell^+ \ell^- + Wb. \tag{4.1}$$

The cascade is sensitive to CP-violating couplings in both the $\tilde{t}_i$ and $\tilde{\chi}_j^0$ decay. Thus the chain is sensitive to CP-violating couplings in both the neutralino and stop mixing matrices (Sec. 2.4.1 and Sec. 2.4.3). In this thesis we set the phase $\phi_\mu = 0$ due to EDM constraints, Sec. 2.5, and therefore concentrate on the phases ϕ_{M_1} and ϕ_{A_t} in this chapter.

As our main observable we use triple product correlations that are explained in detail in Sec. 3.3. The correlation allows us to create a CP-sensitive asymmetry that is explained in Sec. 3.4.

The first CP-odd asymmetry we consider is formed from $\mathcal{T}_t = \vec{p}_t \cdot (\vec{p}_{\ell^+} \times \vec{p}_{\ell^-})$. This quantity has been studied at the parton level in [130], assuming pure gaugino-like neutralinos. In this chapter we extend that work by providing fully analytic expressions for the squared amplitude of the whole cascade process including full spin correlations. In addition, we study the complete neutralino mixing matrix in

order to see the effect of higgsino states and include scenarios where the neutralinos of interest may be mainly higgsino-like.

A major open question of [130] was the exact effect that including the production process and Parton Distribution Functions (PDFs) would have on the asymmetry, see Sec. 3.5. The effect was only estimated in the previous study as being an order of magnitude but here we calculate the dilution explicitly by completing the full phase-space calculation. We see that including the PDFs has a big dilution effect on the measurability of a CP-odd asymmetry.

In [129], further CP sensitive asymmetries formed from the momentum of the top decay products were studied under the assumption of 2-body neutralino decays into on-shell sleptons, namely $\mathcal{T}_b = \vec{p}_b \cdot (\vec{p}_{\ell^+} \times \vec{p}_{\ell^-})$ and $\mathcal{T}_{tb} = \vec{p}_b \cdot (\vec{p}_t \times \vec{p}_{\ell^\pm})$. These variables are sensitive to ϕ_{M_1} and ϕ_{A_t}, but have different dependences on the CP-violating phases as described in Section 4.2.4. Both of these CP-violating triple products are produced at the stop decay vertex and therefore our decay chain is also sensitive to these effects. Indeed, we can go further by combining all three observables which would in principle allow one to disentangle the influences of both ϕ_{M_1} and ϕ_{A_t}.

Since T-odd observables can also be generated by final-state interactions at the one-loop level, one should in principle combine the asymmetry for a process with that of its charge-conjugated process, Eq. (3.40). If a non-zero asymmetry is then observed in this combination, it must correspond to a violation of CP symmetry.

To do this we must tag the charge of the $\tilde{t}_i$ involved in the cascade decay, Eq. (4.1). Tagging the charge is possible if the t, produced by the $\tilde{t}_i$, decays leptonically. Alternatively, since the dominant production channels at the LHC are via pair production, $pp \rightarrow \tilde{t}_i \tilde{t}_i^*$, we could tag the charge of the $\tilde{t}_i^*$ produced in association. If we know the charge of the opposite $\tilde{t}_i^*$, we know the charge of the $\tilde{t}_i$ that we are interested in.

In the following study, both of these approaches are taken, depending upon the triple product being studied. For the triple products $\mathcal{T}_t$ and $\mathcal{T}_{tb}$, we require the momentum of the top to be reconstructed. Therefore, we cannot use a leptonically decaying top in the triple product cascade decay, since the momentum of the associated neutrino is lost. Instead, for these triple products we must use the decay

of the opposite $\tilde{t}_i^*$ to tag the charge. In all the scenarios we consider, the decay $\tilde{t} \to \tilde{\chi}_i^+ b$, is dominant, enabling charge identification from the leptonic decay of the $\tilde{\chi}_i^+$. However, a detailed simulation including all combinatorial aspects and also other background processes would be required to validate this possibility and is not included in this study.

For the triple product, $\mathcal{T}_b$, we do not require the momentum of the top. Therefore, it may be possible to use a leptonically decay t to tag the charge of the $\tilde{t}_i$. This approach has the potential advantage that we can ignore the opposite cascade decay. However, it must be noted that fully hadronic top decays will also work with this triple product, using the opposite cascade decay tag mentioned previously.

In addition to looking for CP-violating effects in triple products we also consider the possibility of looking at the masses and branching ratios of the particles involved our decay chain, Eq. 4.1. Both of these observables are CP-even quantities and are therefore not an unambiguous indicator of CP-violation though. However, it may be possible to use these observables in combination with the triple products to constrain the CP-violating phases more accurately. We also consider the accuracy of these measurements at the LHC to see whether this is a realistic proposition.

We begin this chapter by describing the process under consideration in Sec. 4.2, including the calculation method, the phases involved and their various effects. In Sec. 4.3 we present numerical results for three specific benchmark scenarios and discuss the potential for a measurement at the LHC. The Appendices A-C contain details of the Lagrangian, the expression for the squared amplitude including full spin correlations and the kinematics of the phase space in the laboratory system.

4.2 Formalism

4.2.1 Process studied

We study the dominant stop production process at the LHC, namely
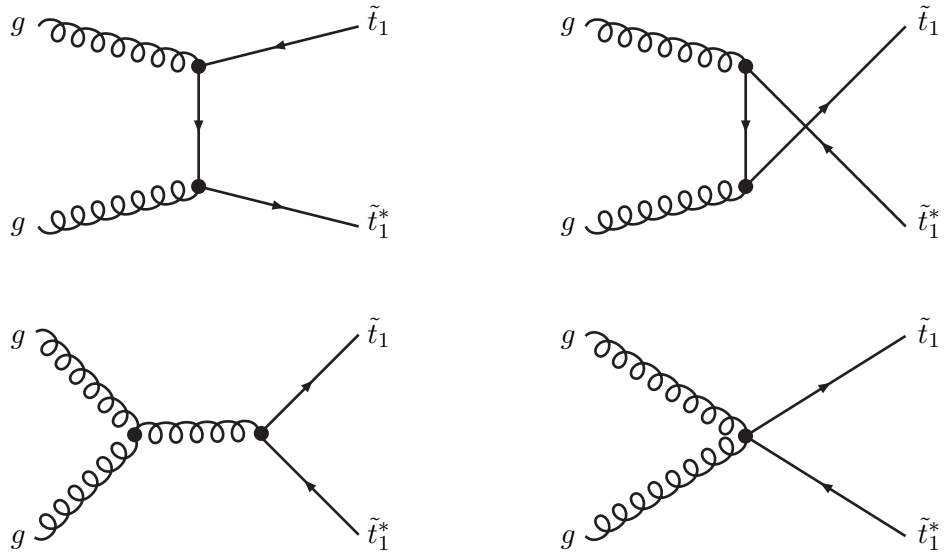
$$gg \to \tilde{t}_i \tilde{t}_i^*, \tag{4.2}$$

Figure 4.1: Feynman diagrams for the production process $gg \to \tilde{t}_1 \tilde{t}_1^*$.

with the subsequent decay chain

$$\tilde{t}_i \to \tilde{\chi}_j^0 + t \to \tilde{\chi}_1^0 \ell^+ \ell^- + Wb. \tag{4.3}$$

At tree level, the production process (4.2) proceeds via g exchange in the direct channel and $\tilde{t}$ exchange in the crossed channel, and via a quartic coupling, as shown in Fig. 4.1. Another possible source of $\tilde{t}_i$s is their production in gluino decays, $\tilde{g} \to \tilde{t}_i t$. However this leads to an experimentally more complex topology than the direct production and consequently we do not investigate this channel.

Since gluons do not couple to off-diagonal combinations of stop mass eigenstates, $\tilde{t}_1 \bar{\tilde{t}}_2$ production occurs only at the loop level, and we do not consider it here. We focus here on $\tilde{t}_1 \bar{\tilde{t}}_1$ production, since the reconstruction of full decay chains of $\tilde{t}_1$ seems achievable, even in the complex experimental environment at the LHC. With the exception of the stop mass eigenvalues, see Sec. 2.4.1, no effects from supersymmetric CP-violating couplings occur in the tree-level production process.

The first step in the cascade decay chain is the two-body process,

$$\tilde{t}_i \to t \tilde{\chi}_2^0. \tag{4.4}$$

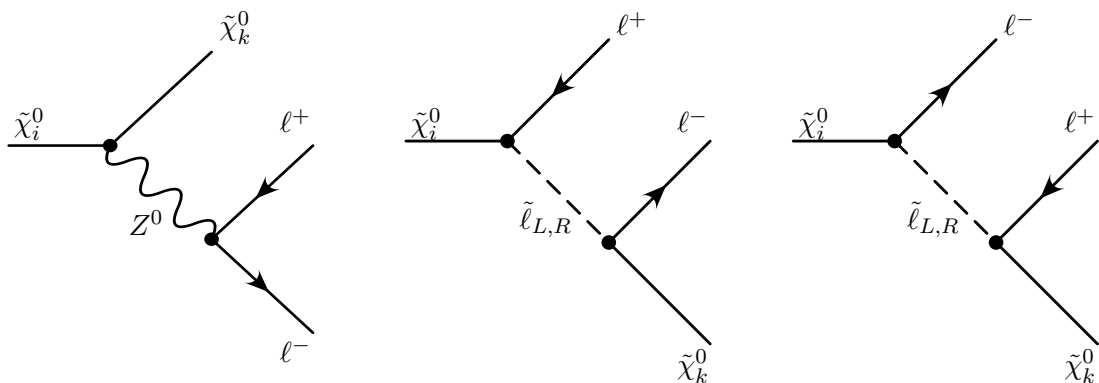Here CP-violating couplings of the $\tilde{t}_1$ enter as well as those of the $\tilde{\chi}_2^0$, and are

Figure 4.2: Feynman diagrams for the three-body decays $\tilde{\chi}_i^0 \to \tilde{\chi}_k^0 \ell^+ \ell^-$.

dominated by the phases ϕ_{A_t} and ϕ_{M_1}, see Appendix B.1 [1]. We consider spectra where the second steps in the cascade decay chains are the three-body decays of the neutralino,

$$\tilde{\chi}_2^0 \to \tilde{\chi}_1^0 \ell^+ \ell^- \, , \tag{4.5}$$

(cf. Appendix B.3) and the dominant top decay $t \to Wb$ (cf. Appendix B.6). The neutralino decay occurs via Z^0 or $\tilde{\ell}_{L,R}$ exchanges, see Fig. 4.2. It is very sensitive to CP-violating supersymmetric couplings, and its structure has been studied in detail in [112, 140]. The phase ϕ_{M_1} (and also ϕ_μ, which has been set to zero here) affects the mass of the $\tilde{\chi}_2^0$, as well as its couplings and decay rates.

4.2.2 Narrow width formalism and spin correlations

In principle we should not split the production and various decays of the cascade into separate steps. Instead, we should just take the initial state and calculate all possible diagrams (including interference terms) that lead to the final state. However, in practice we would need to calculate a large number of diagrams and each individual diagram would have significant complexities.

Therefore, we use the narrow width formalism [141] to factorize the full process

---

[1]Their structure has also been studied in detail in [129].

into the production and each individual decay. The formalism assumes that each intermediate particle (apart from the off-shell exchange particles) in the decay chain can be approximated as being on-shell. This can be considered a good estimate when the width of the particular particle in the decay chain is small compared to its mass, $\Gamma << m$. This implies that the Breit-Wigner resonance shape can be approximated by a δ function in the decays,

$$\frac{1}{(q^2 - m^2)^2 + m^2\Gamma^2} \to \frac{\pi}{m\Gamma}\delta(q^2 - m^2)\,. \tag{4.6}$$

Studies have now been performed in the MSSM to look at the validity of the approximation and where it breaks down [142, 143]. An additional requirement is found that the sum of the mass of the daughter particles should be less than $\sim 90\%$ of the mass of the parent.

We use the definition of the narrow width propagator [140], $|\Delta|^2$, in this thesis that absorbs the factor of π into the phase-space calculation, and introduces a factor of E, so that the partial width, $\hat{\Gamma}$ (Appendix C), is calculated in the laboratory frame,

$$|\Delta|^2 = \frac{E}{m\Gamma}\delta(q^2 - m^2)\,. \tag{4.7}$$

However, to correctly calculate the angular distribution of the decay chain and produce the triple product correlations that we are interested in, the narrow width formalism alone is not sufficient. If the 'on-shell' propagator has spin (e.g a fermion in our decays), an angular correlation will form between the production and decay of the particle. Therefore, we need to include the spin dependence for each decay and the correlation between decays.

We follow the Bouchiat-Michel formalism [141, 144, 145] and introduce 3 four vectors s^a_μ, $a = 1, 2, 3$ for the spin of each 'on-shell' fermion propagator. The s^a and p/m form an orthonormal set of four-vectors,

$$p \cdot s^a = 0\,, \tag{4.8}$$

$$s^a \cdot s^b = -\delta^{ab}\,, \tag{4.9}$$

$$s^a_\mu s^a_\nu = -g_{\mu\nu} + \frac{p_\mu p_\nu}{m^2}\,, \tag{4.10}$$

where repeated indices are implicitly summed over. We can explicitly choose a

particular basis for the set of 3 four vectors for the $\tilde{\chi}_2^0$, Eqs. (B.7.45-B.7.47), or $\tilde{t}_1$, Eqs. (B.7.48-B.7.50).

The above formalism has the advantage of allowing the calculation to be performed with or without explicit spin vectors. One possible method is to contract the spin vectors between the production and decay of a particular particle analytically and effectively merge the squared matrix elements. Alternatively, the amplitudes can be calculated with an explicit set of spin vectors and the correlation will only be visible when the phase-space integral is performed. Hence, we are able to check that the spin correlations have been calculated correctly by comparing the two results.

4.2.3 Squared amplitude

Using the above formalism, Sec. 4.2.2, the squared amplitude $|T|^2$ of the full process can be factorized into the processes of production $gg \to \tilde{t}_1 \bar{\tilde{t}}_1$ and the subsequent decays $\tilde{t}_1 \to t\tilde{\chi}_2^0$, $\tilde{\chi}_2^0 \to \tilde{\chi}_1^0 \ell^+ \ell^-$ and $t \to Wb$, with the second $\tilde{t}_1$ being neglected in the analysis. We apply the narrow-width approximation for the propagators of the intermediate particles, $\tilde{t}_1$, $\tilde{\chi}_2^0$ and t, which is appropriate since the widths of the respective particles are in all cases much smaller than their masses, cf. Table 4.3.1. The squared amplitude can then be expressed in the form

$$
\begin{aligned}
|T|^2 &= |\Delta(\tilde{t}_1)|^2 |\Delta(\tilde{\chi}_2^0)|^2 |\Delta(t)|^2 P(\tilde{t}_1 \tilde{t}_1) \Big\{ P(\tilde{\chi}_2^0 t) D(\tilde{\chi}_2^0) D(t) + \sum_{a=1}^{3} \Sigma_P^a(\tilde{\chi}_2^0) \Sigma_D^a(\tilde{\chi}_2^0) D(t) \\
&\quad + \sum_{b=1}^{3} \Sigma_P^b(t) \Sigma_D^b(t) D(\tilde{\chi}_2^0) + \sum_{a,b=1}^{3} \Sigma_P^{ab}(\tilde{\chi}_2^0 t) \Sigma_D^a(\tilde{\chi}_2^0) \Sigma_D^b(t) \Big\},
\end{aligned}
\tag{4.11}
$$

where $a = 1, 2, 3$ refers to the polarisation states of the neutralino $\tilde{\chi}_i^0$ and top quark, which are described by the polarisation vectors $s^a(\tilde{\chi}_i^0)$, $s^b(t)$ given in Appendix B.1. In addition,

- $\Delta(\tilde{t}_1)$, $\Delta(\tilde{\chi}_2^0)$ and $\Delta(t)$ are the 'propagators' of the intermediate particles which lead to the factors $E_{\tilde{t}_1}/m_{\tilde{t}_1}\Gamma_{\tilde{t}_1}$, $E_{\tilde{\chi}_2^0}/m_{\tilde{\chi}_2^0}\Gamma_{\tilde{\chi}_2^0}$ and $E_t/m_t\Gamma_t$ in the narrow-width approximation, Eqs. (4.6,4.7).

- $P(\tilde{t}_1 \tilde{t}_1)$, $P(t\tilde{\chi}_2^0)$, $D(\tilde{\chi}_i^0)$ and $D(t)$ are the terms in the production and decay, Sec. B.1, B.3, B.6 respectively, that are independent of the polarisations of the

decaying neutralino and top, whereas

- $\Sigma_P^a(\tilde{\chi}_i^0)$, $\Sigma_P^b(t)$, $\Sigma_P^{ab}(\tilde{\chi}_2^0 t)$ and $\Sigma_D^a(\tilde{\chi}_i^0)$, $\Sigma_D^b(t)$, Sec. B.1, B.3, B.6 respectively, are the terms containing the correlations between production and decay spins of the $\tilde{\chi}_2^0$ and t.

According to our choice of the polarisation vectors $s^a(\tilde{\chi}_i^0)$ $[s^b(t)]$, see Eqs. (B.7.45)–(B.7.50) in Appendix B.1, Σ_P^3/P is the longitudinal polarisation, Σ_P^1/P is the transverse polarisation in the production plane, and Σ_P^2/P is the polarisation perpendicular to the reference plane of the neutralino $\tilde{\chi}_i^0$ [top quark t].

4.2.4   Structure of the T-odd asymmetries

As introduced in Sec. 3.3, suitable tools to study CP-violating effects are T-odd observables based on triple products of momenta or spin vectors of the involved particles. In this chapter we study the following T-odd observables,

$$\mathcal{T}_t = \vec{p}_t \cdot (\vec{p}_{\ell^+} \times \vec{p}_{\ell^-}) , \tag{4.12}$$

$$\mathcal{T}_b = \vec{p}_b \cdot (\vec{p}_{\ell^+} \times \vec{p}_{\ell^-}) , \tag{4.13}$$

$$\mathcal{T}_{tb} = \vec{p}_t \cdot (\vec{p}_b \times \vec{p}_{\ell^\pm}). \tag{4.14}$$

The T-odd asymmetries, Sec. 3.4 can then be defined for each triple product as,

$$\mathcal{A}_{T_f} = \frac{N_{\mathcal{T}_f+} - N_{\mathcal{T}_f-}}{N_{\mathcal{T}_f+} + N_{\mathcal{T}_f-}} = \frac{\int \mathrm{sign}\{\mathcal{T}_f\}|T|^2 d\mathrm{lips}}{\int |T|^2 d\mathrm{lips}}, \qquad f = t, b \text{ and } tb, \tag{4.15}$$

where $N_{\mathcal{T}_f+}$, $N_{\mathcal{T}_f-}$ are the numbers of events for which $\mathcal{T}_f$ is positive and negative respectively, and the second denominator in (4.15), $\int |T|^2 d\mathrm{lips}$, is proportional to the corresponding cross section, namely $\sigma(gg \to \tilde{t}_1 \tilde{t}_1^* \to t\tilde{\chi}_1^0 \ell^+ \ell^-)$ in Eq.(4.12) and $\sigma(gg \to \tilde{t}_1 \tilde{t}_1^* \to Wb\tilde{\chi}_1^0 \ell^+ \ell^-)$ in Eqs. (4.13) and (4.14). In the second numerator in (4.15), the triple-product correlations only enter via the spin-dependent terms, as explained in Eq. (4.17) and the following sections.

The observable $\mathcal{A}_{T_b}$ has the advantage that it is not necessary to reconstruct the momentum of the decaying t quark. However, as explained below, in order to disentangle the effects of both phases of A_t and M_1, it will be necessary to study all possible observables.

As can be seen from the numerator of $\mathcal{A}_{T_f}$, in order to identify the T-odd contributions, we have to identify those terms in $|T|^2$, Eq. (4.11), which contain a triple product of the form shown in Eqs. (4.12)–(4.14).

As shown in Eq. (3.34), triple products are produced when covariant products, $i\epsilon_{\mu\nu\rho\sigma}a^\mu b^\nu c^\rho d^\sigma$, are found in the amplitude squared of the process. In our process, T-odd terms with ϵ-tensors are only contained in the spin-dependent contributions to the production, $\Sigma_P^{ab}(\tilde{\chi}_j^0 t)$, and in the spin-dependent terms in neutralino decay, $\Sigma_D^a(\tilde{\chi}_j^0)$. It is therefore convenient to split $\Sigma_P^{ab}(\tilde{\chi}_j^0 t)$ and $\Sigma_D^a(\tilde{\chi}_j^0)$ into T-odd terms $\Sigma_P^{ab,\mathrm{O}}(\tilde{\chi}_j^0 t)$ and $\Sigma_D^{a,\mathrm{O}}(\tilde{\chi}_j^0)$ containing the respective triple products, and T-even terms $\Sigma_P^{ab,\mathrm{E}}(\tilde{\chi}_j^0 t)$ and $\Sigma_D^{a,\mathrm{E}}(\tilde{\chi}_j^0)$ without triple products,

$$\Sigma_P^{ab}(\tilde{\chi}_j^0 t) = \Sigma_P^{ab,\mathrm{O}}(\tilde{\chi}_j^0 t) + \Sigma_P^{ab,\mathrm{E}}(\tilde{\chi}_j^0 t), \qquad \Sigma_D^a(\tilde{\chi}_j^0) = \Sigma_D^{a,\mathrm{O}}(\tilde{\chi}_j^0) + \Sigma_D^{a,\mathrm{E}}(\tilde{\chi}_j^0). \quad (4.16)$$

The other spin-dependent contributions $\Sigma_P^a(\tilde{\chi}_j^0)$ and $\Sigma_P^b(t)$, as well as $\Sigma_D^b(t)$, are T-even.

When multiplying these terms together and composing a T-odd quantity, the only terms of $|T|^2$, Eq. (4.11), which contribute to the numerator of $\mathcal{A}_{T_f}$ are therefore,

$$|T|^2 \supset \sum_{a,b=1}^{3} \left[\Sigma_P^{ab,\mathrm{O}}(\tilde{\chi}_j^0 t)\Sigma_D^{a,\mathrm{E}}(\tilde{\chi}_j^0)\Sigma_D^b(t) \quad + \quad \Sigma_P^{a,\mathrm{E}}(\tilde{\chi}_j^0)\Sigma_D^{a,\mathrm{O}}(\tilde{\chi}_j^0) \right. $$
$$\left. + \quad \Sigma_P^{ab,\mathrm{E}}(\tilde{\chi}_j^0 t)\Sigma_D^{a,\mathrm{O}}(\tilde{\chi}_j^0)\Sigma_D^b(t) \right]. \quad (4.17)$$

The first term in Eq. (4.17) is sensitive to the T-odd contributions from the production of the top and the neutralinos $\tilde{\chi}_j^0$. Comparing Eq.(B.1.9) with Eq.(B.3.25) and (B.6.44) leads to the following possible combination of contributing momenta,

$$\Sigma_P^{ab,\mathrm{O}}(\tilde{\chi}_j^0 t)\Sigma_D^{a,\mathrm{E}}(\tilde{\chi}_j^0)\Sigma_D^b(t) \sim \epsilon_{\mu\nu\rho\sigma}s^{a,\mu}(\tilde{\chi}_j^0)p_{\tilde{\chi}_j^0}^\nu s^{b,\rho}(t)p_t^\sigma \times (p_{[\ell^+,\ell^-]}s^a)(p_{[b,W]}s^b). \quad (4.18)$$

The second term and third terms in Eq. (4.17) are only sensitive to T-odd contributions from the neutralino $\tilde{\chi}_j^0$ decay. The second term depends only on the polarization of $\tilde{\chi}_j^0$, comparing Eq.(B.3.32) with Eq.(B.1.5) therefore leads to the only possible combination of momenta,

$$\Sigma_P^{a,\mathrm{E}}(\tilde{\chi}_j^0)\Sigma_D^{a,\mathrm{O}}(\tilde{\chi}_j^0) \sim (p_t s^a) \times \epsilon_{\mu\nu\rho\sigma}s^{a\mu}p_{\tilde{\chi}_j^0}^\nu p_{\ell^-}^\rho p_{\ell^+}^\sigma. \quad (4.19)$$

Since the third term depends on the polarization of both fermions, $\tilde{\chi}_j^0$ and t, the possible combinations, comparing Eq.(B.3.32) with Eq.(B.1.8) and (B.6.44), are,

$$\Sigma_P^{ab,\mathrm{E}}(\tilde{\chi}_j^0 t)\Sigma_D^{a,\mathrm{O}}(\tilde{\chi}_j^0)\Sigma_D^b(t) \quad \sim \quad (p_t s^a)(p_{\tilde{\chi}_j^0} s^b)(s^b p_{[b,W]}) \times \epsilon_{\mu\nu\rho\sigma} s^{a\mu} p_{\tilde{\chi}_j^0}^\nu p_{\ell-}^\rho p_{\ell+}^\sigma \quad (4.20)$$

$$\text{and} \quad (s^a s^b)(s^b p_{[b,W]}) \times \epsilon_{\mu\nu\rho\sigma} s^{a\mu} p_{\tilde{\chi}_j^0}^\nu p_{\ell-}^\rho p_{\ell+}^\sigma. \quad (4.21)$$

As can be seen by substituting Eqs. (B.7.45)–(B.7.50) into Eq. (B.1.9) in Appendix B.1, $\Sigma_P^{ab,\mathrm{O}}(\tilde{\chi}_j^0 t)$ vanishes for the combinations $(ab) = (11), (22), (33), (13), (31)$, because they contain cross products of three linearly-dependent vectors. Only for the remaining combinations, $(ab) = (12), (21), (23), (32)$, do we get a T-odd contribution to the production density matrix.

Similarly, the expression for the T-even contributions, $\Sigma_P^{ab,E}(\tilde{\chi}_j^0 t)$, Eq. (B.1.8) in Appendix B.1, has non-zero components for $a = 1, 3$ but vanishes when $a = 2$. These expressions are multiplied by $\Sigma_D^{a,\mathrm{O}}(\tilde{\chi}_j^0)$, Eq. (B.3.32), and therefore only $\Sigma_D^{1,\mathrm{O}}(\tilde{\chi}_j^0)$ and $\Sigma_D^{3,\mathrm{O}}(\tilde{\chi}_j^0)$ contribute.

In the following section we derive the three triple products, study their different dependence on phases and provide explicitly a strategy for determining ϕ_{A_t} and ϕ_{M_1} and disentangling their effects.

4.2.5 Strategy for determining ϕ_{A_t} and ϕ_{M_1}

Derivation of the triple products

Contracting the spin indices via Eq.(4.10) on Eqs.(4.18)–(4.21) lead to kinematic expressions that only contain explicit momenta. We can the expand the terms with covariant products ($\epsilon_{\mu\nu\rho\sigma}$), as explained before, Eq. (3.34), in explicit momentum components to produce scalar triple products of the momentum between three independent particles.

In our process we can classify the terms of Eq.(4.17) as follows:

- The terms of Eq.(4.18) lead to a combination between $\mathcal{T}_{tb}$ and $\mathcal{T}_b$.

- The terms of Eq.(4.19) lead only to $\mathcal{T}_t$.

- The terms of Eq.(4.20) lead again only to $\mathcal{T}_t$ but terms of Eq.(4.21) produce $\mathcal{T}_t$ as well as $\mathcal{T}_b$, due to interference effects between both spin vectors of p_t and $p_{\tilde{\chi}_j^0}$.

T-odd terms sensitive to $\mathcal{T}_t$

We consider first $\mathcal{T}_t$, Eq. (4.12). As this includes the reconstructed top quark momentum, there are no spin terms from the decay of the top quark and the contributing terms are the second and third term in Eq. (4.17) as explained in the previous paragraph. The CP-sensitive terms of the decay density matrix are given by Eqs. (B.3.32)–(B.3.35) and the contributing kinematical factor is g_4^a, Eq.(B.3.36),

$$g_4^a = im_k \epsilon_{\mu\nu\rho\sigma} s^{a\mu} p_{\tilde{\chi}_j^0}^{\nu} p_{\ell^-}^{\rho} p_{\ell^+}^{\sigma}. \tag{4.22}$$

We note that g_4^a is purely imaginary. When inserted, for instance, in Eq. (B.3.34) it is multiplied by the coupling,

$$\mathrm{Im}\{a_{Lj}^{\tilde{\ell}*} a_{Lk}^{\tilde{\ell}} O_{kj}^L\}. \tag{4.23}$$

See Eq. (A.2.8) and Eq. (A.4.23) for exact parameter dependence.

Both couplings depend on the phases ϕ_{M_1} (and ϕ_μ) and the factor contributes to $\Sigma_D^{a,\mathrm{O}}$. Analogous contributions follow from Eqs. (B.3.33) and (B.3.35). The corresponding T-even terms of the production density matrix also entering in Eq. (4.17) are obtained from Eq. (B.1.5).

T-odd terms sensitive to $\mathcal{T}_{tb}$

For the triple product $\mathcal{T}_{tb}$, Eq. (4.14), only the first term in Eq. (4.17) contributes, but the kinematics are complicated by the fact that we need to include the decay of the t in addition to that of the $\tilde{\chi}_2^0$. This comes from the fact that the kinematical term that generates the triple product is f_4^{ab}, Eq.(B.1.10):

$$f_4^{ab} = \epsilon_{\mu\nu\rho\sigma} s^{a,\mu}(\tilde{\chi}_j^0) p_{\tilde{\chi}_j^0}^{\nu} s^{b,\rho}(t) p_t^{\sigma}. \tag{4.24}$$

As both $s^{a,\mu}(\tilde{\chi}_j^0)$ and $s^{b,\rho}(t)$ are contained in this term, we need to include their spin correlated decays in order to produce a non-zero contribution.

This term occurs only once in the $\tilde{t}$ decay amplitude, Eq. (B.1.9), and is multiplied by the complex pre-factor $g^2 Im(a_{ij} b_{ij}^*)$, Eq. (B.1.11). Both a_{ij} and b_{ij} contain terms from the $\tilde{t}$ and $\tilde{\chi}_j^0$ mixing matrices, and so are sensitive to both the phases ϕ_{A_t} and ϕ_{M_1} (and ϕ_μ).

T-odd terms sensitive to $\mathcal{T}_b$

The triple product $\mathcal{T}_b$, Eq. (4.13), is the most complicated, as it contains contributions from both the $\tilde{t}$ and $\tilde{\chi}_2^0$ decays (the first and third terms in Eq. (4.17)). The kinematics is rendered more complex by the need to multiply each T-odd contribution by the terms from the other two decays. Each T-odd component is generated through g_4^a and f_4^{ab}, as for the other two triple products. As a consequence of having a dependence on both the $\tilde{t}$ and $\tilde{\chi}_2^0$ decays, $\mathcal{T}_b$ is also sensitive to both phases ϕ_{A_t} and ϕ_{M_1} (and ϕ_μ).

Disentangling of effects of ϕ_{A_t} and ϕ_{M_1}

The T-odd asymmetries, Eq.(4.15), are determined by those CP-violating couplings that are multiplied with the respective triple product. Under the assumption that ϕ_μ is small, the neutralino sector depends only on ϕ_{M_1} and the stop sector only on ϕ_{A_t}. Since the involved triple product momenta show different dependence on the CP-violating phases, as discussed above, it is possible in principle to disentangle the effects of ϕ_{A_t} and ϕ_{M_1} in our process and to determine the phases separately.

The decoupling is possible as the triple product $\mathcal{T}_t$, can only be produced by the term, $\Sigma_P^{a,\mathrm{E}}(\tilde{\chi}_j^0)\Sigma_D^{a,\mathrm{O}}(\tilde{\chi}_j^0)$, cf. section 4.2.5. The T-odd contribution in this term comes from the decay of the $\tilde{\chi}_j^0$ and consequently is only sensitive to the phase ϕ_{M_1}. Once we have used the triple product $\mathcal{T}_t$ to determine the phase ϕ_{M_1} we can then use the value as an input for the triple products, $\mathcal{T}_{tb}$ and $\mathcal{T}_b$, in order to determine the phase ϕ_{A_t}.

4.3   Results

4.3.1   Scenarios

In this Section we analyse numerically the various triple-product asymmetries introduced in Eqs. (4.12)–(4.14) at both the parton level and with the inclusion of parton distribution functions (PDFs) to study the discovery potential at the LHC. In particular, we study the dependences of these triple-product asymmetries on the MSSM parameters $M_1 = |M_1|e^{i\phi_{M_1}}$ and $A_t = |A_t|e^{i\phi_{A_t}}$. We also analyse the effects of these parameters on the masses and branching ratios of the particles involved in our process.

Scenario	A: Reference	B: NUHM - γ	C: Higgsino
M_1	109	97.6	105
M_2	240	184	400
μ	220	316	-190
$\tan\beta$	10	20	20
M_L	298	366	298
M_E	224	341.7	224
M_{Q3}	511	534.5	511
M_{U3}	460	450	460
A_t	-610	-451.4	-610

Table 4.1: Parameters for the three scenarios A, B, C considered in this chapter. The parameters M_2, $|\mu|$ and $\tan\beta$ in scenario B are chosen as for the scenario SPS1a in [146]. We used $m_t = 171.2$ GeV [20] and the SM value for the top width $\Gamma_t \sim 1.5$ GeV [147] for our study. All masses and widths are given in GeV.

For our numerical analysis we study in detail at both the partonic and PDF level a reference scenario, A, where the $\tilde{\chi}_2^0$ is a gaugino-higgsino mixture. For comparison, we also study at the partonic level a non-universal Higgs masses (NUHM) scenario, B, and a third scenario, C, in which the $\tilde{\chi}_2^0$ is higgsino-like. The particle spectra for these scenarios have been computed with the program SPheno [148]. These three

$M_{\tilde{t}_1}$	396.5		447.8		402.6	
$M_{\tilde{t}_2}$	595		609.6		591.6	
$M_{\tilde{\chi}_1^\pm}$	177		172.8		186.3	
$M_{\tilde{\chi}_2^\pm}$	301.6		346.05		421.1	
$m_{\tilde{\ell}_L}$	302.4		369.8		303.1	
$m_{\tilde{\ell}_R}$	229.2		345.2		229.2	
ϕ_{M_1}	0	π	0	π	0	π
$m_{\tilde{\chi}_1^0}$	100.8	106.1	94.8	96.3	99.2	97.6
$m_{\tilde{\chi}_2^0}$	177.0	171.3	167.1	166.6	186.2	179.8
$m_{\tilde{\chi}_3^0}$	227.9	231.8	323.8	325.5	199.4	206.2
$m_{\tilde{\chi}_4^0}$	299.1	297.6	343.4	341.8	419	418.9
$\Gamma_{\tilde{t}_1}$	3.88	3.88	3.48	3.48	5.29	5.29
$\Gamma_{\tilde{\chi}_2^0}$	1.4×10^{-4}	1.4×10^{-4}	2.3×10^{-5}	2.3×10^{-5}	3.0×10^{-3}	3.0×10^{-3}

Table 4.2: Particle spectra for the three scenarios A, B, C considered in this chapter. We used $m_t = 171.2$ GeV [20] and the SM value for the top width $\Gamma_t \sim 1.5$ GeV [147] for our study. All masses and widths are given in GeV.

scenarios have been chosen to have similar masses, as displayed in Table 4.3.1, so that the kinematic effects are similar in each case. We perform our studies using our own program based on the analytic formulae we have derived for the various cross sections and spin correlations. The program uses the VEGAS [149, 150] routine to perform the multi-dimensional phase-space integral. We constrain ourselves to cases where $m_{\tilde{\chi}_2^0} < m_{\tilde{\chi}_1^0} + m_{Z^0}$ and $m_{\tilde{\chi}_2^0} < m_{\tilde{\ell}_{L,R}}$, so as to forbid the two-body decay of the $\tilde{\chi}_2^0$. The branching ratios for both processes have been calculated with Herwig++ [151, 152] [2].

The feasibility of measuring these asymmetries at the LHC depends heavily on the integrated luminosity at the LHC. For this reason we look closely at the cross section, $\sigma = \sigma(gg \to \tilde{t}_1\bar{\tilde{t}}_1) \times BR(\tilde{t}_1 \to t\tilde{\chi}_2^0) \times BR(\tilde{\chi}_2^0 \to \tilde{\chi}_1^0\ell^+\ell^-) \times BR(t \to Wb)$

---

[2]Beyond the Standard Model physics was produced using the algorithm of [153] and, in the running of α_{EM}, the parameterisation of [154] was used.

and determine the nominal luminosity required to observe a statistically significant result.

4.3.2 CP asymmetry at the parton level

Dependence of $m_{\tilde{\chi}_1^0}$ and $\mathcal{A}_T$ on ϕ_{M_1} and ϕ_{A_t}

We start by discussing the dependence of $M_1 = |M_1|e^{i\phi_{M_1}}$ on the parton-level, rest frame asymmetries for each of the three scenarios. In order to see the maximum dependence upon ϕ_{M_1}, we use the reconstructed t quark momentum and the triple product $\mathcal{T}_t = \vec{p}_t \cdot (\vec{p}_{\ell+} \times \vec{p}_{\ell-})$. It should be noted from the following plots that the asymmetry is obviously a CP-odd quantity that in addition to a measurement of the phase, also gives the sign, as seen in Fig. 4.3(a). In comparison, using CP-even quantities, for example the mass, it is not possible to determine if the phase is above or below π, as seen in Fig. 4.3(b).

We see in Fig. 4.3(a) that the biggest asymmetry appears in scenario A, which attains $|\mathcal{A}_{T_t}|_{\max} \approx 12\%$ when $\phi_{M_1} \approx 0.3\pi$. One aspect of the plot that may be surprising is that the asymmetry is not largest at the maximal value of the phase ($\phi_{M_1} = \frac{\pi}{2}$). This is due to the coupling combinations and interferences and can be seen from the equations in Sections 4.2.5. In Fig. 4.3(b), the dependence of the masses of the neutralinos is shown. It can be seen clearly that the variations are too small to be used to determine the phase.

In the cases of the two other scenarios shown in Fig. 4.3(a), the dependence of the asymmetry on the phase ϕ_{M_1} is similar but slightly smaller. In the case of scenario B (NUHM), the peak asymmetry is $|\mathcal{A}_{T_t}|_{\max} \approx 9\%$ when $\phi_{M_1} \approx 0.3\pi$ and in scenario C (Higgsino) it is $|\mathcal{A}_{T_t}|_{\max} \approx 7\%$ when $\phi_{M_1} \approx 0.25\pi$. Again, the asymmetry does not peak when the phase is maximal.

To study the dependence upon ϕ_{A_t} we need to use the triple products sensitive to this phase, $\mathcal{T}_b = \vec{p}_t \cdot (\vec{p}_{\ell+} \times \vec{p}_{\ell-})$ and $\mathcal{T}_{tb} = \vec{p}_t \cdot (\vec{p}_b \times \vec{p}_{\ell\pm})$. Fig. 4.4(a) shows $\mathcal{A}_{\mathcal{T}_b}$ and we see that the biggest asymmetry again occurs in Scenario A, but the maximal asymmetry is only about half of $|\mathcal{A}_{\mathcal{T}_t}|_{\max}$ with $|\mathcal{A}_{\mathcal{T}_b}|_{\max} \approx 6\%$. Scenario C produces a very similar asymmetry to Scenario A, with $|\mathcal{A}_{\mathcal{T}_b}|_{\max} \approx 5.5\%$, whereas
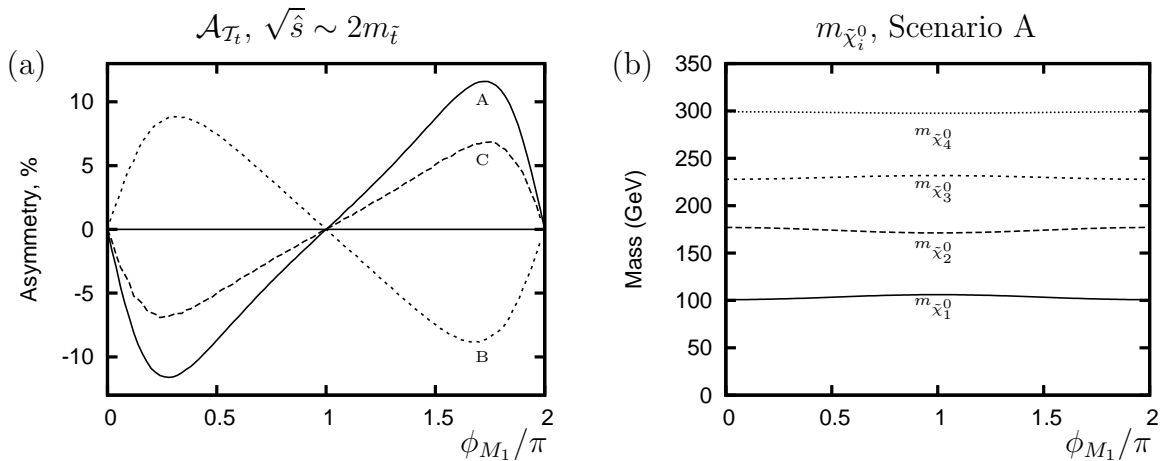
Figure 4.3: The asymmetry at threshold for the production process $gg \longrightarrow \tilde{t}\tilde{t}^*$ for scenarios A, B and C for (a) $\mathcal{A}_{\mathcal{T}_t}$ as a function of ϕ_{M_1}, and (b) the masses of the neutralinos as functions of ϕ_{M_1}.
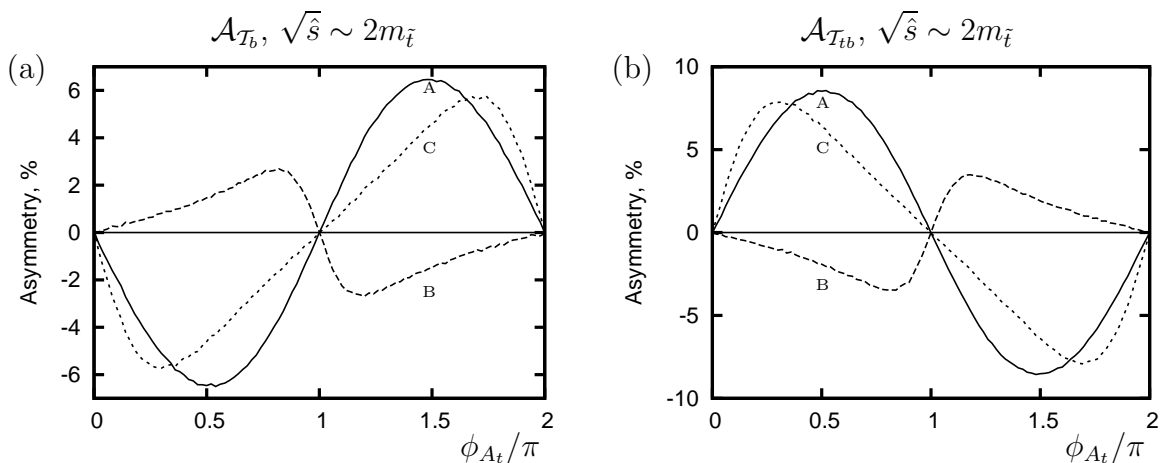

Figure 4.4: (a) The asymmetry $\mathcal{A}_{\mathcal{T}_b}$ at threshold for the production process $gg \longrightarrow \tilde{t}\tilde{t}^*$ for scenarios A, B and C, and (b) the asymmetry $\mathcal{A}_{\mathcal{T}_b}$ at threshold, both as functions of ϕ_{A_t}.

the asymmetry in Scenario B is much smaller: $|\mathcal{A}_{\mathcal{T}_b}|_{\max} \approx 2.5\%$. Fig. 4.4(b) shows that the general shape of the asymmetries for $\mathcal{A}_{\mathcal{T}_{tb}}$ is similar to that of $\mathcal{A}_{\mathcal{T}_b}$ apart from a difference in sign and that all the asymmetries are actually slightly larger. In fact, for Scenario C, the largest asymmetry is generated using $\mathcal{T}_{tb}$ with $\mathcal{A}_{\mathcal{T}_{tb}} \approx 8\%$ when $\phi_{A_t} \approx 0.3\pi$.

In the subsequent analysis, we concentrate on the favourable Scenario A, with just a few remarks on the others.
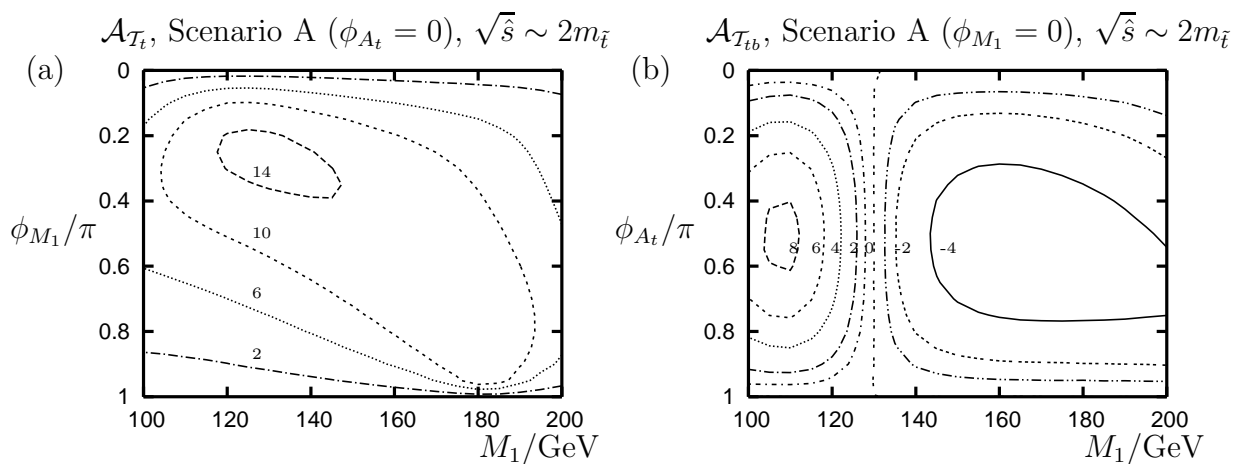
Figure 4.5: Contours in scenario A (in %) of the parton-level asymmetries (a) $\mathcal{A}_{T_t}$ for the triple product $\mathcal{T}_t = \vec{p}_t \cdot (\vec{p}_{\ell^+} \times \vec{p}_{\ell^-})$, as functions of the variables M_1 and ϕ_{M_1}, and (b) $\mathcal{A}_{T_{tb}}$ for the triple product $\mathcal{T}_{tb} = \vec{p}_{\ell^+} \cdot (\vec{p}_t \times \vec{p}_b)$, as functions of the variables M_1 and ϕ_{A_t}.

4.3.3   Contour plots of $\mathcal{A}_{T_t}$ and $\mathcal{A}_{T_{tb}}$ for variables M_1 and A_t

If we now lift the restriction of the GUT relation for $|M_1|$, we can see how the asymmetry varies with $|M_1|$ while leaving all the other parameters the same, for Scenario A. Fig. 4.5(a) shows that the asymmetry peaks at $|M_1| \approx 130$ GeV and $\phi_{M_1} \approx 0.25\pi$ when $|\mathcal{A}_{T_t}| \approx 15\%$. Importantly though, the asymmetry can remain above 10% between $|M_1| = 110$ GeV and $|M_1| = 190$ GeV, which is most of the range allowed in this scenario.

By including the decay of the t quark that was produced in the $\tilde{t}$ decay, we can also study the effect of ϕ_{A_t} on our asymmetries. As the spin-correlation information is now carried by the t quark, we have to change the triple product used to measure the asymmetry, Eq. (4.15). It is found that the largest asymmetry can be measured using the triple product, $\mathcal{T}_{tb} = \vec{p}_{\ell^+} \cdot (\vec{p}_t \times \vec{p}_b)$ where $|\mathcal{A}_{T_{tb}}|_{\max} \approx 8.5\%$ when $\phi_{A_t} \approx 0.5\pi$ in Scenario A, as seen in Fig. 4.5(a). It may be noted that this asymmetry is slightly smaller than those of [129] that can be reconstructed experimentally. In that paper, scenarios were chosen where the $\tilde{\chi}_2^0$ decays via a two-body process, whereas here we concentrate on scenarios where the $\tilde{\chi}_2^0$ decays via a three-body process, so to maximise the sensitivity to ϕ_{M_1}. A more detailed discussion of [129] is given in
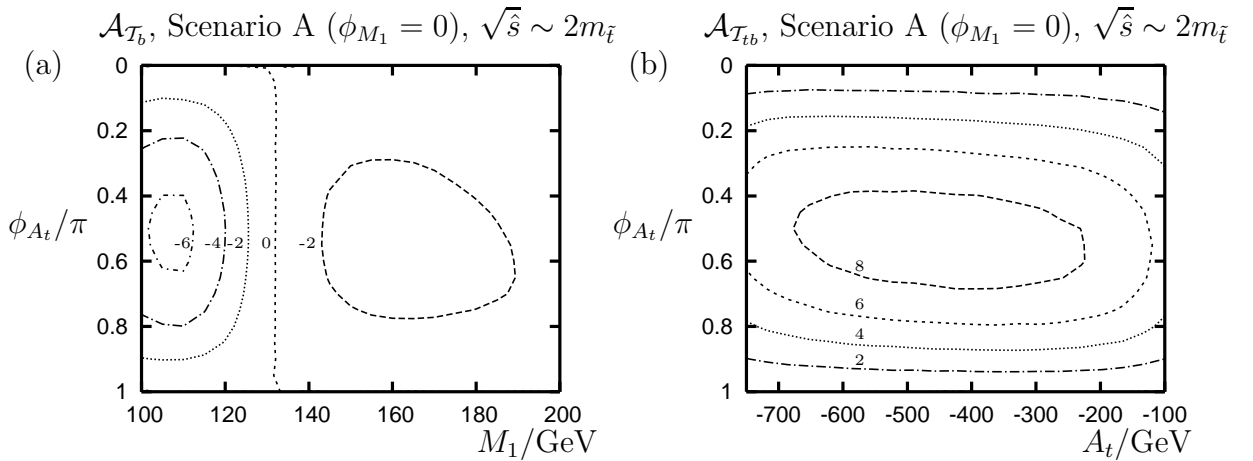
Figure 4.6: Contours in scenario A (in %) of the asymmetries (a) $\mathcal{A}_b$ for the triple product $\mathcal{T} = \vec{p}_b \cdot (\vec{p}_{\ell-} \times \vec{p}_{\ell+})$, as functions of the variables M_1 and ϕ_{A_t} and (b) $\mathcal{A}_{tb}$ for the triple product $\mathcal{T} = \vec{p}_{\ell+} \cdot (\vec{p}_t \times \vec{p}_b)$, as functions of the common variables $A = A_t = A_b = A_\tau$ and ϕ_{A_t}.

Sec. 3.7.1.

The phase dependence can also be seen with the triple product $\mathcal{T}_b = \vec{p}_b \cdot (\vec{p}_{\ell+} \times \vec{p}_{\ell+})$ although the asymmetry is found to be smaller here with $|\mathcal{A}_{T_b}|_{\text{max}} \approx 6\%$, see Fig. 4.6(a).

We have also considered the dependence of the asymmetry on the trilinear coupling, A_t, in scenario A, as shown in Fig. 4.6(b). It can be seen that the asymmetry is stable for the bulk of the region scanned, and only decreases near the edge of the acceptable region for our scenario. The peak is now $|\mathcal{A}_{T_{tb}}|_{\text{max}} \approx 9\%$, when $A_t \approx -500$ GeV, and the region where $|\mathcal{A}_{T_{tb}}| > 8\%$ extends from $A_t \approx -650$ GeV to $A_t \approx -250$ GeV.

We now consider the effect on the asymmetry of varying simultaneously both the phases ϕ_{M_1} and ϕ_{A_t}. The triple products $\mathcal{T}_b = \vec{p}_b \cdot (\vec{p}_{\ell+} \times \vec{p}_{\ell-})$ and $\mathcal{T}_{tb} = \vec{p}_t \cdot (\vec{p}_b \times \vec{p}_{\ell\pm})$ can have contributions from both phases, so we concentrate on these. For $\mathcal{T}_b$, Fig. 4.7(a) shows that the area of parameter space where ϕ_{M_1} and ϕ_{A_t} constructively interfere is actually quite small and peaked around $\phi_{M_1} \approx 0.2\pi$ and $\phi_{A_t} \approx 0.5\pi$. Apart from this area, varying both phases generally results in a reduction in the asymmetry observed, caused by the neutralino and squark mixing entering the cou-
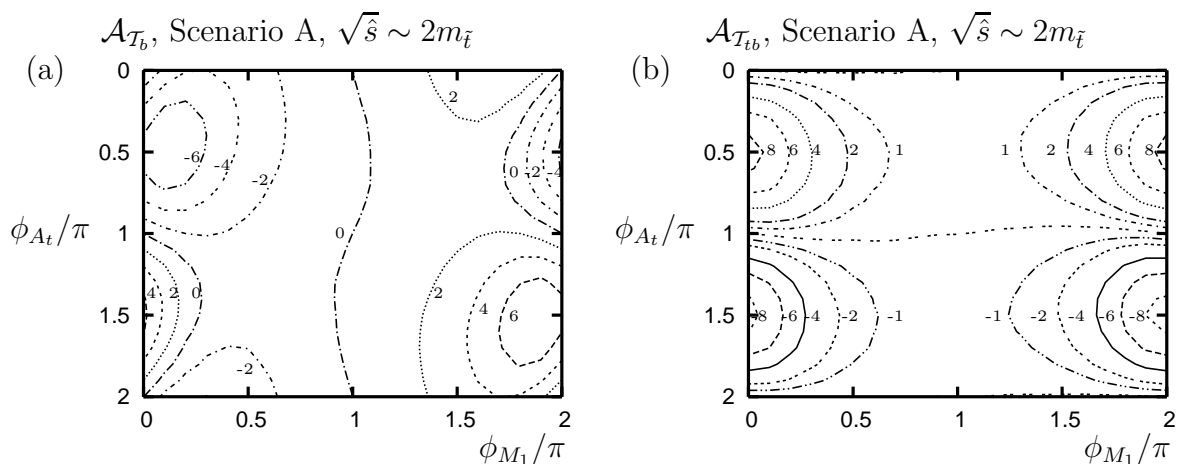
Figure 4.7: Contours (in %) of the asymmetry at the parton level in scenario A with $M_1 = 109$ GeV for the triple products (a) $\mathcal{T}_b = \vec{p}_b \cdot (\vec{p}_{\ell^+} \times \vec{p}_{\ell^-})$ and (b) $\mathcal{T}_{tb} = \vec{p}_{\ell^+} \cdot (\vec{p}_b \times \vec{p}_t)$ for varying phases ϕ_{M_1} and ϕ_{A_t}.

plings, Section 4.2.5. Importantly when $\phi_{M_1} \approx \pi$ the asymmetry vanishes, due to the fact that the mixing between the wino and bino states becomes much weaker. These mixing terms are the dominant entries in the coupling factor where ϕ_{A_t} enters (the last term in Eq. (B.1.11)).

Fig. 4.7(b) demonstrates that, for this scenario, ϕ_{M_1} generates virtually no asymmetry for $\mathcal{T}_b$. However, ϕ_{M_1} can still significantly reduce the asymmetry that ϕ_{A_t} can produce and, again, when $\phi_{M_1} \approx \pi$ we see that $|\mathcal{A}_{T_{tb}}| \approx 0$ as expected.

If we now modify scenario A slightly by setting $|M_1| = 160$ GeV, this results in a more interesting scenario as the phases ϕ_{M_1} and ϕ_{A_t} can interfere constructively to produce an asymmetry larger than that seen before. When $\phi_{M_1} \approx 0.4\pi$ and $\phi_{A_t} \approx 1.8\pi$, we observe a peak asymmetry, $|\mathcal{A}_{T_b}| \approx 7\%$ for the triple product $\mathcal{T}_b$, as seen in Fig. 4.8.

4.3.4   Dependences of branching ratios on ϕ_{M_1} and ϕ_{A_t}

In order to determine whether an asymmetry could be observed at the LHC, we need to calculate the cross section for the total process. Important factors in the total cross section are the branching ratios $BR(\tilde{t}_1 \to \tilde{\chi}_2^0 t)$ (for CP-violating case see [155]) and $BR(\tilde{\chi}_2^0 \to \tilde{\chi}_1^0 \ell^+ \ell^-)$ [112]. Both of these change considerably with ϕ_{M_1}
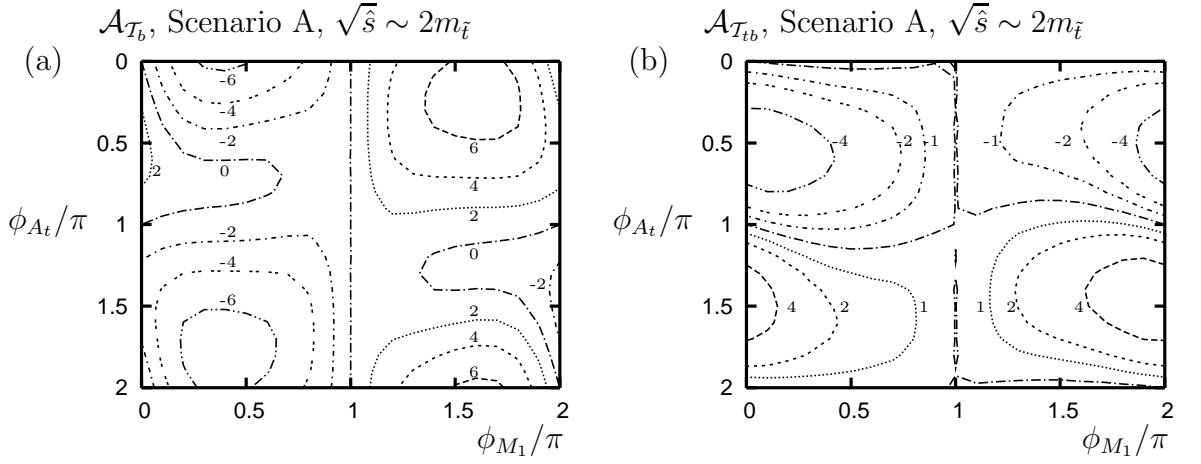
Figure 4.8: Contours (in %) of the asymmetries in scenario A at the parton level with $M_1 = 160$ GeV for the triple products (a) $\mathcal{T}_b = \vec{p}_b \cdot (\vec{p}_{\ell^+} \times \vec{p}_{\ell^-})$ and (b) $\mathcal{T}_{tb} = \vec{p}_{\ell^+} \cdot (\vec{p}_b \times \vec{p}_t)$, as functions of the varying phases ϕ_{M_1} and ϕ_{A_t}.
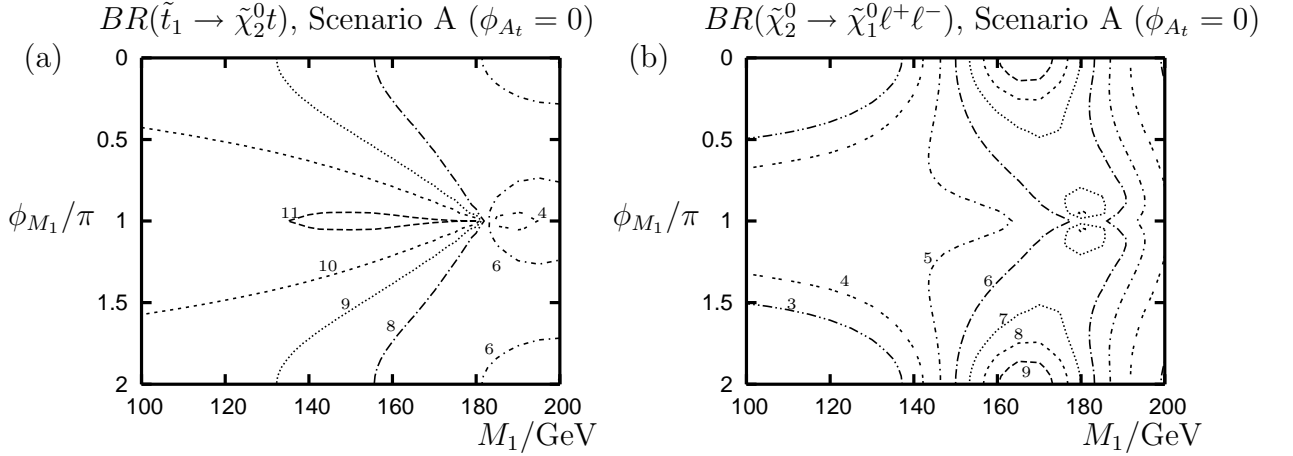

Figure 4.9: Contours (in %) of branching ratios in scenario A as functions of M_1 and ϕ_{M_1}: (a) $BR(\tilde{t}_1 \to \tilde{\chi}_2^0 t)$ and (b) $BR(\tilde{\chi}_2^0 \to \tilde{\chi}_1^0 \ell^+ \ell^-)$, $\ell = e$ or μ.

and ϕ_{A_t}, altering the statistical significance of any measurement of $|\mathcal{A}_{T_f}|$. Analyzing first the variation with M_1, seen in Figs. 4.9 and 4.10(a), we see that the branching ratio $BR(\tilde{t}_1 \to \tilde{\chi}_2^0 t)$ is indeed sensitive to variation of the phase, but can vary more strongly with $|M_1|$. For example, if $\phi_{M_1} = \pi$ when $|M_1| \approx 150$ GeV then $BR \approx 11\%$, but if we keep the phase the same and change to $|M_1| \approx 180$ GeV then $BR \approx 4\%$ (i.e., it drops by almost a factor of three), as seen in Fig. 4.9(a). The general reduction of $BR(\tilde{t}_1 \to \tilde{\chi}_2^0 t)$ as M_1 increases is to be expected as the
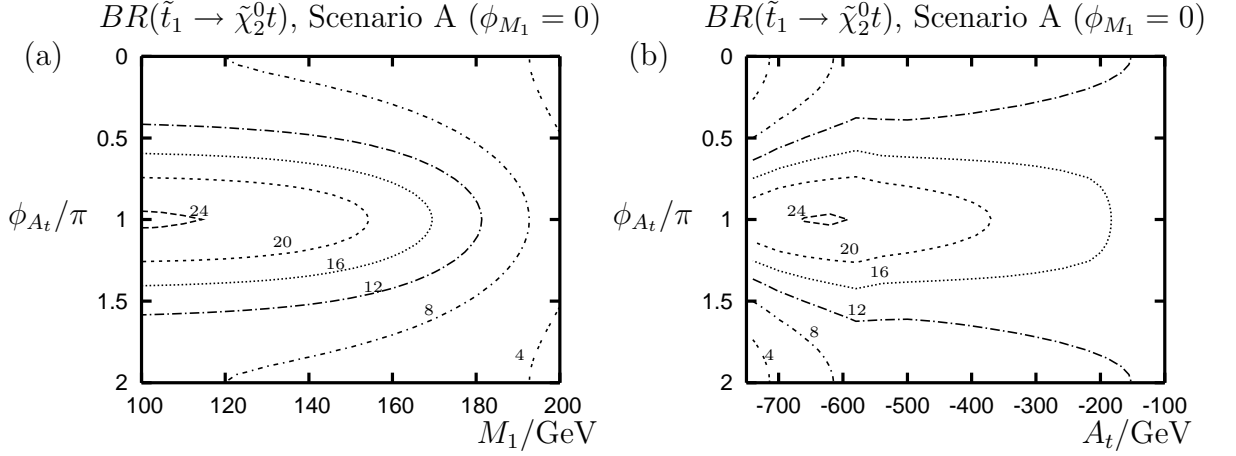
Figure 4.10: Contours (in %) of the branching ratio $BR(\tilde{t}_1 \to \tilde{\chi}_2^0 t)$, in scenario A as functions of varying (a) M_1 and ϕ_{A_t} and (b) the common trilinear coupling $A_t = A_b = A_\tau$ and the phase of the top-quark trilinear coupling ϕ_{A_t}.

mass of the $\tilde{\chi}_2^0$ will rise resulting in a kinematic suppression for this decay state. Similar large differences are found in $BR(\tilde{\chi}_2^0 \to \tilde{\chi}_1^0 \ell^+ \ell^-)$ which varies between 3% for $M_1 < 135$GeV and 9% for $M_1 \approx 165$GeV Fig. 4.9(b).

The phase ϕ_{A_t} does not enter $BR(\tilde{\chi}_2^0 \to \tilde{\chi}_1^0 \ell^+ \ell^-)$, but can have a large effect on $BR(\tilde{t}_1 \to \tilde{\chi}_2^0 t)$. In scenario A, we see in Fig. 4.10 that $BR \approx 8\%$ at $\phi_{A_t} = 0$ but increases to $BR \approx 24\%$ at $\phi_{A_t} = \pi$ (i.e. a factor of 3 increase). The branching ratio $BR(\tilde{t}_1 \to \tilde{\chi}_2^0 t)$ also has a dependence on $|A_t|$ an this is shown in Fig. 4.10(b). We see that if $\phi_{A_t} = 0$ then the branching vary between, $BR \approx 4\%$ when $|A_t| \approx -750$GeV and $BR \approx 12\%$ when $|A_t| \approx -100$GeV.

In the range of $M_1 = |M_1|e^{i\phi_{M_1}}$ and $A_t = |A_t|e^{i\phi_{A_t}}$ studied, we find that $BR(\tilde{t}_1 \to \tilde{\chi}_2^0 t)$ varies between 4% and 24% and $BR(\tilde{\chi}_2^0 \to \tilde{\chi}_1^0 \ell^+ \ell^-)$ between 2.5% and 9% for scenario A. Similar plots can also be produced for scenarios B and C but are not presented here. It is found that $BR(\tilde{t}_1 \to \tilde{\chi}_2^0 t)$ varies between 4% and 14% for scenario B and between 8% and 35% for scenario C. For $BR(\tilde{\chi}_2^0 \to \tilde{\chi}_1^0 \ell^+ \ell^-)$ the variation is between 3% and 12% for scenario B and between 2% and 5% for scenario C.

4.3.5 Influence of Parton Distribution Functions (PDFs) on CP asymmetries

So far we have studied the triple-product asymmetries only when the production process is close to threshold, and the $\tilde{t}_1$ pair are produced almost at rest. However, production at the LHC is not in general close to threshold, and we must include PDFs in our analysis to see how an initial boost to the $\tilde{t}_1$ affects the asymmetry. As explained in Sec. (3.5), whilst the covariant product is a Lorentz invariant quantity, the triple products are not. Therefore, we must analyse the optimal reference frame to observe an asymmetry and compare this frame to the one that will be seen at the LHC.

We first analyse the triple product, $\mathcal{T}_t$, Eq. (4.12),

$$\mathcal{T}_t = \vec{p}_t \cdot (\vec{p}_{\ell+} \times \vec{p}_{\ell-}) , \tag{4.25}$$

which is produced by the covariant product present in the $\tilde{\chi}_2^0$ decay amplitude,

$$(p_t s^a) \cdot \epsilon_{\mu\nu\rho\sigma} s^{a\mu} p_{\tilde{\chi}_j^0}^{\nu} p_{\ell-}^{\rho} p_{\ell+}^{\sigma} \longrightarrow \epsilon_{\mu\nu\rho\sigma} p_t^{\mu} p_{\tilde{\chi}_j^0}^{\nu} p_{\ell-}^{\rho} p_{\ell+}^{\sigma} . \tag{4.26}$$

Following the argument presented in Sec. 3.3 we can see that the optimal reference frame is that of the $\tilde{\chi}_2^0$ rest frame. In this frame all the momentum components of the $\tilde{\chi}_2^0$ vanish and we are left with the single triple product, $\mathcal{T}_t$. However, the rest frame of the $\tilde{\chi}_2^0$ is not the only optimal frame, if we apply momentum conservation at the $\tilde{t}_1$ decay vertex, we trivially find that $p_{\tilde{t}_1} = p_{\tilde{\chi}_2^0} + p_t$. Applying this identity to the covariant product results in,

$$\epsilon_{\mu\nu\rho\sigma} p_t^{\mu} p_{\tilde{\chi}_j^0}^{\nu} p_{\ell-}^{\rho} p_{\ell+}^{\sigma} \longrightarrow \epsilon_{\mu\nu\rho\sigma} p_t^{\mu} p_{\tilde{t}_1}^{\nu} p_{\ell-}^{\rho} p_{\ell+}^{\sigma} , \tag{4.27}$$

and hence, we see that both the $\tilde{\chi}_2^0$ and $\tilde{t}_1$ rest frame can be considered equivalent and optimum for the triple product $\mathcal{T}_t$. For the triple products $\mathcal{T}_{tb}$ and $\mathcal{T}_b$ the same argument can be made that shows both the the $\tilde{\chi}_2^0$ and $\tilde{t}_1$ rest frame are equivalent.

We now present the numerical results and in this section we focus exclusively on scenario A but very similar conclusions are obtained in both Scenarios B and C.
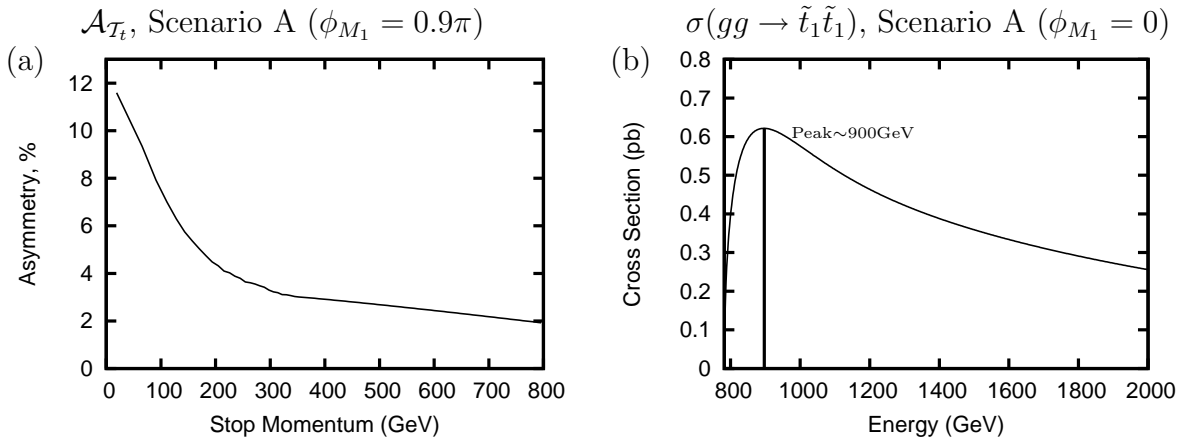
Figure 4.11: (a) Asymmetry $\mathcal{A}_{T_t}$ for scenario A as a function of the $\tilde{t}$ momentum. (b) Total cross section for scenario A for $gg \longrightarrow \tilde{t}\tilde{t}^*$ as a function of the parton-parton centre-of-mass energy.

Fig. 4.11(a) shows the asymmetry $|\mathcal{A}_{T_t}|$ as a function of the $\tilde{t}_1$ momentum. The plot clearly verifies the conclusion that the $\tilde{t}_1$ rest frame is optimal and that the asymmetry falls sharply as the energy of the $\tilde{t}_1$ increases. Fig. 4.11(b) shows the total cross section in 14 TeV collisions at the LHC for $gg \rightarrow \tilde{t}_1 \tilde{t}_1^*$ as a function of the parton-parton centre-of-mass energy, and demonstrates that the peak production occurs close to threshold with a long tail of production at high energy. In addition, even when production occurs at a low parton-parton centre-of-mass energy, in the majority of cases one gluon may be carrying significantly more momentum than the other in the collision. Consequently the produced $\tilde{t}_1$ can have a large longitudinal component to its momenta. Both these factors mean that the asymmetry observed at the LHC will be substantially smaller than if the all $\tilde{t}_1$ were produced at threshold [3]. In should be noted that similar results were found for all asymmetries and scenarios, and this 'dilution' factor, Sec. 3.5, is always present.

We use the `MRST 2004LO` pdf set [156] in our analysis of the asymmetry, and plot the integrated asymmetry $|\mathcal{A}_{T_t}|$ as a function of ϕ_{M_1} and ϕ_{A_t} at the LHC in Fig. 4.12(a), as the solid line. We see that the inclusion of the PDFs reduces the

---

[3]Both these effects could be overcome if one could measure the stop momenta and this possibility is explored in the following chapters.

$\mathcal{A}_{\mathcal{T}_t}$, Scenario A ($M_1 = 130$ GeV, $\phi_{A_t} = 0$), $\sqrt{\hat{s}} = 14$ TeV

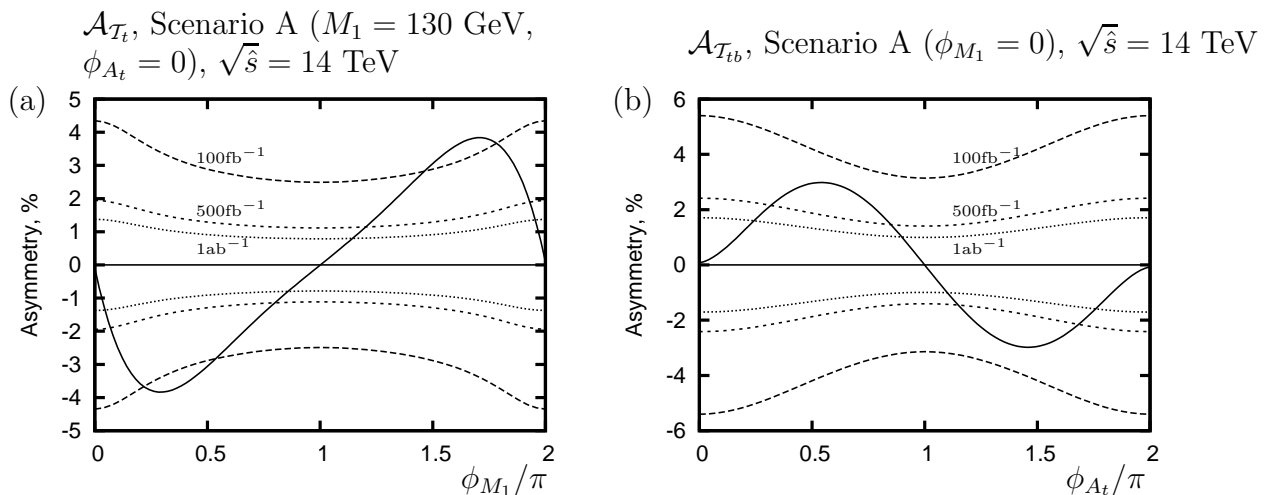$\mathcal{A}_{\mathcal{T}_{tb}}$, Scenario A ($\phi_{M_1} = 0$), $\sqrt{\hat{s}} = 14$ TeV

Figure 4.12: Integrated asymmetries with parton density functions included in the production process. The dotted and dashed lines indicate the asymmetry required in order to observe a 1σ deviation from zero with the indicated luminosities, see the text: (a) $\mathcal{T}_t = \vec{p}_t \cdot (\vec{p}_{\ell+} \times \vec{p}_{\ell-})$ in scenario A as a function of ϕ_{M_1} with $M_1 = 130$ GeV, and (b) $\mathcal{T}_{tb} = \vec{p}_{\ell+} \cdot (\vec{p}_t \times \vec{p}_b)$ in scenario A as a function of ϕ_{A_t} with $M_1 = 109$ GeV.

asymmetry by about a factor of four in this case. This reduction is unsurprising, given the reduction in asymmetry when one moves away from threshold shown in Fig. 4.11(a), though the dilution factor does depend on the scenario[4].

Using the production cross sections and branching ratios we can then estimate the integrated luminosity required to observe an asymmetry at the LHC. We explain in Sec. 3.6 the method used to calculate the statistical significance of any particular asymmetry.

Figs. 4.12 (a), (b) and 4.13(a) show the expected levels of the integrated asymmetries in scenario A with PDF effects included (solid line) together with dotted and dashed lines showing the level of asymmetry one would need with the corresponding integrated luminosity in order to obtain a statistical error $\mathcal{A}_T > \Delta(A_T)$. In other words, the asymmetry could only be seen at the level of 1σ where the solid line is above the relevant dotted or dashed line. For example, in scenario A after

---

[4]These results have been checked independently using `Herwig++` [151,152] with three-body spin correlations included.
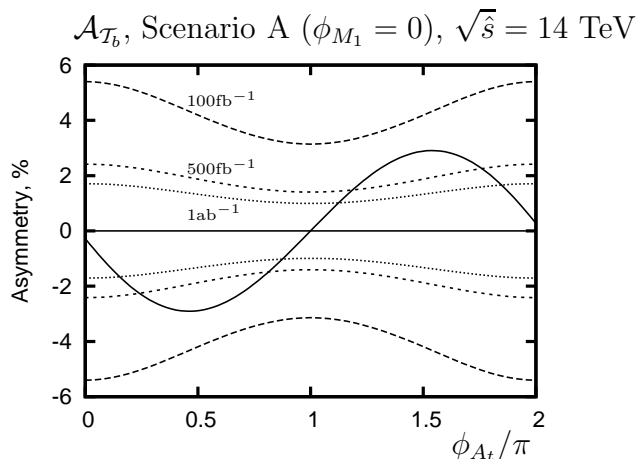
Figure 4.13: Integrated asymmetry with parton density functions included in the production process. The dotted and dashed lines indicate the asymmetry required in order to observe a 1σ deviation from zero with the indicated luminosities. The asymmetry is for the triple product, $\mathcal{T}_b = \vec{p}_b \cdot (\vec{p}_{\ell^+} \times \vec{p}_{\ell^-})$ in scenario A as a function of ϕ_{A_t} with $M_1 = 109$ GeV.

100 fb^{-1}, the asymmetry could only be seen for a small area of parameter space around $\phi_{M_1} = 0.35\pi$ and 1.7π. Figs. 4.12 (a) and (b) show that even if ϕ_{M_1} or ϕ_{A_t} has a value that produces a maximal asymmetry, we require a substantial integrated luminosity if we are to find a statistically significant result. In addition, it must be noted that we have not included any detector effects into our analysis. One can expect that the required integrated luminosity would rise substantially after the inclusion of backgrounds and experimental cuts (for more details on these effects in similar observables see Chapter 5 and Chapter 6). Therefore, an observation of a statistically significant CP-asymmetry using only this decay chain looks difficult at the LHC.

4.3.6 Determination of the CP-violating phases

As we have shown, it will be challenging to determine the phases ϕ_{M_1} and ϕ_{A_t} in our process using the triple-product asymmetries alone. However, it would be very worthwhile, as a non-zero measurement of a T-odd asymmetry would provide unique
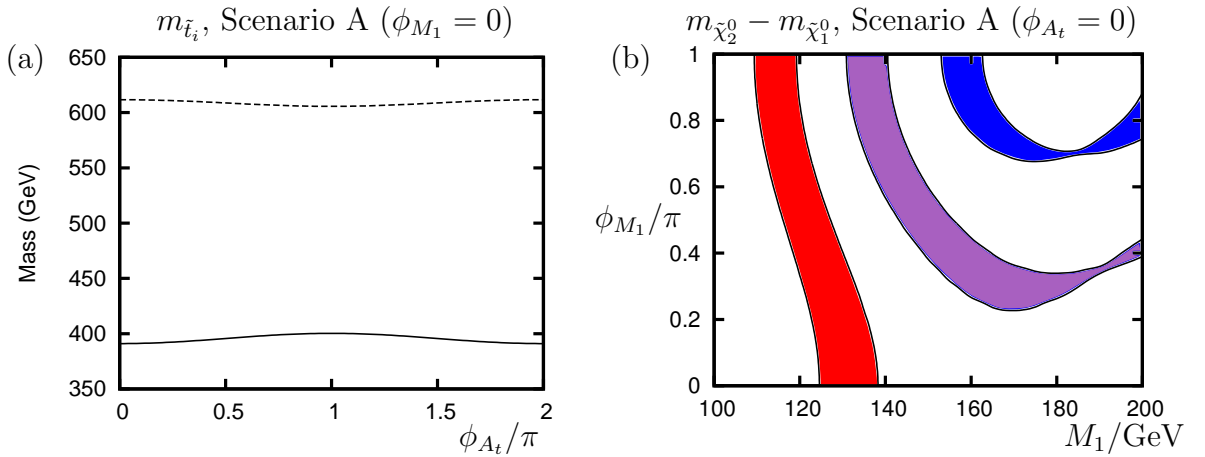
Figure 4.14: (a) The mass of the stop squarks $\tilde{t}_j$, j=1,2 as functions of ϕ_{A_t}/π, and (b) contour plot showing the areas of the (M_1, ϕ_{M_1}) parameter plane consistent with a mass difference between $\tilde{\chi}_2^0$ and $\tilde{\chi}_1^0$ of 20 GeV (blue), 40 GeV (purple) and 60 GeV (red) respectively. The bands assume a 1% error in experimental measurement of the mass difference and a 5% error in M_2.

evidence of CP violation. In the rest of this chapter, we examine briefly the potential for a measurement using other variables, again concentrating on Scenario A.

Masses as a CP observable

Fig. 4.4(b) showed how the masses of the $\tilde{\chi}_i^0$s vary with ϕ_{M_1} and Fig. 4.14(a) shows how the masses of the $\tilde{t}_i$ vary with ϕ_{A_t} in scenario A. The variations in both of these observables are only about $1 - 2\%$ as we vary the phases over the complete range. Unfortunately, the variation is significantly smaller than the expected determination of the MSSM mass scale at the LHC. For example, a detailed analysis of a 2-body cascade decay chain [157], concluded that in a relatively light scenario, the absolute masses for $\tilde{\chi}_2^0$ and $\tilde{\chi}_1^0$ could be measured with an accuracy of 4 GeV. The method relies on the clean dilepton edge produced from the decaying $\tilde{\chi}_2^0$.

A measurement of the $\tilde{t}$ masses will be substantially more difficult due to the fact that the final state contains jets. However, using the ideas of kinematic reconstruction, [158], a new study [159], claims that an error of 10% on the mass may be possible with 20 fb^{-1} of data for an optimistic scenario. Unfortunately, the error is

still far to large for us to be able to place a constraint on the $\tilde{t}$ masses.

Whilst the absolute mass measurements may not prove promising, a far more accurate measurement at the LHC will be the mass difference between the $\tilde{\chi}_2^0$ and $\tilde{\chi}_1^0$. As stated above, this can be determined in our scenario with a clear dilepton end-point. The accuracy of this measurement is expected to be $< 1\%$ for a two body cascade decay chain [157] and a study that considers a three body $\tilde{\chi}_2^0$ decay [160], suggests that a similarly clear dilepton end-point should be visible in these scenarios as well.

If we assume that M_2 can be determined to 5% [161] at the LHC, we find the regions plotted in Fig. 4.14(b). At the smaller values allowed for M_1 in scenario A, we see that this observable does not depend sensitively enough on ϕ_{M_1} for a measurement to become possible. However, as M_1 increases we see that the sensitivity to ϕ_{M_1} becomes much clearer. Importantly, in scenario A, it is only possible to have a mass difference, $\tilde{\chi}_2^0 - \tilde{\chi}_1^0 \lesssim 40$ GeV if ϕ_{M_1} is present. We must state though, that this conclusion relies on the other MSSM parameters in the scenario being known. The observable is not CP-odd and therefore cannot be used as unambiguous measurement of CP-violation.

A more detailed discussion regarding MSSM mass measurements is given in Sec. 5.3.5 and Sec. 6.3.4. For comprehensive reviews of the different studies that have been completed for determining the sparticle masses at the LHC, see [162,163].

Inclusion of branching ratios

Other observables sensitive to the phases ϕ_{M_1} and ϕ_{A_t} are the branching ratios $BR(\tilde{\chi}_2^0 \to \tilde{\chi}_1^0 \ell^+ \ell^-)$ and $BR(\tilde{t}_1 \to \tilde{\chi}_2^0 t)$, as discussed in Section 4.3.4. As is the case for the masses, though, our current expectation of the accuracy of this measurement at the LHC looks insufficient to constrain the phases although a detailed study has not been performed.

Ideas to improve the situation are to study ratios of branching ratios [98, 161, 164]. By taking a ratio of different branching ratios, the production cross section dependence is removed. However, many problems still remain including a severe dependence on the reconstruction efficiency and possible backgrounds. In addition,
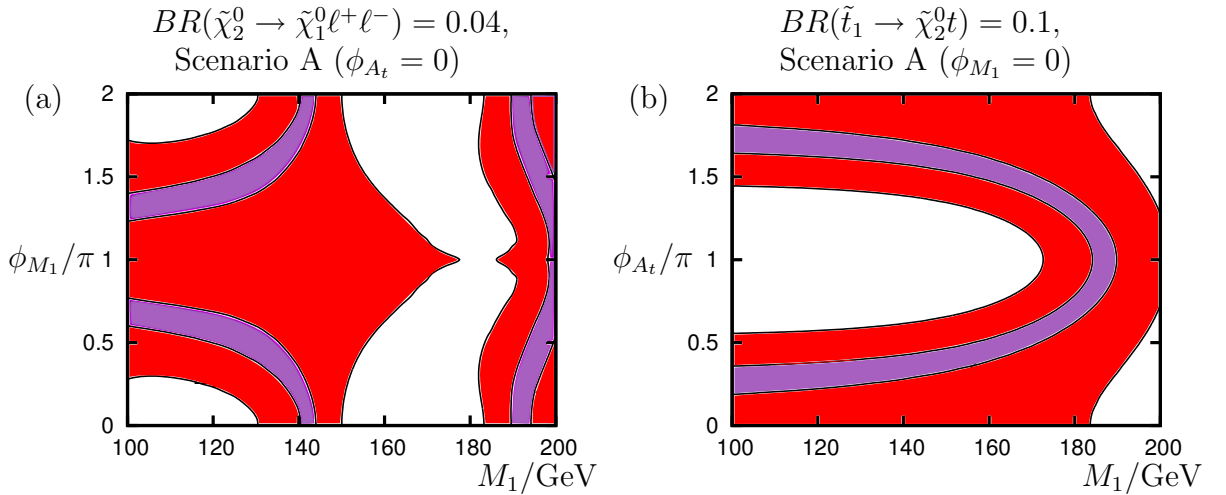
Figure 4.15: Parameter space allowed when the experimental accuracy of the branching ratio measurement is 50% (red) or 10% (purple) for (a) $BR(\tilde{\chi}_2^0 \to \tilde{\chi}_1^0 \ell^+ \ell^-) = 0.04$ and (b) $BR(\tilde{t}_1 \to \tilde{\chi}_2^0 t) = 0.1$.

other parameters of the theory will need to be well constrained.

However, we include a illustrative example here to show how an accurate determination of the branching ratios could be extremely useful if a measurement was made. Fig. 4.15(a) shows in the context of scenario A that, if a measurement $BR(\tilde{\chi}_2^0 \to \tilde{\chi}_1^0 \ell^+ \ell^-) = 0.4$ is made and we assume that the accuracy is 50% (Δ_1), then the constraints on M_1 and ϕ_{M_1} are rather weak. However, if the accuracy could be improved to 10% (Δ_2), a determination of M_1 and ϕ_{M_1} looks possible if this analysis is combined with information from the $\tilde{\chi}_2^0$, $\tilde{\chi}_1^0$ mass difference and that of the triple-product correlations. For the branching ratio, $BR(\tilde{t}_1 \to \tilde{\chi}_2^0 t)$, the conclusion is similar, as seen in Fig. 4.15(b). With a measurement at 50% (Δ_1), we again see that a determination of the CP-violating parameter is not possible but, if a measurement can be made with an accuracy of 10% (Δ_2), then a determination of ϕ_{A_t} would be more plausible.

Thus, we may be able to to pin the model parameters down with greater accuracy by combining information on the CP-violating asymmetries with masses, branching ratios and possibly even cross sections.

4.4 Conclusions

In this chapter we studied direct stop production followed by the decay $\tilde{t}_1 \to t\tilde{\chi}_2^0$, $\tilde{\chi}_2^0 \to \ell^+\ell^-\tilde{\chi}_1^0$, where the latter is a three-body decay and provide compact analytical expressions for the amplitude and phase space. We have specifically concentrated on measuring the CP-violating phases of the parameters M_1 and A_t.

We have provided a thorough analysis of the contributions to this process which lead to non-zero asymmetries in the parameters $\mathcal{T}_t$, $\mathcal{T}_b$ and $\mathcal{T}_{tb}$ formed from triple products of reconstructible final-state particles. These are sensitive to different combinations of the phases mentioned above. We studied three spectra which had different neutralino characteristics at the parton level and also studied the (large) effect of including PDFs which had previously only been roughly estimated in the literature.

We found that with the design integrated luminosity of the LHC of 100 fb^{-1}, the statistical errors would probably remain too great to distinguish a non-zero asymmetry measurement from zero for most of the ranges of ϕ_{M_1} and ϕ_{A_t}, and we recall that this initial study did not include detector or background effects. However, with a luminosity upgrade, the accuracy will improve and it could be possible either to measure a non-zero value or else to provide limits on the possible phases.

Triple products are not the only variables sensitive to the phases of the parameters. We found that a good measurement of the mass difference between the $\tilde{\chi}_2^0$ and $\tilde{\chi}_1^0$ neutralinos could constrain significantly the (M_1, ϕ_{M_1}) parameter space. It is possible that measurements of the two branching ratios $BR(\tilde{t}_1 \to \tilde{\chi}_2^0 t)$ and $BR(\tilde{\chi}_2^0 \to \tilde{\chi}_1^0 \ell^+\ell^-)$ could also constrain both ϕ_{M_1} and ϕ_{A_t}, although this is heavily dependent on the experimental accuracy achieved. However, the disadvantage of both mass differences and branching ratios is that a difference for the expected value can potentially be faked by other values of the real parameters. This is in contrast to the asymmetries from triple products which are uniquely due to CP violation.

Chapter 5

Squark gluino production and three body neutralino decay

5.1 Introduction

In the previous study that considered $\tilde{t}$ pair production we saw that large CP-violating asymmetries can be produced at the parton level. However, we also saw that limited statistics and the dilution of the asymmetry due to fact that the stops are produced with a significant boost will make the observation of these asymmetries challenging at the LHC. The study in this chapter attempts to address these two issues to demonstrate an analysis that may be realistic at the LHC.

We study the production of squarks at the LHC and the subsequent cascade decay chain [136],

$$\tilde{q}_i \to \tilde{\chi}_j^0 + q \to \tilde{\chi}_1^0 \ell^+ \ell^- + q. \tag{5.1}$$

which is analogous to the chain shown in Eq. (4.1) but with a first or second generation $\tilde{q}_i$ replacing the $\tilde{t}_i$.

5.1.1 Advantages of squark decay

The first advantage of studying this chain is that if the masses are similar, the production cross section of squarks at the LHC is substantially higher than that of stops. The higher production cross section is due to the fact that the proton contains

valence up and down quarks. The valence quarks open up many new production channels, including those in association with a gluino, Fig. 5.1, which lead to the higher rate. When analysing the CP-violating asymmetries at the LHC, the higher production rate directly corresponds to an improved statistical significance.

The production channel mentioned above,

$$qg \rightarrow \tilde{q}\tilde{g}\,, \tag{5.2}$$

is of additional importance in this study as the cross section for $\tilde{q}$ production, is substantially higher than the anti-particle, $\tilde{q}^*$, at the LHC. The asymmetry in production occurs since the LHC collides two protons where the valence quarks will all be quarks and not anti-quarks. Thus, a quark is far more likely to be present in the initial collision than an antiquark leading to the process shown in Eq. (5.2) having a higher cross section than that of the charge conjugate.

The asymmetry mentioned above has already been exploited in the literature as a possible method to measure the spin of SUSY particles at the LHC [165]. For this study, the production asymmetry was required as the observable was an asymmetry that had an opposite sign depending on whether a squark or anti-squark was produced. Thus the observable would vanish if no production asymmetry was present.

For our triple product asymmetries, we encounter a similar effect. As the triple products are CP-odd, our asymmetries also have the opposite sign depending on the particle/anti-particle nature of the squark in the cascade decay. Thus, we would also have no net triple product asymmetry if there was not a production asymmetry between the squarks and anti-squarks.

An additional advantage of considering squarks is that when we consider the associated production with gluinos, some decay topologies allow the full kinematic reconstruction of the event even with missing momentum, Sec. 5.3. As shown in Eq. (3.35), if we can fully reconstruct the kinematics of a decay we can boost into a reference frame in which the asymmetry is maximal. Hence, we can recover the rest frame asymmetry and have the potential to substantially reduce the number of reconstructed events required to see an asymmetry at the LHC.

5.1.2 Disadvantages of squark decay

Unfortunately, there are also some disadvantages when comparing squark cascade decays to those of stops. Firstly, we are no longer sensitive to any spin correlation carried by the q in the decay, $\tilde{q}_i \rightarrow \tilde{\chi}_j^0 + q$, as it will not decay to two separate reconstructible particles. Hence, we cannot probe any CP-violating effects in the squark mixing matrix and we are only sensitive to CP phases in the neutralino mass matrix.

A second disadvantage with the squark decay, is that we are not able to tag the charge of the produced quark. As mentioned above, the charge conjugate decay has an asymmetry of the opposite sign so if we had an equal sample of squarks and anti-squarks, the asymmetry would completely cancel and become unobservable. However, due to the production asymmetry between squarks and anti-squarks, this problem can be overcome at the LHC. In principle though, for the asymmetry to be unambiguously CP-violating, we need to define a true CP-odd asymmetry between the charge conjugate decays, Eq. (3.40). This is not possible for the decay shown in Eq. (5.1) but there are good arguments as to why this quantity should be considered a 'good' CP-odd observable. We have shown in Sec. 3.2 that a T_N-odd observable may not correspond to a CP-odd observable in the presence of final state interactions (FSI). However, the only FSI possible in our decay chain are electroweak in nature. These are expected to be a small total effect and therefore, the effect on the asymmetry are assumed to be even smaller. In addition, similar decay chains where no CP-violating effects are expected should be studied for triple product correlations. If no correlations are found in these chains, we should be able to assume that the correlations produced in the decays of interest are really CP-violating.

5.1.3 The study

We calculate the process shown in Eq. (5.1) fully analytically at the parton level to see the effect of CP-violating phases, Sec. 5.2. We also include the dominant production process and PDFs to understand the boosted frame dilution. To counteract the dilution we present the method that allows full kinematic reconstruction

of the events, Sec. 5.3. In Sec. 5.4 we present the numerical results of the study. We also produce Monte Carlo events with explicit CP-violation included. We perform basic selection cuts and include some experimental effects on these events to try and accurately gauge the luminosity required to see CP-violation at the LHC.

5.2 Formalism

5.2.1 The process studied and the amplitude squared

As stated in the introduction, one of the dominant SUSY channels in many scenarios at the LHC is associated squark-gluino production. At the tree level the production process Eq. (5.3) proceeds via the light quark exchange in the direct channel and squark/gluino exchange in the t channel, as seen in Fig. 5.1,

$$gq \to \tilde{g}\tilde{q}_L. \tag{5.3}$$

We study the case where the squark subsequently decays via the following chain:

$$\tilde{q}_L \to \tilde{\chi}_j^0 + q \to \tilde{\chi}_1^0 \ell^+ \ell^- + q. \tag{5.4}$$

The first step in the cascade decay chain is the two-body process $\tilde{q}_L \to q\tilde{\chi}_2^0$. As in Chapter 4 we consider spectra where the second step in the cascade decay chain is the three-body decay of the neutralino, $\tilde{\chi}_2^0 \to \tilde{\chi}_1^0 \ell^+ \ell^-$ (cf. Appendix B.3). The relevant diagrams can be seen in Fig. 4.2. CP-violating couplings of both the $\tilde{\chi}_2^0$ and $\tilde{\chi}_1^0$ are present in this decay and the phases affect the masses of $\tilde{\chi}_1^0$ and $\tilde{\chi}_2^0$, as well as the couplings and decay rates. In addition, the spin vector of the $\tilde{\chi}_2^0$ has to be explicitly included in the amplitude since the full spin correlations have to be taken into account.

We again use the narrow-width approximation, Sec. 4.2.2, so that the squared amplitude $|T|^2$ of the full process can be factorised into the processes of production $pp \to \tilde{g}\tilde{q}_L$ and the subsequent decays $\tilde{q}_L \to q\tilde{\chi}_2^0$, $\tilde{\chi}_2^0 \to \tilde{\chi}_1^0 \ell^+ \ell^-$. We also include the spin correlations between the production and decay of the $\tilde{\chi}_2^0$. For the purpose of analysing neutralino decays we do not need to include decays of the gluino produced with a squark but they will be needed later for momentum reconstruction,
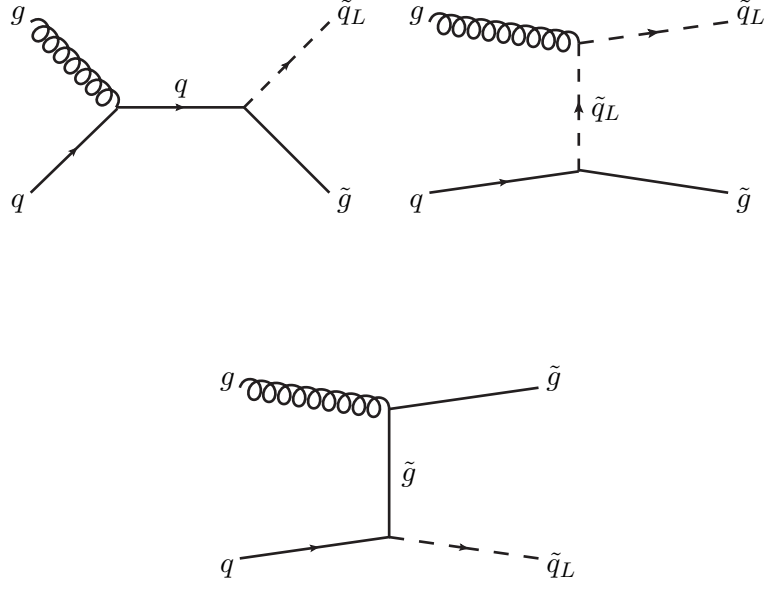
Figure 5.1: Feynman diagrams for the associated production process of squarks and gluinos at the LHC, $gq \to \tilde{g}\tilde{q}_L$.

see Sec. 5.3. Applying the narrow-width approximation for the masses of the intermediate particles, $\tilde{q}_L$ and $\tilde{\chi}_2^0$, is appropriate since the widths of the respective particles are in all cases much smaller than their masses and the mass differences between them are large enough, see Appendix C. The squared amplitude can then be expressed in the form,

$$|T|^2 \;=\; 4|\Delta(\tilde{q}_L)|^2|\Delta(\tilde{\chi}_2^0)|^2 P(\tilde{g}\tilde{q}_L)\Big\{ P(\tilde{\chi}_2^0)D(\tilde{\chi}_2^0) + \sum_{a=1}^{3} \Sigma_P^a(\tilde{\chi}_2^0)\Sigma_D^a(\tilde{\chi}_2^0)\Big\}, \quad (5.5)$$

where $a = 1, 2, 3$ refers to the polarisation states of the neutralino $\tilde{\chi}_2^0$, which are described by the polarisation vectors $s^a(\tilde{\chi}_2^0)$, given in Appendix B.2. In addition,

- $\Delta(\tilde{q}_L)$ and $\Delta(\tilde{\chi}_2^0)$ are the propagators of the intermediate particles which lead to the factors $E_{\tilde{q}_L}/m_{\tilde{q}_L}\Gamma_{\tilde{q}_L}$ and $E_{\tilde{\chi}_2^0}/m_{\tilde{\chi}_2^0}\Gamma_{\tilde{\chi}_2^0}$ in the narrow-width approximation,

- $P(\tilde{g}\tilde{q}_L)$, $P(\tilde{\chi}_2^0)$ and $D(\tilde{\chi}_2^0)$ are the terms in the production and decay that are independent of the polarisations of the decaying neutralino, whereas

- $\Sigma_P^a(\tilde{\chi}_2^0)$ and $\Sigma_D^a(\tilde{\chi}_2^0)$ are the terms containing the correlations between production and decay spin of the $\tilde{\chi}_2^0$.

According to our choice of the polarisation vectors $s^a(\tilde{\chi}_2^0)$, see Eq. (B.7.45-B.7.47) in Appendix B.7, $\Sigma_P^3/P(\tilde{\chi}_2^0)$ is the longitudinal polarisation, $\Sigma_P^1/P(\tilde{\chi}_2^0)$ is the transverse polarisation in the production plane, and $\Sigma_P^2/P(\tilde{\chi}_2^0)$ is the polarisation perpendicular to the reference plane of the neutralino $\tilde{\chi}_2^0$.

5.2.2 Structure of the T-odd asymmetry

We again use the triple products introduced in Sec. 3.3 to study the CP-violating effects at the LHC. In this chapter we study the triple product analogous to one previously studied in relation to stop decay, Eq. (4.12),

$$\mathcal{T} = \vec{p}_q \cdot (\vec{p}_{\ell^+} \times \vec{p}_{\ell^-}). \tag{5.6}$$

The T-odd asymmetry, Sec. 3.4, can again be defined for the triple product as,

$$\mathcal{A}_\mathcal{T} = \frac{N_{\mathcal{T}_+} - N_{\mathcal{T}_-}}{N_{\mathcal{T}_+} + N_{\mathcal{T}_-}} = \frac{\int \text{sign}\{\mathcal{T}\}|T|^2 d\,\text{lips}}{\int |T|^2 d\,\text{lips}}, \tag{5.7}$$

where $N_{\mathcal{T}_+}$ ($N_{\mathcal{T}_-}$) are the numbers of events for which $\mathcal{T}$ is positive (negative) and d lips denotes Lorentz invariant phase space. The denominator in Eq. (5.7), $\int |T|^2 d\,\text{lips}$, is equal to the total cross section, namely $\sigma(pp \rightarrow \tilde{q}_L \tilde{g} \rightarrow q\tilde{\chi}_1^0 \ell^+ \ell^- \tilde{g})$. In the corresponding numerator of Eq. (5.7), the triple-product correlations only enter via the spin-dependent terms. If the spin of the particles is neglected in the calculation, the asymmetry will vanish. In addition, in order to identify the T-odd contributions, we have to identify those terms in $|T|^2$, Eq. (5.5), which contain the triple product shown in Eq. (5.6).

As shown in Eq. (3.34), triple products are produced when covariant products, $i\epsilon_{\mu\nu\rho\sigma}a^\mu b^\nu c^\rho d^\sigma$, are found in the amplitude squared of the process. In our process, T-odd terms with ϵ-tensors are only contained in the spin-dependent contribution to the three body neutralino decay, $\Sigma_D^a(\tilde{\chi}_j^0)$. As stated in the introduction, we cannot probe the polarisation of the quark produced in the decay $\tilde{q}_i \rightarrow q\tilde{\chi}_2^0$ and therefore, we have no T-odd contribution coming from this decay, Eq. (B.2.14).

For the decay of the $\tilde{\chi}_2^0$, it is convenient to split the spin dependent term $\Sigma_D^a(\tilde{\chi}_j^0)$ into a T-odd term, $\Sigma_D^{a,O}(\tilde{\chi}_j^0)$, containing the respective triple products and a T-even term, $\Sigma_D^{a,E}(\tilde{\chi}_j^0)$, without triple products,

$$\Sigma_D^a(\tilde{\chi}_j^0) = \Sigma_D^{a,O}(\tilde{\chi}_j^0) + \Sigma_D^{a,E}(\tilde{\chi}_j^0). \tag{5.8}$$

The contributions to $\Sigma_D^{a,O}(\tilde{\chi}_j^0)$ and $\Sigma_D^{a,E}(\tilde{\chi}_j^0)$ are given in Eq. (B.3.32) and Eq. (B.3.25) respectively. We must also remember that these terms are multiplied by the spin dependent (but T-even) contribution to the squark decay, $\Sigma_P^a(\tilde{\chi}_j^0)$, Eq. (B.2.14).

When multiplying these terms together and composing a T-odd quantity, the only term of $|T|^2$ that contributes to the numerator of $\mathcal{A}_T$ is therefore,

$$|T|^2 \supset \sum_{a,b=1}^{3} \left[\Sigma_P^a(\tilde{\chi}_j^0) \Sigma_D^{a,O}(\tilde{\chi}_j^0) \right]. \tag{5.9}$$

Comparing Eq. (B.2.14) in the squark decay to Eqs. (B.3.33-B.3.35) in the $\tilde{\chi}_2^0$ decay leads to the following combination of momenta,

$$\Sigma_P^a(\tilde{\chi}_j^0) \Sigma_D^{a,O}(\tilde{\chi}_j^0) \sim (p_q s^a(\tilde{\chi}_2^0)) \times i\epsilon_{\mu\nu\rho\sigma} s^{a\mu}(\tilde{\chi}_2^0) p_{\tilde{\chi}_2^0}^{\nu} p_{\ell-}^{\rho} p_{\ell+}^{\sigma}. \tag{5.10}$$

Contracting the spin indices using Eq. (4.10), leads the following covariant product in the numerator of Eq. (5.7),

$$i\epsilon_{\mu\nu\rho\sigma} p_q^{\mu} p_{\tilde{\chi}_2^0}^{\nu} p_{\ell-}^{\rho} p_{\ell+}^{\sigma}, \tag{5.11}$$

which in turn produces the triple product that we use as our observable, Eq. (5.6).

Any CP-violating phases enter via the coupling constants shown in Eqs. (B.3.33-B.3.35). For example, in the Z^0, $\tilde{\ell}$ interference channel, Eq. (B.3.34), the following coupling constant contributes,

$$a_j^{\tilde{\ell}} a_k^{\tilde{\ell}*} O_{kj}^{L*}, \tag{5.12}$$

where $a_j^{\tilde{\ell}}$ is a coupling between $\tilde{\chi}_j^0 \, \tilde{\ell} \, \ell$, Eq. (A.4.17), and O_{kj}^{L*} is the coupling between $\tilde{\chi}_j^0 \, \tilde{\chi}_k^0 \, Z^0$. CP phases in the neutralino mass matrix, Eq. (2.26), enter all of these couplings, giving rise to the CP-violating triple products.

5.3 Momentum reconstruction

5.3.1 Dilution effects

The triple product that is constructed from momenta in the laboratory frame suffers from dilution factors at the LHC. The dilution is due to the lab frame being boosted with respect to the rest frame of the $\tilde{\chi}_2^0$, for a more detailed discussion see Sec. 3.5.

$$\mathcal{T} = \vec{p}_q \cdot (\vec{p}_{\ell^+} \times \vec{p}_{\ell^-})$$

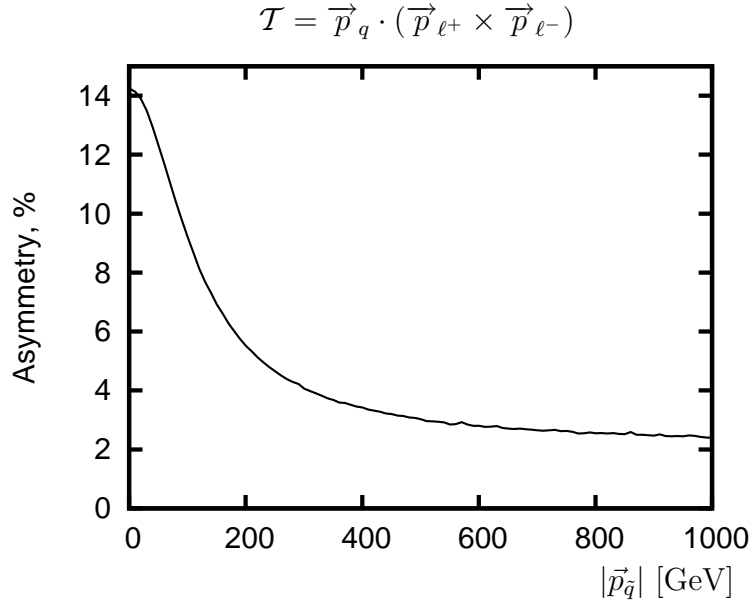Figure 5.2: The parton-level asymmetry $\mathcal{A}_{\mathcal{T}}$, Eq. (5.7), for the single decay chain given in Eq. (5.4) as a function of the squark momentum, $|\vec{p}_{\tilde{q}}|$, in the laboratory frame. Only the $\tilde{q}$ asymmetry is shown and the dilution due to $\tilde{q}^*$ is not included. The scenario is given in Table 5.1 with the phase $\phi_{M_1} = 3\pi/2$.

In Sec. 4.3.5 we also explained how the $\tilde{t}_1$ rest frame is equivalent to the $\tilde{\chi}_2^0$ rest frame and this argument follows for the $\tilde{q}$ rest frame as well.

Just as in the stop study presented in Chapter 4 we see a considerable reduction in the maximum asymmetry observable when we introduce the PDFs which causes an undetermined boost to the system. To illustrate the dilution, Fig. 5.2 shows how the parton-level asymmetry $\mathcal{A}_{\mathcal{T}}$, Eq. (5.7), is diluted in the laboratory frame when we produce the $\tilde{q}$ with varying initial momenta. The plot was produced with an analytical calculation for the single decay chain given in Eq. (5.4). The scenario displayed in Tab. 5.1 was used but with the phase set to $\phi_{M_1} = 3\pi/2$.

We see that the asymmetry is maximal, $\mathcal{A}_{\mathcal{T}} \sim 14\%$, when the $\tilde{q}$ is at rest but drops to, $\mathcal{A}_{\mathcal{T}} \sim 2.5\%$, when $|\vec{p}_{\tilde{q}}| \sim 1$ TeV. We must state that the magnitude of the dilution depends on the chosen scenario and in particular on the masses of the particles involved in the process. If it were possible to reconstruct the momentum of the $\tilde{q}$, we could however perform a Lorentz transformation of all the momenta and bypass the dilution factor, potentially recovering the full asymmetry.
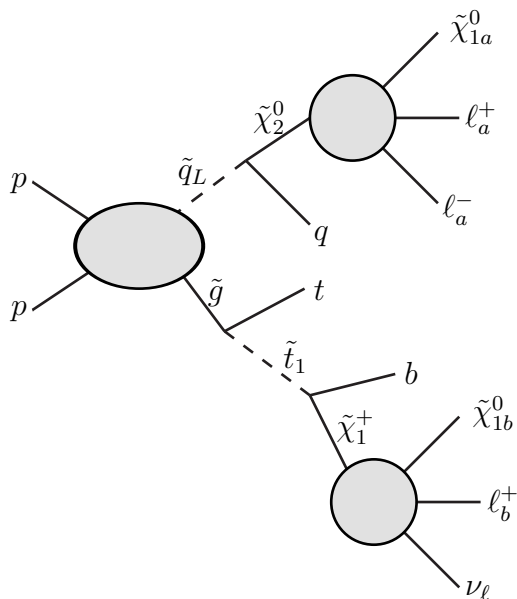
Figure 5.3: The process studied for momentum reconstruction.

5.3.2 Reconstruction procedure

In the mSUGRA scenario that we have chosen to study in this paper (see Section 5.4.1) the full reconstruction of the event is made possible by considering the decay chains of both the particles produced in the hard collision. We include all the particles coming from both the $\tilde{q}_L$ and the $\tilde{g}$ because there are not enough kinematic constraints to perform reconstruction if only the $\tilde{q}$ chain is considered. Therefore we exclusively consider the production of $\tilde{q}_L$ and $\tilde{g}$ and their subsequent decays, see Fig. 5.3. The $\tilde{q}_L$ decay chain will be the same as considered in Eq. (5.4) and the $\tilde{g}$ will decay as follows:

$$\tilde{g} \rightarrow \tilde{t} + t \rightarrow \tilde{\chi}_1^+ + b + t \rightarrow \tilde{\chi}_1^0 \ell^+ \nu_\ell + b + t. \tag{5.13}$$

In many scenarios the production of $\tilde{q}_L$ along with $\tilde{g}$ is the dominant source of the first and second generation squarks at the LHC and in the considered scenarios the branching ratios for these decay chains are favourable (cf. Sec 5.4).

Assuming that all the masses in the decay chains are known, Sec. 5.3.5, the kinematics can be fully reconstructed using the set of invariant conditions and the measured missing transverse momentum. For our procedure we follow the methods for solving the kinematic equations very closely to those presented in [166, 167]. The novelty here is the inclusion of three-body decays of sparticles and allowing for additional missing momentum due to neutrinos in the final state. The difference

lies also in using the mass constraints. For our purpose we assume that masses of sparticles are known and aim at the reconstruction of the momenta, whereas the previous studies used the above conditions to reconstruct masses.

Rather than fully reconstructing the kinematics of both decay chains, an alternative idea may be to estimate the momentum of the $\tilde{\chi}_2^0$ and then boost into this approximate frame. A formula that estimates the momentum was presented in [168] and is shown below,

$$\vec{p}_{\tilde{\chi}_2^0}^{\text{approx}} \equiv \left(1 + \frac{m_{\tilde{\chi}_1^0}}{M_{\ell\ell}} \right) \vec{p}_{\ell\ell} \,. \tag{5.14}$$

This approach does not work in our study however as the approximation only becomes valid when $\vec{p}_{\tilde{\chi}_1^0} \to 0$ in the rest frame of the $\tilde{\chi}_2^0$. At this kinematical endpoint the two leptons are back to back which causes the plane spanned by $\vec{p}_{l+}$ and $\vec{p}_{l-}$ to become badly defined. The triple product is therefore small and inaccurate leading to an asymmetry that is close to zero. Therefore the approach is not valid in our case.

In our process the following invariant equations can be formed.

- $\tilde{q}$ decay chain,

$$m_{\tilde{\chi}_1^0}^2 = (P_{\tilde{\chi}_{1a}^0})^2 \,, \tag{5.15}$$

$$m_{\tilde{\chi}_2^0}^2 = (P_{\tilde{\chi}_{1a}^0} + P_{\ell_a^+} + P_{\ell_a^-})^2 \,, \tag{5.16}$$

$$m_{\tilde{q}}^2 = (P_{\tilde{\chi}_2^0} + P_q)^2 \,. \tag{5.17}$$

- $\tilde{g}$ decay chain,

$$m_{\tilde{\chi}_1^+}^2 = (P_{\tilde{\chi}_{1b}^0} + P_{\nu_\ell} + P_{\ell_b^+})^2 \,, \tag{5.18}$$

$$m_{\tilde{t}}^2 = (P_{\tilde{\chi}_1^+} + P_b)^2 \,, \tag{5.19}$$

$$m_{\tilde{g}}^2 = (P_{\tilde{t}} + P_t)^2 \,, \tag{5.20}$$

where P denote 4-momenta of respective particles, and where necessary we label particles coming from squark and gluino decays with subscripts a and b, respectively.

- We also have the missing transverse momentum constraint,

$$\overrightarrow{p}^T_{miss} \quad = \quad \overrightarrow{p}^T_{\tilde{\chi}^0_{1a}} + \overrightarrow{p}^T_{\tilde{\chi}^0_{1b}} + \overrightarrow{p}^T_{\nu_\ell}. \tag{5.21}$$

- We combine the momenta of $\tilde{\chi}^0_{1b}$ and ν_ℓ coming from the gluino together as it is impossible to resolve these two particles,

$$P_{\tilde{g}ME} = P_{\tilde{\chi}^0_{1b}} + P_{\nu_\ell}. \tag{5.22}$$

- An additional condition on the solutions is that the invariant $P^2_{\tilde{g}ME}$ has to be greater than the mass of the LSP, $m^2_{\tilde{\chi}^0_1}$,

$$P^2_{\tilde{g}ME} > m^2_{\tilde{\chi}^0_1}. \tag{5.23}$$

We apply this condition to each solution and discard as unphysical any that does not meet it.

After expressing the momenta of intermediate particles in terms of the final-state particles,

$$P_{\tilde{\chi}^0_2} \quad = \quad P_{\tilde{\chi}^0_{1a}} + P_{l^+_a} + P_{l^-_a}, \tag{5.24}$$

$$P_{\tilde{\chi}^+_1} \quad = \quad P_{\tilde{g}ME} + P_{\ell^+_b}, \tag{5.25}$$

$$P_{\tilde{t}} \quad = \quad P_b + P_{\tilde{\chi}^0_{1b}} + P_{\ell^+_b} + P_{\nu_\ell}, \tag{5.26}$$

we now have a total of eight equations, Eq. (5.15) - (5.21), and eight unknowns,

$$\left(E_{\tilde{\chi}^0_{1a}}, p_{\tilde{\chi}^0_{1a}}(x), p_{\tilde{\chi}^0_{1a}}(y), p_{\tilde{\chi}^0_{1a}}(z) \right), \tag{5.27}$$

$$\left(E_{\tilde{g}ME}, p_{\tilde{g}ME}(x), p_{\tilde{g}ME}(y), p_{\tilde{g}ME}(z) \right). \tag{5.28}$$

In principle the system can be solved to find $P_{\tilde{\chi}^0_1}$ and $P_{\tilde{g}ME}$. Equations Eq. (5.15) and Eq. (5.18) are quadratic in $P_{\tilde{\chi}^0_1}$ and $P_{\tilde{g}ME}$ respectively, so we consider these last. Using on-shell conditions, quadratic terms in the remaining equations can be removed giving 6 linear equations, therefore we can simply use a matrix to give us solutions in terms of the energies $E_{\tilde{\chi}^0_1}$ and $E_{\tilde{g}ME}$. We first expand $\overrightarrow{p}_{\tilde{\chi}^0_1}$ and $\overrightarrow{p}_{\tilde{g}ME}$ in terms of other momenta contained in the respective decay chains,

$$\overrightarrow{p}_{\tilde{\chi}^0_{1a}} \quad = \quad A\overrightarrow{p}_{\ell^+_a} + B\overrightarrow{p}_{\ell^-_a} + C\overrightarrow{p}_q, \tag{5.29}$$

$$\overrightarrow{p}_{\tilde{g}ME} \quad = \quad D\overrightarrow{p}_{\ell^+_b} + E\overrightarrow{p}_b + F\overrightarrow{p}_t. \tag{5.30}$$

We can now form the system of 6 linear equations for unknowns A-F with $E_{\tilde{\chi}^0_{1a}}$ and $E_{\tilde{g}ME}$ as free parameters,

$$
\mathcal{M}
\begin{pmatrix} A \\ B \\ C \\ D \\ E \\ F \end{pmatrix}
=
\begin{pmatrix}
\frac{1}{2}(m^2_{\tilde{\chi}^0_1} - m^2_{\tilde{\chi}^0_2}) + P_{\ell^+_a} \cdot P_{\ell^-_a} + E_{\tilde{\chi}^0_{1a}}(E_{\ell^+_a} + E_{\ell^-_a}) \\
\frac{1}{2}(m^2_{\tilde{\chi}^0_2} - m^2_{\tilde{q}}) + P_{\ell^+_a} \cdot P_q + P_{\ell^-_a} \cdot P_q + E_{\tilde{\chi}^0_{1a}} E_q \\
\frac{1}{2}(m^2_b + m^2_{\tilde{\chi}^+_1} - m^2_{\tilde{t}}) + P_{\ell^+_b} \cdot P_b + E_{\tilde{g}ME} E_b \\
\frac{1}{2}(m^2_{\tilde{t}} + m^2_t - m^2_{\tilde{g}}) + P_{\ell^+_b} \cdot P_t + P_b \cdot P_t + E_{\tilde{g}ME} E_t \\
p^T_{miss}(x) \\
p^T_{miss}(y)
\end{pmatrix} , \quad (5.31)
$$

where,

$$
\mathcal{M} =
\begin{pmatrix}
(\vec{p}_{\ell^+_a} + \vec{p}_{\ell^-_a})\vec{p}_{\ell^+_a} & (\vec{p}_{\ell^+_a} + \vec{p}_{\ell^-_a})\vec{p}_{\ell^-_a} & (\vec{p}_{\ell^+_a} + \vec{p}_{\ell^-_a})\vec{p}_q & 0 & 0 & 0 \\
\vec{p}_{\ell^+_a}\vec{p}_q & \vec{p}_{\ell^-_a}\vec{p}_q & \vec{p}_q\vec{p}_q & 0 & 0 & 0 \\
0 & 0 & 0 & \vec{p}_b\vec{p}_{\ell^+_b} & \vec{p}_b\vec{p}_b & \vec{p}_b\vec{p}_t \\
0 & 0 & 0 & \vec{p}_t\vec{p}_{\ell^+_b} & \vec{p}_b\vec{p}_t & \vec{p}_t\vec{p}_t \\
p_{\ell^+_a}(x) & p_{\ell^-_a}(x) & p_q(x) & p_{\ell^+_b}(x) & p_b(x) & p_t(x) \\
p_{\ell^+_a}(y) & p_{\ell^-_a}(y) & p_q(y) & p_{\ell^+_b}(y) & p_b(y) & p_t(y)
\end{pmatrix}
$$
$$(5.32)$$

The matrix $\mathcal{M}$ can then be inverted to give solutions for each of the momentum components of $\vec{p}_{\tilde{\chi}^0_1}$ and $\vec{p}_{\tilde{g}ME}$ in terms of $E_{\tilde{\chi}^0_{1a}}$ and $E_{\tilde{g}ME}$. These solutions are substituted into the two quadratic equations, Eq. (5.15) and Eq. (5.18), to produce two equations of the form,

$$
a_{11}E^2_{\tilde{\chi}^0_{1a}} + a_{12}E_{\tilde{\chi}^0_{1a}}E_{\tilde{g}ME} + a_{22}E^2_{\tilde{g}ME} + a_1 E_{\tilde{\chi}^0_{1a}} + a_2 E_{\tilde{g}ME} + a \equiv F_A \quad = \quad 0 ,
$$
$$(5.33)$$

$$
b_{11}E^2_{\tilde{\chi}^0_{1a}} + b_{12}E_{\tilde{\chi}^0_{1a}}E_{\tilde{g}ME} + b_{22}E^2_{\tilde{g}ME} + b_1 E_{\tilde{\chi}^0_{1a}} + b_2 E_{\tilde{g}ME} + b \equiv F_B \quad = \quad 0 ,
$$
$$(5.34)$$

where the coefficients a_{ij}, a_i, a and b_{ij}, b_i, b are functions only of masses and measured momenta. We use,

$$
F_A - \frac{a_{11}}{b_{11}} \times F_B = 0 , \quad (5.35)
$$

to produce the linear equation for $E_{\tilde{\chi}_{1a}^0}$,

$$E_{\tilde{\chi}_{1a}^0} = \frac{a_{11}b - a\,b_{11} - a_2 b_{11} E_{\tilde{g}ME} + a_{11} b_2 E_{\tilde{g}ME} - a_{22} b_{11} E_{\tilde{g}ME}^2 + a_{11} b_{22} E_{\tilde{g}ME}^2}{-a_{11}b_1 + a_1 b_{11} + a_{12} b_{11} E_{\tilde{g}ME} - a_{11} b_{12} E_{\tilde{g}ME}}\,. \tag{5.36}$$

This result can then be substituted into Eq. (5.33) to obtain a quartic equation of the following form,

$$Q_4 E_{\tilde{g}ME}^4 + Q_3 E_{\tilde{g}ME}^3 + Q_2 E_{\tilde{g}ME}^2 + Q_1 E_{\tilde{g}ME} + Q_0 = 0\,, \tag{5.37}$$

where the various Q's are functions of the a's and b's in Eqs. (5.33) and (5.34).

5.3.3 Discussion of graphical solutions

Analysing the roots of the quartic equations, Eq. (5.37), we select the solutions that are real and discard the solutions that contain imaginary parts. The selected roots are substituted into Eq. (5.36) to find the corresponding solutions for $E_{\tilde{\chi}_{1a}^0}$. Using the values of $E_{\tilde{g}ME}$ and $E_{\tilde{\chi}_{1a}^0}$ together with the inverted matrix we can now calculate A, B, C, D, E, F, see Eqs. (5.29),(5.30) and hence the components of $\overrightarrow{p}_{\tilde{g}ME}$ and $\overrightarrow{p}_{\tilde{\chi}_{1a}^0}$.

In general, taking into account multiple roots, Eq. (5.37) has 4 solutions. Thus we would have 4 real, 2 real and 1 complex pair or 2 complex pairs of roots. Only the real roots can yield physical solutions, therefore for each event we normally expect real solutions. As Eq. (5.37) is derived from Eqs. (5.33) and (5.34) they share the same set of solutions. Both Equations (5.33) and (5.34) are polynomials of degree 2 in $E_{\tilde{\chi}_{1a}^0}$ and $E_{\tilde{g}ME}$ so they correspond to degree 2 curves in the $E_{\tilde{\chi}_{1a}^0}$ and $E_{\tilde{g}ME}$ plane (ellipses, hyperbolas or parabolas). The intersection points solve simultaneously both equations and at the same time the quartic Equation (5.37). A graphical solution to this set of equations is shown in Fig. 5.4 for one sample event. In this example we have two real solutions, of which only one corresponds to the actual momenta in the event.

In the realistic physical case one has to include uncertainties on measured momenta and masses. This will of course affect above equations and solutions. Smearing of momenta will typically result in shifting of the curves shown in Fig. 5.4.
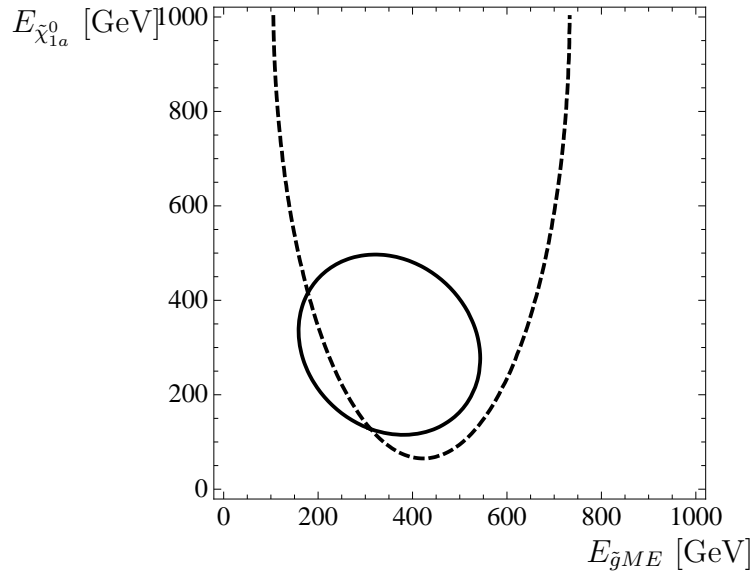
Figure 5.4: Ellipses in the $E_{\tilde{\chi}_{1a}^0}$ and $E_{\tilde{g}ME}$ plane corresponding to Equations (5.33) (solid line) and (5.34) (dashed line) for one sample event. Out of the two real solutions the lower right one gives the correct momenta of the original event.

Therefore it is possible that one can get two additional solutions or no real solutions at all. The consequences of experimental effects on our analysis will be discussed in Sec. 5.5.2.

5.3.4 Practical approach

In general more than one solution to the above system will remain depending upon the resolvent. In some cases Eq. (5.23) reduces the number of solutions further. For the application of this study we therefore calculate the triple product, Eq. (5.6), for each individual solution. If all solutions produce the same sign triple product we keep the event and use it in our asymmetry. If any of the solutions disagrees on the sign of the triple product we will discard the whole event and it will not contribute. This method has the disadvantage that we lose events and therefore statistical significance.

An additional issue when trying to complete the momentum reconstruction procedure are combinatorial problems when attempting to assign the measured momenta to the correct particle in the given event. If we take the leptons as an

example, we know that opposite sign, same flavour leptons must come from the $\tilde{\chi}_2^0$. However, it is possible that a same flavour lepton could be produced from the $\tilde{\chi}_1^+$ in the opposite decay chain and be confused with those coming from the $\tilde{\chi}_2^0$. In order to assign the leptons correctly to the decay chains one can use the conditions for invariant masses. In the squark decay chain a useful observable is the invariant mass of two leptons and in the gluino decay chain one can use the invariant mass of the b-jet from the stop decay and the lepton from chargino decay. The end points of these distributions are given by

$$M_{\ell_a^+ \ell_a^-} \quad < \quad m_{\tilde{\chi}_2^0} - m_{\tilde{\chi}_1^0}\,, \tag{5.38}$$

$$M_{b\ell_b^+} \quad < \quad \sqrt{\frac{(m_{\tilde{t}_1}^2 - m_{\tilde{\chi}_1^+}^2 - m_b^2)(m_{\tilde{\chi}_2^0}^2 - m_{\tilde{\chi}_1^0}^2)}{m_{\tilde{\chi}_1^+} m_{\tilde{\chi}_2^0}}}\,. \tag{5.39}$$

It turns out that only a small fraction of the events, around 5% in our scenario, satisfies both conditions simultaneously for the two possible assignments of the leptons in question. Moreover, if we run the momentum reconstruction algorithm, we find that physically acceptable solutions are only found in roughly 10% of events where a wrong assignment has occurred. These conditions act as a strong discriminant, therefore we do not expect lepton combinatorics to be a relevant issue for this study.

Another possible approach to this problem would be the subtraction of the opposite-sign opposite-flavour (OSOF) lepton pairs. In that case the quantities $N_{\mathcal{T}_+}$ and $N_{\mathcal{T}_-}$ in Eq. (5.7) would be defined as

$$N_{\mathcal{T}_+} \quad = \quad [N_{e^+ e^-} + N_{\mu^+ \mu^-} - N_{e^+ \mu^-} - N_{e^- \mu^+}]_{\mathcal{T}_+}\,, \tag{5.40}$$

$$N_{\mathcal{T}_-} \quad = \quad [N_{e^+ e^-} + N_{\mu^+ \mu^-} - N_{e^+ \mu^-} - N_{e^- \mu^+}]_{\mathcal{T}_-}\,. \tag{5.41}$$

In Eqs. (5.40) and (5.41) one adds the number of events with a positive (negative) triple product using $e^+ e^-$ pairs (and the jet) to the number of events with a positive (negative) triple product using $\mu^+ \mu^-$ pairs and subtract the number of events with positive triple product using $e^+ \mu^-$ and $e^- \mu^+$ pairs. For the combinatorial background one gets equal rates for same flavour and opposite flavour lepton pairs since the leptons are uncorrelated. Hence, this "flavour subtraction" procedure removes (up to statistical fluctuations) all combinatorial background resulting from the lepton pairing problem and also all background coming from $\tilde{\chi}_2^0 \rightarrow \tilde{\chi}_1^0 \tau^+ \tau^-$.

5.3.5 Mass reconstruction at the LHC

Since our procedure requires the sparticle masses to be known, we wish to comment on the possibility of mass determination in our scenario. One of the standard approaches at the LHC is to study kinematic edges and endpoints of the invariant mass distributions, see e.g. [157, 161, 169, 170]. In our case the masses of $\tilde{g}$, $\tilde{q}_L$, $\tilde{t}_1$, $\tilde{\chi}_{1,2}^0$ and $\tilde{\chi}_1^\pm$ are required. The possible invariant mass observables would include:

- quark and leptons in the decay chain of $\tilde{q}_L$ followed by the squark decay to chargino or neutralino $\tilde{\chi}_2^0$,

- lepton pair in the neutralino $\tilde{\chi}_2^0$ decay, cf. Eq. (5.38),

- top and bottom quarks in the gluino decay chain Eq. (5.13),

- bottom quark and lepton in the stop decay chain, cf. Eq. (5.39),

- quark pairs in the decay of gluino to the 1st and 2nd generation squarks [171, 172].

Fitting the above invariant masses to experimentally measured edges and endpoints should provide enough number of constraints to obtain the required information. However we must make it clear that all of the above studies examined two, 2-body decays for the $\tilde{\chi}_2^0$ and not the single three body decay that takes place in our scenario. Mass measurements for the three body decay were studied in [160] and similar mass end-points were found. A mass fit for a particular scenario was not attempted though so the expected accuracy cannot be given.

Whilst measuring the masses of the individual particles is obviously important, for the majority of our equations in Eq. (5.31), we actually require the difference between various m^2's in the decay chains. The mass differences are measured directly by the respective end-points and it is hoped that this method will measure these mass differences with high accuracy $\mathcal{O}(1\%)$ for leptonic final-states [157]. Final-states involving jets will obviously be less well constrained but it is hoped measurements of $\mathcal{O}(5\ \mathrm{GeV})$ may be possible. Errors at this level were tested on the reconstruction procedure but very little degradation was noted. For stops and charginos, some

model assumptions may be required on the masses before we can begin to use the kinematic reconstruction.

The on-shell mass condition for the $\tilde{\chi}_1^0$ requires the absolute mass scale and this should be measured at the LHC to a precision of better than 10% [157] for low mass scenarios similar to the phenomenology presented in this chapter. As an extra check on the numerical stability of the reconstruction procedure, up to 20 GeV absolute mass errors were tested on the absolute mass scale of the decay chain as a conservative estimate. This had a negligible effect on the reconstruction efficiency and the CP-asymmetry and is therefore not considered to be a problem.

In addition new methods have been proposed for measuring the sparticle masses from the kinematic invariants directly [158, 159, 166, 167, 173, 174]. These methods also employ the mass invariants on an event-by-event basis but use this information to reconstruct the masses of the particles in the decay chain. Therefore, these methods are directly measuring the inputs we require for Eq. (5.31). We then use the output from these methods to reconstruct the $\tilde{\chi}_1^0$ on an event-by-event basis.

The impact of the mass uncertainties will be discussed in Section 5.5.2. Comprehensive reviews of all the major mass reconstruction methods proposed for the LHC are given in [162, 163].

5.4 Numerical results

5.4.1 Chosen scenario: spectrum and decay modes

In order to study the experimental prospects of measuring CP-violating effects at the LHC we use an MSSM scenario derived from mSUGRA parameters defined at the GUT scale, as shown in Tab. 5.1. This scenario has been already used to analyse the properties of the neutralino sector in [113]. The values of the parameters at the electroweak scale have been derived using the RGE code `SPheno` [148]. Masses of the coloured particles are of order 500 GeV, apart from the light stop $\tilde{t}_1$, which has a mass of 171.0 GeV. The lightest supersymmetric particle (LSP) is the lightest neutralino with a mass of 78.1 GeV. The second neutralino and the light chargino have masses around 150 GeV, whereas the sleptons are around 200 GeV. Therefore

Parameter	Value	Particle	Mass [GeV]	Particle	Mass [GeV]
m_0	150 GeV	$\tilde{g}$	496.5	$\tilde{\chi}_1^0$	78.1
$m_{1/2}$	200 GeV	$\tilde{d}_L$	484.1	$\tilde{\chi}_2^0$	148.4
A_0	-650 GeV	$\tilde{d}_R$	466.4	$\tilde{\chi}_1^\pm$	148.2
$\tan\beta$	10	$\tilde{u}_L$	477.9	$\tilde{\chi}_2^\pm$	436.0
$\text{sign}\,\mu$	+	$\tilde{u}_R$	465.9	$\tilde{e}_L$	207.5
$|M_1|$	80.5 GeV	$\tilde{b}_1$	397.2	$\tilde{e}_R$	173.1
M_2	153.3 GeV	$\tilde{b}_2$	462.6	$\tilde{\nu}_e$	192.0
M_3	484.6 GeV	$\tilde{t}_1$	171.0	$\tilde{\tau}_1$	149.4
μ	419.0 GeV	$\tilde{t}_2$	498.0	$\tilde{\tau}_2$	212.5
				$\tilde{\nu}_\tau$	187.2

Table 5.1: mSUGRA input parameters at the GUT scale, MSSM parameters and particle masses in GeV from SPheno 2.2.3 [148] for $\phi_{M_1} = 0$ and with $m_t = 171$ GeV.

we note that the two-body decay channels of $\tilde{\chi}_2^0$ and $\tilde{\chi}_1^\pm$ are closed and this gives a good opportunity to study CP-violation effects in their three-body decay modes. Details of the mass spectrum can be found in Tab. 5.1. The values of the gaugino mass parameters reproduce the given spectrum in the case when all the CP phases are set to 0. In order to generate CP-violating effects in the following we will attribute a non-zero phase ϕ_{M_1} to the bino mass parameter,

$$M_1 = |M_1|e^{i\phi_{M_1}}, \qquad 0 \le \phi_{M_1} < 2\pi, \tag{5.42}$$

while keeping the absolute value $|M_1|$ fixed as given in Tab. 5.1.

Although we chose a specific scenario our method is applicable in a wider range of parameter points. For the decay chain that we concentrate on, we require the three-body decay of the $\tilde{\chi}_2^0$ which places the following constraints on the SUSY

masses,

$$m_{\tilde{\chi}_2^0} < m_{\tilde{\ell}}, \tag{5.43}$$

$$m_{\tilde{\chi}_2^0} - m_{\tilde{\chi}_1^0} < m_Z. \tag{5.44}$$

Equation (5.43) ensures that the decay, $\tilde{\chi}_2^0 \to \tilde{\ell}\ell$ cannot occur whereas Eq. (5.44) forbids the decay $\tilde{\chi}_2^0 \to Z\tilde{\chi}_1^0$.

To complete momentum reconstruction from the gluino side, other decay modes can contribute with regard to the scenario presented here but their impact on the final result would be scenario dependent. For example if the decay $\tilde{t} \to t\tilde{\chi}_2^0$ became kinematically open the momentum reconstruction would actually become easier as there would be no neutrino in the final state and the system would become over-constrained. However, there would now be one additional top and one additional lepton in the final state that may cause new combinatorial difficulties.

As already mentioned, the highest production rate is typically obtained for coloured final-states containing squarks and gluinos at the LHC. In our scenario, where their masses are not very heavy, the total cross section for production of strongly interacting supersymmetric particles reaches 140 pb, see Tab. 5.2. For our purpose we will be interested in the inclusive production of left squarks and the associated production of left squark and gluino[1]. As was mentioned in Sec. 3.3, anti-squarks give a CP asymmetry with exactly the opposite sign to squarks. We note however that the inclusive cross section for left squark production is almost a factor of 4 larger than the cross section for left anti-squark production. This is a direct consequence of the fact that we have two protons in the initial state for which the abundance of quarks is significantly higher than of anti-quarks. Since we cannot distinguish experimentally squarks and anti-squarks of the first two generations this fraction of anti-squarks will cause some dilution in the asymmetry. A similar situation occurs for associated squark-gluino production for which the ratio of squarks

---

[1]Triple product asymmetry in right squarks decay chain has the opposite sign as compared to the left squarks (and the same sign as that of left anti-squarks), however in our case where the coupling of the right squark to the second lightest neutralino is suppressed due to small bino component of $\tilde{\chi}_2^0$, this contribution remains negligible.

Produced Particles	Cross Section (pb)
At least one coloured SUSY particle.	148
At least one $\tilde{g}$.	58.8
$\tilde{q}_L\tilde{q}_L + \tilde{q}_L\tilde{q}_L^* + \tilde{q}_L\tilde{q}_R + \tilde{q}_L\tilde{q}_R^* + \tilde{q}_L\tilde{g}$	30.0
$\tilde{q}_L^*\tilde{q}_L + \tilde{q}_L^*\tilde{q}_L^* + \tilde{q}_L^*\tilde{q}_R + \tilde{q}_L^*\tilde{q}_R^* + \tilde{q}_L^*\tilde{g}$	8.3
$\tilde{q}_L\tilde{g}$	18.2
$\tilde{q}_L^*\tilde{g}$	3.1
$\tilde{t}_1\tilde{t}_1^*$	66.3

Table 5.2: Leading order cross sections at $\sqrt{s} = 14$TeV for direct production of various particles from `Herwig++ 2.3.2` [151, 152] using `MRST 2004LO` PDF set [156]. $\tilde{q}$ stands for squarks of the first and second generation.

to anti-squarks is 18.2 pb to 3.1 pb, see Tab. 5.2. Together with left squarks we also have the production of right squarks at a comparable rate. However, since the latter decay almost exclusively to the lightest neutralino in our scenario, as shown in Tab. 5.3, they do not give rise to the CP-odd asymmetry.

Following the production process we include subsequent decays of squarks and gluinos. The dominant decay mode of the gluino is to the light stop and the top with a branching ratio of $BR = 53.8\%$. The light stop then decays almost exclusively to $\tilde{\chi}_1^{\pm}b$. Left squarks decay mainly to the light chargino and the second lightest neutralino with branching fractions of 65% and 33% respectively. Finally we consider the decays of chargino $\tilde{\chi}_1^{\pm}$ and neutralino $\tilde{\chi}_2^0$. Leptonic decays constitute in total $BR = 61\%$ for the chargino and $BR = 68\%$ for the neutralino decay modes. For decays into light leptons we have $BR = 24.3\%$ and $BR = 9\%$ for chargino and neutralino, respectively. The most interesting are the neutralino decays to electrons and muons that are used to construct the CP-sensitive triple product, Eq. (5.6). The summary of the relevant branching ratios can be found in Tab. 5.3. It may be noted that in the scenario presented, the branching ratio $\tilde{\chi}_2^0 \to \tilde{\chi}_1^0\tau^+\tau^-$ is high (59.3%).

Decay	BR	Decay	BR	Decay	BR
$\tilde{g} \to \tilde{t}_1 \bar{t} + \text{c.c.}$	53.8%	$\tilde{q}_L \to \tilde{\chi}_1^{\pm} q$	65%	$\tilde{t}_1 \to \tilde{\chi}_1^+ b$	98.1%
$\tilde{g} \to \tilde{b}_1 \bar{b} + \text{c.c.}$	26.6%	$\tilde{q}_L \to \tilde{\chi}_2^0 q$	33%	$\tilde{t}_1 \to \tilde{\chi}_2^0 c$	1.6%
$\tilde{g} \to \tilde{q}_R \bar{q} + \text{c.c.}$	11.8%	$\tilde{q}_L \to \tilde{\chi}_1^0 q$	1.5%	$\tilde{\chi}_2^0 \to \tilde{\chi}_1^0 \tau^- \tau^+$	59.3%
$\tilde{g} \to \tilde{b}_2 \bar{b} + \text{c.c.}$	3.8%	$\tilde{\chi}_1^+ \to \tilde{\chi}_1^0 \nu_\tau \tau^+$	37.2%	$\tilde{\chi}_2^0 \to \tilde{\chi}_1^0 \nu \bar{\nu}$	23.6%
$\tilde{g} \to \tilde{q}_L \bar{q} + \text{c.c.}$	3.3%	$\tilde{\chi}_1^+ \to \tilde{\chi}_1^0 q_u \bar{q}_d$	38.5%	$\tilde{\chi}_2^0 \to \tilde{\chi}_1^0 q \bar{q}$	8.1%
$\tilde{q}_R \to \tilde{\chi}_1^0 q$	98%	$\tilde{\chi}_1^+ \to \tilde{\chi}_1^0 \nu_\mu \mu^+$	12.2%	$\tilde{\chi}_2^0 \to \tilde{\chi}_1^0 e^+ e^-$	4.5%
$\tilde{q}_R \to \tilde{\chi}_2^0 q$	1%	$\tilde{\chi}_1^+ \to \tilde{\chi}_1^0 \nu_e e^+$	12.1%	$\tilde{\chi}_2^0 \to \tilde{\chi}_1^0 \mu^+ \mu^-$	4.5%

Table 5.3: Branching ratios for the scenario defined in Tab. 5.1 from `SPheno 2.2.3` [148] for $\phi_{M_1} = 0$.

This is due to the masses of the $\tilde{\chi}_2^0$ and $\tilde{\tau}$ being very close and hence the kinematic factors are favourable. The particular branching ratio is simply a coincidence in the scenario chosen however and is not a required feature for our study.

When we vary the phase of the M_1 parameter, the masses and couplings in the neutralino sector are affected. First we note that the changes in the neutralino masses are negligible and smaller than the possible experimental accuracy. It turns out however, that the phase ϕ_{M_1} has large impact on neutralino couplings and therefore the pattern of its decay modes. The most significant change is for the light chargino decays to the LSP and a fermion pair. With increasing phase the branching ratio for $\tilde{\chi}_1^+ \to \tilde{\chi}_1^0 \nu_\tau \tau^+$ rises and eventually reaches 70% for $\phi_{M_1} = \pi$. At the same time the branching ratios for decays to light leptons remain roughly at the level of 10%. As we will explain later, a chargino decay to tau, followed by a leptonic tau decay can be used for momentum reconstruction in the same way as a chargino decay to an electron and a muon. On the other hand, the decay $\tilde{\chi}_2^0 \to \tilde{\chi}_1^0 \tau^+ \tau^-$ followed by a leptonic tau decay will be a background, since it gives incorrectly reconstructed momenta. Finally, we note that in the case of neutralino $\tilde{\chi}_2^0$ decays to light leptons, the respective branching ratios increase up to 5.5% for $\phi_{M_1} = \pi/2$.
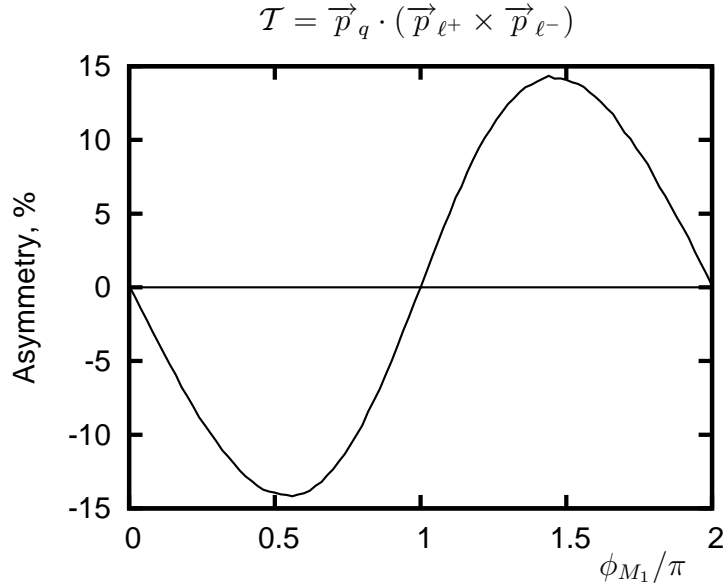
$$\mathcal{T} = \overrightarrow{p}_q \cdot (\overrightarrow{p}_{\ell^+} \times \overrightarrow{p}_{\ell^-})$$

Figure 5.5: The parton-level asymmetry $\mathcal{A}_\mathcal{T}$, Eq. (5.7), for the single decay chain given in Eq. (5.4) in the rest frame of $\tilde{q}_L$ as a function of ϕ_{M_1}. The scenario is given in Tab 5.1.

5.4.2   CP asymmetry at the parton level

We start by discussing the dependence of the asymmetry on ϕ_{M_1}, Eq. (5.7), at the partonic level studying only the decay chain presented in Eq. (5.4). In order to see a maximal effect, we place the $\tilde{q}_L$ at rest and calculate the triple product and the asymmetry in its distribution, Sec. 5.2.2.

We see from Fig. 5.5 that the maximal asymmetry in this scenario is roughly 14% and this occurs when the phase ϕ_{M_1} is just above $\pi/2$ and just below $3\pi/2$. The asymmetry is produced by a complex interplay between different couplings in the $\tilde{\chi}_2^0$ decay, cf. Eqs. (B.3.33)-(B.3.35), and can vary significantly between scenarios. These couplings can all have different behaviour with respect to ϕ_{M_1} and in other scenarios the maximum asymmetry can be seen far from $\pi/2$.

It should be noted from the previous plot that the asymmetry is obviously a CP-odd quantity that in addition to a measurement of the phase, also determines whether it lies above or below π, as seen in Fig. 5.5. In comparison, using CP-even quantities, for example the mass, it is not possible to determine if the phase is above or below π. It must also be noted that these quantities have a weak dependence upon the phase and will be challenging to study. Moreover CP-even quantities alone do

not give unambiguous proof of CP violation in the model, that can only be provided by CP-odd observables, see Sec. 3.2.

5.4.3 Influence of parton distribution functions on CP asymmetries

Experimentally the situation becomes significantly more complicated since in general, particles are not produced at rest but can be heavily boosted in the laboratory frame. Our observables can be significantly reduced in size by this effect as triple product correlations induced by spin effects are largest in the rest frame of the decaying particle. Essentially, a boosted frame can make the momentum vector of the quark appear to come from the opposite side of the plane formed by ℓ^+ and ℓ^-. As explained in Sec. 5.2.2 and before in Sec. 4.3.5, this causes a severe dilution in the asymmetry that is measured at the LHC.

There are two other dilution factors that have to be taken into account and give a further reduction in the observed asymmetry. The first one we consider is the contamination from anti-squarks $\tilde{q}_L^*$ that will be produced at the LHC along with squarks $\tilde{q}_L$. There is no way of identifying the charge of the produced quark in contrast to the top discussed in chapter 4 and chapter 6. Consequently we need to include the effect of the $\tilde{q}_L^*$ in our analysis. Anti-squarks produce an asymmetry of the opposite sign to $\tilde{q}_L$ so if for example we had equal numbers of each of them, no overall asymmetry could be seen. However, the production cross section for $\tilde{q}_L^*$ is substantially lower than that of $\tilde{q}_L$ due to the valence quarks in the proton, see Tab. 5.2 and at the LHC we would expect only roughly 20% of the sample to be $\tilde{q}_L^*$.

The other background contribution is that of neutralinos decaying to a tau pair, $\tilde{\chi}_2^0 \to \tilde{\chi}_1^0 \tau^+ \tau^-$ followed by leptonic tau decays to the pair of opposite-sign same-flavour leptons. Since the branching ratio for the above decay is large, even after inclusion of leptonic tau decays there is a significant number of events faking our signal, i.e.

$$BR(\tilde{\chi}_2^0 \to \tilde{\chi}_1^0 \tau^+ \tau^- \to \tilde{\chi}_1^0 \ell^+ \ell^- \nu_\ell \bar{\nu}_\ell \nu_\tau \bar{\nu}_\tau) \approx 2 \times 0.6 \times 0.175 \times 0.175 = 3.7\%. \quad (5.45)$$

compared with

$$BR(\tilde{\chi}_2^0 \rightarrow \tilde{\chi}_1^0 \ell_{e,\mu}^+ \ell_{e,\mu}^-) \approx 2 \times 0.045 = 9\%. \tag{5.46}$$

As the asymmetry calculated for such leptons is diluted, this background introduces a further dilution factor. However, this background can be easily removed using the flavour subtraction technique described above, Eqs. (5.40) and (5.41). In addition we will see later that much of this background is removed after the application of simple selection cuts on the lepton energy and the invariant mass.

We use the `MRST 2004LO` [156] PDF set in our analysis of the asymmetry and plot the integrated asymmetry $\mathcal{A}_\mathcal{T}$ as a function of ϕ_{M_1} in Fig. 5.6. We see that the inclusion of the PDFs and the $\tilde{q}_L^*$ sample reduce the asymmetry by about a factor of 8 in this scenario as compared to the result of Sec. 5.4.2. The maximum asymmetry is now $|\mathcal{A}_\mathcal{T}| = 1.7\%$. It must be noted that the dilution factor does depend on the scenario studied and changes in particular with the mass of the sparticle that is initially produced.

For the calculation of the asymmetry we included the production channels shown in rows 3 and 4 of Table 5.2 but we only take decays of individual $\tilde{q}_L$ and $\tilde{q}_L^*$ following the decay chain in Eq. (5.4). At this point correct identification was assumed for the final-state particles and no hadronisation or detector effects were included but these assumptions will be relaxed in Sec. 5.5. The only backgrounds in the study are those discussed above.

Using the total production cross sections[2] for $\tilde{q}_L$ and $\tilde{q}_L^*$, and respective branching ratios from Table 5.3 we can now estimate the integrated luminosity required to observe the asymmetry at the LHC with a certain significance.

We use the definition of statistical given in Sec. 3.6 and the significance of any particular asymmetry is given in Eq. (3.45). The horizontal lines in Fig. 5.6 show an estimate of the amount of luminosity required for a 3σ observation of a non-zero

---

[2]Note that the total rate of squark production is actually larger than 30.0 pb quoted in Table 5.2, as some of the subprocesses give a pair of squarks e.g. $(\tilde{q}_L\tilde{q}_L)$ and both can contribute to our analysis. The total number of squarks in the sample at the given luminosity $\mathcal{L}$ and $\sqrt{s} = 14$ TeV is therefore $33.2 \times \mathcal{L}$. In case of anti-squarks the number is $8.5 \times \mathcal{L}$.

$$\mathcal{T} = \overrightarrow{p}_q \cdot (\overrightarrow{p}_{\ell^+} \times \overrightarrow{p}_{\ell^-}), \quad \sqrt{s} = 14 \text{ TeV}$$
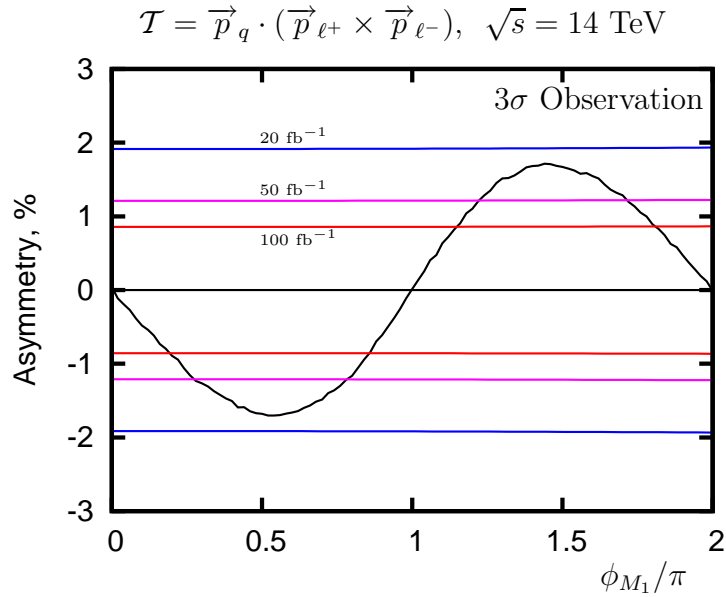

Figure 5.6: The parton-level asymmetry $\mathcal{A}_{\mathcal{T}}$, Eq. (5.7), in the laboratory frame with PDFs included in the analysis using the scenario shown in Tab. 5.1. The coloured lines show the size of the asymmetry needed for a 3σ observation at the given luminosity, $\mathcal{L}$=(20 fb^{-1}, 50 fb^{-1}, 100 fb^{-1}), assuming squarks were produced via the channels shown in rows 3 and 4 of Tab. 5.2. All produced $\tilde{q}$ and $\tilde{q}^*$ that follow the decay chain given in Eq. (5.4) are taken into account.

asymmetry. In other words, an asymmetry can be seen at the 3σ level where the asymmetry curve in Fig. 5.6 lies outside the luminosity band.

5.4.4 Impact of momentum reconstruction on the observable CP asymmetry

In order to increase the statistical significance of our CP asymmetry we investigate the possibility of reconstructing the momenta of the invisible particles in our process. In principle a perfect reconstruction would return the magnitude of the asymmetry to that where the $\tilde{q}_L$ is at rest but in reality there are additional complications with this procedure, see Sec. 5.3. The reconstruction is performed at the partonic level with PDF's included in the production process.

Again our sample of events will contain $\tilde{q}_L^*$ which have an asymmetry of the opposite sign to that of $\tilde{q}_L$ as has already been discussed in Sec. 5.4.3. As we are looking

$$\mathcal{T} = \overrightarrow{p}_q \cdot (\overrightarrow{p}_{\ell^+} \times \overrightarrow{p}_{\ell^-}), \ \sqrt{s} = 14 \text{ TeV}$$
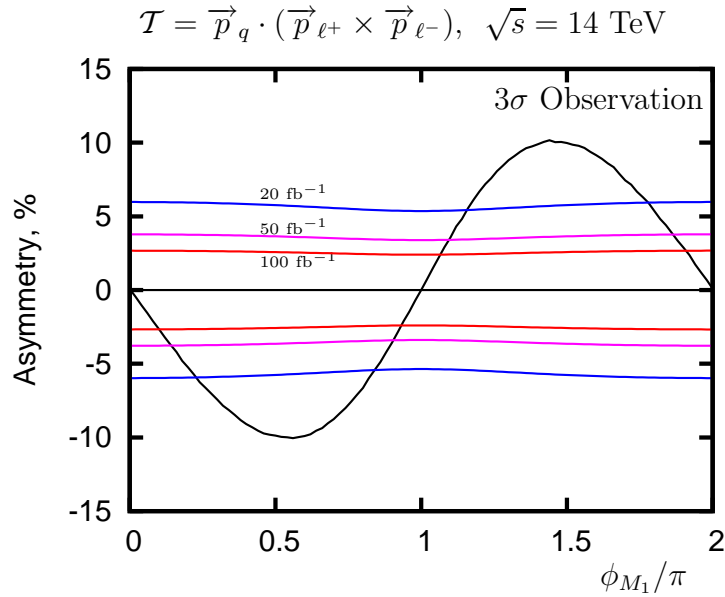
Figure 5.7: The parton-level asymmetry $\mathcal{A}_{\mathcal{T}}$, Eq. (5.7), in the reconstructed $\tilde{q}_L$ rest frame. The coloured lines show the size of the asymmetry needed for a 3σ observation at the given luminosity, $\mathcal{L}=(20 \text{ fb}^{-1}, 50 \text{ fb}^{-1}, 100 \text{ fb}^{-1})$ for the production channels $\tilde{q}_L\tilde{g}$, $\tilde{q}_L^*\tilde{g}$ Tab. 5.2. The decay chains included are shown in Eq. (5.4) and Eq (5.13). As explained in the text correct jet and lepton assignment is assumed.

exclusively at $\tilde{q}_L\tilde{g}$ and $\tilde{q}_L^*\tilde{g}$ production however when applying the momentum reconstruction, we actually have a smaller number of $\tilde{q}_L^*$ that dilute the asymmetry (15%, see Table 5.2). After including this dilution factor we see our maximum asymmetry reduced from $\mathcal{A}_{\mathcal{T}} \sim 14\%$ to $\mathcal{A}_{\mathcal{T}} \sim 11\%$, see Figs. 5.5 and 5.7, respectively.

To calculate the luminosity we require to see a statistically significant effect at the LHC we include the production cross sections for channels $\tilde{q}_L\tilde{g}$, $\tilde{q}_L^*\tilde{g}$ (Tab. 5.2) and the branching ratios from both the $\tilde{q}_L$ and $\tilde{g}$ decay chains Eq. (5.4) and Eq. (5.13). No hadronisation or detector effects were included in this section and correct identification was assumed for the quarks. For the leptons the correct assignment is made as is explained in Sec. 5.3.4. For the jets, a detailed experimental study would be required to look at this question as we need to include hard radiation, reconstruction and b-tagging efficiencies. However, a cursory examination suggests that the individual jets may be resolvable. For example, the jet coming from the $\tilde{q}_L$ decay is the hardest one for a high proportion of events. We would also require three other

jets to have the invariant mass m_t. Finally we would then require at least one b-jet to be tagged. We would like to state here that the only backgrounds included in the study are those of $\tilde{q}_L^* \tilde{g}$ production and the decay chain Eq. (5.45).

After inclusion of all branching ratios the production rate for our process drops down to 200 fb (after hadronic top decay), which results in approximately $20\,000$ events at the integrated luminosity $\mathcal{L} = 100$ fb^{-1}. One extra point to note is that we are able to use events where the $\tilde{\chi}_1^\pm$ in the opposite decay chain produces a $\tau^\pm$. Kinematically these events are similar to our normal signal events but we have one extra neutrino ν_τ that will be invisible and simply contribute to our missing transverse momenta. An additional factor that reduces the number of reconstructed and accepted events are the multiple solutions, as discussed in Sec. 5.3. We only use events when all solutions produce the same sign triple product and this allows us to use approximately $\sim 60\%$ of the events.

The horizontal lines in Fig. 5.7 again show an estimate of the amount of luminosity required for a 3σ observation of a non-zero asymmetry. It can be seen that the luminosity lines are not flat but actually give a narrower band as $\phi_{M_1} \to \pi$. This effect is caused by the branching ratios, $\tilde{q}_L \to q\tilde{\chi}_2^0$, $\tilde{\chi}_2^0 \to \tilde{\chi}_1^0 \ell^+ \ell^-$ and $\tilde{\chi}_1^+ \to \tilde{\chi}_1^0 \overline{\nu}_\ell \ell^-$ altering with the change in phase and producing more events. We see that after 20 fb^{-1} of well understood LHC data it may be possible to start seeing a statistically significant effect if large phases are present. It must be noted however that for this method to be successful we will require mass measurements of the individual particles involved in the decay chains. This will obviously require significant running time and may even need the help of a precision linear collider.

5.5 Inclusion of experimental factors

To more realistically estimate if the study will be possible at the LHC some additional experimental factors need to be included in the analysis. For this purpose we simulate events using the Monte Carlo event generator `Herwig++ 2.3.2` [151, 152]. These events will be used in the following to perform momentum reconstruction and as a cross check for our analytic calculations.

We start with the inclusion of the selection cuts that have to be used to resolve leptons and jets and these are listed below:

$$E_T(j_1) \geq 100 \text{ GeV}, \tag{5.47}$$

$$E_T(j) \geq 25 \text{ GeV}, \tag{5.48}$$

$$E_T(\ell_{e,\mu}) \geq 10 \text{ GeV}, \tag{5.49}$$

$$M_{\ell^+\ell^-} \geq 20 \text{ GeV}, \tag{5.50}$$

$$|\eta| \leq 2.5. \tag{5.51}$$

Here $E_T(j_1)$ is the transverse energy of the hardest jet, $E_T(j)$ is the transverse energy of all other jets, $E_T(\ell_{e,\mu})$ is the transverse energy of the leptons, $M_{\ell^+\ell^-}$ is the invariant mass of the opposite-sign same flavour lepton pair, and η is the pseudo-rapidity of all the final-state particles in the decay chain. Moreover we require at least two b-jets and that 1 b-jet plus 2 other jets (typically with the lowest p_T) should reconstruct the top quark. Since we need the top momentum to be reconstructed we only take into account tops that decay hadronically.

One of the consequences of the application of the above cuts, especially Eq. (5.49) and (5.50) is the significant reduction in the background originating from τ's, Eq. (5.45). This is due to the rather low energy of the leptons coming from τ decays and the even lower invariant mass of the resulting lepton pair, which is peaking around 0. Already at this point, approximately 95% of this background is removed.

Another factor we include is the momenta of the resolved particles being smeared due to the intrinsic experimental precision. The accuracy for both jets and electrons follows the same function but with different coefficients [175]:

$$\frac{\sigma_E}{E} = \sqrt{\frac{a_{j,e}^2}{E} + \frac{b_{j,e}^2}{E^2} + c_{j,e}^2}, \tag{5.52}$$

where

- for jets $a_j = 0.6 \text{ GeV}^{\frac{1}{2}}$, $b_j = 1.5 \text{ GeV}$ and $c_j = 0.03$;

- for electrons the accuracy is better, with $a_e = 0.12 \text{ GeV}^{\frac{1}{2}}$, $b_e = 0.2 \text{ GeV}$ and $c_e = 0.01$.

The resolution for muons has a different functional dependence,

$$\frac{\sigma_{p_T}}{p_T} = \begin{cases} 0.00008(p_T/\text{GeV} - 100) + 0.03, & p_T > 100\,\text{GeV}, \\ 0.03, & p_T < 100\,\text{GeV}. \end{cases} \tag{5.53}$$

In addition we also have a finite resolution on the measurement of missing transverse energy,

$$\frac{\sigma^x_{MET}}{E_T} = \frac{\sigma^y_{MET}}{E_T} = \frac{0.57}{\sqrt{E_T/\text{GeV}}}, \tag{5.54}$$

which are the errors on the x and y components of the MET vector and E_T is the scalar sum of all visible transverse energy .

The momenta smearing will only affect the observables when we perform momentum reconstruction as the LSP momenta will be reconstructed with limited precision. The triple product will not suffer however as the measurement only relies on the direction of the measured particles and not on the energy measurement. The direction can be found far more accurately and this error happens to be negligible for our observables.

Finally, we also investigate the fact that the masses of the particles in the decay chains we are interested in will only be known with a certain precision at the LHC (we assume 10% error), see Section 5.4.1. This error will again only affect the observables when we perform momentum reconstruction in order to boost into the rest frame of the $\tilde{\chi}^0_2$ and can cause the frame to be mis-measured, see Section 5.5.2 for more details.

5.5.1 Experimental factors without momentum reconstruction

Out of the experimental factors mentioned above, only the cuts affect the result for the triple product correlation measured in the laboratory frame. These cuts reduce the number of detectable events by $\approx 50\%$ and consequently significantly increase the luminosity required to make a statistically significant measurement at the LHC, see Fig. 5.8. For example if large phases are present we may begin to see hints with integrated luminosity $\mathcal{L} = 50$ fb^{-1}. With $\mathcal{L} = 300$ fb^{-1} we could become sensitive

$$\mathcal{T} = \overrightarrow{p}_q \cdot (\overrightarrow{p}_{\ell^+} \times \overrightarrow{p}_{\ell^-}), \quad \sqrt{s} = 14 \text{ TeV}$$
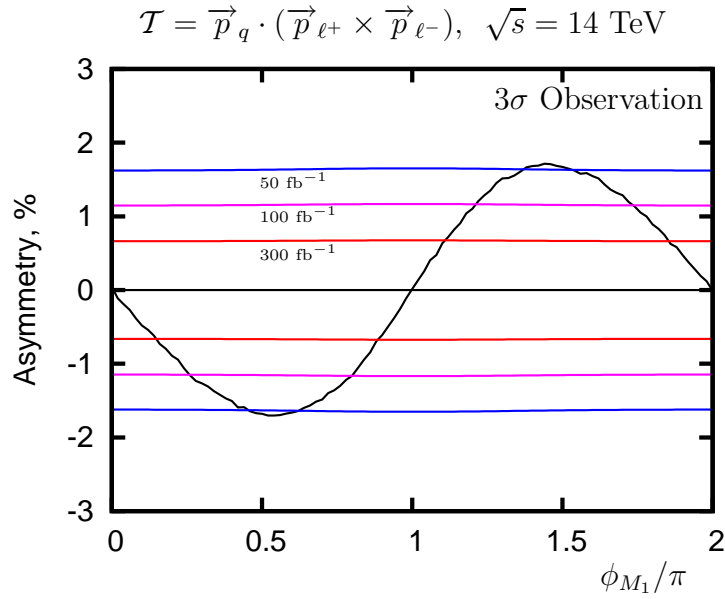
Figure 5.8: The asymmetry $\mathcal{A}_{\mathcal{T}}$, Eq. (5.7), in the laboratory frame for the decay chain Eq. (5.4) after the cuts, Eqs. (5.47)-(5.51), have been applied. The coloured lines show the size of the asymmetry needed for a 3σ observation at the given luminosity, $\mathcal{L}$=(50 fb^{-1}, 100 fb^{-1}, 300 fb^{-1}), assuming squarks were produced via the channels shown in rows 3 and 4 of Tab. 5.2. Momentum smearing for both the leptons and quarks was studied and found to have a negligible effect. All other relevant experimental details are mentioned in the text.

to phases in the ranges $0.15\,\pi \lesssim \phi_{M_1} \lesssim 0.9\,\pi$ and $1.1\,\pi \lesssim \phi_{M_1} \lesssim 1.85\,\pi$ where the asymmetry $|\mathcal{A}_{\mathcal{T}}| > 0.7\%$.

For the calculation of the asymmetry we included the production channels shown in rows 3 and 4 of Table 5.2 taking into account the decays of individual $\tilde{q}_L$ and $\tilde{q}_L^*$ as listed in Eq (5.4). No explicit hadronisation was included but momentum smearing is expected to simulate some of this effect. We also need to include additional hard QCD radiation and other detector effects (for example fakes) in a full experimental study. Correct identification was assumed for the quark and two leptons. The backgrounds in the study are those from $\tilde{q}_L^*$ and Eq. (5.45).

It must be noted however, that significant pollution due to backgrounds will be expected for this signal from both the Standard Model and the MSSM. Further experimental cuts will certainly be required to improve the signal/background ratio

and without a more detailed study it is hard to predict what effect this will have on the ability to complete this measurement at the LHC, especially as the asymmetries are rather small.

5.5.2 Experimental factors with momentum reconstruction

When we perform the momentum reconstruction we need to include the experimental precision on the momentum of the visible particles. This resolution is $\sim 3\%$ for leptons and follows Eq. (5.52) for jets. The corresponding effect on momentum reconstruction is a reduction in the number of events that have the same sign triple product. As stated in Sec. 5.4.4 we discard any events where we have solutions with opposite sign triple products. Discarding these events reduces the percentage we can use from $\sim 60\%$ without momentum smearing down to $\sim 30\%$ when we include it.

The other difficulty momentum smearing creates is that all the reconstructed solutions can now have the wrong sign triple product as we no longer correctly reproduce the rest frame of the neutralino $\tilde{\chi}_2^0$. Inevitably this effect produces a decrease in the observed asymmetry from $\sim 11\%$ to $\sim 8\%$.

We again include the cuts on all visible particles in our decay chain given by Eqs. (5.47)-(5.51). These cuts significantly reduce the number of visible events and remove $\sim 80\%$ of the events compared with our initial naïve estimates. When we combine the cuts with the momentum reconstruction efficiency we are left with $\sim 6\%$ of the initial events and this clearly increases the luminosity needed to make an observation statistically significant. After inclusion of these effects the number of events drops from 20000 down to 1200 at the integrated luminosity of $\mathcal{L} = 100 \text{ fb}^{-1}$. This results in a 1σ absolute uncertainty of order $\sim 3\%$ on the asymmetry, according to Eq. (3.43).

Another possible experimental aspect we investigate is a 20 GeV uncertainty on the absolute mass scale of the supersymmetric particles used in the momentum reconstruction. We found that this has a negligible effect on the momentum reconstruction as long as the mass differences between different particles in the decay chain are known better than $\mathcal{O}(5 \text{ GeV})$. The assumption that the mass differences
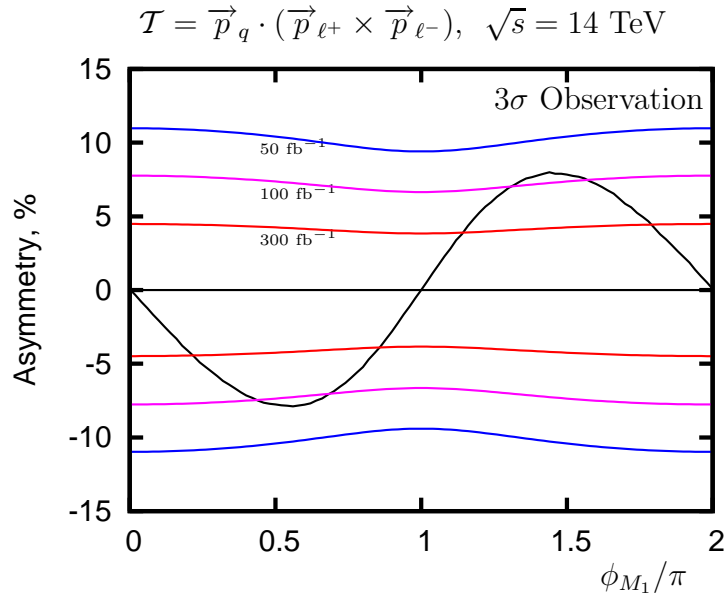
$$\mathcal{T} = \overrightarrow{p}_q \cdot (\overrightarrow{p}_{\ell^+} \times \overrightarrow{p}_{\ell^-}), \quad \sqrt{s} = 14 \text{ TeV}$$

Figure 5.9: The asymmetry $\mathcal{A}_\mathcal{T}$, Eq. (5.7), in the reconstructed $\tilde{q}_L$ frame for $\tilde{q}_L \tilde{g}$, $\tilde{q}_L^* \tilde{g}$ production followed by the decay chains shown in Eq. (5.4) and Eq (5.13) with cuts Eqs. (5.47)-(5.51). The coloured lines show the size of the asymmetry needed for a 3σ observation at the given luminosity, $\mathcal{L}$=(50 fb^{-1}, 100 fb^{-1}, 300 fb^{-1}). The momenta of the final-state particles have been smeared according to Eq. (5.52)-(5.54) to replicate the LHC detector effects. All other relevant experimental details are mentioned in the text.

are known to a higher accuracy is reasonable as the main method of measuring masses in SUSY decay chains at the LHC will be via kinematic end points that are measured with high precision.

Figure 5.9 shows the asymmetry and the luminosity required at the LHC to see a statistically significant result at the 3σ level at the LHC once all the above factors have been taken into account. The production channels are $\tilde{q}_L \tilde{g}$, $\tilde{q}_L^* \tilde{g}$ and the branching ratios are included from both the $\tilde{q}_L$ and $\tilde{g}$ decay chains. No explicit hadronisation effects were included here and possible additional hard jets in the final state require further study. Also correct identification was assumed for all the leptons and quarks in both decay chains as explained in Sec. 5.4.4 and Sec. 5.3.4. Again the only backgrounds included in the study are those of $\tilde{q}_L^* \tilde{g}$ production and of taus that decay to visible leptons, Eq. (5.45). In chapter 6 we extend the analysis,

albeit with stop production, to include all Standard Model and SUSY backgrounds.

We can see that using this method, with integrated luminosity $\mathcal{L} \sim 100\,\text{fb}^{-1}$ we start to become sensitive if large phases happen to be present. After $\mathcal{L} \sim 300\,\text{fb}^{-1}$ we expect to have sensitivity to phases in the ranges $0.2\,\pi \lesssim \phi_{M_1} \lesssim 0.85\,\pi$ and $1.15\,\pi \lesssim \phi_{M_1} \lesssim 1.8\,\pi$, and obviously more luminosity will improve this further.

Note that a direct comparison between the methods with and without momentum reconstruction based on the above plots should not be performed. The backgrounds from both SM and MSSM will be more severe when we do not perform momentum reconstruction and clearly many new cuts will be required to isolate the signal, which is the consequence of being totally inclusive. For the method when we perform momentum reconstruction, we have a well defined final state that is difficult to be faked by Standard Model processes and is also uncommon for SUSY cascade decays. Moreover the multiple cuts on all the particles and the need for the missing momentum to be successfully reconstructed mean that many backgrounds will be rejected. In Sec. 6.5.4 we show the potential power of the momentum reconstruction technique for rejecting backgrounds when applied to stop production.

However, for the study shown in Fig. 5.8, none of these extra benefits of momentum reconstruction are present. It can be expected that the backgrounds may be substantial (especially from competing SUSY decays) and will require conventional kinematic cuts to reduce. Both the cuts and backgrounds will increase the luminosity required to observe a CP signal for this analysis in comparison to Fig. 5.9.

5.5.3 Conclusion

In this chapter we studied squark production, followed by the decay, $\tilde{q}_L \rightarrow \tilde{\chi}_2^0 q \rightarrow \ell^+\ell^- \tilde{\chi}_1^0 q$. We again used CP-violating asymmetries composed of triple product correlations to examine the sensitivity of the LHC to CP phases within the MSSM. In this study, CP-asymmetries were only formed from the three body decay of the $\tilde{\chi}_2^0$. Therefore we were only sensitive to phases in the neutralino mixing matrix and in particular we concentrated on the phase, ϕ_{M_1}.

Again, we found that when we calculated the full production process and included the PDFs, the asymmetry was significantly diluted. We therefore applied

the technique of momentum reconstruction to boost all the final-state particles of interest into the rest frame of the produced $\tilde{q}_L$. We found that it was almost possible to recover the rest frame asymmetry. Using the momentum reconstruction technique we estimate that with 300 fb^{-1} we should see sensitivity in the range $0.2\pi \lesssim \phi_{M_1} \lesssim 0.85\pi$.

However, we wish to emphasise that we need to study fully hadronic events to confirm these preliminary findings. In addition, these events should be passed through a detector simulation to see if the momentum reconstruction of the final state is valid. We also need to run the same analysis on both Standard Model and MSSM backgrounds to make sure that the signal to background ratio is acceptable.

Chapter 6

Stop Production with two-body decays

6.1 Introduction

For the final study presented in this thesis, we again consider the production of stops but with the following decay chain [133],

$$\tilde{t}_i \rightarrow \tilde{\chi}_2^0 + t \rightarrow \tilde{\ell}^\pm + \ell^\mp + Wb \rightarrow \tilde{\chi}_1^0 + \ell^\pm + \ell^\mp + Wb \,. \tag{6.1}$$

The difference from the decay chains previously studied is that in the scenarios considered in this chapter the mass of at least one slepton is less than the $\tilde{\chi}_2^0$ ($m_{\tilde{\chi}_2^0} > m_{\tilde{\ell}}$). Consequently, the $\tilde{\chi}_2^0$ decays via a two body decay to an on-shell $\tilde{\ell}$ which in turn undergoes a two-body decay.

Unfortunately, the decay of the $\tilde{\chi}_2^0$ now produces no triple product correlations because the $\tilde{\ell}$ cannot carry any spin correlations since it is a scalar. Therefore, we are only sensitive to correlations in the stop decay and the two triple products we can form are,

$$\mathcal{T}_{\ell_N} = \vec{p}_{\ell_N} \cdot (\vec{p}_W \times \vec{p}_t) \,, \tag{6.2}$$

$$\mathcal{T}_{\ell\ell} = \vec{p}_b \cdot (\vec{p}_{\ell^+} \times \vec{p}_{\ell^-}) \,. \tag{6.3}$$

In the scenarios considered in this chapter, these triple products and mainly sensitive to phases in the stop mixing matrix. Since we have set $\phi_\mu = 0$ in this thesis, we

exclusively consider the effect of ϕ_{A_t}. In principle, ϕ_{M_1} could also contribute but we concentrate on scenarios where the $\tilde{\chi}_2^0$ is mainly wino-like and thus the effect of ϕ_{M_1} is negligible.

Following on from the momentum reconstruction technique presented in Chapter 5, we also reconstruct the momentum of the $\tilde{\chi}_1^0$ in this study to recover the rest frame asymmetry. The reconstruction is actually much simpler for the two body decay shown in Eq. (6.1) as the single decay chain alone contains enough invariants to solve the system. Whereas the reconstruction presented in Sec. 5.3 required a quartic equation to be solved which can result in 4 separate solutions, the solution to the two-body decay is only a quadratic.

We begin the chapter by describing the process under consideration and the terms that produce the CP-asymmetry. In Sec. 6.3 we explain the momentum reconstruction technique for the two-body decay chain and consider the combinatorial difficulties that will be faced at the LHC. We discuss the analytical parton-level results in Sec. 6.4 where both the $\tilde{t}_i$ is at rest and where the PDFs and production process is included. Sec. 6.5 describes the hadron level results where we have performed a Monte Carlo study and applied a jet-finder after showering and hadronisation has taken place. We also include the cuts required at the LHC and some of the most important experimental efficiencies. Both Standard Model and SUSY backgrounds have been simulated to examine how these effect our results. Finally, we conclude in Sec. 6.6.

6.2   Formalism

6.2.1   The process studied and the amplitude squared

At the LHC, the light stop ($\tilde{t}_1$) particles can be produced via pair production,

$$pp \rightarrow \tilde{t}_1 \tilde{t}_1^* \tag{6.4}$$

As mentioned in Sec.4.2.1, the dominant production process is from gluon fusion and we again use this channel when performing the analytical calculation.

In our study the CP-violating observables are produced in the following decay,

$$\tilde{t}_1 \rightarrow \tilde{\chi}_2^0 + t. \tag{6.5}$$

We require the $\tilde{\chi}_2^0$ to decay via two, 2-body leptonic channels,

$$\tilde{\chi}_2^0 \rightarrow \tilde{\ell}_R^\pm \ell_N^\mp \rightarrow \tilde{\chi}_1^0 \ell_N^\mp \ell_F^\pm, \tag{6.6}$$

where N and F denote the near and far leptons respectively. In addition, we only consider events where the t is fully reconstructible and hence decays hadronically,

$$t \rightarrow Wb \rightarrow q_u \bar{q}_d b. \tag{6.7}$$

We again apply the narrow-width approximation (Sec. 4.2.2) and include the full spin correlations for production and decay of the intermediate particles, $\tilde{t}_1$, $\tilde{\chi}_2^0$, $\tilde{\ell}$ and t. The squared amplitude $|T|^2$ of the full process can then be factorised into the processes of production $gg \rightarrow \tilde{t}_1 \tilde{t}_1^*$ and the subsequent decays $\tilde{t}_1 \rightarrow t\tilde{\chi}_2^0$, $\tilde{\chi}_2^0 \rightarrow \tilde{\ell}\ell_N$, $\tilde{\ell} \rightarrow \tilde{\chi}_1^0 \ell_F$ and $t \rightarrow Wb$. The use of the narrow-width approximation is appropriate since the widths of the respective particles are much smaller than the masses in all cases. The squared amplitude can then be expressed in the form,

$$
\begin{aligned}
|T|^2 &= 4|\Delta(\tilde{t}_1)|^2 |\Delta(\tilde{\chi}_2^0)|^2 |\Delta(\tilde{\ell})|^2 |\Delta(t)|^2 P(\tilde{t}_1 \tilde{t}_1^*) \Big\{ P(\tilde{\chi}_2^0 t) D(\tilde{\chi}_2^0) D(\tilde{\ell}) D(t) \\
&\quad + \sum_{a=1}^{3} \Sigma_P^a(\tilde{\chi}_2^0) \Sigma_D^a(\tilde{\chi}_2^0) D(\tilde{\ell}) D(t) + \sum_{b=1}^{3} \Sigma_P^b(t) \Sigma_D^b(t) D(\tilde{\chi}_2^0) D(\tilde{\ell}) \\
&\quad + \sum_{a,b=1}^{3} \Sigma_P^{ab}(\tilde{\chi}_2^0 t) \Sigma_D^a(\tilde{\chi}_2^0) \Sigma_D^b(t) D(\tilde{\ell}) \Big\},
\end{aligned} \tag{6.8}
$$

where $a, b = 1, 2, 3$ refers to the polarisation states of the neutralino $\tilde{\chi}_i^0$ and top quark t. In addition,

- $\Delta(\tilde{t}_1)$, $\Delta(\tilde{\chi}_2^0)$, $\Delta(\tilde{\ell})$ and $\Delta(t)$ are the pseudo-propagators of the intermediate particles which lead to the factors $E_{\tilde{t}_1}/m_{\tilde{t}_1}\Gamma_{\tilde{t}_1}$, $E_{\tilde{\chi}_2^0}/m_{\tilde{\chi}_2^0}\Gamma_{\tilde{\chi}_2^0}$, $E_{\tilde{\ell}_R}/m_{\tilde{\ell}_R}\Gamma_{\tilde{\ell}_R}$ and $E_t/m_t\Gamma_t$ in the narrow-width approximation.

- $P(\tilde{t}_1 \tilde{t}_1)$, $P(t\tilde{\chi}_2^0)$, $D(\tilde{\chi}_2^0)$, $D(\tilde{\ell})$ and $D(t)$ (Appendix B) are the terms in the production and decay that are independent of the spin of the decaying neutralino and top, whereas,

- $\Sigma_P^a(\tilde{\chi}_i^0)$, $\Sigma_P^b(t)$, $\Sigma_P^{ab}(\tilde{\chi}_2^0 t)$ and $\Sigma_D^a(\tilde{\chi}_2^0)$, $\Sigma_D^b(t)$ (Appendix B) are the spin-dependent terms giving the correlations between production and decay of the $\tilde{\chi}_2^0$ and t. We follow the formalism and conventions described in [141].

- It must be noted that the slepton $\tilde{\ell}$ produces no spin correlation term in the amplitude since it is a scalar.

Explicit expressions are given in Appendix B.

6.2.2 Structure of the T-odd asymmetry

As in chapter 4 and chapter 5, we classify all terms of the corresponding amplitude squared, Eq.(6.8), with respect to their T_N–odd or T_N–even character. Only the products that contain a T_N-odd contribution will lead to CP-odd violating observables (Sec. 5),

- The spin–independent terms introduced in the previous section, $P(\tilde{t}_1\tilde{t}_1)$, $P(t\tilde{\chi}_2^0)$, $D(\tilde{\chi}_2^0)$, $D(\tilde{\ell})$, $D(t)$ do not cause any T_N-odd terms.

- The spin-dependent terms, $\Sigma_P^a(\tilde{\chi}_i^0)$, $\Sigma_P^b(t)$, $\Sigma_P^{ab}(\tilde{\chi}_2^0 t)$, $\Sigma_D^a(\tilde{\chi}_2^0)$, $\Sigma_D^b(t)$, however, often can be divided up into T_N-even and T_N-odd terms, depending on the processes studied. In our case, a sequence of 2-body decays, however, we can only split $\Sigma_P^{ab}(\tilde{\chi}_2^0 t) = \Sigma_P^{ab,E}(\tilde{\chi}_2^0 t) + \Sigma_P^{ab,O}(\tilde{\chi}_2^0 t)$, all other spin-dependent terms only lead to T_N-even terms.

- Therefore, the T_N-odd term in the amplitude is,
  $\sum_{a,b=1}^3 \Sigma_P^{ab,O}(\tilde{\chi}_2^0 t)\Sigma_D^a(\tilde{\chi}_2^0)\Sigma_D^b(t)D(\tilde{\ell})$.

When we contract the spin indices of the t and $\tilde{\chi}_2^0$ and evaluate the T_N-odd contribution we find that the following covariant product appears in the amplitude,

$$\Sigma_P^{ab,O}(\tilde{\chi}_2^0 t)\Sigma_D^a(\tilde{\chi}_2^0)\Sigma_D^b(t) \quad \sim \quad i\epsilon_{\mu\nu\rho\sigma}s^{a,\mu}(\tilde{\chi}_2^0)p_{\tilde{\chi}_2^0}^\nu s^{b,\rho}(t)p_t^\sigma \times (p_{\ell_N}s^a)(p_{[b,W]}s^b), \quad (6.9)$$

$$\sim \quad i\epsilon_{\mu\nu\rho\sigma}p_{\tilde{\chi}_2^0}^\nu p_{\ell_N}^\mu p_W^\rho p_t^\sigma, \quad (6.10)$$

where $\Sigma_P^{ab,O}$, $\Sigma_D^a(\tilde{\chi}_2^0)$ and $\Sigma_D^b(t)$ are given by Eq. (B.1.9), Eq. (B.4.39) and Eq. (B.6.44) respectively.

Eq. (6.9) is multiplied by the imaginary part of the coupling, Eq. (B.1.11) that contain terms from both the $\tilde{t}$, Eq. (2.4.1), and $\tilde{\chi}^0$, Eq. (2.26), mixing matrices. Hence, any complex phases contained in those mixing matrices will yield CP-violating effects that can be seen in an observable that exploits the covariant product.

If we expand the covariant product (as in Sec. 3.3) we find the triple product,

$$\mathcal{T}_{\ell_N} = \vec{p}_{\ell_N} \cdot (\vec{p}_W \times \vec{p}_t) \,, \tag{6.11}$$

The triple product is analogous to the one presented in Eq. (4.14). However, whereas in the three body decay of the $\tilde{\chi}_2^0$ we only needed to know the charge of the lepton in the triple product, for the sequence of 2 two-body decays we also need to know if the lepton originated from the first or second decay.

An alternative triple product that uses both leptons can be found though. The covariant product can be re-expressed in the following form by exploiting momentum conservation, $p_{\tilde{\chi}_2^0} = p_{\tilde{\ell}} + p_{\ell_N}$, $p_{\tilde{\ell}} = p_{\ell_F} + p_{\tilde{\chi}_1^0}$, $p_W = p_t + p_b$,

$$\epsilon_{\mu\nu\rho\sigma} p_{\tilde{\chi}_2^0}^\mu p_{\ell_N}^\nu p_W^\rho p_t^\sigma = \epsilon_{\mu\nu\rho\sigma} (p_{\ell_F} + p_{\tilde{\chi}_1^0})^\mu p_{\ell_N}^\nu p_W^\rho p_b^\sigma \,. \tag{6.12}$$

This covariant product leads to the triple product,

$$\mathcal{T}_{\ell\ell} = \vec{p}_b \cdot (\vec{p}_{\ell^+} \times \vec{p}_{\ell^-}) \,. \tag{6.13}$$

However, Eq. (6.12) shows that we have effectively two covariant products, one which contains the momentum of the $\tilde{\chi}_1^0$. Thus, there is no kinematical frame in which the triple product, $\mathcal{T}_{\ell\ell}$ will be completely equivalent to the covariant product in Eq. (6.12). We can understand this since the far lepton is not directly correlated with the spin of $\tilde{\chi}_2^0$ and therefore triple products containing the momentum of the far lepton will be lower.

Using the triple products, we can again define the asymmetry parameter using Eq. (3.36). We then define,

$$\mathcal{A}_{\ell_N} = \mathcal{A}_T(\mathcal{T}_{\ell_N}), \qquad \mathcal{A}_{\ell\ell} = \mathcal{A}_T(\mathcal{T}_{\ell\ell}), \tag{6.14}$$

where $\mathcal{A}_{\ell_N}$ is the asymmetry from the triple product $\mathcal{T}_{\ell_N}$ and $\mathcal{A}_{\ell\ell}$ is the asymmetry from the triple product $\mathcal{T}_{\ell\ell}$.

Once again, the asymmetries formed from triple products will suffer a dilution at the LHC due to boosted frames, see Sec. 3.5 Hence, we again use the ideas of momentum reconstruction to find the optimal reference frame for the asymmetry and evaluate the triple product.

For all our observables we require that we know the charge of the decaying $\tilde{t}_1$ and can therefore distinguish the particle and anti-particle. We can combine the process with the charge-conjugated decay to make an unambiguous observation of CP-violation via T_N-odd observables. In addition, since the charge conjugate decay has an asymmetry of the opposite sign, if we do not know the charge of the decaying stop, the asymmetry would simply cancel. The charge of the $\tilde{t}_1$ can be found by demanding that the opposite cascade produces a single lepton and thus a tri-lepton final-state overall.

An extra subtlety in the two-body decay chain is that changing the charge of the near lepton ℓ_N reverses the sign of the triple product, $\mathcal{T}_{\ell_N}$, Eq. (6.11). We can distinguish the near and far leptons using the momentum reconstruction technique, Sec. 5.3. However if for some reason the leptons cannot be identified we can still use the triple product $\mathcal{T}_{\ell\ell}$, Eq. (6.13). No lepton distinction is required as exchanging the near and far leptons has an extra sign change that cancels the change produced by the charge exchange.

6.3 Momentum reconstruction

6.3.1 Dilution effects

The triple product that is constructed from momenta in the laboratory frame suffers from dilution factors (~ 4) at the LHC. This is due to the lab frame being boosted with respect to the rest frame of the $\tilde{\chi}_2^0$ or $\tilde{t}_1$, see Eq. (3.5). It results in a considerable reduction in the maximum asymmetry observable when we introduce the PDFs which causes an undetermined boost to the system. Fig. 6.1 shows how the asymmetry is diluted in the laboratory frame when we produce the $\tilde{t}_1$ with varying initial momenta. If we were able to reconstruct the momentum of the $\tilde{t}_1$, we could perform a Lorentz transformation of all the momenta in the triple product into the
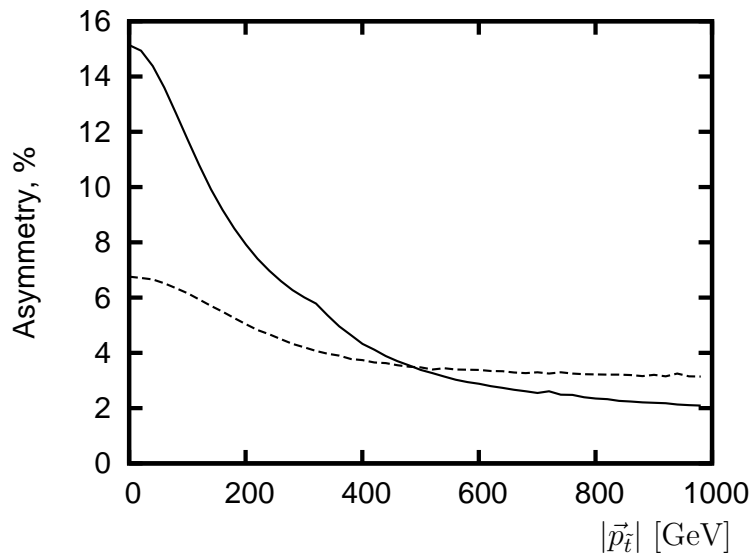
Figure 6.1: The asymmetry $\mathcal{A}_{\mathrm{T}}$, Eq. (3.36), as a function of the stop momentum, $|\vec{p}_{\tilde{t}}|$, in the laboratory frame. The solid line is the asymmetry for the triple product $\mathcal{T}_{\ell_N}$, Eq. (6.11) and the dotted line is for the triple product $\mathcal{T}_{\ell\ell}$, Eq. (6.13). The respective masses are given in Tab. 6.2, Tab. 6.3 and Tab. 6.4.

$\tilde{t}_1$ rest frame and potentially recover the full asymmetry.

6.3.2 Reconstruction procedure

We are able to reconstruct the $\tilde{\chi}_1^0$ four momentum by reconstructing the following two body decay chain in full,

$$\tilde{t} \to t + \tilde{\chi}_2^0 \to t + \tilde{\ell}^{\pm} + \ell_N^{\mp} \to t + \tilde{\chi}_1^0 + \ell_N^{\mp} + \ell_F^{\pm}. \tag{6.15}$$

Assuming that all the masses in the decay chains are known, the kinematics can be fully reconstructed using the set of invariant mass conditions,

$$m_{\tilde{\chi}_1^0}^2 = (P_{\tilde{\chi}_1^0})^2, \tag{6.16}$$

$$m_{\tilde{\ell}^{\pm}}^2 = (P_{\tilde{\chi}_1^0} + P_{\ell_F^{\pm}})^2, \tag{6.17}$$

$$m_{\tilde{\chi}_2^0}^2 = (P_{\tilde{\ell}^{\pm}} + P_{\ell_N^{\mp}})^2 = (P_{\tilde{\chi}_1^0} + P_{\ell_F^{\pm}} + P_{\ell_N^{\mp}})^2, \tag{6.18}$$

$$m_{\tilde{t}_1}^2 = (P_{\tilde{\chi}_2^0} + P_t)^2 = (P_{\tilde{\chi}_1^0} + P_{\ell_F^{\pm}} + P_{\ell_N^{\mp}} + P_t)^2, \tag{6.19}$$

where P denote the four momenta of the respective particles.
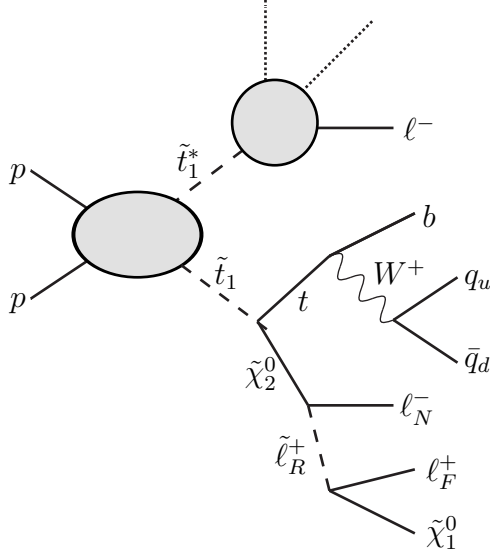
Figure 6.2: The process studied for momentum reconstruction.

We see that with the four equations we have enough information to solve the system and find each component of the $\tilde{\chi}_1^0$ four momentum. A solution to the above set of equations is presented in [167] and we outline the procedure here. We first expand the $\tilde{\chi}_1^0$ momentum in terms of the final-state momentum of the $\ell_F^{\mp}$, $\ell_N^{\pm}$ and t,

$$\overrightarrow{p}_{\tilde{\chi}_1^0} = a\,\overrightarrow{p}_{\ell_F^{\pm}} + b\,\overrightarrow{p}_{\ell_N^{\mp}} + c\,\overrightarrow{p}_t\,. \tag{6.20}$$

In order to derive a system of 3 linear equations for the unknowns $a-c$, we calculate $\vec{p}_{\tilde{\chi}_1^0} \cdot \vec{p}_{\ell_F}$, $\vec{p}_{\tilde{\chi}_1^0} \cdot \vec{p}_{\ell_N}$ and $\vec{p}_{\tilde{\chi}_1^0} \cdot \vec{p}_t$. Inserting Eq. (6.20) and exploiting Eqs. (6.17-6.19) we form the system of equations,

$$\mathcal{M} \begin{pmatrix} a \\ b \\ c \end{pmatrix} = \begin{pmatrix} \frac{1}{2}(m_{\tilde{\chi}_1^0}^2 - m_{\tilde{\ell}}^2) + E_{\tilde{\chi}_1^0} E_{\ell_F} \\ \frac{1}{2}(m_{\tilde{\ell}}^2 - m_{\tilde{\chi}_2^0}^2) + p_{\ell_F} \cdot p_{\ell_N} + E_{\tilde{\chi}_1^0} E_{\ell_N} \\ \frac{1}{2}(m_{\tilde{\chi}_2^0}^2 + m_t^2 - m_{\tilde{t}_1}^2) + p_{\ell_F} \cdot p_t + p_{\ell_N} \cdot p_t + E_{\tilde{\chi}_1^0} E_t \end{pmatrix}, \tag{6.21}$$

where,

$$\mathcal{M} = \begin{pmatrix} \overrightarrow{p}_{\ell_F} \cdot \overrightarrow{p}_{\ell_F} & \overrightarrow{p}_{\ell_F} \cdot \overrightarrow{p}_{\ell_N} & \overrightarrow{p}_{\ell_F} \cdot \overrightarrow{p}_t \\ \overrightarrow{p}_{\ell_N} \cdot \overrightarrow{p}_{\ell_F} & \overrightarrow{p}_{\ell_N} \cdot \overrightarrow{p}_{\ell_N} & \overrightarrow{p}_{\ell_N} \cdot \overrightarrow{p}_t \\ \overrightarrow{p}_t \cdot \overrightarrow{p}_{\ell_F} & \overrightarrow{p}_t \cdot \overrightarrow{p}_{\ell_N} & \overrightarrow{p}_t \cdot \overrightarrow{p}_t \end{pmatrix}. \tag{6.22}$$

We invert the matrix $\mathcal{M}$ to find solutions for a, b and c in terms of constants and

$E_{\tilde{\chi}_1^0}$. The on shell mass condition for the $\tilde{\chi}_1^0$, Eq. (6.16), can then be expressed as,

$$E_{\tilde{\chi}_1^0}^2 = (a, b, c)\mathcal{M} \begin{pmatrix} a \\ b \\ c \end{pmatrix} + m_{\tilde{\chi}_1^0}^2. \tag{6.23}$$

We solve the above quadratic, to find two solutions for $E_{\tilde{\chi}_1^0}$. These solutions are then substituted back into Eq. (6.20) to find all components of the $\tilde{t}_1$ momentum on an event-by-event basis.

6.3.3   Challenges from multiple solutions

We encounter a complication in the reconstruction as Eq. (6.16) is quadratic in $(p_{\tilde{\chi}_1^0})$. Consequently we have two solutions for $(p_{\tilde{\chi}_1^0})$ for each reconstructed event but we have no extra information in the single decay chain to determine which solution is physically correct. As we cannot distinguish which of these solutions corresponds to the physically correct configuration, we need to analyse both. Therefore, we calculate the $\tilde{t}_1$ momentum for both configurations and boost all final-state particles in the triple product into the reconstructed $\tilde{t}_1$ rest frame. If the sign of both triple products are the same then the event is recorded but if the sign of the triple products are different, we discard the event since we cannot know which of the reconstructed solutions is correct. The method has the disadvantage that we lose events and therefore statistical significance.

However, we find that the asymmetry can actually rise ($\approx 1.5\%$) due to the nature of the events that are removed. The events most likely to be removed are those with small triple products. This is because the smaller the triple product of a particular event, the more likely that the triple product will change sign if the rest frame is mis-measured. Another property of events with small triple products is that the asymmetry is lower than that of events with large triple products. Therefore, if these events are removed from our sample, proportionally more events are removed in the denominator of the asymmetry, Eq. (3.36) and the asymmetry will rise in value.

When performing the momentum reconstruction at the LHC we have additional problems from multiple solutions that come from combinatorial effects in the event.

Firstly, to complete the reconstruction we need to correctly identify the near and far lepton in the decay chain Eq. (6.15) if we wish to compute the triple product $\mathcal{T}_{\ell_N}$, Eq. (6.11) (although this information is not required for the triple product $\mathcal{T}_{\ell\ell}$, Eq. (6.13)). We find that in $\approx 20\%$ of events the wrong assignment of near and far leptons satisfy the kinematic equations Eq. (6.16)-(6.19) and produce two extra solutions for the momentum of the $\tilde{\chi}_1^0$ in addition to the solutions found from the correct configuration. In addition, we always require a third lepton in the event coming from the opposite decay chain to correctly identify the stop charge. For example the lepton produced in the decay chain $\tilde{t}_1^* \to \tilde{\chi}^- \bar{b}$, $\tilde{\chi}^- \to \ell^- + X$, where X are neutral decay products. If this lepton is of the same flavour as those in the triple product decay chain there is a small chance that it can also reconstruct the $\tilde{\chi}_2^0$. All of these combinatorial issues are removed by again demanding that all calculated triple products are of the same sign and discarding any events where opposite sign solutions occur.

Further combinatorial issues occur with the reconstructed top in the event. Firstly a second b is always present in the opposite decay chain and this can occasionally combine with a reconstructed W to give a fake t. The opposite decay chain also can contain extra quarks that can produce more reconstructed t's. Finally, the parton shower can sometimes radiate hard gluons that are also seen as extra jets and further complicate the combinatorial problem. Whenever extra t quarks are found that satisfy the event kinematics we perform the same procedure as for combinatorial leptons. Triple products are calculated for all reconstructed rest frames and only events, that yield the same sign for all the reconstructed triple products, are recorded.

6.3.4 Mass measurements

As mentioned above, we assume that the masses of all the SUSY particles in the decay chain will be known. In Sec. 5.3.5, we briefly discussed the measurement of the SUSY mass states at the LHC and the main studies on this topic. We found that for the mass differences we require in Eq. (6.21), the mass end-point method is well established. It is hoped that the method will measure these mass differences

with high accuracy $\mathcal{O}(\,1\%)$ [157].

Whereas the cascade decay studied in chapter 5 involved a three body decay of the $\tilde{\chi}_2^0$ the decay presented in this chapter involves,

$$\tilde{\chi}_2^0 \rightarrow \tilde{\ell}^{\pm}\ell^{\mp}, \ \ \tilde{\ell}^{\pm} \rightarrow \tilde{\chi}_1^0 \ell^{\pm}\,. \tag{6.24}$$

The vast majority of the studies presented in Sec. 5.3.5 actually studied this decay chain. Therefore, we can have far more confidence that the mass reconstruction methods will provide the required accuracy. We again test errors on the absolute mass scale of up to 20 GeV and an error on the mass differences of 5 GeV. Both of these errors have a negligible impact on the reconstruction efficiency.

These errors can be viewed as conservative apart from the mass of the stop. However, using the method of kinematic invariants and high luminosity, such an accuracy may become possible [167].

6.4 Parton level results

In this section we analyse numerically the CP-asymmetry at the parton level, with the inclusion of parton distribution functions, whilst in Sec. 6.5 we complete a hadronic level study to estimate the realistic environment and the discovery potential at the LHC. In particular, we focus on a specific mSUGRA parameter point, Tab. 6.1, at the parton level before discussing more general low mass mSUGRA scenarios for our hadronic study.

6.4.1 Chosen scenario: spectrum and decay modes

We choose for this study the mSUGRA scenario shown in Tab. 6.1 with an added CP-phase to the trilinear coupling ϕ_{A_t}. The spectrum at the electroweak scale have been derived using the RGE code `SPheno 2.2.3` [148] and the masses of the gauginos and scalars are shown in Tab. 6.2, Tab. 6.3 and Tab. 6.4 respectively. Using the low energy soft SUSY breaking parameters and the phase of the trilinear coupling ϕ_{A_t}, we calculate the masses and mixing of the $\tilde{t}_i$'s, see Sec 2.4.1 for details.

Parameter	m_0	$m_{1/2}$	$\tan\beta$	$\text{sign}(\mu)$	A_0
Value	65	210	5	+	0

Table 6.1: mSUGRA benchmark scenario (masses in GeV).

Particle	$m_{\tilde\chi_1^0}$	$m_{\tilde\chi_2^0}$	$m_{\tilde\chi_3^0}$	$m_{\tilde\chi_4^0}$	$m_{\tilde\chi_1^\pm}$	$m_{\tilde\chi_2^\pm}$	$m_{\tilde g}$
Mass(GeV)	77.7	142.4	305.1	330.3	140.7	329.9	514.116

Table 6.2: Masses (in GeV) of the gauginos calculated by `SPheno 2.2.3` [148].

Particle	$m_{\tilde t_1}$	$m_{\tilde t_2}$	$m_{\tilde b_1}$	$m_{\tilde b_2}$	$m_{\tilde q_{dL}}$	$m_{\tilde q_{dR}}$	$m_{\tilde q_{uL}}$	$m_{\tilde q_{uR}}$
Mass(GeV)	345.7	497.8	443.4	466.0	484.7	465.2	478.7	464.9

Table 6.3: Masses (in GeV) of the SUSY squarks calculated by `SPheno 2.2.3` [148] except for $\tilde t_i$ that were calculated at tree level with phase $\phi_{A_t} = |\frac{4}{5}\pi|$.

Particle	$m_{\tilde\ell_L}$	$m_{\tilde\ell_R}$	$m_{\tilde\tau_2}$	$m_{\tilde\tau_1}$
Mass(GeV)	163.4	110.8	164.9	108.0

Table 6.4: Masses (in GeV) of the SUSY sleptons calculated by `SPheno 2.2.3` [148].

For the presented analysis to work, we require the SUSY spectrum to have the following mass hierarchy,

$$m_{\tilde t_1} - m_t > m_{\tilde\chi_2^0} > m_{\tilde\ell_R^\pm} > m_{\tilde\chi_1^0}, \tag{6.25}$$

to allow for full momentum reconstruction. This hierarchy is often a feature in the mSUGRA parameter space. In addition we concentrate on light mass scenarios as the study is statistically limited and consequently we require a large production cross section.

The feasibility of the study at the LHC depends heavily on the integrated lumi-

Parameter	Value
$BR(\tilde{t}_1 \to \tilde{\chi}_1^0 t)$	34.6
$BR(\tilde{t}_1 \to \tilde{\chi}_2^0 t)$	7.5
$BR(\tilde{t}_1 \to \tilde{\chi}_1^+ b)$	50.1
$BR(\tilde{t}_1 \to \tilde{\chi}_2^+ b)$	7.8
$BR(\tilde{\chi}_2^0 \to \tilde{\mu}_R^+ \mu^- / \tilde{e}_R^+ e^-)$	11.6
$BR(\tilde{\chi}_1^+ \to \tilde{\tau}_1^+ \nu_\tau)$	95.1
$\sigma(pp \to \tilde{t}_1 \tilde{t}_1^*)$ [pb]	3.44

Table 6.5: Nominal values of the branching ratios (in %) for various decays calculated in `Herwig++` [151, 176] with phase $\phi_{A_t} = |\frac{4}{5}\pi|$. In the last row, cross sections for stop pair production at the LHC with $\sqrt{s} = 14$ TeV at leading order (LO) from `Herwig++`.

nosity. For this reason we look closely at the predicted cross section of the asymmetry decay chain,

$$\sigma = \sigma(pp \to \tilde{t}_1 \tilde{t}_1^*) \times BR(\tilde{t}_1 \to t \tilde{\chi}_2^0) \times BR(\tilde{\chi}_2^0 \to \tilde{\ell}^\pm \ell^\mp) \times BR(\tilde{\ell}^\pm \to \tilde{\chi}_1^0 \ell^\pm) \times BR(t \to q_u \bar{q}_d b),$$

(6.26)

and the relevant values for our scenario are shown in Tab. 6.5. In our study we also need to identify the charge of the $\tilde{t}_1$ in the opposite decay chain and this is possible when the decay products contain a single lepton (any number of jets are allowed). We see that the dominant production of single leptons from $\tilde{t}_1$ decays are via the channel $\tilde{t}_1 \to \tilde{\chi}_1^+ b$. However, as only the right sleptons and the bino-like $\tilde{\chi}_1^0$ are lighter than the wino-like $\tilde{\chi}_1^+$, the decay of the $\tilde{\chi}_1^+$ is via mixing terms or Yukawa couplings and hence the decay $BR(\tilde{\chi}_1^+ \to \tilde{\tau}_1^+ \nu_\tau)$ dominates, Tab. 6.5. For this reason we find that our study is far more promising if τ identification is possible and we compare results where τ identification has and has not been used later in the next section, Sec. 6.5.

6.4.2 CP asymmetry at the parton level

We start by discussing the dependence of ϕ_{A_t} on the parton level asymmetry, Eq. (3.36), for both the triple products $\mathcal{T}_{\ell_N}$ and $\mathcal{T}_{\ell\ell}$, Eqs. (6.11), (6.13). In order to see the maximum dependence upon ϕ_{A_t} we reconstruct the $\tilde{t}_1$ at rest and calculate the triple product in this frame.

We see from Fig. 6.3(a) that the largest asymmetry occurs for the triple product $\mathcal{T}_{\ell_N}$, which attains $|\mathcal{A}_{\ell_N}|_{\max} \approx 15\%$ when $\phi_{A_t} \approx 0.8\pi$. For the triple product $\mathcal{T}_{\ell\ell}$, the asymmetry is smaller, $|\mathcal{A}_{\ell\ell}|_{\max} \approx 6.5\%$, because the 'true' CP triple product correlation is only partially measured, see Sec. 6.2.2.

If we now include the dominant production process at the LHC ($gg \rightarrow \tilde{t}_1\bar{\tilde{t}}_1$) and relevant parton distribution functions (`MRST 2004LO` [156]), we see that the asymmetries are significantly diluted, Fig. 6.3(b). The asymmetry for the triple product $\mathcal{T}_{\ell_N}$, drops from $|\mathcal{A}_{\ell_N}|_{\max} \approx 15\%$ to $|\mathcal{A}_{\ell_N}|_{\max} \approx 4.5\%$ and the reduction is due to the boosted frame of the produced $\tilde{t}_1$ as discussed in Sec. 6.2.2. For the triple product $\mathcal{T}_{\ell\ell}$, the reduction in the asymmetry is far less, from $|\mathcal{A}_{\ell\ell}|_{\max} \approx 6.5\%$ to $|\mathcal{A}_{\ell\ell}|_{\max} \approx 3.8\%$. This is because the triple product, relies on the ℓ_F being correlated with the $\tilde{\ell}$ by the intrinsic boost of the $\tilde{\chi}_2^0$, $\tilde{\ell}$ system which already has a boost, even when the $\tilde{t}_1$ is at rest. As the $\tilde{t}_1$ becomes boosted, the boost of the $\tilde{\chi}_2^0$, $\tilde{\ell}$ system becomes proportionally less so, as the momentum of the $\tilde{t}_1$ is distributed throughout the decay chain. The difference in the dilution of the two asymmetries with $\tilde{t}$ momentum can be seen in Fig. 6.1.

6.5 Hadron level results

In order to estimate the potential for observing CP-violating effects in $\tilde{t}_1$ decays at the LHC more realistically, we perform the analysis at the hadronic level. For the first study in this thesis, Chapter 4, we made no attempt to analyse the hadronic effects at all (apart from the PDFs) and indeed every other study on this topic have only investigated at the parton level. Hadronic effects were partially estimated in Chapter 5, for example by applying a momentum smearing technique, Sec. 5.5. However, we go one step further with this analysis and generate Monte Carlo events
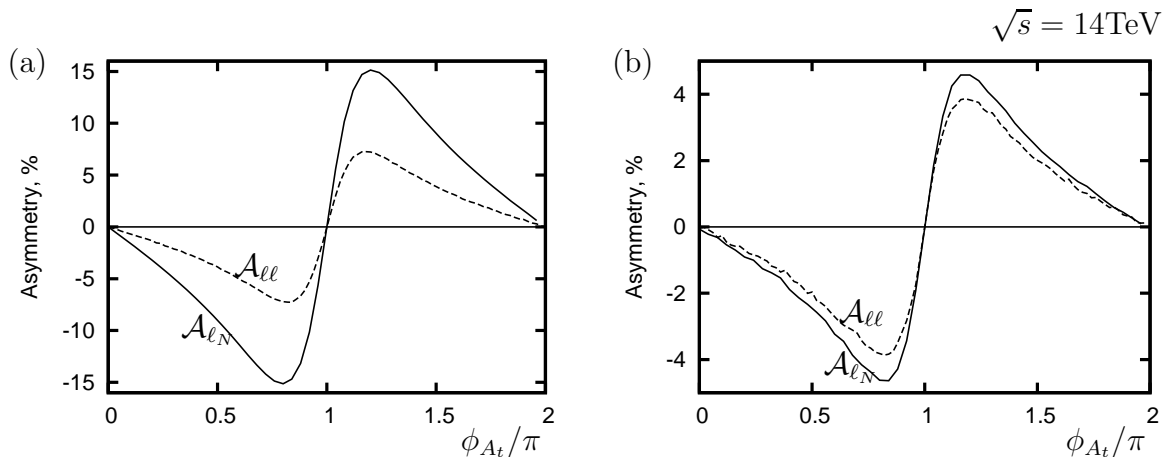
$$\sqrt{s} = 14\text{TeV}$$

Figure 6.3: (a) The asymmetry $\mathcal{A}_\text{T}$, Eq. (3.36), in the rest frame of $\tilde{t}_1$ as a function of ϕ_{A_t}. (b) The asymmetry $\mathcal{A}_\text{T}$, Eq. (3.36), in the laboratory frame as a function of ϕ_{A_t} at the LHC at 14TeV. The solid line is the asymmetry for the triple product $\mathcal{T}_{\ell_N}$, Eq. (6.11) and the dotted line is for the triple product $\mathcal{T}_{\ell\ell}$, Eq. (6.13).

where the final state is the same that would be seen in a detector. We apply a jet finder to these events and our analysis uses no truth information from the hard interaction. In addition, this is the first study in which both Standard Model and SUSY backgrounds were produced and analysed to explore how they may effect the observation of CP-phases.

We use the `Herwig++` [151, 176] event generator to calculate all the matrix elements in the process, the initial hard interaction, the subsequent SUSY particle decays, the parton shower and the hadronisation. We again emphasise the important feature of `Herwig++` is that it calculates the spin correlations in the SUSY cascade decay and allows the input of complex mixing matrices. Consequently, the triple product CP-asymmetry can be automatically calculated within `Herwig++`.

6.5.1   Cuts used and signal identification

The hadronic analysis of the produced events has been performed within the program `Rivet` [177,178]. We used the anti-k_t [179,180] jet algorithm with R=0.5 and applied the following acceptance cuts,

- $p_{T\ell_i} > 10\text{GeV}$,

- $p_{Tj_i} > 20\text{GeV}$,

- invariant mass of opposite sign same flavour (OSSF) leptons: $M_{\ell^+\ell^-} > 10\text{GeV}$,

- $|\eta_{\ell_i}| < 2.5$,

- $|\eta_{j_i}| < 3.5$,

- lepton jet isolation, $\Delta\text{R} = 0.5$,

- b-tag efficiency $= 60\%$ [14],

- hadronic τ-tag efficiency (whenever used) $= 40\%$ [14].

To identify the events we demand three charged leptons in the final state, so that we can correctly identify the charge of each $\tilde{t}_1$ produced in the event, Sec. 6.2.2. In addition, we demand that a pair of these leptons are OSSF as is the case for light leptons from $\tilde{\chi}_2^0$ decay. Whenever a $\tilde{t}_1$ decays in our scenarios a b is produced and therefore we require at least one b-tag in the final state (in principle we could require 2 b-tags including the opposite decay chain but we loose 40% of events due to b-tagging efficiency). On top of the b we require at least 2 more jets to be found in the final state so the full reconstruction of the t is possible. As all of our triple products and momentum reconstruction need a t we require at least one hadronic t to be reconstructed. For this procedure, we first demand that 2 jets (not b's) reconstruct a $W^\pm$ ($70\text{GeV} < M_{jj} < 90\text{GeV}$). We then impose that a reconstructed $W^\pm$ and one b jet reconstruct a t ($150\text{GeV} < M_{W^\pm b} < 190\text{GeV}$).

Once these cuts have been passed we then perform the kinematical reconstruction shown in Sec. 5.3 with any t's and OSSF leptons found in the final state. If the particles satisfy the kinematic constraints Eq. (6.16)-(6.19), we will have at least two different solutions on event-by-event basis for the momentum of the $\tilde{\chi}_1^0$. For each solution, the relevant rest frame triple product is calculated and only if all the signs of the triple products agree the event is accepted.

6.5.2 Standard model background

The following Standard Model backgrounds were produced with `Herwig++`: $t\bar{t}$, Drell-Yan gauge boson production (Z, γ, W), WW, WZ, ZZ, $W\gamma$. In addition, we generate $t\bar{t}\ell^+\ell^-$ events with `MadGraph` [181] and then use `Herwig++` to perform the parton shower and hadronisation. These backgrounds were selected as the Standard Model processes most likely to pass our analysis cuts. We find that the only background to pass the event selection is $t\bar{t}\ell^+\ell^-$ with the very low rate of 0.03 events/fb^{-1} after kinematical reconstruction. This corresponds to only $\approx 1\%$ of the signal process for our particular scenario.

Although the above result is encouraging, it must be stated that our analysis contains no jets mis-identified as leptons. As the dominant standard model processes produced by `Herwig++` only contain a maximum of two hard leptons in the initial process, the lack of a tri-lepton signal is not surprising. However, we do not expect major problems from Standard Model backgrounds if we limit the study to leptons from the first and second generation. $t\bar{t}$ can be expected to provide the largest background when both $W^\pm$ decay leptonically and an extra lepton is produced from a b or a mis-identified jet. Even when this occurs though, we still require an additional two hard jets in the event that have to combine with a b to form a t. Moreover, the final state then has to fulfill the reconstructed particular kinematics of our signal and finally all the calculated triple products have to agree.

To improve the statistical significance of our analysis, we also investigated the possibility of using τ-tagging in the opposite decay chain to that of our signal. In this analysis, we now change the original tri-lepton signal to a first or second lepton OSSF and additional hadronic τ. The mis-identification of a jet for a τ is much higher than for the other leptons and the standard model backgrounds may now become an issue [14]. However, this analysis is currently postponed to future studies.
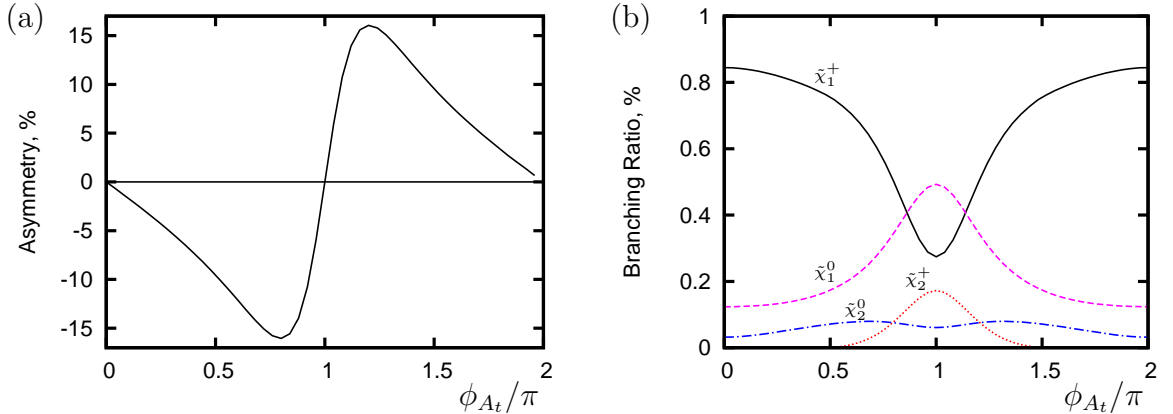
Figure 6.4: (a) The asymmetry $\mathcal{A}_{\ell_N}$, Eq. (3.36), for the decay chain shown in Eq. (6.27)-(6.28) as a function of ϕ_{A_t} at the hadronic level after momentum reconstruction has been performed. (b) The branching ratios: $\tilde{t}_1 \to \tilde{\chi}_1^+ b$ (black solid), $\tilde{t}_1 \to \tilde{\chi}_2^+ b$ (red dotted), $\tilde{t}_1 \to \tilde{\chi}_1^0 t$ (purple slashed), $\tilde{t}_1 \to \tilde{\chi}_2^0 t$ (blue slash-dot).

6.5.3 Stop Production

We begin by studying $\tilde{t}_1 \tilde{t}_1^*$ production along with the following decay chain,

$$\tilde{t}_1 \rightarrow \tilde{\chi}_2^0 t \to \tilde{\chi}_1^0 e^+ e^- jjb, \tag{6.27}$$

$$\tilde{t}_1^* \rightarrow \tilde{\chi}_1^0 \bar{t} \to \tilde{\chi}_1^0 \mu^- \bar{\nu}_\mu \bar{b}. \tag{6.28}$$

to test the momentum reconstruction procedure. The above decay chain is the cleanest signal process from a combinatorial point of view. We find a reconstruction efficiency of $\approx 5\%$ for this particular topology after cuts and the requirement for same sign triple products. The decay chain Eq. (6.28) has a single lepton in the final state allowing us to tag the charge of both the $\tilde{t}_1$ and $\tilde{t}_1^*$ in the process.

For the CP-asymmetry, we now concentrate purely on the triple product $\mathcal{T}_{\ell_N}$, Eq. (6.11) calculated in the reconstructed rest frame of the $\tilde{t}_1$, as this is the observable with high significance at the LHC. Fig. 6.4(a) shows that there is virtually no dilution when we move to the hadronic level and the asymmetry stays at $|\mathcal{A}_{\ell_N}|_{\max} \approx 15\%$. In fact, the hadronic level reconstruction does induce a degree of dilution, $\approx 1.5\%$ but this is cancelled by our procedure of removing opposite sign triple products which enhances the asymmetry by a similar amount, Sec. 6.3.3.

	$\tilde{t}_1\tilde{t}_1^*$	$\tilde{g},\tilde{q}$
Herwig++ LO (pb^{-1})	3.44	75.8
Prospino LO (pb^{-1})	$3.34^{+1.15}_{-0.8}$	$76.7^{+24.8}_{-17.3}$
Prospino NLO (pb^{-1})	$5.04^{+1.19}_{-0.92}$	$99.5^{+7.7}_{-9.6}$

Table 6.6: Cross section at the LHC with $\sqrt{s} = 14$ TeV production channel $\tilde{t}_1\tilde{t}_1^*$ and coloured SUSY production for both leading order (LO) and next-to-leading order (NLO). All cross sections were calculated using Herwig++ [151, 176] or Prospino [182–184]. The errors indicated next to the Prospino cross sections relate to varying the factorisation and renormalisation scales from $0.5m_{\tilde{t}_1} \rightarrow 2m_{\tilde{t}_1}$.

The plot was constructed by producing a large number of Herwig++ events (2×10^7) with the precise cascade decays given in Eq. (6.27) and Eq. (6.28). These events were all produced with a scenario where $\phi_{A_t} = 0.8\pi$ and thus the asymmetry was maximal. Due to the factors mentioned above we saw no difference in the asymmetry within the statistical errors of the simulation. For all other values of the phase, ϕ_{A_t}, we assumed that this conclusion would hold and no dilution would be seen. Thus, the other points on the plot are an extrapolation of this behaviour.

In order to estimate whether it is possible to observe a CP-asymmetry in $\tilde{t}_1$ decays at the LHC we need to calculate the statistical significance of any result and we again use the definition shown in Eq. (3.45). The total cross section used to calculate the statistical significance of any result in this chapter has been calculated using Herwig++ at the leading order (LO) for consistency. However, next-to-leading order production cross sections are available and have been calculated using Prospino [182–184], cf. Tab. 6.6. We see that in general the cross sections at NLO are higher than those at LO suggesting that the effective luminosity at the LHC will be more optimistic than those shown in the following results. In addition, the factorisation and renormalisation scale uncertainties are shown that indicates an estimate of the underlying theoretical uncertainty.

Due to the phase dependence of both the $\tilde{t}_1$ branching ratios, see Fig. 6.4(b),

and production cross section, the statistical significance for different values of ϕ_{A_t} cannot be trivially extrapolated. The total number of events observed will be an interplay between the branching ratios and the production cross section. However, in the case of branching ratios, each of the decays, $\tilde{t}_1 \to \tilde{\chi}_1^+ b$, $\tilde{t}_1 \to \tilde{\chi}_2^+ b$ and $\tilde{t}_1 \to \tilde{\chi}_1^0 t$ has a different reconstruction efficiency and asymmetry dilution that needs to be calculated. For example, we see from Fig. 6.4(b) that the branching ratio for the decay $\tilde{t}_1 \to \tilde{\chi}_2^+ b$ increases noticeably as we vary ϕ_{A_t} from $\phi_{A_t} = 0$ to $\phi_{A_t} = |\pi|$ due to this decay becoming kinematically more favourable. The $\tilde{\chi}_2^+$ has a large number of final states with no lepton however, so consequently the number of signal events decreases. Also, the $\tilde{\chi}_2^+$ decays generally contain extra jets that make the reconstruction of the event more difficult and thus reduce the efficiency of this channel.

Fig. 6.5(a) shows the asymmetry when all $\tilde{t}_1$ decay channels are considered and an estimate of the amount of luminosity required for a 3σ-observation of a non-zero asymmetry for pure $\tilde{t}_1 \tilde{t}_1^*$ production at the LHC. We can see that the asymmetry is slightly diluted when all $\tilde{t}_1$ decay modes are included from $|\mathcal{A}_{\ell_N}|_{\max} \approx 15\%$ to $|\mathcal{A}_{\ell_N}|_{\max} \approx 12.5\%$. The dilution is due to reconstructed events that are not originating from the signal process, Eq. (6.15). These events have no overall asymmetry and therefore simply dilute the signal. The horizontal lines show the estimate of the required luminosity required to see a certain asymmetry; an asymmetry can be seen at the 3σ level where the asymmetry curve in Fig. 6.5(a) lies outside the luminosity band. The luminosity bands are not flat because as discussed before, both the branching ratios and production cross section of the $\tilde{t}_1$ vary with the phase ϕ_{A_t}. We can see that in our scenario for pure $\tilde{t}_1 \tilde{t}_1^*$ production, we expect a sensitivity for $|0.5\pi| < \phi_{A_t} < |0.9\pi|$ with 500 fb^{-1}.

We can see the effect of varying the mSUGRA parameters $\tan\beta$ and A_0 in Fig. 6.5(b). It is shown that as the value of either $\tan\beta$ or A_0 is increased, we require more luminosity to see a statistically significant observation even with maximum asymmetry. An increase in $\tan\beta$ decreases the sensitivity because the branching ratio $\tilde{\chi}_2^0 \to \tilde{\ell}^\pm \ell^\mp$ is reduced. The reduction is due to $\tilde{\tau}$'s becoming more mixed which increases the left handed component in the lighter $\tilde{\tau}$. Therefore, the $\tilde{\tau}_1$ cou-
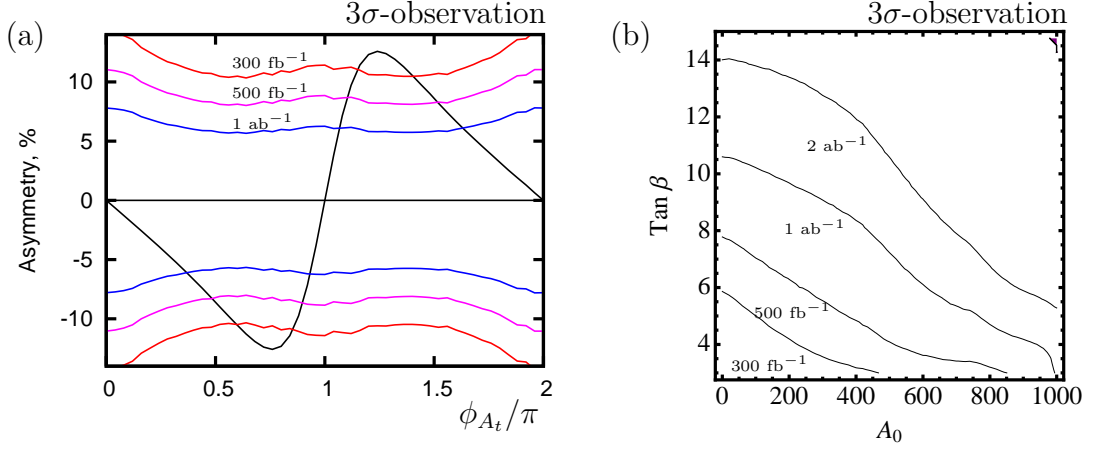
Figure 6.5: Pure $\tilde{t}_1\tilde{t}_1^*$ production, all decay channels included, see Tab. 6.5 for branching ratios for the specific parameter point and Fig. 6.4 for how these alter with ϕ_{A_t}. τ tagging is included in both plots. (a) Asymmetry, $\mathcal{A}_{\ell_N}$, at reference point with 3σ-luminosity lines shown. (b) Minimum luminosity required for 3σ-discovery in $\tan\beta, A_0$ plane when asymmetry, $\mathcal{A}_{\ell_N}$, is maximal.
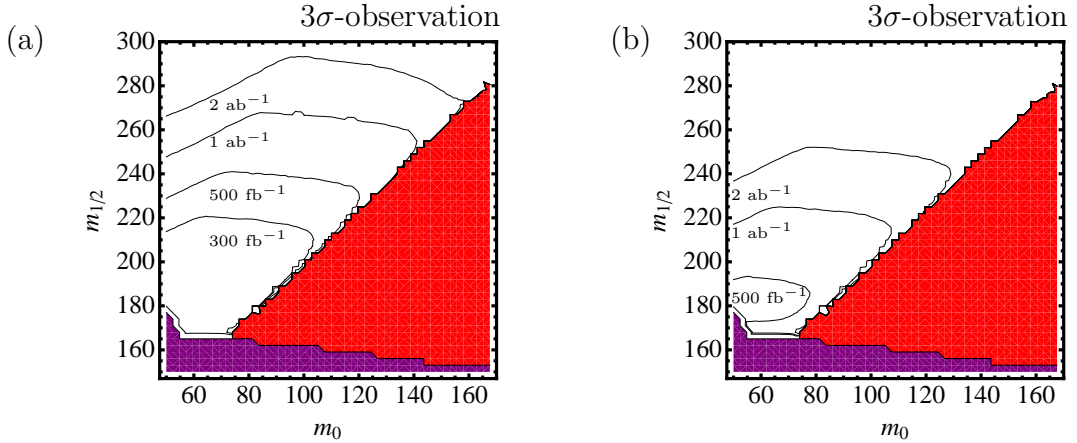
Figure 6.6: Minimum luminosity required for 3σ-discovery in $m_0, m_{1/2}$ plane when asymmetry, $\mathcal{A}_{\ell_N}$, is maximal. Pure $\tilde{t}_1\tilde{t}_1^*$ production, all decay channels included, see Tab. 6.5 for branching ratios for the specific parameter point and Fig. 6.4 for how these alter with ϕ_{A_t}. Purple area is ruled out by LEP direct detection [20] and red area has no two body decay $\tilde{\chi}_2^0 \to \tilde{\ell}^\pm \ell^\mp$. (a) With τ tagging. (b) Without τ tagging.

ples more strongly to the predominantly wino $\tilde{\chi}_2^0$ and begins to dominate this decay channel at the expense of the signal process. A rise in A_0 decreases sensitivity mainly because the CP-asymmetry is reduced. The reason is that after RGE running, an

increase in A_0 reduces the magnitude of the trilinear coupling A_t that contains the phase, ϕ_{A_t} that we are interested in. Hence the CP effects are reduced.

Similarly, Fig. 6.6(a) shows the effect of varying the mSUGRA parameters m_0 and $m_{1/2}$ on the minimum luminosity required for an observation of CP effects. We note as general trend that as $m_{1/2}$ is increasing, we need more luminosity to observe the CP-violating triple products. This is due to the increase in $\tilde{t}_1$ mass which reduces the production cross section for $\tilde{t}_1\tilde{t}_1^*$. If we increase m_0 we see that a large area of the parameter space has no two body decay $\tilde{\chi}_2^0 \to \tilde{\ell}^\pm \ell^\mp$ as $\tilde{\ell}^\pm > \tilde{\chi}_2^0$.

Fig. 6.6(b) indicates the effect of having no hadronic τ-tagging for the decay $\tilde{\chi}_1^+ \to \tilde{\tau}_1^+ \nu_\tau$. The τ final-state dominates the $\tilde{\chi}_1^+$ decay which in turn is the dominant product of the $\tilde{t}_1$ in low mass mSUGRA scenarios, Tab. 6.5. As stated in the beginning of Sec. 6.5 we assume a 40% τ-tagging efficiency and without this we lose approximately a factor of 2 in effective luminosity for our signal process.

6.5.4 Impact of momentum reconstruction on SUSY background separation

All of the previous sections results have assumed that the $\tilde{t}_1\tilde{t}_1^*$ process can be isolated effectively. However, in the mSUGRA scenarios investigated many other SUSY particles will be produced. Tab. 6.7 shows that the total production cross section for SUSY is ≈ 25 times greater than for $\tilde{t}_1\tilde{t}_1^*$ production and we can therefore expect sizable backgrounds. We can also expect that the vast majority of the SUSY background processes will have no other spin correlated CP-sensitive triple product with the same final state and will therefore just act as a dilution to the CP-asymmetry by contributing to the denominator of Eq. (3.36).

Tab. 6.7 shows that after the initial event selection and top reconstruction, the SUSY background is still ≈ 10 times larger than the signal process. Note that if we apply the kinematical reconstruction to these events we see that we substantially reduce the background to be only ≈ 3 times larger.

In order to observe CP-violating effects in $\tilde{t}_1\tilde{t}_1^*$ production at the LHC, however, the signal to background ratio may still be too high and consequently we need further cuts to isolate the signal process. We notice that in mSUGRA scenarios, the largest

	$\tilde{t}_1\tilde{t}_1^*$	SUSY	$\tilde{t}_1\tilde{t}_1^*$ Signal / SUSY Background
Cross Section (pb^{-1})	3.44	80.1	
Events with 500 fb^{-1}	1.7×10^6	4×10^7	
Events with 500 fb^{-1} Initial selection	32389	410735	0.079
Events with 500 fb^{-1} Top Reconstruction	7117	64729	0.11
Events with 500 fb^{-1} Kinematic Reconstruction	1213	3759	0.32
Events with 500 fb^{-1} Extra SUSY cuts	901	967	0.93

Table 6.7: Cross section, number of events and signal to background ratio at the LHC with $\sqrt{s} = 14$ TeV at LO for both the production channel $\tilde{t}_1\tilde{t}_1^*$ and inclusive SUSY production. All cross sections were calculated using `Herwig++` [151, 176].

background comes from $\tilde{g}$ production followed by the dominant decay to either sbottom, $\tilde{g} \rightarrow \tilde{b}_i b$ with a branching ratio of $\approx 30\%$. The $\tilde{b}_i$ decays dominantly to $\tilde{\chi}_2^0 b$ or $\tilde{\chi}_1^+ t$ which leads to a very similar final state as the signal process when combined with the opposite decay chain. The difference between the SUSY background and the $\tilde{t}_1$'s is that the $\tilde{g}$ and first and second generation $\tilde{q}$ have a higher mass. In addition, a gluino has in general one more decay vertex in the cascade decay producing another hard jet. These two factors mean that the average p_T of the particles produced in the event will be higher and the number of jets will be greater, thus we can use these characteristics to discriminate the signal from the background. Hence we cut on the number of jets reconstructed in an event,

$$\text{Number of jets} < 6. \tag{6.29}$$

For the p_T cuts, we have,

$$p_T(\text{Hardest Jet}) \quad < \quad 200 \text{ GeV}, \tag{6.30}$$

$$p_T(\text{2nd Jet}) \quad < \quad 130 \text{ GeV}, \tag{6.31}$$

$$p_T(\text{3rd Jet}) \quad < \quad 80 \text{ GeV (if applicable)}, \tag{6.32}$$

$$p_T(\text{Any } b \text{ Jet}) \quad < \quad 150 \text{ GeV}, \tag{6.33}$$

$$p_T(\text{Any Lepton}) \quad < \quad 100 \text{ GeV}. \tag{6.34}$$

Tab. 6.7 shows that after all these cuts are performed the signal to background ratio improves significantly and we now have roughly the same number of signal and background events in the sample.

If we now re-evaluate the luminosity plots with the SUSY background included, Fig. 6.7,6.8, we see that more luminosity is now required to observe a statistically significant effect. Due to the background dilution of the asymmetry, we now have $|\mathcal{A}_{\ell_N}|_{\max} \approx 6.5\%$ for our scenario Fig. 6.7. Consequently we are now only sensitive to phases between $0.6\pi < \phi_{A_t} < 0.85\pi$ with 1 ab^{-1} of data. If we look at the tanβ, A_0 contour plot we see that sensitivity at the LHC for 1 ab^{-1} is only possible for small values of tanβ.
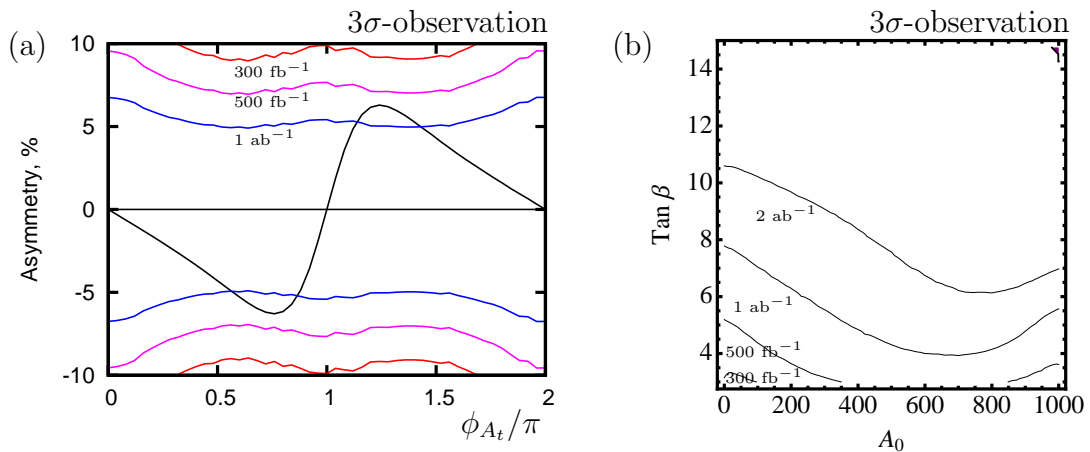
Figure 6.7: General SUSY production for the asymmetry $\mathcal{A}_{\ell_N}$. τ tagging is included in both plots. (a) Asymmetry, $\mathcal{A}_{\ell_N}$, at reference point with 3σ-luminosity lines shown. (b) Minimum luminosity required for 3σ-discovery in tanβ, A_0 plane when asymmetry, $\mathcal{A}_{\ell_N}$, is maximal.
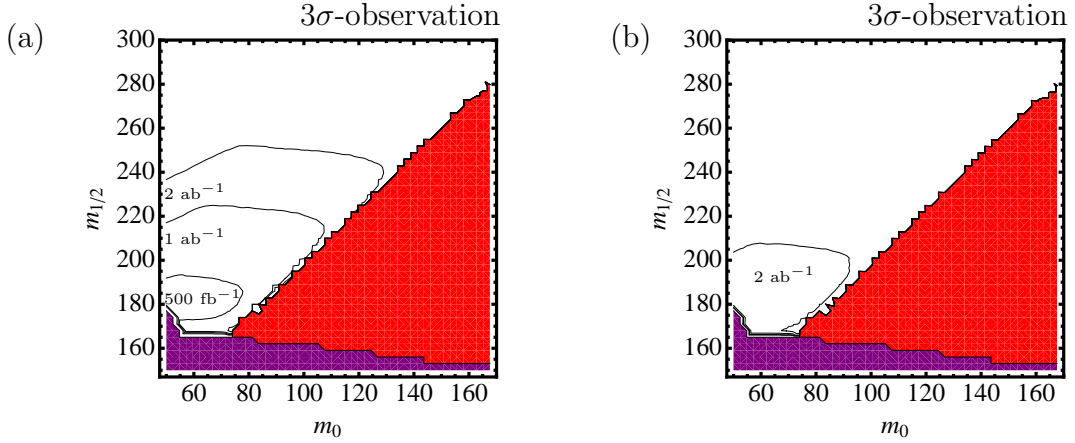
Figure 6.8: General SUSY production for the asymmetry $\mathcal{A}_{\ell_N}$. Minimum luminosity required for 3σ-discovery in $m_0, m_{1/2}$ plane when asymmetry, $\mathcal{A}_{\ell_N}$, is maximal. Purple area is ruled out by LEP direct detection [20] and red area has no two body decay $\tilde{\chi}_2^0 \to \tilde{\ell}^{\pm}\ell^{\mp}$. (a) With τ tagging. (b) Without τ tagging.

However, we would like to emphasise that it may be possible to substantially improve the statistical significance of an asymmetry measurement and return to close to the significance achieved when looking at a purely $\tilde{t}_1\tilde{t}_1^*$ process, even with the same SUSY background. Namely, via measuring the SUSY spectra (in particular the $\tilde{g}$ and $\tilde{b}$) a good estimate of the background should be possible. The background events can then be subtracted from the denominator of the asymmetry, Eq. (3.36), to give the true value of the asymmetry. Thus, the statistical significance should be much improved.

We would also like to remind the reader that this subtraction only becomes reliable if the signal to background ratio is good enough otherwise the signal is swamped by statistical fluctuations. Thus the momentum reconstruction procedure is vital since it significantly reduces the backgrounds that are present.

Similarly, a more constrained area of observability is seen in the m_0, $m_{1/2}$ plane, Fig. 6.8(a). With 1 ab^{-1} of data, our study suggests that only if $m_{1/2} < 220$ GeV will it be possible to observe a CP-phase in the stop sector. Again, we see the importance of τ-tagging to our study from the difference between Fig. 6.8(a) and Fig. 6.8(b). If τ-tagging is not used in the study, no CP-violation in the $\tilde{t}_1$ sector can be observed with 1 ab^{-1} of data.

6.5.5 Open experimental issues

Although the presented study was completed at the hadronic level, a full detector simulation should be completed to confirm the conclusions of this chapter. The most obvious experimental issue that could affect our results is the finite momentum resolution of the detector for both jets and leptons when performing momentum reconstruction. However, the resolution was tested with regards to momentum reconstruction in chapter 5, with a significantly more complicated final state and it was found to have only a small effect.

In terms of background suppression the mis-tagging of various objects could increase both the Standard Model and SUSY background. For the Standard Model background, the most obvious example is the $t\bar{t}$ process generating a tri-lepton signal [14]. The process requires a jet to be mistagged as a lepton, which is not investigated in this study. The suitability of hadronic τ-tagging in the study also needs to be investigated thoroughly as these are expected to have significant mis-identification rates [14]. However, this is beyond the scope of this theoretical study.

6.6 Conclusions

In this chapter we studied $\tilde{t}_1 \tilde{t}_1^*$ production and subsequent two body decays. We again form triple product correlations from the final-state particles that are sensitive to the presence of complex phases in the model. We find that in the mSUGRA scenario studied one can expect an asymmetry in the triple product distribution of up to 15% when calculated in the rest frame of the produced stop. The source of the CP violation in our case was the phase of the trilinear coupling A_t that attains a value of $\phi_{A_t} \sim 0.8$ when the asymmetry is maximum in our scenario.

The investigation was the first to analyse Monte Carlo hadronic events when using triple products to look for CP-violation in SUSY. We again find that the rest frame CP-odd asymmetry is diluted by the high boosts of the produced particles and this makes an observation difficult. Therefore we again studied the impact of momentum reconstruction of invisible LSPs to get access to the rest frame of the $\tilde{t}_1$. Having fully reconstructed events we are able to boost particle momenta back to the

rest frame of the $\tilde{t}_1$ and the maximum asymmetry is recovered to 15%. In addition, momentum reconstruction leads to a significant increase in the signal background ratio and thus is very important in attempting to isolate the process of interest.

If we consider exclusive $\tilde{t}_1$ production and all possible $\tilde{t}_1$ decay chains the maximum asymmetry is diluted slightly to $\sim 12.5\%$. In the mSUGRA scenario considered in this chapter one should expect to see a 3σ effect at $\mathcal{L} = 500$ fb^{-1} for phases in the range $0.5\,\pi \lesssim \phi_{A_t} \lesssim 0.9\,\pi$. If general SUSY production is considered, significant backgrounds to our signal process are present and extra kinematical cuts are required to remove this background. Even after these cuts some SUSY background remains and our maximum asymmetry is reduced to $\sim 6.5\%$. To see a 3σ effect at the LHC would require $\mathcal{L} = 1$ ab^{-1} of data for sensitivity to phases in the range $0.6\,\pi \lesssim \phi_{A_t} \lesssim 0.85\,\pi$.

We emphasise that the asymmetry after momentum reconstruction is a much cleaner observable from a theoretical point of view, thanks to a well defined final state. Therefore, using the above technique provides prospects for the observation of CP-violating effects for a range of the phase ϕ_{A_t} after a few years of LHC running at the high luminosity. The full assessment of LHC's ability to resolve CP violation in the MSSM, however, will definitely require a detailed simulation of detector effects, SM and SUSY backgrounds which is beyond the scope of the present phenomenological analysis.

Chapter 7

Conclusions

Supersymmetry has garnered significant interest from the particle physics community. This is due to both the theory's elegance and also the ability of particular models to solve some of the most pressing issues facing fundamental physics today. If supersymmetry is to provide a solution to the hierarchy problem, then we can expect that the model should reveal itself over the next few years at the LHC. If new states start being discovered, the challenge we immediately face is to measure and characterise the new physics. Of particular importance is the possibility that a model of supersymmetry may contain CP-violating phases. This thesis explores ideas of how these phases may be uncovered in supersymmetry at the LHC.

The main tool we used to study CP-violation within supersymmetry were triple product correlations. These correlations are formed from the momenta or spin vectors of three independent final-state particles. Supersymmetry is particularly suited for these observables due to the common occurrence in the theory of cascade decays, with many separate final-state particles. The correlations studied are all T_N-odd and using the CPT theorem (neglecting higher orders) correspond to CP-violating observables.

Our first study looked at stop pair production at the LHC with the following cascade decay,

$$\tilde{t}_i \to \tilde{\chi}_j^0 + t \to \tilde{\chi}_1^0 \ell^+ \ell^- + Wb. \tag{7.1}$$

We found that the decay was sensitive to phases in both the stop and neutralino mixing matrices. At the parton level and in the rest frame of the stop, we found that

the asymmetry could be as high as $\sim 12\%$. However, when we included the production process and PDFs at the LHC we found that the asymmetry was significantly diluted to the boosted initial state. The boost reduces the maximum asymmetry in the scenarios studied to $\sim 4\%$. When we include the production cross section and branching ratios, we estimate that a 1σ deviation from zero asymmetry may be seen with 500 fb^{-1}.

We also studied how the masses and branching ratios of the particles involved in the cascade decay vary with CP-phases. However, these are both CP-even quantities and we conclude that the LHC is unlikely to be able to make an unambiguous observation of CP-violation from these observables.

The first study highlighted two key difficulties we face when searching for CP-violation in SUSY cascade decays at the LHC. One issue is that the study has statistical limitations and it will be challenging to record enough events to make an unambiguous measurement of an asymmetry. Another issue is that the asymmetry is significantly diluted by the boosted production process which makes an observation much harder. Our second study attempted to resolve both of these issues.

Progress was made on the statistics front by looking at first and second generation squark production. The cross section is substantially higher for first and second generation squarks than for stops and consequently we can expect more events of interest to be observed. Secondly, if we look at squark production in association with a gluino we find that for some decay modes, the whole event is kinematically reconstructible. Thus we can boost all final-state particles into the rest frame of the squark and recover the full asymmetry.

We found that the rest frame parton-level asymmetry could be as large as 15% for the scenario discussed. Although we see a large dilution from the production process and PDFs, once momentum reconstruction is performed, the full asymmetry is almost recovered. We also added experimental cuts and final-state momentum smearing in the analysis and estimated that the sensitivity to phases at the LHC could be seen at the 3σ-level with 300 fb^{-1}.

For the last study in this thesis we again investigated stop pair production but the scenario had a different mass hierarchy. In this scenario, $m_{\tilde{\chi}_2^0} > m_{\tilde{\ell}}$, and therefore

the $\tilde{\chi}_2^0$ undergoes a two-body decay. Hence, the cascade decay of interest is,

$$\tilde{t}_i \rightarrow \tilde{\chi}_2^0 + t \rightarrow \tilde{\ell}^{\pm} + \ell^{\mp} + Wb \rightarrow \tilde{\chi}_1^0 + \ell^{\pm} + \ell^{\mp} + Wb\,. \qquad (7.2)$$

Any triple products are now only sensitive to phases that enter in the $\tilde{t}_i$ decay. Despite this restriction, rest frame, parton-level asymmetries of up to 15% can be in seen the scenarios studied. As usual, these asymmetries are significantly diluted when the production process and PDFs are included so we employ momentum reconstruction. Compared with the squark-gluino study, kinematic reconstruction is far simpler as we have enough invariants to solve the system with just one decay chain. Once the reconstruction is complete, we find that the asymmetry returns to the $\tilde{t}_i$ rest frame level.

As an additional facet to this study, we produced Monte Carlo events at the hadronic level and employed a jet finder to try and produce a realistic analysis for the LHC. With this analysis, we found that if we just consider $\tilde{t}_i$ decays that a 3σ-sensitivity at the LHC to phases in low mass scenarios of this kind could be expected with 500 fb^{-1}. We also considered the effect of supersymmetric backgrounds and found that the kinematic reconstruction can act as an effective cut to isolate the signal. If we assume no knowledge of the background, the luminosity required to see a 3σ-signal is estimated as 1 ab^{-1}. However, subtraction of the background has the potential to reduce this luminosity requirement.

These studies show, that whilst challenging, searching for CP-violation in cascade decays will be worthwhile if low mass supersymmetry is seen at the LHC. However, we must perform a full detector simulation with all backgrounds included to confirm the findings we have made. The simulations will also act as a valuable training ground to see how far precision physics can be pushed at the LHC. We have already seen how potentially useful kinematic reconstruction can be in recovering the asymmetry and suppressing background. Hopefully, new ideas will emerge, using all the final-state information, so that we can really begin to decode the full supersymmetric Lagrangian.

Appendix A

Interaction Lagrangians and couplings

A.1 Production process

The interaction Lagrangian terms for the production processes are,

$$\mathcal{L}_{ggg} = g_s \partial^\nu G^a_\mu g^{\mu\rho} f_{abc} G^b_\nu G^c_\rho \,, \tag{A.1.1}$$

$$\mathcal{L}_{qqg} = -g_s T^a_{rs} G^a_\mu \bar{q}_r \gamma^\mu q_s \,, \tag{A.1.2}$$

$$\mathcal{L}_{\tilde{q}_i \tilde{q}_j g} = i g_s T^a_{rs} \delta_{ij} G^a_\mu \tilde{q}^*_{jr} \overleftrightarrow{\partial^\mu} \tilde{q}_{is} \,, \tag{A.1.3}$$

$$\mathcal{L}_{q\tilde{q}_i \tilde{g}} = -\sqrt{2} g_s T^a_{rs} \left[\bar{q}_r (R^{\tilde{q}}_{i1} P_R - R^{\tilde{q}}_{i2} P_L) \tilde{g}^a \tilde{q}_{i,s} + \tilde{g}^a (R^{\tilde{q}}_{i1} P_L - R^{\tilde{q}}_{i2} P_R) q_r \tilde{q}^*_{i,s} \right] \,, \tag{A.1.4}$$

$$\mathcal{L}_{g\tilde{g}\tilde{g}} = \frac{ig_s}{2} f_{abc} G^a_\mu \tilde{g}^b \gamma^\mu \tilde{g}^c \,, \tag{A.1.5}$$

$$\mathcal{L}_{\tilde{q}_i \tilde{q}_j gg} = \tfrac{1}{2} g_s^2 (\tfrac{1}{3} \delta_{ab} + d_{abc} T^c) G^a_\mu G^{b\mu} \tilde{q}^*_j \tilde{q}_i \,. \tag{A.1.6}$$

where g_s is the strong coupling constant and $P_{L,R} = \frac{1}{2}(1 \mp \gamma_5)$. T^a are the generators of $SU(3)$ while f_{abc} and d_{abc} are colour factors derived from $SU(3)$. For more details see [185, 186]

A.2 Stop Decay

The interaction Lagrangian for the stop decay ($\tilde{t}_i \to \tilde{\chi}^0_j t$) is,

$$\mathcal{L}_{t\tilde{t}\tilde{\chi}^0} = \bar{\tilde{\chi}}^0_j \left(a^{\tilde{t}}_{ij} P_L + b^{\tilde{t}}_{ij} P_R \right) t \, \tilde{t}^*_i + \text{h.c.} \,, \tag{A.2.7}$$

137

The couplings are given by,

$$a_{ij}^{\tilde{t}} = -\frac{e}{\sqrt{2}\,s_W c_W}\,\mathcal{R}_{i1}^{\tilde{t}}\left(\frac{1}{3}s_W N_{j1}^* + c_W N_{j2}^*\right) - Y_t\,\mathcal{R}_{i2}^{\tilde{t}} N_{j4}^*, \qquad (A.2.8)$$

$$b_{ij}^{\tilde{t}} = \frac{2\sqrt{2}\,e}{3c_W}\,\mathcal{R}_{i2}^{\tilde{t}} N_{j1} - Y_t\,\mathcal{R}_{i1}^{\tilde{t}} N_{j4}, \qquad (A.2.9)$$

where $\mathcal{R}_{ij}^{\tilde{t}}$ are the entries of stop mixing matrix, Eq. (2.14), and N_{ij} are the entries of the neutralino mixing matrix, Eq. (2.28). $s_W = \sin\theta_W$ and $c_W = \cos\theta_W$ where θ_W is the weak mixing angle. e is the electromagnetic coupling constant ($e = g_2 s_W = g_1 c_W$) and the top Yukawa coupling is given by,

$$Y_t = \frac{e\,m_t}{\sqrt{2}\,m_W s_W \sin\beta}\,. \qquad (A.2.10)$$

where m_t is the mass of the top quark and m_W is the mass of the $W^{\pm}$ boson. $\tan\beta = \nu_2/\nu_1$ and is the ratio of the expectation value of the two neutral Higgs fields.

A detailed discussion of the stop decay couplings and decays to neutralinos and charginos is given in [98].

A.3 Squark decay

The lagrangian for the coupling of the first and second generation squarks to neutralinos can be considered a simplifiction of that for stops. Firstly, we neglect the small Yukawa terms and thus we have no couplings to the higgsino components. Secondly, mixing between the left and right squark states can be neglected, Eq. (2.8). For the decay ($\tilde{q}_i \to \tilde{\chi}_j^0 q$) we therefore have,

$$\mathcal{L}_{q\tilde{q}_i\tilde{\chi}_j^0} = a_{Lj}^{\tilde{q}}\,\bar{\tilde{\chi}}_j^0 P_L\,q\,\tilde{q}_L^* + b_{Rj}^{\tilde{q}}\,\bar{\tilde{\chi}}_j^0 P_R\,q\,\tilde{q}_R^* + \text{h.c.}\,, \qquad (A.3.11)$$

where the couplings are given by,

$$a_{Lj}^{\tilde{q}_u} = -\frac{e}{\sqrt{2}\,s_W c_W}\left(\frac{1}{3}s_W N_{j1}^* + c_W N_{j2}^*\right), \qquad (A.3.12)$$

$$b_{Rj}^{\tilde{q}_u} = \frac{2\sqrt{2}\,e}{3c_W}\,N_{j1}\,, \qquad (A.3.13)$$

$$a_{Lj}^{\tilde{q}_d} = -\frac{e}{\sqrt{2}\,s_W c_W}\left(\frac{1}{3}s_W N_{j1}^* - c_W N_{j2}^*\right), \qquad (A.3.14)$$

$$b_{Rj}^{\tilde{q}_d} = -\frac{\sqrt{2}\,e}{3c_W}\,N_{j1}\,. \qquad (A.3.15)$$

$\tilde{q}_{L(R)}$ are the left (right) squarks respectively of the first and second generation. Under the approximation of no squark mixing, $\tilde{q}_R = \tilde{q}_1$ and $\tilde{q}_L = \tilde{q}_2$.

A.4 Neutralino and slepton decay

In our analytical calculations we concentrate on neutralino decays to electrons and muons (followed by slepton decay if the 2-body process is on-shell). We ignore taus and therefore neglect the small Yukawa terms present in the same way as for the 1st and 2nd generation squarks. In addition, we again make the assumption that the mixing effects will be negligible.

The interaction lagrangian for the vertex $\tilde{\chi}_j^0 \tilde{\ell}^\pm \ell^\pm$ is,

$$\mathcal{L}_{\ell\tilde{\ell}_i\tilde{\chi}_j^0} = a_{Lj}^{\tilde{\ell}} \bar{\tilde{\chi}}_j^0 P_L \, \ell \, \tilde{\ell}_L^* + b_{Rj}^{\tilde{\ell}} \bar{\tilde{\chi}}_j^0 P_R \, \ell \, \tilde{\ell}_R^* + \text{h.c.} \,, \tag{A.4.16}$$

where the couplings are given by,

$$a_{Lj}^{\tilde{\ell}} = \frac{e}{\sqrt{2}\, s_W c_W} \left(s_W N_{j1}^* + c_W N_{j2}^* \right) , \tag{A.4.17}$$

$$b_{Rj}^{\tilde{\ell}} = -\frac{\sqrt{2}\, e}{c_W} N_{j1} \,. \tag{A.4.18}$$

Identically to the squarks, under the approximation of no slepton mixing, $\tilde{\ell}_R = \tilde{\ell}_1$ and $\tilde{q}_L = \tilde{q}_2$.

For the 3-body neutralino decay, $\tilde{\chi}_j^0 \to \tilde{\chi}_k^0 \ell^\pm \ell^\pm$, we also have a contribution from the exchange of a Z^0. Therefore the following Lagrangians are required to calculate this decay,

$$\mathcal{L}_{Z^0\ell^+\ell^-} = -Z_\mu \bar{\ell} \gamma^\mu [L_\ell P_L + R_\ell P_R]\ell \,, \tag{A.4.19}$$

$$\mathcal{L}_{Z^0\tilde{\chi}_j^0\tilde{\chi}_k^0} = Z_\mu \bar{\tilde{\chi}}_j^0 \gamma^\mu [O_{jk}^L P_L + O_{jk}^R P_R]\tilde{\chi}_k^0 \,, \tag{A.4.20}$$

where the couplings are given by,

$$L_\ell = \frac{e}{c_W s_W} \left(-\frac{1}{2} + s_W^2 \right) , \tag{A.4.21}$$

$$R_\ell = \frac{e}{c_W s_W} \left(s_W^2 \right) , \tag{A.4.22}$$

$$O_{jk}^L = \frac{e}{2c_W s_W} (N_{m4} N_{n4}^* - N_{m3} N_{n3}^*) \,, \tag{A.4.23}$$

$$O_{jk}^R = -\frac{e}{2c_W s_W} (O_{mn}^{L*}) \,, \tag{A.4.24}$$

The full interaction Lagrangian for the MSSM can be found in [187, 188].

Appendix B

Amplitudes

B.1 Stop decay $\tilde{t}_1 \to \tilde{\chi}_j^0 t$

We give the analytic expression for the stop decay density matrix which produces the $\tilde{\chi}_j^0$ and t. The decay can be decomposed as,

$$|M(\tilde{t}_1 \to \tilde{\chi}_j^0 t)|^2 = P(\tilde{\chi}_j^0 t) + \Sigma_P^a(\tilde{\chi}_j^0) + \Sigma_P^b(t) + \Sigma_P^{ab}(\tilde{\chi}_j^0 t)\,, \tag{B.1.1}$$

whose spin-independent contribution reads,

$$P(\tilde{\chi}_j^0 t) = (|a_{1j}^{\tilde{t}}|^2 + |b_{1j}^{\tilde{t}}|^2)(p_t p_{\tilde{\chi}_j^0}) - 2 m_t m_{\tilde{\chi}_j^0} Re(a_{1j}^{\tilde{t}} b_{1j}^*)\,, \tag{B.1.2}$$

where p_t and $p_{\tilde{\chi}_k^0}$ denote the four-momenta of the t-quark and the neutralino $\tilde{\chi}_k^0$. The coupling constants a_{ij} and b_{ij} are shown in Eq. (A.2.8, A.2.9) and by substituting the explicit matrix elements of Eq. (2.14) we can show the specific parameter dependence,

$$
\begin{aligned}
|a_{1j}^{\tilde{t}}|^2 + |b_{1j}^{\tilde{t}}|^2 \;\; = \;\; & \cos^2\theta_{\tilde{t}} \left(\frac{e^2}{2 s_W^2 c_W^2} \left| \frac{1}{3} s_W N_{j1} + c_W N_{j2} \right|^2 + Y_t^2 |N_{j4}|^2 \right) \\
& + \; \sin^2\theta_{\tilde{t}} \left(\frac{8e^2}{9 c_W^2} |N_{j1}|^2 + Y_t^2 |N_{j4}|^2 \right) \\
& + \; 2\sin\theta_{\tilde{t}}\cos\theta_{\tilde{t}} \, Y_t \left(\frac{e}{\sqrt{2}\, s_W c_W} \operatorname{Re}\left[\mathrm{e}^{\mathrm{i}\phi_{\tilde{t}}} \left(\frac{1}{3} s_W N_{j1}^* + c_W N_{j2}^* \right) N_{j4} \right] \right. \\
& \left. - \; \frac{2\sqrt{2}\, e}{3 c_W} \operatorname{Re}\left[\mathrm{e}^{-\mathrm{i}\phi_{\tilde{t}}} N_{j1} N_{j4}^* \right] \right). \tag{B.1.3}
\end{aligned}
$$

$$\text{Re}\left[a_{1j}^{\tilde{t}} b_{1j}^{\tilde{t}*}\right] = \cos^2\theta_{\tilde{t}} \frac{e}{\sqrt{2}\, s_W c_W} Y_t \, \text{Re}\left[\left(\frac{1}{3} s_W N_{j1}^* + c_W N_{j2}^*\right) N_{j4}^*\right]$$

$$+ \sin^2\theta_{\tilde{t}} \frac{2\sqrt{2}\, e}{3 c_W} Y_t \, \text{Re}[N_{j4}^* N_{j1}^*]$$

$$+ \sin\theta_{\tilde{t}} \cos\theta_{\tilde{t}} \left(Y_t^2 \, \text{Re}\left[e^{-i\phi_{\tilde{t}}} N_{j4}^{*2}\right]\right.$$

$$\left. - \frac{2}{3} \frac{e^2}{s_W c_W^2} \, \text{Re}\left[e^{i\phi_{\tilde{t}}} \left(\frac{1}{3} s_W N_{j1}^* + c_W N_{j2}^*\right) N_{j1}^*\right]\right). \qquad \text{(B.1.4)}$$

The spin-dependent terms that depend on individual spin contributions are T-even and are given by,

$$\Sigma_P^a(\tilde{\chi}_j^0) = (|b_{ij}|^2 - |a_{ij}|^2) m_{\tilde{\chi}_j^0}(p_t s^a(\tilde{\chi}_j^0)), \qquad \text{(B.1.5)}$$

$$\Sigma_P^b(t) = (|b_{ij}|^2 - |a_{ij}|^2) m_t(p_{\tilde{\chi}_j^0} s^b(t)), \qquad \text{(B.1.6)}$$

where $s^a(\tilde{\chi}_j^0)$ ($s^b(t)$) denote the spin-basis vectors of the neutralino $\tilde{\chi}_j^0$ (t-quark) respectively (for an explicit representation see Eq. (B.7.45-B.7.50)). Again the coupling constants can be expanded as,

$$|b_{1j}^{\tilde{t}}|^2 - |a_{1j}^{\tilde{t}}|^2 = \cos^2\theta_{\tilde{t}} \left(Y_t^2 |N_{j4}|^2 - \frac{e^2}{2 s_W^2 c_W^2}\left|\frac{1}{3} s_W N_{j1} + c_W N_{j2}\right|^2\right)$$

$$+ \sin^2\theta_{\tilde{t}} \left(\frac{8 e^2}{9 c_W^2}|N_{j1}|^2 - Y_t^2 |N_{j4}|^2\right)$$

$$- 2\sin\theta_{\tilde{t}} \cos\theta_{\tilde{t}} Y_t \left(\frac{e}{\sqrt{2}\, s_W c_W} \, \text{Re}\left[e^{i\phi_{\tilde{t}}}\left(\frac{1}{3} s_W N_{j1}^* + c_W N_{j2}^*\right) N_{j4}\right]\right.$$

$$\left. + \frac{2\sqrt{2}\, e}{3 c_W} \, \text{Re}\left[e^{-i\phi_{\tilde{t}}} N_{j1} N_{j4}^*\right]\right). \qquad \text{(B.1.7)}$$

The terms that depend simultaneously on the spin of the top quark and of the neutralino can be split into T-even, $\Sigma_P^{ab,E}(\tilde{\chi}_j^0 t)$, and T-odd, $\Sigma_P^{ab,O}(\tilde{\chi}_j^0 t)$. The T-even contributions are as follows,

$$\Sigma_P^{ab,E}(\tilde{\chi}_j^0 t) = 2 Re(a_{ij} b_{ij}^*)[(s^a(\tilde{\chi}_j^0) p_t)(s^b(t) p_{\tilde{\chi}_j^0}) - (p_t p_{\tilde{\chi}_j^0})(s^a(\tilde{\chi}_j^0) s^b(t))]$$

$$+ m_t m_{\tilde{\chi}_j^0}(s^a(\tilde{\chi}_j^0) s^b(t))(|a_{ij}|^2 + |b_{ij}|^2). \qquad \text{(B.1.8)}$$

The T-odd contributions that generate the triple product correlations that we are interested in are,

$$\Sigma_P^{ab,O}(\tilde{\chi}_j^0 t) = -g^2 Im(a_{ij} b_{ij}^*) f_4^{ab}, \qquad \text{(B.1.9)}$$

where the T-odd kinematical factor is given by,

$$f_4^{ab} = \epsilon_{\mu\nu\rho\sigma} s^{a,\mu}(\tilde{\chi}_j^0) p_{\tilde{\chi}_j^0}^\nu s^{b,\rho}(t) p_t^\sigma. \qquad \text{(B.1.10)}$$

Sec.5.2.2 explains how this epsilon product generates the triple product observable. We again expand the coupling constant to see the functional dependence,

$$
\begin{aligned}
\text{Im}\left[a_{1j}^{\tilde{t}} b_{1j}^{\tilde{t}*}\right] &= \cos^2\theta_{\tilde{t}} \frac{e}{\sqrt{2}\, s_W c_W} Y_t \,\text{Im}\left[\left(\frac{1}{3} s_W N_{j1}^* + c_W N_{j2}^*\right) N_{j4}^*\right] \\
&+ \sin^2\theta_{\tilde{t}} \frac{2\sqrt{2}\, e}{3 c_W} Y_t\, \text{Im}[N_{j4}^* N_{j1}^*] \\
&+ \sin\theta_{\tilde{t}}\cos\theta_{\tilde{t}}\bigg(Y_t^2\,\text{Im}\left[\mathrm{e}^{-\mathrm{i}\phi_{\tilde{t}}} N_{j4}^{*2}\right] \\
&- \frac{2}{3}\frac{e^2}{s_W c_W^2}\,\text{Im}\left[\mathrm{e}^{\mathrm{i}\phi_{\tilde{t}}}\left(\frac{1}{3} s_W N_{j1}^* + c_W N_{j2}^*\right) N_{j1}^*\right]\bigg). \quad (\text{B.1.11})
\end{aligned}
$$

B.2 Squark decay $\tilde{q}_L \to \tilde{\chi}_j^0 q$

The analytic expression for the squark decay density matrix which produces the $\tilde{\chi}_j^0$ and q can be decomposed as,

$$
|M(\tilde{q}_L \to \tilde{\chi}_j^0 q)|^2 = P(\tilde{\chi}_j^0 q) + \Sigma_P^a(\tilde{\chi}_j^0)\,, \quad (\text{B.2.12})
$$

whose spin-independent contribution reads,

$$
P(\tilde{\chi}_j^0 q) = |a_{Lj}^{\tilde{q}}|^2 (p_q p_{\tilde{\chi}_j^0})\,, \quad (\text{B.2.13})
$$

where p_q and $p_{\tilde{\chi}_j^0}$ denote the four-momenta of the quark q and the neutralino $\tilde{\chi}_j^0$. The spin-dependent contributions is T-even and given by,

$$
\Sigma_P^a(\tilde{\chi}_j^0) = -|a_{Lj}^{\tilde{q}}|^2 m_{\tilde{\chi}_j^0}(p_q s^a(\tilde{\chi}_j^0))\,, \quad (\text{B.2.14})
$$

where $s^a(\tilde{\chi}_j^0)$ denotes the spin-basis vector of the neutralino $\tilde{\chi}_j^0$, see Eq. (B.7.45-B.7.47) for an explicit representation.

B.3 Neutralino 3-body decay $\tilde{\chi}_j^0 \to \tilde{\chi}_k^0 \ell^+ \ell^-$

The analytic expression for the squark decay density matrix can be decomposed as,

$$
|M(\tilde{\chi}_j^0 \to \tilde{\chi}_k^0 \ell^+ \ell^-)|^2 = D(\tilde{\chi}_j^0) + \Sigma_D^a(\tilde{\chi}_j^0)\,. \quad (\text{B.3.15})
$$

The contributions independent of the polarisation of the neutralino $\tilde{\chi}_j^0$ are,

$$
D(\tilde{\chi}_j^0) = D(ZZ) + D(Z\tilde{\ell}_L) + D(Z\tilde{\ell}_R) + D(\tilde{\ell}_L\tilde{\ell}_L) + D(\tilde{\ell}_R\tilde{\ell}_R)\,, \quad (\text{B.3.16})
$$

where,

$$
\begin{aligned}
D(ZZ) &= 32|\Delta(Z)|^2(L_\ell^2 + R_\ell^2) \\
&\quad \times \left[|O_{kj}^L|^2(g_1 + g_2) + (\text{Re } O_{kj}^L)^2 - (\text{Im } O_{kj}^L)^2)g_3\right], \qquad \text{(B.3.17)} \\
D(Z\tilde{\ell}_L) &= 8L_\ell \,\text{Re}\left\{\Delta(Z)\Big[a_{Lj}^{\tilde{\ell}}a_{Lk}^{\tilde{\ell}*}\Delta_t^*(\tilde{\ell}_L)(2O_{kj}^L g_1 + O_{kj}^{L*}g_3)\right. \\
&\qquad\qquad\qquad \left.+ a_{Lj}^{\tilde{\ell}*}a_{Lk}^{\tilde{\ell}}\Delta_u^*(\tilde{\ell}_L)(2O_{kj}^{L*}g_2 + O_{kj}^L g_3)\Big]\right\}, \;\; \text{(B.3.18)} \\
D(\tilde{\ell}_L\tilde{\ell}_L) &= 2\left[|a_{Lj}^{\tilde{\ell}}|^2|a_{Lk}^{\tilde{\ell}}|^2\big(|\Delta_t(\tilde{\ell}_L)|^2 g_1 + |\Delta_u(\tilde{\ell}_L)|^2 g_2\big)\right. \\
&\qquad \left.+ \,\text{Re}\left\{(a_{Lj}^{\tilde{\ell}*})^2(a_{Lk}^{\tilde{\ell}})^2\Delta_t(\tilde{\ell}_L)\Delta_u^*(\tilde{\ell}_L)\right\}g_3\right]. \qquad \text{(B.3.19)}
\end{aligned}
$$

$\Delta(Z)$ and $\Delta_{t,u}(\tilde{\ell}_L)$ denote the propagators of the virtual particles in the direct channel and in both crossed channels (labelled t, u, cf. Fig. 4.2). The quantities $D(Z\tilde{\ell}_R)$ and $D(\tilde{\ell}_R\tilde{\ell}_R)$ can be derived from Eqs. (B.3.18) and (B.3.19) by the substitutions,

$$
L_\ell \to R_\ell, \quad \Delta_{t,u}(\tilde{\ell}_L) \to \Delta_{t,u}(\tilde{\ell}_R), \quad O_{kj}^L \to O_{kj}^R, \quad a_{Lj,k}^{\tilde{\ell}} \to b_{Rj,k}^{\tilde{\ell}}. \qquad \text{(B.3.20)}
$$

The kinematic factors are,

$$
\begin{aligned}
g_1 &= (p_{\tilde{\chi}_k^0}p_{\ell^-})(p_{\tilde{\chi}_j^0}p_{\ell^+}), &\text{(B.3.21)} \\
g_2 &= (p_{\tilde{\chi}_k^0}p_{\ell^+})(p_{\tilde{\chi}_j^0}p_{\ell^-}), &\text{(B.3.22)} \\
g_3 &= m_j m_k (p_{\ell^-}p_{\ell^+}). &\text{(B.3.23)}
\end{aligned}
$$

We can split the terms depending on the polarisation of the neutralino into T-even and T-odd contributions,

$$
\Sigma_D^a(\tilde{\chi}_j^0) = \Sigma_D^{a,E}(\tilde{\chi}_j^0) + \Sigma_D^{a,O}(\tilde{\chi}_j^0). \qquad \text{(B.3.24)}
$$

The T-even contributions depending on the polarisation of the decaying neutralino $\tilde{\chi}_j^0$ are,

$$
\Sigma_D^{a,E}(\tilde{\chi}_j^0) = \Sigma_D^{a,E}(ZZ) + \Sigma_D^{a,E}(Z\tilde{\ell}_L) + \Sigma_D^{a,E}(Z\tilde{\ell}_R) + \Sigma_D^{a,E}(\tilde{\ell}_L\tilde{\ell}_L) + \Sigma_D^{a,E}(\tilde{\ell}_R\tilde{\ell}_R) \quad \text{(B.3.25)}
$$

where,

$$
\begin{aligned}
\Sigma_D^{a,E}(ZZ) &= 32|\Delta(Z)|^2(R_\ell^2 - L_\ell^2) \\
&\quad \times \Big[-[(\mathrm{Re}\,O_{kj}^L)^2 - (\mathrm{Im}\,O_{kj}^L)^2]g_3^a + |O_{kj}^L|^2(g_1^a - g_2^a) \Big], \quad \text{(B.3.26)}
\end{aligned}
$$

$$
\begin{aligned}
\Sigma_D^{a,E}(Z\tilde{\ell}_L) &= 8L_\ell\,\mathrm{Re}\Big\{\Delta(Z)\Big[a_{Lj}^{\tilde{\ell}}a_{Lk}^{\tilde{\ell}*}\Delta_t^*(\tilde{\ell}_L)\big(-2O_{kj}^Lg_1^a + O_{kj}^{L*}g_3^a\big) \\
&\qquad\qquad + a_{Lj}^{\tilde{\ell}*}a_{Lk}^{\tilde{\ell}}\Delta_u^*(\tilde{\ell}_L)\big(2O_{kj}^{L*}g_2^a + O_{kj}^Lg_3^a\big)\Big]\Big\} \quad \text{(B.3.27)}
\end{aligned}
$$

$$
\begin{aligned}
\Sigma_D^{a,E}(\tilde{\ell}_L\tilde{\ell}_L) &= 2\Big[|a_{Lj}^{\tilde{\ell}}|^2|a_{Lk}^{\tilde{\ell}}|^2[|\Delta_u(\tilde{\ell}_L)|^2g_2^a - |\Delta_t(\tilde{\ell}_L)|^2g_1^a] \\
&\qquad + \mathrm{Re}\big\{(a_{Lj}^{\tilde{\ell}*})^2(a_{Lk}^{\tilde{\ell}})^2\Delta_t(\tilde{\ell}_L)\Delta_u^*(\tilde{\ell}_L)g_3^a\big\}\Big], \quad \text{(B.3.28)}
\end{aligned}
$$

The contributions $\Sigma_D^{a,E}(Z\tilde{\ell}_R)$ and $\Sigma_D^{a,E}(\tilde{\ell}_R\tilde{\ell}_R)$ are derived from Eqs. (B.3.27) and (B.3.28) by applying the substitutions given by Eq. (B.3.20) and in addition $g_{1,2,3}^a \to -g_{1,2,3}^a$. The kinematic factors are,

$$
g_1^a = m_j(p_{\tilde{\chi}_k^0}p_{\ell^-})(p_{\ell^+}s^a(\tilde{\chi}_j^0)), \quad \text{(B.3.29)}
$$

$$
g_2^a = m_j(p_{\tilde{\chi}_k^0}p_{\ell^+})(p_{\ell^-}s^a(\tilde{\chi}_j^0)), \quad \text{(B.3.30)}
$$

$$
g_3^a = m_k[(p_{\tilde{\chi}_j^0}p_{\ell^+})(p_{\ell^-}s^a(\tilde{\chi}_j^0)) - (p_{\tilde{\chi}_j^0}p_{\ell^-})(p_{\ell^+}s^a(\tilde{\chi}_j^0))]. \quad \text{(B.3.31)}
$$

The T-odd contributions depending on the polarisation of the decaying neutralino $\tilde{\chi}_j^0$ are,

$$
\Sigma_D^{a,O}(\tilde{\chi}_j^0) = \Sigma_D^{a,O}(ZZ) + \Sigma_D^{a,O}(Z\tilde{\ell}_L) + \Sigma_D^{a,O}(Z\tilde{\ell}_R) + \Sigma_D^{a,O}(\tilde{\ell}_L\tilde{\ell}_L) + \Sigma_D^{a,O}(\tilde{\ell}_R\tilde{\ell}_R) \quad \text{(B.3.32)}
$$

where,

$$
\Sigma_D^{a,O}(ZZ) = 32|\Delta(Z)|^2(L_\ell^2 - R_\ell^2)\Big[2\mathrm{Re}\,(O_{kj}^L)\,\mathrm{Im}\,(O_{kj}^L)ig_4^a\Big], \quad \text{(B.3.33)}
$$

$$
\begin{aligned}
\Sigma_D^{a,O}(Z\tilde{\ell}_L) &= 8L_\ell\,\mathrm{Re}\Big\{\Delta(Z)\Big[-a_{Lj}^{\tilde{\ell}}a_{Lk}^{\tilde{\ell}*}O_{kj}^{L*}\Delta_t^*(\tilde{\ell}_L) \\
&\qquad\qquad + a_{Lj}^{\tilde{\ell}*}a_{Lk}^{\tilde{\ell}}O_{kj}^L\Delta_u^*(\tilde{\ell}_L)\Big]g_4^a\Big\}, \quad \text{(B.3.34)}
\end{aligned}
$$

$$
\Sigma_D^{a,O}(\tilde{\ell}_L\tilde{\ell}_L) = 2\,\mathrm{Re}\Big\{(a_{Lj}^{\tilde{\ell}*})^2(a_{Lk}^{\tilde{\ell}})^2\Delta_t(\tilde{\ell}_L)\Delta_u^*(\tilde{\ell}_L)g_4^a\Big\}. \quad \text{(B.3.35)}
$$

The contributions $\Sigma_D^{a,O}(Z\tilde{\ell}_R)$ and $\Sigma_D^{a,O}(\tilde{\ell}_R\tilde{\ell}_R)$ are derived from Eqs. (B.3.27) and (B.3.28) by applying the substitutions given by Eq. (B.3.20). The kinematic factor is

$$
g_4^a = im_k\epsilon_{\mu\nu\rho\sigma}s^{a\mu}(\tilde{\chi}_j^0)p_{\tilde{\chi}_j^0}^\nu p_{\ell^-}^\rho p_{\ell^+}^\sigma. \quad \text{(B.3.36)}
$$

B.4 Neutralino 2-body decay $\tilde{\chi}_j^0 \to \tilde{\ell}_R^\pm \ell^\mp$

The analytic expression for the 2-body neutralino decay density matrix can be decomposed as,

$$|M(\tilde{\chi}_j^0 \to \tilde{\ell}_R^\pm \ell^\mp)|^2 = D(\tilde{\chi}_j^0) + \Sigma_D^a(\tilde{\chi}_j^0)\,, \tag{B.4.37}$$

whose spin-independent contribution reads,

$$D(\tilde{\chi}_2^0) = \frac{|a_{Rj}^{\tilde{\ell}}|^2}{2}\{m_{\tilde{\chi}_j^0}^2 - m_{\tilde{\ell}_R}^2\}\,. \tag{B.4.38}$$

The spin-dependent contribution is T-even and reads,

$$\Sigma_D^a(\tilde{\chi}_2^0) = -|f_{L2}^l|^2 m_{\tilde{\chi}_2^0}\{(s^a(\tilde{\chi}_2^0)p_{\ell^\mp}\}\,. \tag{B.4.39}$$

where $s^a(\tilde{\chi}_j^0)$ denotes the spin-basis vector of the neutralino $\tilde{\chi}_j^0$, see Eq. (B.7.45-B.7.47) for the explicit representations.

B.5 Slepton decay $\tilde{\ell}_R^\pm \to \tilde{\chi}_k^0 \ell^\pm$

The slepton is a scalar and consequently carries no spin correlation. Therefore, we only have a spin independent component for the decay,

$$\begin{aligned} |M(\tilde{\ell}_R^\pm \to \tilde{\chi}_k^0 \ell^\pm)|^2 &= D(\tilde{\chi}_j^0)\,, & \text{(B.5.40)} \\ &= \frac{|a_{Rk}^{\tilde{\ell}}|^2}{2}\{m_{\tilde{\ell}_R}^2 - m_{\tilde{\chi}_k^0}^2\}\,. & \text{(B.5.41)} \end{aligned}$$

B.6 Top decay $t \to W^+ b$

The analytical expression for the 2-body decay of the top quark into a W-boson and the final-state bottom quark can be decomposed as,

$$|M(t \to W^+ b)|^2 = D(t) + \Sigma_D^b(t)\,, \tag{B.6.42}$$

whose spin-independent contribution reads,

$$D(t) = \frac{e^2}{4s_W^2}\{m_t^2 - 2m_W^2 + \frac{m_t^4}{m_W^2}\}\,. \tag{B.6.43}$$

The spin-dependent contribution is T-even and reads,

$$\Sigma_D^b(t) = -\frac{e^2}{2s_W^2}m_t\{(s^b(t)p_b) + \frac{m_t^2 - m_W^2}{m_W^2}(s^b(t)p_W)\}. \tag{B.6.44}$$

where $s^b(t)$ denotes the spin-basis vector of the neutralino t, see Eq. (B.7.48-B.7.50) for the explicit representations.

B.7   Spin vectors

Spin correlations can be carried by both the neutralino and the top depending on the decay chain. For the numerical calculations we perform the computation with explicit spin vectors in the amplitudes. The three spin-basis four-vectors s^1, s^2 and s^3 form a right-handed system and provide, together with the momentum, an orthogonal basis system. They are chosen as,

$$s^1(\tilde{\chi}_j^0) = \left(0, \frac{(\vec{p}_{\tilde{\chi}_j^0} \times \vec{p}_{\tilde{t}_i}) \times \vec{p}_{\tilde{\chi}_j^0}}{|(\vec{p}_{\tilde{\chi}_j^0} \times \vec{p}_{\tilde{t}_i}) \times \vec{p}_{\tilde{\chi}_j^0}|}\right), \tag{B.7.45}$$

$$s^2(\tilde{\chi}_j^0) = \left(0, \frac{\vec{p}_{\tilde{\chi}_j^0} \times \vec{p}_{\tilde{t}_i}}{|\vec{p}_{\tilde{\chi}_j^0} \times \vec{p}_{\tilde{t}_i}|}\right), \tag{B.7.46}$$

$$s^3(\tilde{\chi}_j^0) = \frac{1}{m_{\tilde{\chi}_j^0}}\left(|\vec{p}_{\tilde{\chi}_j^0}|, \frac{E_{\tilde{\chi}_j^0}}{|\vec{p}_{\tilde{\chi}_j^0}|}\vec{p}_{\tilde{\chi}_j^0}\right). \tag{B.7.47}$$

The spin-system for the top quark has been chosen analogously,

$$s^1(t) = \left(0, \frac{(\vec{p}_t \times \vec{p}_{\tilde{\chi}_j^0}) \times \vec{p}_t}{|(\vec{p}_t \times \vec{p}_{\tilde{\chi}_j^0}) \times \vec{p}_t|}\right), \tag{B.7.48}$$

$$s^2(t) = \left(0, \frac{\vec{p}_t \times \vec{p}_{\tilde{\chi}_j^0}}{|\vec{p}_t \times \vec{p}_{\tilde{\chi}_j^0}|}\right), \tag{B.7.49}$$

$$s^3(t) = \frac{1}{m_t}\left(|\vec{p}_t|, \frac{E_t}{|\vec{p}_t|}\vec{p}_t\right), \tag{B.7.50}$$

and E_t and $E_{\tilde{\chi}_j^0}$ denote the energies of the top quark and the neutralino $\tilde{\chi}_j^0$, respectively.

Appendix C

Kinematics

C.1 Phase space

Here we consider the generic phase space terms that can be applied to any process discussed in this thesis.
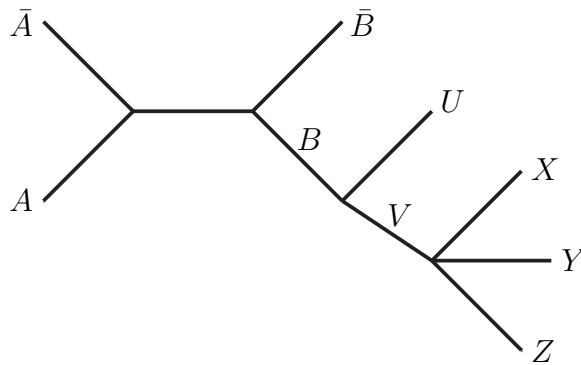
Figure C.1: Example process, $A\bar{A} \to B\bar{B}$, $B \to UV$, $V \to XYZ$, used to illustrate phase space factors.

The complete cross section for all the processes discussed in this thesis can be decomposed into the production cross section and the branching ratios of the subsequent decays. For the example process shown in Fig. C.1,

$$d\sigma_{\text{tot}} = d\sigma(A\bar{A} \to B\bar{B}) \cdot \frac{E_B}{m_B \Gamma_B} d\hat{\Gamma}(B \to UV) \cdot \frac{E_V}{m_V \Gamma_V} d\hat{\Gamma}(V \to XYZ),$$

$$(\text{C.1.1})$$

where the factors $E/m\Gamma$ come from the use of the narrow-width approximation for

the propagators of the unstable particles B and V. This approximation is valid for $(\Gamma/m)^2 \ll 1$, which is satisfied for all cases studied in our scenarios.

C.2   2-body decay, 1 massive final state particle

For the 2-body decay $B \to UV$ where $m_U^2 = 0$ and $m_V^2 \neq 0$ we have,

$$d\hat{\Gamma}_{2,1}(B \to UV) = \frac{1}{4E_V} D(B \to UV) \, d\Phi_{2,1}, \tag{C.2.2}$$

where $D(B \to UV)$ is the amplitude for the decay $B \to UV$. $d\Phi_{2,1}$ is the phase space factor in the laboratory system for the 2-body decay with 1 massive particle in the final state,

$$d\Phi_{2,1} = \frac{1}{(2\pi)^2} \frac{1}{2||\vec{p}_B| \cos\theta_U - E_V - E_U|} \, d\Omega_U \,, \tag{C.2.3}$$

where $d\Omega_U = d\phi_U d(\cos\theta_U)$ is solid angle of the particle U.

C.3   2-body decay, 2 massive final state particles

For the 2-body decay $B \to UV$ where $m_U^2 \neq 0$ and $m_V^2 \neq 0$ we have,

$$d\hat{\Gamma}_{2,2}(B \to UV) = \frac{2}{E_B} D(B \to UV) \, d\Phi_{2,2} \,, \tag{C.3.4}$$

where $D(B \to UV)$ is the amplitude for the decay $B \to UV$. $d\Phi_{2,2}$ is the phase space factor in the laboratory system for the 2-body decay with 2 massive particles in the final state,

$$d\Phi_{2,2} = \frac{1}{(2\pi)^2} \frac{|\vec{p}_V^{\pm}|^2}{2|E_B|\vec{p}_V^{\pm}| - E_V^{\pm}|\vec{p}_B| \cos\theta_V|} \, d\Omega_V \,, \tag{C.3.5}$$

where $d\Omega_V = d\phi_V d(\cos\theta_V)$ is solid angle of the particle V.

There is a subtlety in the phase-space calculation, namely that there can be two solutions for $\vec{p}_V$. If,

$$|\vec{p}_V| < p_0 \,, \tag{C.3.6}$$

where

$$p_0 = \lambda^{\frac{1}{2}}(m_B^2, m_U^2, m_V^2)/2m_V \,, \tag{C.3.7}$$

and

$$\lambda(m_B^2, m_U^2, m_V^2) = (m_B^2 - m_U^2 - m_V^2)^2 - 4m_U^2 m_V^2 \,, \qquad (C.3.8)$$

then the decay angle, $\theta_V = \measuredangle(\vec{p}_B, \vec{p}_V)$, is unconstrained and there is only one solution. However, if

$$\vec{p}_V > p_0 \,, \qquad (C.3.9)$$

then the angle is constrained by

$$\sin \theta_V^{max} = \frac{p_0}{|\vec{p}_B|} = \frac{\lambda^{\frac{1}{2}}(m_B^2, m_U^2, m_V^2)}{2|\vec{p}_B|m_V} \,, \qquad (C.3.10)$$

and there are two physical solutions,

$$|\vec{p}_V| = \frac{(m_B^2 + m_V^2 - m_U^2)|\vec{p}_B| \cos\theta_V \pm E_B \sqrt{\lambda(m_B^2, m_U^2, m_V^2) - 4|\mathbf{p}_B|^2 \, m_V^2 \, (1 - \cos^2\theta_V)}}{2|\mathbf{p}_B|^2(1 - \cos^2\theta_V) + 2m_B^2} \,. \qquad (C.3.11)$$

For the region of phase space where two solutions exist the cross section becomes a summation of the solutions for each of the subsequent decay chains.

C.4 3-body decay, 1 massive final state particle

For the 3-body decay $B \to UV$ where $m_X^2 = 0$, $m_Y^2 = 0$ and $m_Z^2 \neq 0$ we have,

$$d\hat{\Gamma}_{3,1}(V \to XYZ) = \frac{1}{4E_V} D(V \to XYZ) \, d\Phi_{3,1}, \qquad (C.4.12)$$

where $D(V \to XYZ)$ is the amplitude for the decay $V \to XYZ$. $d\Phi_{3,1}$ is the phase space factor in the laboratory system for the 3-body decay with 1 massive particle in the final state,

$$d\Phi_{3,1} = \frac{1}{8(2\pi)^5} \frac{E_X}{||\vec{p}_V| \cos\theta_X - E_Z - E_X - E_Y \cos\alpha|} \, E_Y \, dE_Y d\Omega_X d\Omega_Y \,, \qquad (C.4.13)$$

where $d\Omega_{X(Y)} = d\phi_{X(Y)} d(\cos\theta_{X(Y)})$ is solid angle of the particle $X(Y)$ respectively and the opening angle between X and Y is $\alpha = \measuredangle(\vec{p}_X, \vec{p}_Y)$.

When evaluating the phase-space integral at the parton level, kinematical limits need to be determined on some of the variables and these are listed below,

$$E_Y \;<\; \frac{m_V^2 - m_Z^2}{2(E_V - |\vec{p}_V|)} \,, \qquad (C.4.14)$$

$$\cos\theta_Y \;<\; \frac{2E_V E_Y + m_Z^2 - m_V^2}{2E_Y|\vec{p}_V|} \,. \qquad (C.4.15)$$

Bibliography

[1] S. Weinberg, "A Model of Leptons," *Phys. Rev. Lett.* **19** (1967) 1264–1266.

[2] S. L. Glashow, "Partial Symmetries of Weak Interactions," *Nucl. Phys.* **22** (1961) 579–588.

[3] A. Salam, "Weak and Electromagnetic Interactions,". Originally printed in *Svartholm: Elementary Particle Theory, Proceedings Of The Nobel Symposium Held 1968 At Lerum, Sweden*, Stockholm 1968, 367-377.

[4] M. Gell-Mann, "A Schematic Model of Baryons and Mesons," *Phys. Lett.* **8** (1964) 214–215.

[5] H. Fritzsch, M. Gell-Mann, and H. Leutwyler, "Advantages of the Color Octet Gluon Picture," *Phys. Lett.* **B47** (1973) 365–368.

[6] D. J. Gross and F. Wilczek, "Ultraviolet behaviour of non-abelian gauge theories," *Phys. Rev. Lett.* **30** (1973) 1343–1346.

[7] P. W. Higgs, "Broken symmetries and the masses of gauge bosons," *Phys. Rev. Lett.* **13** (1964) 508–509.

[8] P. W. Higgs, "Spontaneous Symmetry Breakdown without Massless Bosons," *Phys. Rev.* **145** (1966) 1156–1163.

[9] F. Englert and R. Brout, "Broken symmetry and the mass of gauge vector mesons," *Phys. Rev. Lett.* **13** (1964) 321–322.

[10] G. S. Guralnik, C. R. Hagen, and T. W. B. Kibble, "Global conservation laws and massless particles," *Phys. Rev. Lett.* **13** (1964) 585–587.

[11] T. W. B. Kibble, "Symmetry breaking in non-Abelian gauge theories," *Phys. Rev.* **155** (1967) 1554–1561.

[12] **LEP Working Group for Higgs boson searches** Collaboration, R. Barate *et al.*, "Search for the standard model Higgs boson at LEP," *Phys. Lett.* **B565** (2003) 61–75, `arXiv:hep-ex/0306033`.

[13] **CDF and D0** Collaboration, P. Mastrandrea, "Higgs searches at the Tevatron," `arXiv:1009.1046 [hep-ex]`.

[14] **The ATLAS** Collaboration, G. Aad *et al.*, "Expected Performance of the ATLAS Experiment - Detector, Trigger and Physics," `arXiv:0901.0512 [hep-ex]`.

[15] **CMS** Collaboration, G. L. Bayatian *et al.*, "CMS technical design report, volume II: Physics performance," *J. Phys.* **G34** (2007) 995–1579.

[16] E. Gildener, "Gauge Symmetry Hierarchies," *Phys. Rev.* **D14** (1976) 1667.

[17] L. Susskind, "Dynamics of Spontaneous Symmetry Breaking in the Weinberg- Salam Theory," *Phys. Rev.* **D20** (1979) 2619–2625.

[18] D. A. Dicus and V. S. Mathur, "Upper bounds on the values of masses in unified gauge theories," *Phys. Rev.* **D7** (1973) 3111–3114.

[19] B. W. Lee, C. Quigg, and H. B. Thacker, "Weak Interactions at Very High-Energies: The Role of the Higgs Boson Mass," *Phys. Rev.* **D16** (1977) 1519.

[20] **Particle Data Group** Collaboration, C. Amsler *et al.*, "Review of particle physics," *Phys. Lett.* **B667** (2008) 1.

[21] **ALEPH** Collaboration, "Precision electroweak measurements on the Z resonance," *Phys. Rept.* **427** (2006) 257, `arXiv:hep-ex/0509008`.

[22] F. Zwicky, "Spectral displacement of extra galactic nebulae," *Helv. Phys. Acta* **6** (1933) 110–127.

[23] R. B. Metcalf, L. A. Moustakas, A. J. Bunker, and I. R. Parry, "Spectroscopic Gravitational Lensing and Limits on the Dark Matter Substructure in Q2237+0305," *Astrophys. J.* **607** (2004) 43–59, `arXiv:astro-ph/0309738`.

[24] E. Komatsu *et al.*, "Seven-Year Wilkinson Microwave Anisotropy Probe (WMAP) Observations: Cosmological Interpretation," `arXiv:1001.4538 [astro-ph.CO]`.

[25] G. Bertone, D. Hooper, and J. Silk, "Particle dark matter: Evidence, candidates and constraints," *Phys. Rept.* **405** (2005) 279–390, `arXiv:hep-ph/0404175`.

[26] A. D. Sakharov, "Violation of CP Invariance, c Asymmetry, and Baryon Asymmetry of the Universe," *Pisma Zh. Eksp. Teor. Fiz.* **5** (1967) 32–35.

[27] M. Kobayashi and T. Maskawa, "CP Violation in the Renormalizable Theory of Weak Interaction," *Prog. Theor. Phys.* **49** (1973) 652–657.

[28] A. G. Cohen, D. B. Kaplan, and A. E. Nelson, "Progress in electroweak baryogenesis," *Ann. Rev. Nucl. Part. Sci.* **43** (1993) 27–70, `arXiv:hep-ph/9302210`.

[29] M. B. Gavela, P. Hernandez, J. Orloff, O. Pene, and C. Quimbay, "Standard model CP violation and baryon asymmetry. Part 2: Finite temperature," *Nucl. Phys.* **B430** (1994) 382–426, `arXiv:hep-ph/9406289`.

[30] V. A. Rubakov and M. E. Shaposhnikov, "Electroweak baryon number non-conservation in the early universe and in high-energy collisions," *Usp. Fiz. Nauk* **166** (1996) 493–537, `arXiv:hep-ph/9603208`.

[31] F. Csikor, Z. Fodor, and J. Heitger, "Endpoint of the hot electroweak phase transition," *Phys. Rev. Lett.* **82** (1999) 21–24, `arXiv:hep-ph/9809291`.

[32] P. Ramond, "Dual Theory for Free Fermions," *Phys. Rev.* **D3** (1971) 2415–2418.

[33] A. Neveu and J. H. Schwarz, "Factorizable dual model of pions," *Nucl. Phys.* **B31** (1971) 86–112.

[34] R. Haag, J. T. Lopuszanski, and M. Sohnius, "All Possible Generators of Supersymmetries of the s Matrix," *Nucl. Phys.* **B88** (1975) 257.

[35] M. Drees, "An Introduction to supersymmetry," `arXiv:hep-ph/9611409`.

[36] S. P. Martin, "A Supersymmetry Primer," `arXiv:hep-ph/9709356`.

[37] E. Witten, "Dynamical Breaking of Supersymmetry," *Nucl. Phys.* **B188** (1981) 513.

[38] N. Sakai, "Naturalness in Supersymmetric Guts," *Zeit. Phys.* **C11** (1981) 153.

[39] R. K. Kaul and P. Majumdar, "Cancellation of quadratically divergent mass corrections in globally supersymmetric spontaneoulsy broken gauge theories," *Nucl. Phys.* **B199** (1982) 36.

[40] O. Buchmueller *et al.*, "Predictions for Supersymmetric Particle Masses in the CMSSM using Indirect Experimental and Cosmological Constraints," *JHEP* **09** (2008) 117, `arXiv:0808.4128 [hep-ph]`.

[41] O. Buchmueller *et al.*, "Likelihood Functions for Supersymmetric Observables in Frequentist Analyses of the CMSSM and NUHM1," `arXiv:0907.5568 [hep-ph]`.

[42] P. Bechtle, K. Desch, M. Uhlenbrock, and P. Wienemann, "Constraining SUSY models with Fittino using measurements before, with and beyond the LHC," `arXiv:0907.2589 [hep-ph]`.

[43] H. Pagels and J. R. Primack, "Supersymmetry, Cosmology and New TeV Physics," *Phys. Rev. Lett.* **48** (1982) 223.

[44] H. Goldberg, "Constraint on the photino mass from cosmology," *Phys. Rev. Lett.* **50** (1983) 1419.

[45] U. Chattopadhyay, A. Corsetti, and P. Nath, "WMAP Constraints, SUSY Dark Matter and Implications for the Direct Detection of SUSY," *Phys. Rev.* **D68** (2003) 035005, `arXiv:hep-ph/0303201`.

[46] M. S. Carena, M. Quiros, M. Seco, and C. E. M. Wagner, "Improved results in supersymmetric electroweak baryogenesis," *Nucl. Phys.* **B650** (2003) 24–42, `arXiv:hep-ph/0208043`.

[47] A. Riotto and M. Trodden, "Recent progress in baryogenesis," *Ann. Rev. Nucl. Part. Sci.* **49** (1999) 35–75, `arXiv:hep-ph/9901362`.

[48] M. Trodden, "Electroweak baryogenesis," *Rev. Mod. Phys.* **71** (1999) 1463–1500, `arXiv:hep-ph/9803479`.

[49] S. Dimopoulos and H. Georgi, "Softly Broken Supersymmetry and SU(5)," *Nucl. Phys.* **B193** (1981) 150.

[50] H. P. Nilles, "Supersymmetry, Supergravity and Particle Physics," *Phys. Rept.* **110** (1984) 1–162.

[51] H. E. Haber and G. L. Kane, "The Search for Supersymmetry: Probing Physics Beyond the Standard Model," *Phys. Rept.* **117** (1985) 75–263.

[52] R. Barbieri, "Looking Beyond the Standard Model: The Supersymmetric Option," *Riv. Nuovo Cim.* **11N4** (1988) 1–45.

[53] J. F. Gunion, H. E. Haber, G. L. Kane, and S. Dawson, "The Higgs hunter's guide,". SCIPP-89/13.

[54] S. Heinemeyer, "MSSM Higgs physics at higher orders," *Int. J. Mod. Phys.* **A21** (2006) 2659–2772, `arXiv:hep-ph/0407244`.

[55] M. Frank *et al.*, "The Higgs boson masses and mixings of the complex MSSM in the Feynman-diagrammatic approach," *JHEP* **02** (2007) 047, `arXiv:hep-ph/0611326`.

[56] L. Girardello and M. T. Grisaru, "Soft Breaking of Supersymmetry," *Nucl. Phys.* **B194** (1982) 65.

[57] A. H. Chamseddine, R. L. Arnowitt, and P. Nath, "Locally Supersymmetric Grand Unification," *Phys. Rev. Lett.* **49** (1982) 970.

[58] L. J. Hall, J. D. Lykken, and S. Weinberg, "Supergravity as the Messenger of Supersymmetry Breaking," *Phys. Rev.* **D27** (1983) 2359–2378.

[59] P. Nath and R. L. Arnowitt, "Non-universal soft SUSY breaking and dark matter," *Phys. Rev.* **D56** (1997) 2820–2832, `arXiv:hep-ph/9701301`.

[60] J. R. Ellis, T. Falk, K. A. Olive, and Y. Santoso, "Exploration of the MSSM with Non-Universal Higgs Masses," *Nucl. Phys.* **B652** (2003) 259–347, `arXiv:hep-ph/0210205`.

[61] J. R. Ellis, K. A. Olive, and Y. Santoso, "The MSSM Parameter Space with Non-Universal Higgs Masses," *Phys. Lett.* **B539** (2002) 107–118, `arXiv:hep-ph/0204192`.

[62] B. C. Allanach, A. Dedes, and H. K. Dreiner, "Bounds on R-parity violating couplings at the weak scale and at the GUT scale," *Phys. Rev.* **D60** (1999) 075014, `arXiv:hep-ph/9906209`.

[63] H. K. Dreiner, M. Kramer, and B. O'Leary, "Bounds on R-parity violation from leptonic and semi- leptonic meson decays," *Phys. Rev.* **D75** (2007) 114016, `arXiv:hep-ph/0612278`.

[64] J. R. Ellis, J. S. Hagelin, D. V. Nanopoulos, K. A. Olive, and M. Srednicki, "Supersymmetric relics from the big bang," *Nucl. Phys.* **B238** (1984) 453–476.

[65] J. R. Ellis and D. V. Nanopoulos, "Flavor Changing Neutral Interactions in Broken Supersymmetric Theories," *Phys. Lett.* **B110** (1982) 44.

[66] F. Gabbiani, E. Gabrielli, A. Masiero, and L. Silvestrini, "A complete analysis of FCNC and CP constraints in general SUSY extensions of the standard model," *Nucl. Phys.* **B477** (1996) 321–352, `arXiv:hep-ph/9604387`.

[67] H. E. Haber, "The status of the minimal supersymmetric standard model and beyond," *Nucl. Phys. Proc. Suppl.* **62** (1998) 469–484, `arXiv:hep-ph/9709450`.

[68] S. Dimopoulos and D. W. Sutter, "The Supersymmetric flavor problem," *Nucl. Phys.* **B452** (1995) 496–512, `arXiv:hep-ph/9504415`.

[69] D. W. Sutter, "The Supersymmetric flavor problem and $\mu \to e^+\gamma$," `arXiv:hep-ph/9704390`.

[70] S. Dimopoulos and S. D. Thomas, "Dynamical Relaxation of the Supersymmetric CP Violating Phases," *Nucl. Phys.* **B465** (1996) 23–33, `arXiv:hep-ph/9510220`.

[71] S. M. Bilenky and S. T. Petcov, "Massive Neutrinos and Neutrino Oscillations," *Rev. Mod. Phys.* **59** (1987) 671.

[72] C. A. Baker *et al.*, "An improved experimental limit on the electric dipole moment of the neutron," *Phys. Rev. Lett.* **97** (2006) 131801, `arXiv:hep-ex/0602020`.

[73] B. C. Regan, E. D. Commins, C. J. Schmidt, and D. DeMille, "New limit on the electron electric dipole moment," *Phys. Rev. Lett.* **88** (2002) 071805.

[74] W. C. Griffith *et al.*, "Improved Limit on the Permanent Electric Dipole Moment of Hg-199," *Phys. Rev. Lett.* **102** (2009) 101601.

[75] I. B. Khriplovich and A. R. Zhitnitsky, "What is the value of the neutron electric dipole moment in the Kobayashi-Maskawa model?," *Phys. Lett.* **B109** (1982) 490.

[76] M. B. Gavela *et al.*, "CP violation induced by penguin diagrams and the neutron electric dipole moment," *Phys. Lett.* **B109** (1982) 215.

[77] B. H. J. McKellar, S. R. Choudhury, X.-G. He, and S. Pakvasa, "The neutron electric dipole moment in the standard K-M model," *Phys. Lett.* **B197** (1987) 556.

[78] S. Abel, S. Khalil, and O. Lebedev, "EDM constraints in supersymmetric theories," *Nucl. Phys.* **B606** (2001) 151–182, `arXiv:hep-ph/0103320`.

[79] M. Pospelov and A. Ritz, "Electric dipole moments as probes of new physics," *Annals Phys.* **318** (2005) 119–169, `arXiv:hep-ph/0504231`.

[80] Y. Li, S. Profumo, and M. Ramsey-Musolf, "A Comprehensive Analysis of Electric Dipole Moment Constraints on CP-violating Phases in the MSSM," `arXiv:1006.1440 [Unknown]`.

[81] P. Nath, "CP Violation via electroweak gauginos and the electric dipole moment of the electron," *Phys. Rev. Lett.* **66** (1991) 2565–2568.

[82] Y. Kizukuri and N. Oshimo, "Implications of the neutron electric dipole moment for supersymmetric models," *Phys. Rev.* **D45** (1992) 1806–1809.

[83] T. Falk, K. A. Olive, and M. Srednicki, "Phases in the MSSM, Electric Dipole Moments and Cosmological Dark Matter," *Phys. Lett.* **B354** (1995) 99–106, `arXiv:hep-ph/9502401`.

[84] T. Falk and K. A. Olive, "Electric Dipole Moment Constraints on Phases in the Constrained MSSM," *Phys. Lett.* **B375** (1996) 196–202, `arXiv:hep-ph/9602299`.

[85] T. Falk and K. A. Olive, "More on electric dipole moment constraints on phases in the constrained MSSM," *Phys. Lett.* **B439** (1998) 71–80, `arXiv:hep-ph/9806236`.

[86] T. Ibrahim and P. Nath, "The neutron and the lepton EDMs in MSSM, large CP violating phases, and the cancellation mechanism," *Phys. Rev.* **D58** (1998) 111301, `arXiv:hep-ph/9807501`.

[87] T. Ibrahim and P. Nath, "Large CP phases and the cancellation mechanism in EDMs in SUSY, string and brane models," *Phys. Rev.* **D61** (2000) 093004, `arXiv:hep-ph/9910553`.

[88] J. R. Ellis, J. S. Lee, and A. Pilaftsis, "Electric Dipole Moments in the MSSM Reloaded," *JHEP* **10** (2008) 049, `arXiv:0808.1819 [hep-ph]`.

[89] T. Gajdosik, "EDMs – signs of CP violation from physics beyond the Standard Model," *Acta Phys. Polon.* **B40** (2009) 3171–3177, `arXiv:0910.3512 [Unknown]`.

[90] A. Pilaftsis, "Higgs scalar-pseudoscalar mixing in the minimal supersymmetric standard model," *Phys. Lett.* **B435** (1998) 88–100, `arXiv:hep-ph/9805373`.

[91] D. A. Demir, "Effects of the supersymmetric phases on the neutral Higgs sector," *Phys. Rev.* **D60** (1999) 055006, `arXiv:hep-ph/9901389`.

[92] A. Pilaftsis and C. E. M. Wagner, "Higgs bosons in the minimal supersymmetric standard model with explicit CP violation," *Nucl. Phys.* **B553** (1999) 3–42, `arXiv:hep-ph/9902371`.

[93] S. Y. Choi, M. Drees, and J. S. Lee, "Loop corrections to the neutral Higgs boson sector of the MSSM with explicit CP violation," *Phys. Lett.* **B481** (2000) 57–66, `arXiv:hep-ph/0002287`.

[94] J. L. Kneur and G. Moultaka, "Inverting the supersymmetric standard model spectrum: From physical to Lagrangian ino parameters," *Phys. Rev.* **D59** (1999) 015005, `arXiv:hep-ph/9807336`.

[95] S. Y. Choi *et al.*, "Reconstructing the chargino system at e+ e- linear colliders," *Eur. Phys. J.* **C14** (2000) 535–546, `arXiv:hep-ph/0002033`.

[96] J. L. Kneur and G. Moultaka, "Phases in the gaugino sector: Direct reconstruction of the basic parameters and impact on the neutralino pair production," *Phys. Rev.* **D61** (2000) 095003, `arXiv:hep-ph/9907360`.

[97] A. Bartl, S. Hesselbach, K. Hidaka, T. Kernreiter, and W. Porod, "Top squarks and bottom squarks in the MSSM with complex parameters," *Phys. Rev.* **D70** (2004) 035003, `arXiv:hep-ph/0311338`.

[98] K. Rolbiecki, J. Tattersall, and G. Moortgat-Pick, "Measuring the Stop Mixing Angle at the LHC," `arXiv:0909.3196 [Unknown]`.

[99] H. Eberl, T. Gajdosik, W. Majerotto, and B. Schrausser, "CP-violating asymmetry in chargino decay into neutralino and W boson," *Phys. Lett.* **B618** (2005) 171–181, `arXiv:hep-ph/0502112`.

[100] E. Christova, H. Eberl, W. Majerotto, and S. Kraml, "CP violation in charged Higgs decays in the MSSM with complex parameters," *Nucl. Phys.* **B639** (2002) 263–280, `arXiv:hep-ph/0205227`.

[101] E. Christova, H. Eberl, W. Majerotto, and S. Kraml, "CP violation in charged Higgs boson decays into tau and neutrino," *JHEP* **12** (2002) 021, `arXiv:hep-ph/0211063`.

[102] M. Frank and I. Turan, "CP asymmetry in charged Higgs decays in MSSM," *Phys. Rev.* **D76** (2007) 016001, `arXiv:hep-ph/0703184`.

[103] M. Frank and I. Turan, "CP Asymmetry in Charged Higgs Decays to Chargino- Neutralino," *Phys. Rev.* **D76** (2007) 076008, `arXiv:0708.0026 [hep-ph]`.

[104] E. Christova, H. Eberl, E. Ginina, and W. Majerotto, "CP violation in $H^{\pm}t$ production at the LHC," *Phys. Rev.* **D79** (2009) 096005, `arXiv:0812.4392 [hep-ph]`.

[105] E. Christova, H. Eberl, E. Ginina, and W. Majerotto, "CP violation in charged Higgs decays in the MSSM," *JHEP* **02** (2007) 075, `arXiv:hep-ph/0612088`.

[106] Y. Kizukuri and N. Oshimo, "T odd asymmetry mediated by neutralino in e+ e- annihilation," *Phys. Lett.* **B249** (1990) 449–454.

[107] S. Y. Choi, H. S. Song, and W. Y. Song, "CP phases in correlated production and decay of neutralinos in the minimal supersymmetric standard model," *Phys. Rev.* **D61** (2000) 075004, `arXiv:hep-ph/9907474`.

[108] V. D. Barger *et al.*, "CP-violating phases in SUSY, electric dipole moments, and linear colliders," *Phys. Rev.* **D64** (2001) 056007, `arXiv:hep-ph/0101106`.

[109] A. Bartl, H. Fraas, O. Kittel, and W. Majerotto, "CP asymmetries in neutralino production in e+ e- collisions," *Phys. Rev.* **D69** (2004) 035007, `arXiv:hep-ph/0308141`.

[110] A. Bartl, H. Fraas, O. Kittel, and W. Majerotto, "CP sensitive observables in e+ e- –¿ neutralino(i) neutralino(j) and neutralino decay into Z boson," *Eur. Phys. J.* **C36** (2004) 233–243, `arXiv:hep-ph/0402016`.

[111] J. A. Aguilar-Saavedra, "CP violation in neutralino(1) neutralino(2) production at a linear collider," *Nucl. Phys.* **B697** (2004) 207–224, `arXiv:hep-ph/0404104`.

[112] A. Bartl, H. Fraas, S. Hesselbach, K. Hohenwarter-Sodek, and G. A. Moortgat-Pick, "A T-odd asymmetry in neutralino production and decay," *JHEP* **08** (2004) 038, `arXiv:hep-ph/0406190`.

[113] S. Y. Choi, B. C. Chung, J. Kalinowski, Y. G. Kim, and K. Rolbiecki, "Analysis of the neutralino system in three-body leptonic decays of neutralinos," *Eur. Phys. J.* **C46** (2006) 511–520, `arXiv:hep-ph/0504122`.

[114] A. Bartl, H. Fraas, O. Kittel, and W. Majerotto, "CP violation in chargino production and decay into sneutrino," *Phys. Lett.* **B598** (2004) 76–82, `arXiv:hep-ph/0406309`.

[115] O. Kittel, A. Bartl, H. Fraas, and W. Majerotto, "CP sensitive observables in chargino production and decay into a W boson," *Phys. Rev.* **D70** (2004) 115005, `arXiv:hep-ph/0410054`.

[116] A. Bartl *et al.*, "CP asymmetries in chargino production and decay: The three-body decay case," *Eur. Phys. J.* **C51** (2007) 149–161, `arXiv:hep-ph/0608065`.

[117] S. Kraml, "CP violation in SUSY," `arXiv:0710.5117 [hep-ph]`.

[118] S. Hesselbach, "CP Violation in SUSY Particle Production and Decay," `arXiv:0709.2679 [hep-ph]`.

[119] S. Weinberg, "The Quantum theory of fields. Vol. 1: Foundations,". Cambridge, UK: Univ. Pr. (1995) 609 p.

[120] M. E. Peskin and D. V. Schroeder, "An Introduction to quantum field theory,". Reading, USA: Addison-Wesley (1995) 842 p.

[121] D. Atwood, S. Bar-Shalom, G. Eilam, and A. Soni, "CP violation in top physics," *Phys. Rept.* **347** (2001) 1–222, `arXiv:hep-ph/0006032`.

[122] J. S. Schwinger, "The theory of quantized fields. I," *Phys. Rev.* **82** (1951) 914–927.

[123] J. S. Schwinger, "The theory of quantized fields. II," *Phys. Rev.* **91** (1953) 713–728.

[124] K. Desch, J. Kalinowski, G. Moortgat-Pick, K. Rolbiecki, and W. J. Stirling, "Combined LHC / ILC analysis of a SUSY scenario with heavy sfermions," *JHEP* **12** (2006) 007, `arXiv:hep-ph/0607104`.

[125] A. Bartl, H. Fraas, T. Kernreiter, and O. Kittel, "T-odd correlations in the decay of scalar fermions," *Eur. Phys. J.* **C33** (2004) 433–442, `arXiv:hep-ph/0306304`.

[126] Y. Kizukuri and N. Oshimo, "T-odd asymmetry in chargino pair production processes," `arXiv:hep-ph/9310224`.

[127] A. Bartl, K. Hohenwarter-Sodek, T. Kernreiter, and H. Rud, "CP sensitive observables in chargino production with transverse e+- beam polarization," *Eur. Phys. J.* **C36** (2004) 515–522, `arXiv:hep-ph/0403265`.

[128] A. Bartl *et al.*, "CP-odd observables in neutralino production with transverse e+ and e- beam polarization," *JHEP* **01** (2006) 170, `arXiv:hep-ph/0510029`.

[129] A. Bartl, E. Christova, K. Hohenwarter-Sodek, and T. Kernreiter, "Triple product correlations in top squark decays," *Phys. Rev.* **D70** (2004) 095007, `arXiv:hep-ph/0409060`.

[130] P. Langacker, G. Paz, L.-T. Wang, and I. Yavin, "A T-odd observable sensitive to CP violating phases in squark decay," *JHEP* **07** (2007) 055, `arXiv:hep-ph/0702068`.

[131] J. Ellis, F. Moortgat, G. Moortgat-Pick, J. M. Smillie, and J. Tattersall, "Measurement of CP Violation in Stop Cascade Decays at the LHC," *Eur. Phys. J.* **C60** (2009) 633–651, `arXiv:0809.1607 [hep-ph]`.

[132] F. Deppisch and O. Kittel, "Probing SUSY CP Violation in Two-Body Stop Decays at the LHC," `arXiv:0905.3088 [hep-ph]`.

[133] G. Moortgat-Pick, K. Rolbiecki, and J. Tattersall, "Momentum reconstruction at the LHC for probing CP- violation in the stop sector," `arXiv:1008.2206 [hep-ph]`.

[134] A. Bartl, E. Christova, K. Hohenwarter-Sodek, and T. Kernreiter, "CP asymmetries in scalar bottom quark decays," *JHEP* **11** (2006) 076, `arXiv:hep-ph/0610234`.

[135] F. F. Deppisch and O. Kittel, "CP violation in sbottom decays," `arXiv:1003.5186 [Unknown]`.

[136] G. Moortgat-Pick, K. Rolbiecki, J. Tattersall, and P. Wienemann, "Probing CP Violation with and without Momentum Reconstruction at the LHC," *JHEP* **01** (2010) 004, `arXiv:0908.2631 [hep-ph]`.

[137] K. Kiers, A. Szynkman, and D. London, "CP violation in supersymmetric theories: stop(2) → stop(1) tau- tau+," *Phys. Rev.* **D74** (2006) 035004, `arXiv:hep-ph/0605123`.

[138] A. Szynkman, K. Kiers, and D. London, "CP Violation in Supersymmetric Theories: stop2 → stop1 H H, stop2 → stop1 Z Z, stop2 → stop1 W+ W-,

stop2 → stop1 Z H," *Phys. Rev.* **D75** (2007) 075009,
`arXiv:hep-ph/0701165`.

[139] H. Eberl, S. M. R. Frank, and W. Majerotto, "CP Violating Asymmetry in
Stop Decay into Bottom and Chargino," `arXiv:0912.4675 [Unknown]`.

[140] G. A. Moortgat-Pick, H. Fraas, A. Bartl, and W. Majerotto, "Polarization
and spin effects in neutralino production and decay," *Eur. Phys. J.* **C9**
(1999) 521–534, `arXiv:hep-ph/9903220`.

[141] H. E. Haber, "Spin formalism and applications to new physics searches,"
`arXiv:hep-ph/9405376`.

[142] D. Berdine, N. Kauer, and D. Rainwater, "Breakdown of the Narrow Width
Approximation for New Physics," *Phys. Rev. Lett.* **99** (2007) 111601,
`arXiv:hep-ph/0703058`.

[143] N. Kauer, "Narrow-width approximation limitations," *Phys. Lett.* **B649**
(2007) 413–416, `arXiv:hep-ph/0703077`.

[144] C. Bouchiat and L. Michel, "Mesure de la polarisation des electrons
relativistes," *Nucl. Phys.* **5** (1958) 416.

[145] L. Michel, "Covariant description of polarization," *Il Nuovo Cimento* **14**
(1959) 95.

[146] B. C. Allanach *et al.*, "The Snowmass points and slopes: Benchmarks for
SUSY searches," `arXiv:hep-ph/0202233`.

[147] A. H. Hoang and T. Teubner, "Top quark pair production close to threshold:
Top mass, width and momentum distribution," *Phys. Rev.* **D60** (1999)
114027, `arXiv:hep-ph/9904468`.

[148] W. Porod, "SPheno, a program for calculating supersymmetric spectra,
SUSY particle decays and SUSY particle production at e+ e- colliders,"
Comput. Phys. Commun. **153** (2003) 275–315, `arXiv:hep-ph/0301101`.

[149] G. P. Lepage, "A New Algorithm for Adaptive Multidimensional Integration," *Journal of Computational Physics* **27** (1978) 192.

[150] G. P. Lepage, "VEGAS: An Adaptive Multidimensional Integration Program," *Cornell preprint* (1980) CLNS–80/447.

[151] M. Bahr *et al.*, "Herwig++ Physics and Manual," `arXiv:0803.0883 [hep-ph]`.

[152] M. Bahr *et al.*, "Herwig++ 2.2 Release Note," `arXiv:0804.3053 [hep-ph]`.

[153] M. Gigg and P. Richardson, "Simulation of beyond standard model physics in Herwig++," *Eur. Phys. J.* **C51** (2007) 989–1008, `arXiv:hep-ph/0703199`.

[154] R. Kleiss *et al. CERN 89-08, vol.3, pp129-131* .

[155] A. Bartl, S. Hesselbach, K. Hidaka, T. Kernreiter, and W. Porod, "Impact of SUSY CP phases on stop and sbottom decays in the MSSM," `arXiv:hep-ph/0306281`.

[156] A. D. Martin, W. J. Stirling, R. S. Thorne, and G. Watt, "Update of Parton Distributions at NNLO," *Phys. Lett.* **B652** (2007) 292–299, `arXiv:0706.0459 [hep-ph]`.

[157] B. K. Gjelsten, D. J. Miller, and P. Osland, "Measurement of SUSY masses via cascade decays for SPS 1a," *JHEP* **12** (2004) 003, `arXiv:hep-ph/0410303`.

[158] M. M. Nojiri, G. Polesello, and D. R. Tovey, "Proposal for a new reconstruction technique for SUSY processes at the LHC," `arXiv:hep-ph/0312317`.

[159] D. Casadei, R. Djilkibaev, and R. Konoplich, "Reconstruction of stop quark mass at the LHC," `arXiv:1006.5875 [hep-ph]`.

[160] C. G. Lester, M. A. Parker, and M. J. White, "Three body kinematic endpoints in SUSY models with non- universal Higgs masses," *JHEP* **10** (2007) 051, `arXiv:hep-ph/0609298`.

[161] **LHC/LC Study Group** Collaboration, G. Weiglein *et al.*, "Physics interplay of the LHC and the ILC," *Phys. Rept.* **426** (2006) 47–358, `arXiv:hep-ph/0410364`.

[162] A. J. Barr and C. G. Lester, "A Review of the Mass Measurement Techniques proposed for the Large Hadron Collider," `arXiv:1004.2732 [hep-ph]`.

[163] G. Brooijmans *et al.*, "New Physics at the LHC. A Les Houches Report: Physics at TeV Colliders 2009 - New Physics Working Group," `arXiv:1005.1229 [hep-ph]`.

[164] J. Hisano, K. Kawagoe, and M. M. Nojiri, "A detailed study of the gluino decay into the third generation squarks at the CERN LHC," *Phys. Rev.* **D68** (2003) 035007, `arXiv:hep-ph/0304214`.

[165] A. J. Barr, "Using lepton charge asymmetry to investigate the spin of supersymmetric particles at the LHC," *Phys. Lett.* **B596** (2004) 205–212, `arXiv:hep-ph/0405052`.

[166] H.-C. Cheng, J. F. Gunion, Z. Han, G. Marandella, and B. McElrath, "Mass Determination in SUSY-like Events with Missing Energy," *JHEP* **12** (2007) 076, `arXiv:0707.0030 [hep-ph]`.

[167] K. Kawagoe, M. M. Nojiri, and G. Polesello, "A new SUSY mass reconstruction method at the CERN LHC," *Phys. Rev.* **D71** (2005) 035008, `arXiv:hep-ph/0410160`.

[168] **ATLAS** Collaboration, "ATLAS detector and physics performance. Technical design report. Vol. 2,". CERN-LHCC-99-15.

[169] F. E. Paige, "Determining SUSY particle masses at LHC," `arXiv:hep-ph/9609373`.

[170] D. J. Miller, P. Osland, and A. R. Raklev, "Invariant mass distributions in cascade decays," *JHEP* **03** (2006) 034, `arXiv:hep-ph/0510356`.

[171] B. K. Gjelsten, D. J. Miller, and P. Osland, "Measurement of the gluino mass via cascade decays for SPS 1a," *JHEP* **06** (2005) 015, arXiv:hep-ph/0501033.

[172] W. S. Cho, K. Choi, Y. G. Kim, and C. B. Park, "Gluino Stransverse Mass," *Phys. Rev. Lett.* **100** (2008) 171801, arXiv:0709.0288 [hep-ph].

[173] M. M. Nojiri, G. Polesello, and D. R. Tovey, "A hybrid method for determining SUSY particle masses at the LHC with fully identified cascade decays," *JHEP* **05** (2008) 014, arXiv:0712.2718 [hep-ph].

[174] H.-C. Cheng, J. F. Gunion, Z. Han, and B. McElrath, "Accurate Mass Determinations in Decay Chains with Missing Energy: II," arXiv:0905.1344 [hep-ph].

[175] **ATLAS** Collaboration, G. Aad *et al.*, "The ATLAS Experiment at the CERN Large Hadron Collider," *JINST* **3** (2008) S08003.

[176] M. Bahr *et al.*, "Herwig++ 2.3 Release Note," arXiv:0812.0529 [hep-ph].

[177] A. Buckley *et al.*, "Rivet user manual," arXiv:1003.0694 [Unknown].

[178] B. M. Waugh *et al.*, "HZTool and Rivet: Toolkit and framework for the comparison of simulated final states and data at colliders," arXiv:hep-ph/0605034.

[179] M. Cacciari and G. P. Salam, "Dispelling the N^3 myth for the k_t jet-finder," *Phys. Lett.* **B641** (2006) 57–61, arXiv:hep-ph/0512210.

[180] M. Cacciari, G. P. Salam, and G. Soyez, "The anti-k_t jet clustering algorithm," *JHEP* **04** (2008) 063, arXiv:0802.1189 [hep-ph].

[181] J. Alwall *et al.*, "MadGraph/MadEvent v4: The New Web Generation," *JHEP* **09** (2007) 028, arXiv:0706.2334 [hep-ph].

[182] W. Beenakker, R. Hopker, and M. Spira, "PROSPINO: A program for the PROduction of Supersymmetric Particles In Next-to-leading Order QCD," arXiv:hep-ph/9611232.

[183] W. Beenakker, R. Hopker, M. Spira, and P. M. Zerwas, "Squark and gluino production at hadron colliders," *Nucl. Phys.* **B492** (1997) 51–103, `arXiv:hep-ph/9610490`.

[184] W. Beenakker, M. Kramer, T. Plehn, M. Spira, and P. M. Zerwas, "Stop production at hadron colliders," *Nucl. Phys.* **B515** (1998) 3–14, `arXiv:hep-ph/9710451`.

[185] A. Grozin, "Lectures on QED and QCD," `arXiv:hep-ph/0508242`.

[186] P. Cvitanović, "Group Theory," *http://www.nbi.dk/GroupTheory/* .

[187] J. Rosiek, "Complete Set of Feynman Rules for the Minimal Supersymmetric Extension of the Standard Model," *Phys. Rev.* **D41** (1990) 3464.

[188] J. Rosiek, "Complete set of Feynman rules for the MSSM – ERRATUM," `arXiv:hep-ph/9511250`.

List of Figures

List of Tables